408-SMRM-79-0001

PROCEEDINGS
OF THE
SMRM DEGRADATION STUDY WORKSHOP

Organized by:
The Satellite Servicing Project
Goddard Space Flight Center

May 9-10, 1985

National Aeronautics and Space Administration

GODDARD SPACE FLIGHT CENTER
Greenbelt, Maryland

PROCEEDINGS

OF THE

SMRM DEGRADATION STUDY WORKSHOP

Organized by:

The Satellite Servicing Project
Goddard Space Flight Center

May 9-10, 1985

GODDARD SPACE FLIGHT CENTER
Greenbelt, Maryland

The workshop was organized by the Satellite Servicing Project, Goddard Space Flight Center. Participants include representativies from NASA, JPL, industry and universities.

Single copies of this document can be obtained by writing to:

Gilbert W. Ousley, Jr.
NASA/GSFC
Code 408
Grenbelt, Maryland 20771

CONTENTS

PREFACE

This publication contains the proceedings of the Solar Maximum Repair Mission Degradation Study Workshop, held at the Goddard Space Flight Center in Greenbelt, Maryland on May 9-10, 1985. The main purpose of the workshop was to report on the results of tests and studies of the returned Solar Maximum Mission hardware and materials. Specifically, the workshop was concerned with studies of the effects of four years exposure to a low-earth orbital environment.

A summary of the results reported at the workshop is included in this publication. To provide a background for the reported findings, the summary includes a short description of the Solar Maximum Mission and the Solar Maximum Repair Mission. Some of the papers contained in this publication have been submitted by the participating organizations after the presentations were made at the workshop and may not necessarily have the same title and author/presenter as in the workshop agenda.

AGENDA

SMRM DEGRADATION STUDY WORKSHOP
Goddard Space Flight Center

May 9-10, 1985

	PRESENTER
INTRODUCTION	W. Ousley/GSFC
Solar Max Repair	F. Cepollina/GSFC
Main Electronics Box (MEB)	R. Davis/GSFC
MEB Box Failure Analysis	R. Lee/HAO
Parts Analysis	T. Marquez/Sperry
Radiation Effects on MEB Parts	R. Maurer/APL
ACS Louvers/MEB Honeycomb Studies	H. Frankel/Fairchild R. Eby/Fairchild

BREAK

Inertial Reference Unit (DRIRU) Performance Tests	J. Ritter/Teledyne
DRIRU Bearing and Lubricant Analysis	J. Uber/GSFC
Remote Interface Unit	M. Bay/Fairchild
Magnetometer Performance Tests	J. Rippingale/Schonstedt
Standard Reaction Wheel Performance and Internal Examination	C. Sutter/Sperry
Star Tracker Degradation	P. Newman/GSFC

LUNCH

Initial Examination of Returned SMM Surfaces	J. Triolo/GSFC
Surface Effects on Kapton, Silver Teflon, and Louvers	J. Park/GSFC
Kapton Erosion and Other Surface Effects	R. Fristrom/APL
Micrometeorite and Space Debris Impacts	D. McKay/JSC

Teflon and Kapton Surface Effects	R. Linton/MSFC
Surface Chemistry and Thermal Effects on Kapton and Silver Teflon	B. Mason/Langley
BREAK	
Chemical and Physical Analysis of Kapton and Silver Teflon	J. Robinson/Lockheed
Analysis of Transparent and Normal Silver Teflon	W. Stuckey/Aerospace
Photo-induced Contaminant Deposition on Silver Teflon	W. Stuckey/Aerospace
Teflon Degradation by Oxygen	R. Liang/JPL
Teflon and Kapton Thermal Properties	D. Rhoads/Lockheed

SUMMARY OF THE SMRM DEGRADATION STUDY WORKSHOP

Prepared for the

National Aeronautics and Space Administration
SMRM Degradation Study Workshop
Goddard Space Flight Center
Satellite Servicing Project

by

Computer Technology Associates, Inc.
7501 Forbes Blvd.
Lanham, Maryland 20706

INTRODUCTION

The Solar Maximum Mission (SMM) spacecraft, built at the Goddard Space Flight Center, was launched in February 1980 with solar flare research its primary objective. Launched near the peak of the 11-year solar cycle, the SMM was put in a 310 nm, nearly circular orbit with 28.5° inclination. The spacecraft's longitudinal axis was pointing at the Sun in a 3-axis stabilized mode, so that the seven instruments aboard the spacecraft could monitor the activities of the Sun. Some of the instruments required very fine pointing accuracy and stability to obtain high-resolution data. During the initial period, the pointing accuracy of the SMM was better than 2 arc-sec with stability less than 1 arc-sec.

The following instruments were carried by the SMM spacecraft:

Active Cavity Radiometer Irradiance Monitor
Coronagraph/Polarimeter (C/P)
Gamma Ray Spectrometer
Hard X-Ray Burst Spectrometer
Hard X-Ray Imaging Spectrometer
Ultraviolet Spectrometer/Polarimeter
X-Ray Polychromator

Six of the instruments were designed to observe solar flares in regions of the electromagnetic spectrum ranging from visible light through ultraviolet and x-ray emission to gamma rays. The seventh instrument, the Active Cavity Radiometer Irradiance Monitor, monitored the Sun's total radiation.

Equipment and Instrument Failures

The first months of the mission were very successful. The spacecraft and the instruments operated flawlessly with hundreds of flares monitored and recorded. In September 1980, about 6 1/2 months after launch, one of the three gyro channels (Channel C) of the NASA Inertial Reference Unit failed. The required attitude control was maintained, however, without performance degradation by the two remaining gyro channels (A and B) until November 1980, when three fuses burned out in the reaction wheel control circuits. In December 1980, a yaw magnetic torquer also failed. A coarse attitude control mode was established using the remaining magnetic torquers. The spacecraft was spin stabilized at a rotation rate of 1 deg/sec with a coning motion that moved the Sun pointing spacecraft axis up to 15° off the Sun line. Only two of the seven instruments were 100% operational (Gamma Ray Spectrometer and Hard X-Ray Burst Spectrometer) since they did not require precise pointing. One instrument functioned with limited capability (Active Cavity Radiometer Irradiance Monitor). Two of the instruments were not able to operate due to the backup attitude control mode (Ultraviolet Spectrometer/Polarimeter and X-Ray Polychromator) and two others had failed and were inoperative (Coronagraph/Polarimeter and Hard X-Ray Imaging Spectrometer).

Solar Maximum Repair Mission

The Solar Max spacecraft was the first spacecraft designed to be serviced and repaired in space by the Space Shuttle crew. The Modular Attitude Control System (MACS) module was designed to be an orbital replacement unit, but the instrument repair was more complex because the Instrument Module (IM) was not designed to be repaired or replaced in orbit. Of the two failed scientific instruments, only the C/P was considered repairable. An identical spare MACS module was available from the Landsat program and a new C/P Main Electronics Box (MEB) was built specifically for the repair mission.

The Solar Maximum Repair Mission (SMRM) was performed by the crew of the STS flight 41-C in April 1984. By this time the SMM orbit altitude had decayed to 265 nm. Attempts by the astronaut using the Manned Maneuvering Unit (MMU) to dock to the spacecraft and to stop its rotation failed. The docking attempts imparted to the spacecraft uncontrollable roll, pitch and yaw rates. After the spacecraft was stabilized using specially uplinked software, the spacecraft was grappled by the Orbiter's Remote Manipulator System (RMS) and placed on the Flight Support System (FSS) located in the Orbiter Bay.

The MACS module was removed from the SMM and placed on its temporary storage fixture on the FSS. After the new module was mounted on the SMM, the old module was secured in its landing location on the lower starboard side of the FSS. The entire MACS module replacement took less than an hour.

The replacement of the Main Electronics Box of the Coronagraph/Polarimeter was the next repair operation. The MEB was replaced successfully, even though it was not designed for servicing. The faulty MEB was stowed in a storage area in the FSS tool locker for return to Earth.

After the replacement of the faulty equipment, the SMM was checked out and deployed to provide more data near the Sun's least active solar flare period. The Orbiter landed two days later on April 14, 1984.

Post-Flight Handling of Returned Equipment

After landing at Edwards Air Force Base in California, the Orbiter and its returned payload were flown on the 747 to the Kennedy Space Center (KSC). After three days in the Orbiter Processing Facility (OPF), the FSS with MACS attached was removed from the Orbiter and transported to the Operations and Checkout (O&C) building.

Because of concern that contamination may mask the environmental effects on the returned equipment, the MACS and the MEB were bagged while in the O&C building and under QA control with rigid handling limitations. The MACS and MEB were removed from the FSS and placed in their respective storage containers. A one square foot wash plate and a fallout grid/surface had been attached to the MACS in the OPF before removal from the Orbiter to monitor molecular and particulate contaminants deposited from the time the MACS was taken out of the Orbiter bay to when it was unpacked at GSFC. The same procedure was used with MEB but the sequence started at the O&C building where the MEB was removed from the FSS tool locker.

Clean room attire was used by the handling personnel at all times. Except for the time when the units (MACS & MEB) were packed in their separate shipping containers, the units were protected from contamination by bagging made of Capran 518. When the wash plates and fallout plates were removed after unpacking the units at the GSFC, analyses indicated that the protected surfaces were in better condition than required by Mil Std 1246A level 100A.

The returned hardware was stored in a class 10,000 cleanroom at the GSFC. Thermal blankets were carefully cut and removed, then stored in display containers.

Post-Flight Analysis

The returned MACS unit and the MEB of the Coronagraph/Polarimeter offered an opportunity to examine the hardware in an effort to determine the causes of the failures and to study the effects of 50 months exposure to the Low Earth Orbit (LEO) environment. Natural orbital environments, such as solar ultraviolet radiation, charge particles, atomic oxygen, and micrometeroids have been demonstrated to degrade thermal radiative properties like solar absorptance, and material mechanical properties such as elongation and tensile strength. More subtle effects on surface electrical properties have also been observed. Similar effects can be caused by self-induced environments, such as molecular and particulate contamination and by space debris carried into orbit (or created) by the launch vehicle, the spacecraft, or the payload.

The atomic oxygen and space debris effects were for the most part noted from experiments on STS-3 to 8. The contrasts in effects should provide a gauge to assess the reliability of Orbiter based testing of materials for higher altitude and longer term predictions.

HARDWARE ANALYSES

Main Electronic Box

The Main Electronic Box (MEB) provides the control and data handling functions for the Coronagraph/Polarimeter (C/P) instrument. The coronagraph creates an artificial total eclipse of the Sun by using a series of external disks to prevent direct sunlight from falling on the objective lens of the telescope. The C/P operated successfully taking pictures of Sun's corona for 5 months after launch before the first failure occurred. Fortunately, the failed microcircuit could be bypassed by ground software. The second failure in the electronics occurred about a month later, August 8, 1980, but the instrument was kept operating with only an occasional loss of data. The third electronics failure occurred in early September, but a solution to prevent unnecessary shutdowns was found by modifying the onboard software. The terminal failure in the electronics occurred on September 23, 1980, which rendered the instrument inoperative.

Subsequent post-flight analysis showed that all the failures occurred in one type of integrated circuit MM54C161J/883B manufactured by National Semiconductor. There were a total of 21 such microcircuits in use of which three failed. Electrical testing of two of the devices isolated the failures to short circuited transistors. The third device could not be tested because of damage during removal from the PC board. The short circuits were caused by defects in the gate oxide material as a result of time, temperature and applied bias voltage. Several oxide defects were also observed in the third device.

In addition, nine National Semiconductor MM54C161J microcircuits were removed from the MEB and tested. All nine devices had been operating properly on the MEB. Two of the devices failed marginally the initial electrical tests. One device failed catastrophically a static burn-in test at 125°C for 24 hours. The failures were similar to the in-orbit failures of the parts of the same type. Also the parts had similar defects in the gate oxide material, which indicates a lot related problem. There is some question about the burn-in of these devices before delivery. A proper burn-in is an accepted determinant of a parts reliability and will usually weed out weak devices.

Radiation Effects of Selected MEB Electronic Parts

A total of 29 parts of 9 different types were submitted to static, dynamic and functional electrical tests. The tested parts included flight parts and residual parts from the same date code lot as the original flight parts. The flight parts had been under power or bias for the first 8 months and about 10% of the time thereafter. These parts also had a year to anneal at ambient room temperatures on the ground.

The flight electronic parts showed no adverse effects due to the low earth orbit radiation environment. Complex linear devices (μA108A) begin to degrade at low doses and dose rates and will be susceptible to failure at higher altitudes and/or longer exposures. More detailed evaluation of electronic parts in orbit will be possible from the CRRES mission planned for 1986 and from the Space Station. Radiation detectors will then actually measure the environment experienced by electronic parts which will be simultaneously monitored for electrical performance.

Selected Hardware Studies

The evaluation was performed on the returned module retension system preload bolts, MEB honeycomb panel epoxy film adhesive and the thermal louver blade polyimide adhesive.

The two returned bolts were tested for yield strength and ultimate tensile strength. The tests showed no degradation in either category and the results were comparable to those of an unflown bolt.

The MEB honeycomb panel evaluation produced a conclusion that there was no degradation in room temperature bond strength of the epoxy film adhesive.

The returned louver polyimide blade adhesive was tested for lap shear strength and compared with unflown specimens. The results showed an average of 65% reduction in shear strength as compared to the unflown specimens. However, the reduction was not considered a severe one as evidenced by the bonding which survived the action and environments in good condition.

The returned thermal louver blades had red nodules on both sides of the blades. Evidence suggests that the red nodules represent regions of pure polyimide resin cured in space.

Infrared reflectometer measurements were performed on the returned louver blades and compared with those of unflown spare louver blades. The results showed no degradation of infrared reflectivity. Also the louver blade open and close temperature settings showed no degradation. The measured post-flight settings were well within the specification limits.

NASA Standard Inertial Reference Unit (DRIRU II)

The returned unit was the first production DRIRU II (S/N 1001) used as one of the subsystems of the Modular Attitude Control System (MACS). The DRIRU is a self contained, strapdown, three axis, dual redundant attitude rate sensing unit. Three orthogonally mounted, two-degree-of-freedom gyros and a triplication of electronic modules and power supplies are used to provide full operational capability with any two of the three channels. The gyros in the DRIRU II are Teledyne SDG-5 Dynamically Tuned Gyros.

The investigation concluded that gyro channel C failed because of an intermittent electrical short in the motor control logic. Because the failure occurred near the South Atlantic Anomaly, much effort was devoted to determine if the failure could have been caused by radiation. After extensive tests, it was concluded that radiation was not a probable cause of the failure. Subsequent tests at the GSFC Parts Analysis Laboratory showed that the failures occurred in three logic devices. Two of the devices failed because of an electrical overstress. As of this date, the cause of the overstress has not been determined. The third device most likely failed because time, temperature, and an out-of-tolerance logic supply voltage created a short at a latent defect of the device. The defect apparently was caused by an irregularity in the manufacturing process. (See 'DRIRU II Electronics Parts Analysis.')

After the system was reassembled with two substitute electronic modules, a full series of tests were performed to evaluate the stability of the unit over the full operating temperature range. Also the repeatability of the parameters as compared to the delivered state was investigated. The test series were designed to repeat the complete 1978 acceptance tests.

The physical condition of the system was excellent with no apparent materials degradation. There was no evidence of system performance degradation due to operational and other environments. The system had excellent long-term stability of performance parameters over the launch, orbital operation and retrieval environments during a 74-month period.

There was no measurable degradation of the shock/vibration isolators as evidenced by the excellent alignment stability of the gyro axes through launch environments and over an extended time period.

There was no evidence of structural or mechanical changes and no apparent outgassing or degradation of exposed surfaces.

Examination at Teledyne found that the gyro ball bearings showed no excessive wear to raceways, balls, or retainers. However, there was some dark colored, viscous residue mainly in the ball tracks and the retainer ball pockets. (See 'DRIRU Bearings and Lubricant' for summary of GSFC analysis.)

DRIRU Bearings and Lubricant

One of the DRIRU gryoscopes was disassembled and the bearings were returned to GSFC for examination. The gyroscopes had been running continuously in orbit for 4 years at 6000 RPM.

The bearings showed some wear in the form of tiny pits and scratch-line deformations. Numerous tiny particles were observed clinging to the bearing parts after the case and the hysteresis ring were removed. The particles had originated from the pits of the bearing races and the balls.

The lubricant for the bearings is contained in the retainers which are made from a porous, phenolic material. Examination showed that the bearings were lubricated.

The conclusion was that the bearings showed little wear and had a sufficient amount of lubricant left to perform without problems for their predicted life of 5 years.

DRIRU II Electronics Parts Analysis

The failed part in the gyro channel C of the DRIRU II unit was an RCA CD4017AK microcircuit, a decade counter. The part was submitted to the GSFC Parts Analysis Laboratory for failure analysis. The tests determined that the failure was due to a short circuit through an oxide defect underneath the output metalization. The defect was the result of a manufacturing irregularity during processing.

Two other devices, an RCA CD4049AK and a CD4081BK, both microcircuits of the DRIRU II gyro motor control logic, were submitted to the GSFC Parts Analysis Laboratory for failure analysis. Both devices had failed in flight due to a fused open die metalization track. A pin on each of the devices was open circuited to all other pins. The fused open metalization was a result of electrical overstress.

Remote Interface Unit

The Remote Interface Unit (RIU) was designed and built by the Fairchild Space Company. The first application of the RIU was on the SMM spacecraft. The unit provides two-way communications between electronic packages on the spacecraft and a central command and telemetry unit (CU) which decodes and distributes commands and generates telemetry formats. The CU communicates with the On-Board Computer (OBC) through the Standard Interface and with the ground via the RF equipment.

The standard MACS module carries two redundant RIU's which have three operational modes: 'OFF,' 'Standby 1,' and 'Standby 2.' The last two are sub-modes of the 'ON' mode. During the flight, Unit A was operating in the full 'ON' mode (Standby 2). Unit B was operating in the 'OFF' mode (only Bus Receiver/Control Logic and Power Converter continuously powered). Throughout the flight, no malfunctions of the Units were indicated.

The RIU's were returned to Earth with the MACS module and Unit B underwent a post-flight engineering evaluation from December 1984 until April 1985. The pre-flight tests were performed in 1979.

Post-flight external and internal visual inspection revealed no degradation. Besides the visual inspection, RIU B underwent two other kinds of engineering tests. Automated test equipment was used to qualify the unit as a whole ('GO - NO GO'). In the other test, a parametric test,

each parameter was evaluated separately. The parametric evaluation included user telemetry interface circuitry (active and passive analog linearity), phase lock loop performance, pulsed output current and width, serial digital commands, serial digital telemetry, and power dissipation.

The tests were performed at ambient temperature, -20°C, and +60°C. The cold and hot temperatures are the qualification limits. All parameters evaluated were found to be within specification. When compared to pre-flight test data, in many categories the post-flight data showed some improvement. The test results qualify the unit for reuse in another mission.

Three Axis Magnetometers

Magnetometers are used to sense spacecraft attitude with respect to Earth's magnetic field. Two Three Axis Magnetometers, designated as the primary and secondary magnetometer, are part of the standard MACS module. The magnetometers are fluxgate magnetometers which produce three analog signals proportional to the magnetic field components along their input axes.

The magnetometers together with the magnetic torquers provided an important function during one part of the SMRM when they were used to stabilize the spacecraft's attitude. Only one of the magnetometers was used during the SMM. The other, serving as a backup unit, was never used because the primary unit did not malfunction.

After the magnetometers were returned to the manufacturer, they were subjected to the same performance tests which were performed before the flight. The post-flight tests showed that the magnetometers still satisfied the original specification requirements. The post-flight test data nearly duplicated the pre-flight data.

Standard Reaction Wheels

The four Standard Reaction Wheels are components of the MACS module and are used for attitude control and stabilization. They are essentially flywheels and work on the principle of exchanging angular momentum with the spacecraft body. Normally, three of the wheels are aligned with the principal axes of the spacecraft. The fourth, a redundant skewed wheel, is used to replace any of the orthogonal wheels in case of a wheel failure. In normal operation it is run at a bias speed to keep the other three wheels away from zero speed and to maximize bearing life.

After the return of the wheels to the manufacturer on January 24, 1985, they were subject to visual examination, preliminary electrical checks, performance tests at ambient, hot and cold temperature environments, and internal pressure measurements. One wheel, which showed a slightly deteriorated performance, was selected for teardown.

Visual examination found the wheels in good condition. Preliminary electrical tests, continuity, bonding, and isolation were satisfactory. The bonding resistance for two of the four units was slightly above the requirements but was not considered excessive.

The internal pressure measurements indicated that the pressures were far below atmospheric, confirming that the vacuum seal was still intact.

All four units successfully passed the performance tests with the exception of the 500 RPM torque noise test using a .1 rad/sec high pass filter. However, the units met the torque noise test with the 0.3 rad/sec high pass filter in the test circuit.

Individually, two of the units showed very similar performance results as compared to pre-flight tests. One unit showed decreased bearing drag torques and extended coastdown times. Another unit had a 45% increase in drag torques and reduced coastdown times, although it met all requirements. It had been exposed to a no-load overtemperature (60°C) for approximately 3 hours due to a software problem.

Teardown analysis of the overtemperature-exposed unit showed an 'as new' appearance of the internal components and surfaces. The lubrication analysis showed a greater lubrication loss in the floating cartridge system than in the fixed cartridge system. An investigation package including contamination wipes, lubricant samples, bearing components and photographs of some items was sent to NASA GSFC for analysis (pending).

NASA Standard Star Trackers

The MACS module includes two Fixed Head Star Trackers (FHST) which are used together with the inertial reference unit and the on-board computer to determine and maintain the spacecraft's attitude with the required accuracy. Because the star tracker is a very sensitive instrument, its image dissector tube must be adequately protected from high level light sources such as the Sun. This was done by providing light shades and a shutter operated by a bright object sensor. At the time of the grappling attempt, the trackers and the shutter were powered-off. They remained in this condition until recovery.

The cathode of the image dissector tube detector was extensively damaged by the Sun following the attempts by the astronaut to dock with the spacecraft using the Manned Maneuvering Unit (MMU). The spacecraft was tumbling out of control for many hours before it was finally stabilized so that it could be grappled by the Remote Manipulator System. The tumbling exposed the sensitive cathode to the Sun causing permanent degradation. This prevented proper operation of the tracker after return to Earth and made comparison with pre-flight characteristics impossible. Otherwise, the tracker functioned nominally during testing at the GSFC and the Kennedy Space Center.

The trackers performed flawlessly during the Solar Maximum Mission. Because of inconsistencies in the flight data, some questions arose about the position calibration and alignment. The inconsistencies were attributed partly to a new calibration method and partly to the scarcity of flight data.

During the period from the spacecraft failure to just prior to recovery, the trackers were used occasionally, but were always adequately protected by the shutter.

The tests discovered that the 'tracks' made by the Sun across the cathode were insensitive regions which could not produce an adequate signal to track a star. It was also discovered that the lens of tracker S/N 001 had on its surface large peelings from the lens coating.

MATERIALS ANALYSES

Materials analyses have been performed on materials retrieved from the Solar Max thermal control system, and on various impact particles that were imbedded in the thermal control materials. The materials analyzed were aluminized Kapton and Mylar, and Dacron netting from the multilayer insulation (MLI) blankets, and silver Teflon used on a thermal radiator and as trim on louver assemblies.

MLI is used to thermally insulate various spacecraft components. The portions of the MLI returned to Earth are primarily from the blankets used to insulate the MACS. Other pieces are from the blanket that covered the Main Electronics Box of the Coronagraph/Polarimeter. Aluminized Kapton is used for the top layer of the MLI. Other layers of the MLI are aluminized Kapton (MACS) or aluminized Mylar (MEB) separated by Dacron netting. A summary of the analyses is reported in the following section.

Silver Teflon is used on spacecraft components to increase the thermal radiation performance of exposed surfaces. The silver Teflon removed from the MACS is from the thermal louver assembly.

The chemistry of various impact particles, both natural and man made, has been analyzed. These impact particles were found imbedded in the MLI and in the thermal louvers. A summary of these analyses is reported in section 'Impact Particles.'

Insulation Materials

There are two different forms of MLI insulation blankets returned to Earth from the Solar Max. In both forms, the top layer is made of Kapton with an aluminum layer vapor deposited on the inside surface. The bottom layer, the layer facing the spacecraft systems, is also made of aluminized Kapton, with the aluminum facing the inner layers of the MLI. In both forms, every layer is separated and supported by a Dacron mesh.

The MLI blankets that covered the MACS are composed entirely of aluminized Kapton. The top and bottom layers are made of 2 mil Kapton. There are six to ten inner layers of 1/4 mil Kapton, aluminized on both sides. The MLI taken from the Main Electronics Box is made of aluminized Kapton and aluminized Mylar. The top layer is 3 mil Kapton and the bottom layer is 1 mil Kapton. There are fifteen inner layers of 1/4 mil Mylar, aluminized on both sides.

The MLI materials have been analyzed by various investigators primarily using optical microscopes and Scanning Electron Microscopes (SEM). In addition, infrared spectroscopy was used to detect potential changes in the Kapton polymer structure, and a solar reflectometer measured solar absorptance. Measurements have been made of Kapton samples by exposing them to low pressure atomic oxygen discharge, to a microwave discharge rich in ultraviolet and to a 3 Kv argon ion beam under high vacuum conditions.

Aluminized Kapton Degradation

The most apparent change in the MLI is the dull appearance of the top Kapton layers as compared to the shiny surface of new Kapton samples. Thus, studies of the MLI samples have con-centrated on a possible degradation of the Kapton material. Observations show the outer Kapton surface to be eroded, thereby creating the dull appearance. This finding is similar to the results of tests performed on-orbit during the STS-8 mission. Findings on STS-8 as well as SMM indicate that changes in the Kapton are most likely due to the presence of atomic oxygen.

Degradation of the Kapton surface appears to be greater in areas cleaned during preflight operations with an alcohol based solvent. The same study has revealed tunnel-like substructures under the Kapton surface in the region of the interface between the alcohol wiped and non-wiped areas. It is believed that this is caused by the diffusion of atomic oxygen through the surface, and reaction with the underlying polymers. Associated with the thin tunnel surfaces are small holes believed to be the result of atomic oxygen and UV interaction.

Infrared spectroscopy indicates that while there is obvious degradation in the Kapton, the actual polymer structure has not changed. Measurements of thickness of the top Kapton layer from the front of the MACS indicate that the Kapton suffered mass losses ranging from 0.54 percent to 31.4 percent. One sample from the bottom of the MACS suffered a 41 percent mass loss.

In order to more specifically determine the cause of the Kapton mass losses, Kapton samples were exposed to a variety of atomic oxygen sources, ion sources and ultraviolet (UV) sources. These tests suggest that the greatest surface etching is due to a combination of atomic oxygen coupled with exposure to UV. The angle at which the surface is exposed to these elements is probably significant.

Studies of the back side of the top Kapton layer from the MEB have revealed areas where the deposited aluminum is missing. These areas include scratches most likely caused by the handling of the MLI. Other areas are pinhole in size in a regular pattern, causing the illusion of penetrations in the transparent Kapton layer. These transparent pinholes appear to correspond with the knots in the underlying Dacron mesh, leading to the speculation that the knots have rubbed the aluminum off. While some surface holes appear to be the result of atomic oxygen and UV interaction or the illusion of transparent Kapton, other surface holes appear to be the result of particle impacts. Not all of these holes show a total penetration. The subject of particle impacts is discussed in section 'Impact Particles.'

The significance of the Kapton degradation to spacecraft designers lies in potential changes in the MLI performance. Measurements have been made of solar absorptance of the Kapton material. The solar absorptance of the Kapton material is typically 0.37 to 0.41 prior to on-orbit exposure. The post-flight measurements indicate that the solar absorptance of the SMM Kapton samples has increased by 0.03 to 0.04. This increase is probably due to the optical scattering effect of the degraded Kapton surface. This small increase should have little effect on the performance of the MLI insulation blankets. However, greater degradation of the top Kapton layer that may significantly affect the performance of the MLI, cannot be ruled out in future missions.

Inner Layer Material Degradation

An examination has been made of the aluminized Mylar films and the Dacron mesh from the inner layers of the MLI which was used to cover the MEB. Optical microscopes of up to 400 power have revealed no erosion in these materials. The only apparent damage to these materials was caused by the impact particles (see 'Impact Particles').

Silver Teflon

Silver Teflon is a thin Teflon film on which a layer of silver is vapor deposited. A layer of Inconel is deposited on the silver for protection from the environment. The Teflon film used on the SMM spacecraft is 5 mils thick with a 1500 Angstrom thick layer of silver and a 100 Angstrom thick layer of Inconel. Silver Teflon is used in the thermal protection system to increase the thermal radiative performance of various exposed surfaces. The film is normally applied so that the Teflon side is exposed to the orbit environment.

All silver Teflon samples given to investigators for analyses were exposed to the orbit environment on the Teflon side. Some material was also exposed on the silver/Inconel side, due to its unique application as trim on the MACS louver system (see 'Post-Flight Photographs'). It has been found in both cases that the surfaces were affected by the long duration exposure.

The silver Teflon has been analyzed, as in the case of aluminized Kapton, primarily with optical and Scanning Electron Microscopes. The absorptance of exposed samples has been measured and Energy Dispersive X-Ray Analysis (EDAX) has been used in conjunction with SEM to detect the presence of trace elements. Some samples have been tested with exposure to low pressure atomic oxygen discharge, and other samples have been subjected to tensile strength testing.

Teflon Surface Degradation

Observations of Teflon exposed surfaces show evidence of a reaction to the orbit environment. Unexposed Teflon is smooth in appearance, while the exposed Teflon has been described as having a 'bristle-like' reaction pattern.

The bristle-like structures in exposed Teflon have also been described as cone-like structures. These adjacent cones are easily visible in magnified views of Teflon samples exposed to atomic oxygen and UV. The cause of this Teflon degradation has been studied by exposing a new sample of silver Teflon to atomic oxygen alone. Although the Teflon surface was no longer smooth, it did not have the deep cone structures of the SMM samples. There is speculation that a combination of atomic oxygen fluence and UV exposure will cause a more severe Teflon reaction than atomic oxygen alone, resulting in the cone structures.

Teflon is a fluorocarbon polymer. It has been found that exposure to atomic oxygen depletes Teflon of fluorine. This is evidenced by an increase in the detected carbon/fluorine ratio. Further study is required to determine if longer on-orbit exposures would result in any further breakdown of Teflon.

Silver/Inconel Surface Degradation

The samples exposed on the silver/Inconel surface also show reaction to the orbit environment. Reactions range from cracks in the Inconel layer to a total depletion of silver and Inconel. In the later case, the exposed Teflon surfaces of some samples have developed the cone structures discussed earlier.

Many samples show the whole range of reactions. Between the extremes, a grain pattern of silver/Inconel was formed. Nearing the silver depleted regions, the grain bodies become smaller with the pattern of cracks more widespread.

The cracks in the Inconel surface may be due to temperature cycling under varying orbit conditions. Other evidence has indicated that the reaction of Inconel with atomic oxygen causes removal of the Inconel layer. Silver oxide deposits have been found on sample surfaces. The silver oxide may have come to the Inconel surface through the apparent cracks after the exposed silver reacted with atomic oxygen. Exposure tests indicate that the silver/Inconel depletion may be caused by exposure to atomic oxygen alone, or to a combination of atomic oxygen and UV. This suggests a mechanism for the loss of Inconel and silver. First, the atomic oxygen and temperature cycling causes the loss of Inconel and the formation of cracks. Silver oxide (and perhaps silver peroxide) forms and then flakes off in response to temperature cycling. This cycle continues until Teflon is exposed, and the Teflon reacts to atomic oxygen and UV resulting in the formation of the cone structures.

Tensile strength tests have shown that samples with eroded surfaces have no resilience. Abrupt breaks appear to have occurred in the same direction as thermal expansion/contraction. It was found that the tensile modulus of silver Teflon exposed to atomic oxygen decreased by about 15%, while the modulus of samples exposed to atomic oxygen and UV decreased by about 30%.

Measurements have been made of solar absorptance of the returned Teflon material. The solar absorptance of the Teflon film is typically 0.05 to 0.07 prior to on-orbit exposure. The Teflon samples having the greatest absorptance change, appear to be those exposed to the orbit environment on both sides of the film, and those contaminated by spacecraft outgassing. In these samples, the solar absorptance has increased by as much as 0.22 to 0.29. This large change in absorptance indicates a potentially large change in the performance of the Teflon film. The solar absorptance of Teflon film samples with non-eroded silver/Inconel surfaces had increased by a maximum of 0.04.

Impact Particles

Analyses have begun on some of the particles that impacted the various MLI blankets and the louvers from the MACS. These analyses determine the sources of the various particles and the effect of impacts on the MLI materials and on the aluminum louvers.

A survey of approximately one-half square meter of MLI has revealed over 1500 impact sites. Of these, 432 impacts resulted in craters in the Kapton greater than 40 microns in diameter. In the 75-micron thick Kapton (MEB), craters greater than 100 microns in diameter are

perforations through the Kapton layer. In the 50 micron Kapton (MACS), craters larger than 70 microns in diameter penetrate through the Kapton. When the survey totalled approximately 0.7 square meters of Kapton surface, about 160 impact craters penetrating the Kapton layer were found.

A number of particles completely penetrated all of the MLI layers. One particle penetrated the MLI near a star tracker, making an impression in the star tracker's aluminum shield. Approximately half of the particles that impacted the MACS louvers penetrated the first of the two aluminum sheets, as evidenced by impressions in the second sheet.

Chemical analyses of a number of the impacts has shown that sources of the particles fall into one of four groups. The first group of particles is meteoric material, evidenced by the elements silicon, magnesium, iron, calcium, aluminum with minor amounts of iron-nickel sulfide. The second group of particles is paint particles. This is characterized by titanium and zinc, and the chemistry includes potassium, silicon, aluminum and chlorine. The third group of particles is aluminum droplets, probably from the MLI. The fourth group of particles is waste particles as evidenced by one impact that penetrated three layers of MLI. The chemistry includes sodium, potassium chlorine, phosphorus and minor amounts of sulfur. Investigators believe that this particle may have come from the Orbiter's waste management system.

Two of the large impacts have been investigated in more detail. In both cases, the impact particle apparently disrupted upon impact with the outer Kapton layer of the MLI. The disrupted material was sprayed inward in a cone shaped pattern, lodging on the second layer of the MLI.

In the case of the first impact particle, a small portion of disrupted material penetrated the second layer of the MLI. This impact particle caused a hole 280 microns in diameter with a raised rim. The second MLI layer has a ring of tiny holes and craters surrounding a roughed up area of about 5 millimeters in diameter. Particles from the back of the first layer and from the front of the second layer have been analyzed showing that about 75% are fragments or melted droplets of Kapton. Of the non-Kapton particles, most are composed of magnesium, silicon and iron. Next in number were aluminum particles. Investigators believe that the aluminum is derived from the MLI. Other particles are composed of iron, sulfur and nickel.

The second reported impact particle caused a crater 355 microns in diameter with a raised rim in the Kapton layer. The second layer has a wedge shaped pattern of concentric, elongated holes. Particles of the second impact are composed primarily of iron, sulfur and nickel.

Post-Flight Photographs of
Returned MACS Module

Crewman in MMU approaches SMM. Instrument apertures and solar arrays are seen from "top."

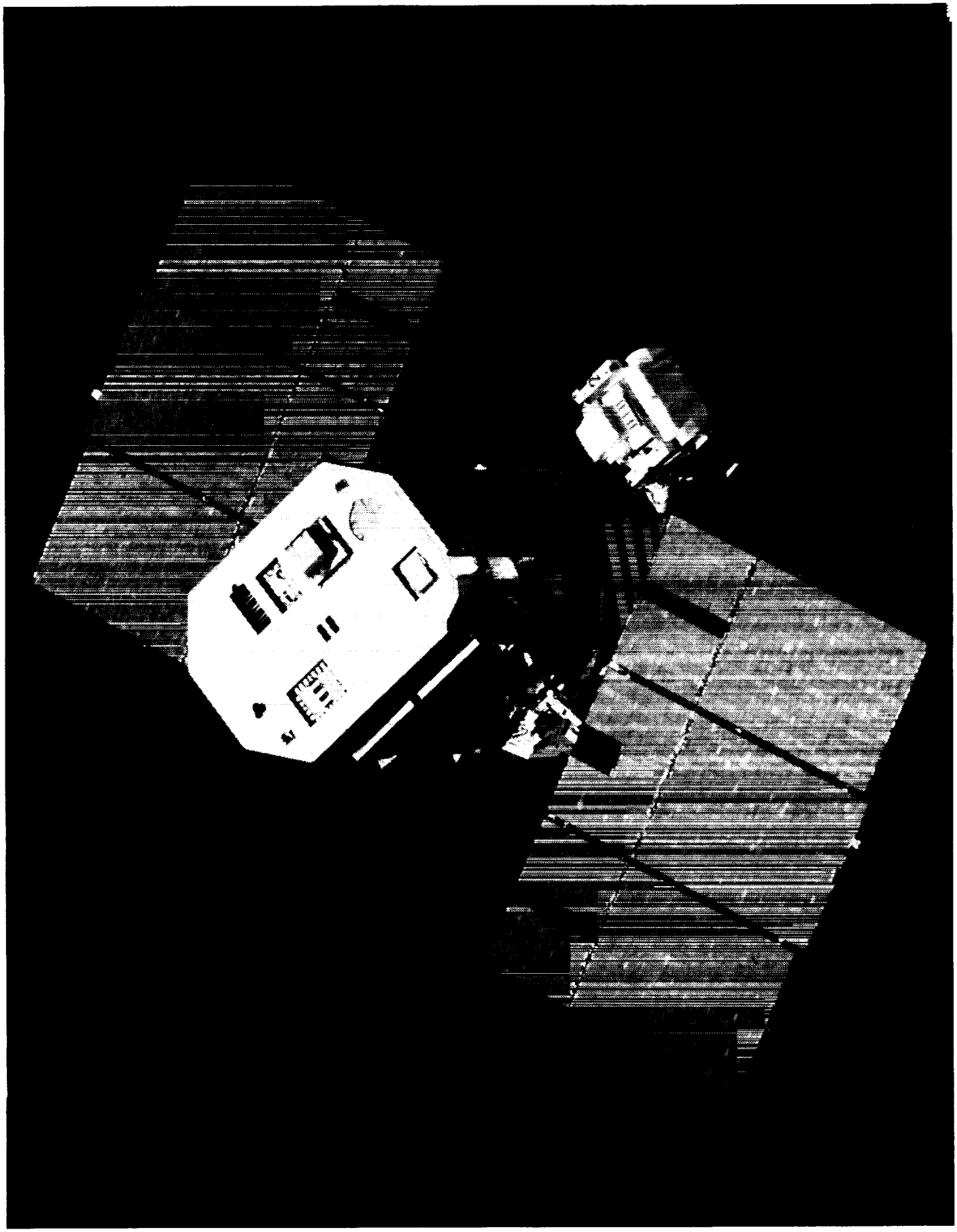

View of MACS module after unsuccessful dock attempt. Most louvers are closed. Degradation of bottom-facing louver trim can be seen.

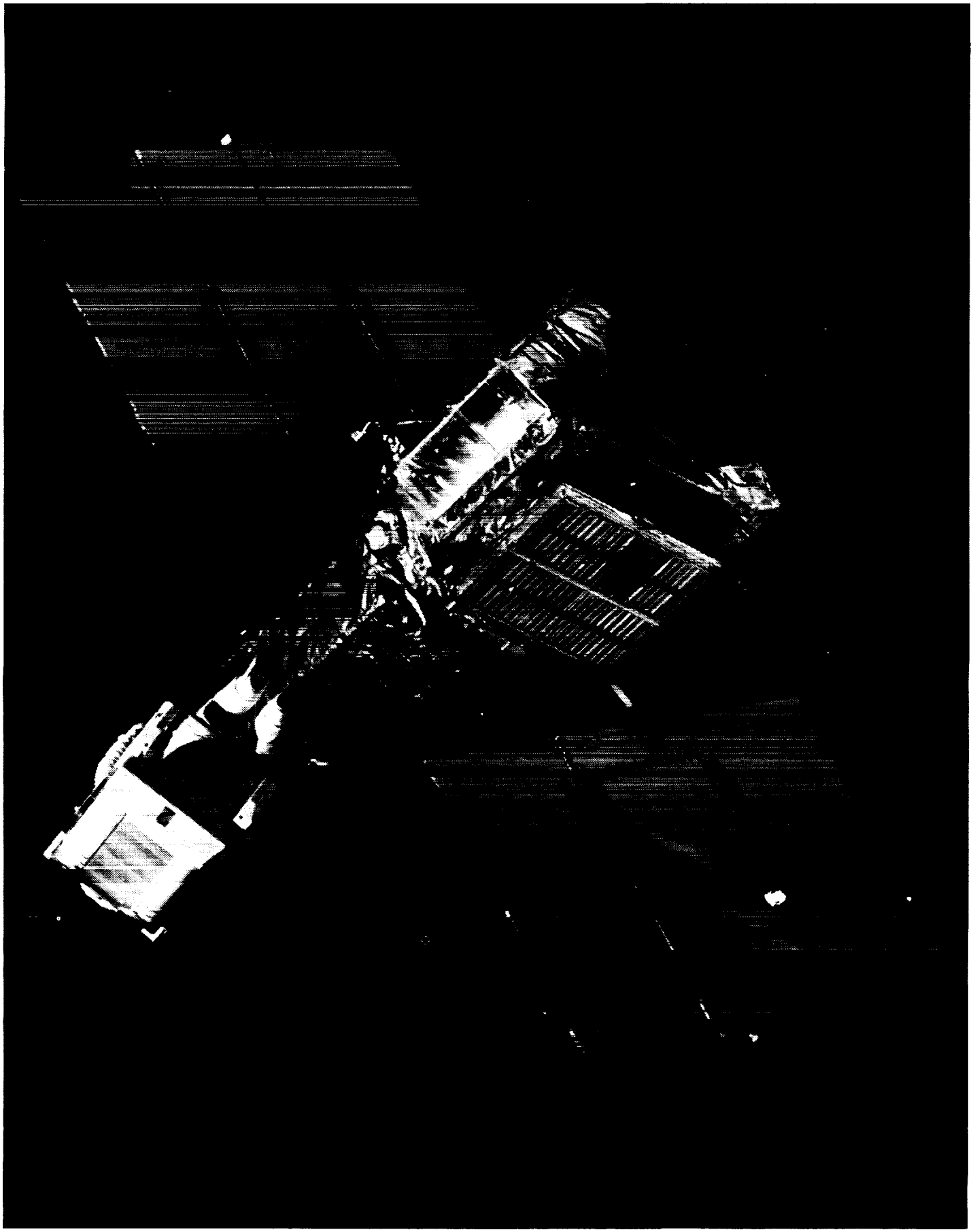

MACS Module Baseplate, after landing. Taken at KSC while still attached to FSS. Fading of black paint was caused by separation and "creep" of oil from thermal grease compound under (gold-colored) louver actuators. Louver blade sent by astronaut is also visible.

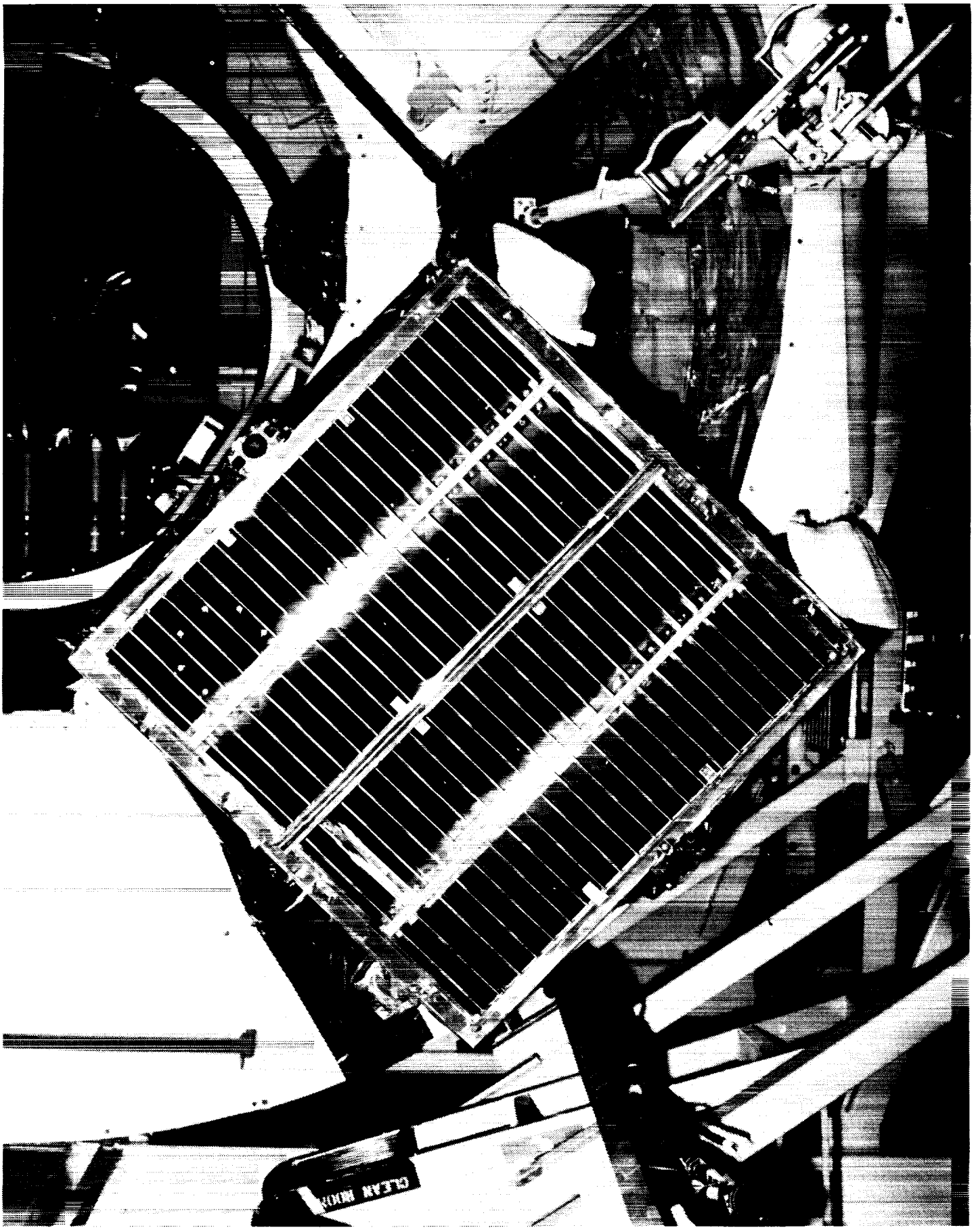

View of "top" (Sun-facing side) of MACS. Discoloration and tearing of silver Teflon, and fading of Kapton, are seen on the corner exposed to solar radiation.

Oblique view of module. Compare silver Teflon trim on the "bottom" (anti-Sun) side with the side facing upper left.

Close-up of the degraded silver Teflon louver trim, on the "bottom" side to solar radiation and the atomic oxygen fluence on the silver/Inconel side of the silver Teflon.

Star-tracker side of the module shows "wash" pattern on the blanket at top center of the photo.

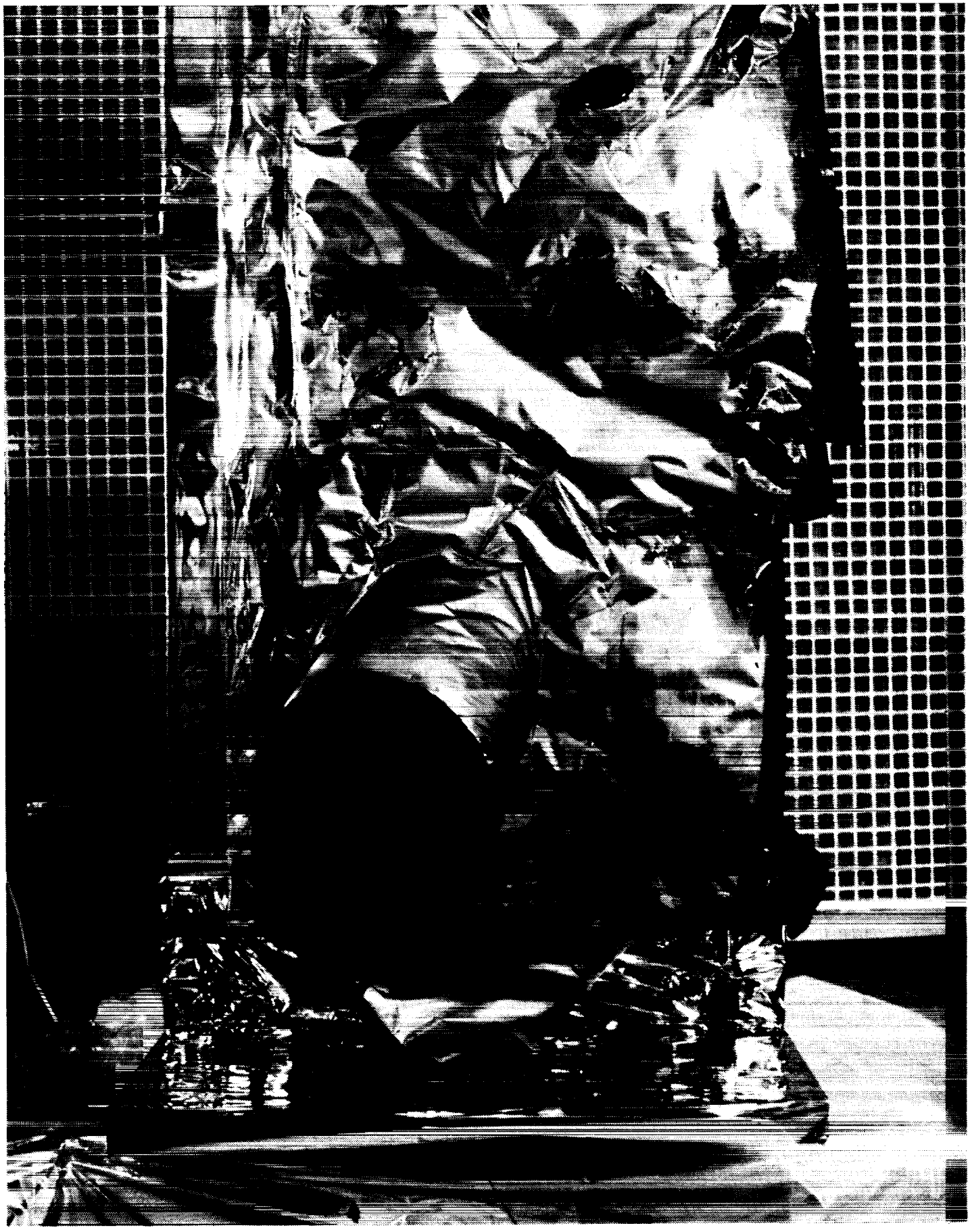

Sun-sensor side of module. Small MLI cover removed from test connector plugs (center) shows unexposed Kapton compared to that exposed to oxygen fluence. The Fine Sun Sensor (upper right) has some white deposits on the radiator surface. These were formed by outgassing from the module interior.

(This page intentionally left blank)

REPORT ON SMRM
C/P MAIN ELECTRONICS BOX
COMPONENT AND MATERIALS DEGRADATION EVALUATIONS

MAY 9, 1985

ROBERT E. DAVIS
SATELLITE SERVICING PROJECT/CODE 408
NASA/GODDARD SPACE FLIGHT CENTER
GREENBELT, MD 20771

C/P MAIN ELECTRONICS BOX HISTORY

- HAO C/P OPERATED SUCCESSFULLY TAKING PICTURES OF SUN'S CORONA UNTIL FAILURE SEPTEMBER 29, 1980 (7 MONTHS)
- AROUND EARLY 1982, DECISION MADE THAT C/P COULD BE REPAIRED BY BUILDING NEW MEB FOR EVA REPLACEMENT
- SMRM MEB REPLACEMENT PERFORMED APRIL 10, 1984
- FAILED MEB RETURNED FOR DEGRADATION STUDIES

SOLAR MAXIMUM MISSION OBSERVATORY IN CLEAN ROOM

(SHOWS MEB AND ITS BLANKET LOCATION BEFORE LAUNCH)

MEB INSTALLED IN SMM P/L COMPARTMENT BEFORE LAUNCH

(SHOWS CABLE INTERCONNECTIONS WITH MEB TEMPORARILY HINGED FOR ACCESSIBILITY - THIS AS FLOWN PHOTO USED TO DETERMINE FEASIBILITY OF REPAIR MISSION)

MEB IS A COMPLICATED ASSEMBLY CONTAINING

- o 15 PLUG-IN STITCH-WELDED CIRCUIT BOARD (APPROX. 4 1/2" x 10" EA.)
- o POWER SUPPLY
- o 11 EXTERNAL SUBMINIATURE CONNECTORS (WITH 362 ACTIVE LEADS)
  - MOUNTED WITH 22 #4/40 SCREWS
  - (PLUS 1 TEST CONNECTOR) CLIPS INSTALLED ON NEW MEB FACILITATING EVA REPLACEMENT
- o ESTIMATED 1,000 COMPONENTS (ABOUT 20% MICROCIRCUITS)

MEB HANDLING CONDITIONS FOLLOWING SMRM REPAIRS

- MEB WITH THERMAL BLANKET FOLDED WAS INSTALLED IN FSS LOCKER BY ASTRONAUTS
- UNHEATED MEB RETURNED TO KSC IN FSSL
- MEB CAREFULLY REMOVED, PHOTOGRAPHED, BAGGED AND PURGED, AND INSTALLED IN SHIPPING BOX FOR RETURN TO GSFC
- BOX STORED IN CLEAN ROOM AT GSFC FOR OVER SIX MONTHS
- THERMAL BLANKET REMOVED DURING STORAGE AND GIVEN TO MATERIALS PERSONNEL FOR ANALYSIS
- ALUMINUM HONEYCOMB PANEL REMOVED FROM MEB AND GIVEN TO FSC FOR ANALYSIS - NO NOTICEABLE INCREASE IN SCREW REMOVAL TORQUE
- MEB GIVEN TO HAO FOR CONFIRMATION OF ON-ORBIT MALFUNCTIONS AND COMPONENT REPLACEMENT (NOT PERFORMED IN A CLEAN ROOM)

PRESENTATORS ON RESULTS OF MEB COMPONENT AND MATERIALS DEGRADATION STUDIES

MAY 9, AM PRESENTATIONS

HAO - BOB LEE, C/P PROJECT ENGINEER

- o MEB MALFUNCTION CONFIRMATION
- o REPAIRS AND RETEST OF REWORKED BOARDS AND MEB

GSFC CODE 311.2/SPERRY - TONY MARQUEZ, FAILURE ANALYSIS ENGINEER

- o MEB PARTS FAILURE ANALYSES
- o REMOVED AND RESIDUAL PARTS RESCREENING

JHU/APL - DICK MAUER, RELIABILITY ENGINEER

- o MEB GENERIC PARTS RADIATION SUSCEPTIBILITY MEASUREMENTS

LATER PRESENTATIONS

FSC - MATERIALS SPECIALIST

- o MEB ALUMINUM HONEYCOMB DEGRADATION MEASUREMENTS

GSFC/JSC/OTHERS - MATERIALS ANALYSTS

- o MEB THERMAL BLANKET DEGRADATION AND SPACE DEBRIS PENETRATIONS

(This page intentionally left blank)

THE MAIN ELECTRONICS BOX (MEB) OF THE HAO CORONAGRAPH/POLARIMETER

ABSTRACT. The SMM satellite was launched in February, 1980 with a complex of instruments designed to study the active sun. The HAO instrument (c/p) operated satisfactorily until July when a series of partial failures began.

This report describes analysis and resolution of problems up to the terminal failure on September 23, 1980. The MEB was replaced in orbit in April, 1984, restoring the observational capability of the c/p instrument.

The process of trouble-shooting and restoration of the failed MEB at GSFC is described. Conclusions are presented regarding the cause of the failures encountered.

Figure 1

A loop transient in the solar corona during the first mission (1980) showing the high activity levels which occur near sunspot maximum. The coronagraph creates an artificial total eclipse of the sun by using a series of external disks to prevent direct sunlight from falling on the objective lens of the telescope. The occulting disk, seen partially in this picture is approximately 1.5 times the diameter of the solar disk.

Figure 1.

Figure 2

The main electronics box (MEB) contains many control and data handling functions. This presentation concerns a failure in the sweep control sequencer (SCS) shown here in block form. The SCS architecture is similar to that of a primitive microprocessor, and it controls an SEC VIDICON camera tube used in an unconventional way to observe the very low light levels involved.

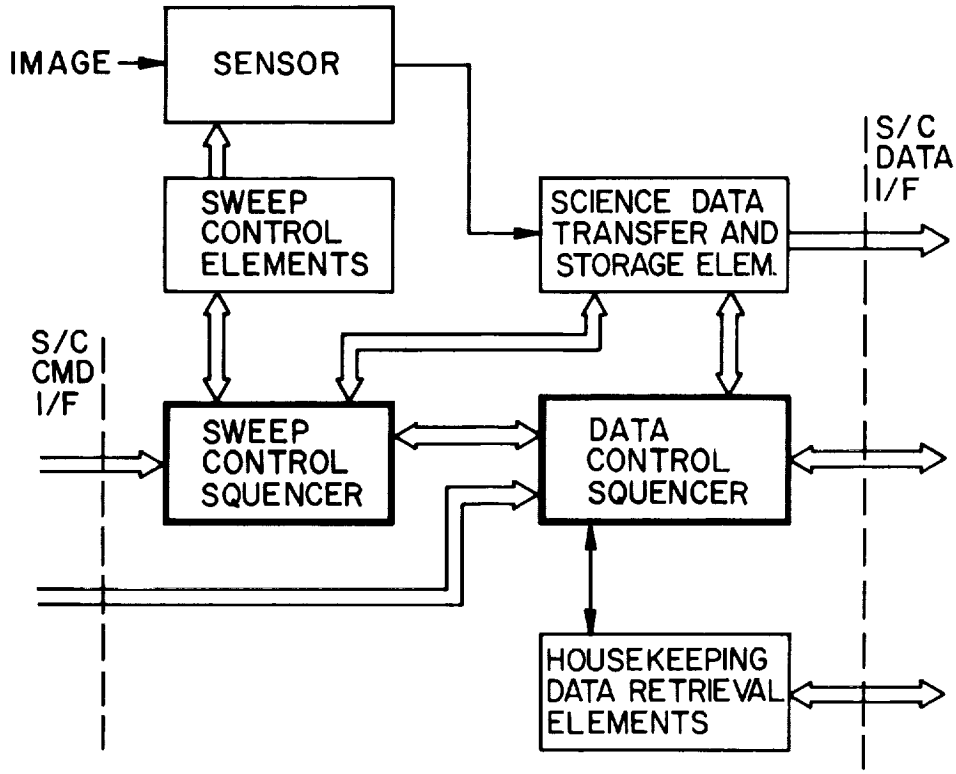
IMAGE
SENSOR
SWEEP CONTROL ELEMENTS
SCIENCE DATA TRANSFER AND STORAGE ELEM.
S/C DATA I/F
S/C CMD I/F
SWEEP CONTROL SQUENCER
DATA CONTROL SQUENCER
HOUSEKEEPING DATA RETRIEVAL ELEMENTS

Figure 2.

Figure 3

This simplified flowchart illustrates the four major control functions which are necessary to obtain the observations. The READ sequence involves interaction between the SCS and another controller called the data control sequencer (DCS), also located in the MEB.

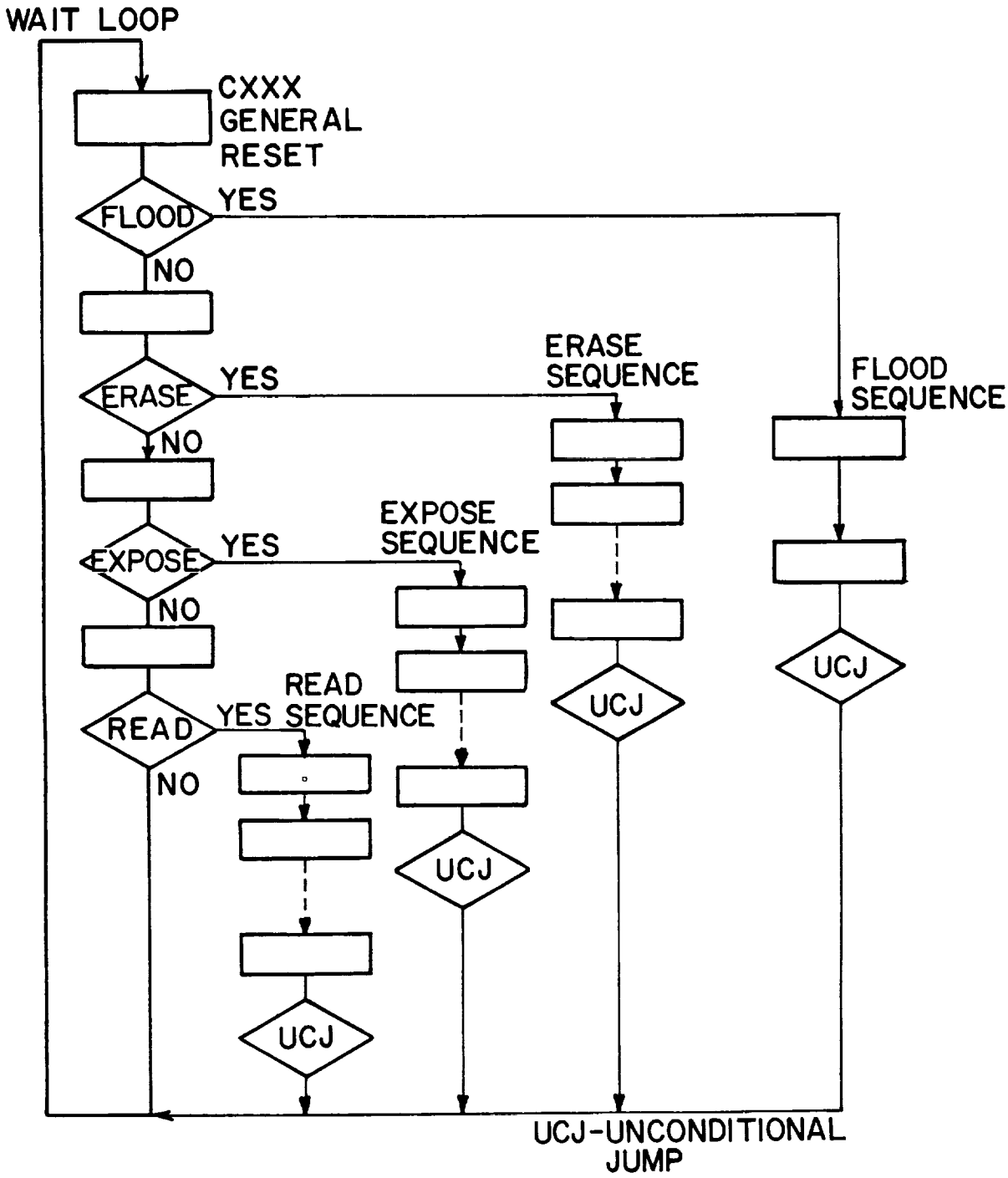
WAIT LOOP
CXXX
GENERAL
RESET
FLOOD
YES
NO
ERASE
YES
NO
EXPOSE
YES
NO
READ
YES
NO
ERASE
SEQUENCE
EXPOSE
SEQUENCE
READ
SEQUENCE
FLOOD
SEQUENCE
UCJ
UCJ
UCJ
UCJ
UCJ-UNCONDITIONAL
JUMP

Figure 3.

Figure 4

The failures discussed here involved a particular type of integrated circuit whose main features are shown here.

FAILED INTEGRATED CIRCUIT (IC)

MM54C161J/883B (4 STAGE BINARY COUNTER)

- o MFR. - NATIONAL SEMICONDUCTOR
- o PKG. - 16 PIN CERAMIC DUAL IN LINE (DIP)
- o FEATURES
  - PRESETTABLE
  - LOOK AHEAD CARRY
  - SYNCHRONOUS

Figure 5, 6, 7

Indicate the characteristics of the failures encountered in the first mission.

FIRST FAILURE (7/10/80)

- LOCATED IN SEGMENT COUNTER
  - 13 BITS (4 CASCADED MM54C161) FOR PURPOSE OF RECONSTRUCTING PICTURE FROM DIGITAL DATA
  - 2^9 BIT STUCK HIGH EXCEPT BETWEEN RESET AND FIRST COUNT
  - ONE WEEK LATER, 2^8 BIT (IN SAME IC) SHOWED SAME FAULT
- SOLUTION - GROUND SOFTWARE WORKAROUND, POSSIBLE BECAUSE OF "FORTUNATE" NATURE OF FAILURE
  - STAGES FAILED WITH OUTPUTS HIGH, SO CARRY COULD BYPASS STUCK STAGES
  - LOOK AHEAD CARRY ALLOWED COUNTING TO CONTINUE IN A PREDICTABLE WAY, EVEN THOUGH COUNTING SEQUENCE APPEARED TO BE SCRAMBLED
- IDENTIFICATION - CLEAR CUT, BECAUSE EVERY COUNT NUMBER IS IN VIDEO DATA STREAM

SECOND FAILURE (FROM 8/6/80)

- o SYMPTOM - INTERMITTENT FAILURE TO COMPLETE THE READ CYCLE ON THE VIDICON CAMERA TUBE
- o LOCATION - UNABLE TO LOCATE SPECIFIC CAUSE IN COMPLEX INTERACTION BETWEEN SWEEP CONTROL SEQUENCER AND DATA CONTROL SEQUENCER
- o SOLUTION - LEAVE MEB RESET ON FOR LONG PERIODS. A "MAGIC" SOLUTION WHICH IS NOT UNDERSTOOD.
  - KEPT INSTRUMENT OPERATING WITH ONLY OCCASIONAL LOSS OF DATA

THIRD FAILURE (EARLY SEPTEMBER)

- o SYNC SLIPS IN HOUSEKEEPING TELEMETRY
  - CAUSED INSTRUMENT SHUTDOWNS DUE TO SAFETY FEATURES IN ON-BOARD COMPUTER PROGRAM
- o CAUSE - SUSPECTED TELEMETRY ADDRESS IC (MM54C161) BUT THIS WAS NEVER PROVEN
- o SOLUTION - MODIFY ON-BOARD SOFTWARE TO PREVENT UNNECESSARY SHUTDOWNS

TERMINAL FAILURE (9/23/80)

- SYMPTOM - UNABLE TO COMPLETE ANY OPERATIONAL SEQUENCE ON VIDICON.
- CAUSE - EXTENSIVE ANALYSIS POINTED TO ADDRESS COUNTER IN SWEEP CONTROL SEQUENCER (3 CASCADED MM54C161 IC'S)
- SOLUTION - NONE - CEASE OPERATION AND AWAIT IN-ORBIT REPAIR

Figure 8

Astronauts replacing the failed MEB with a new one built for this repair mission.

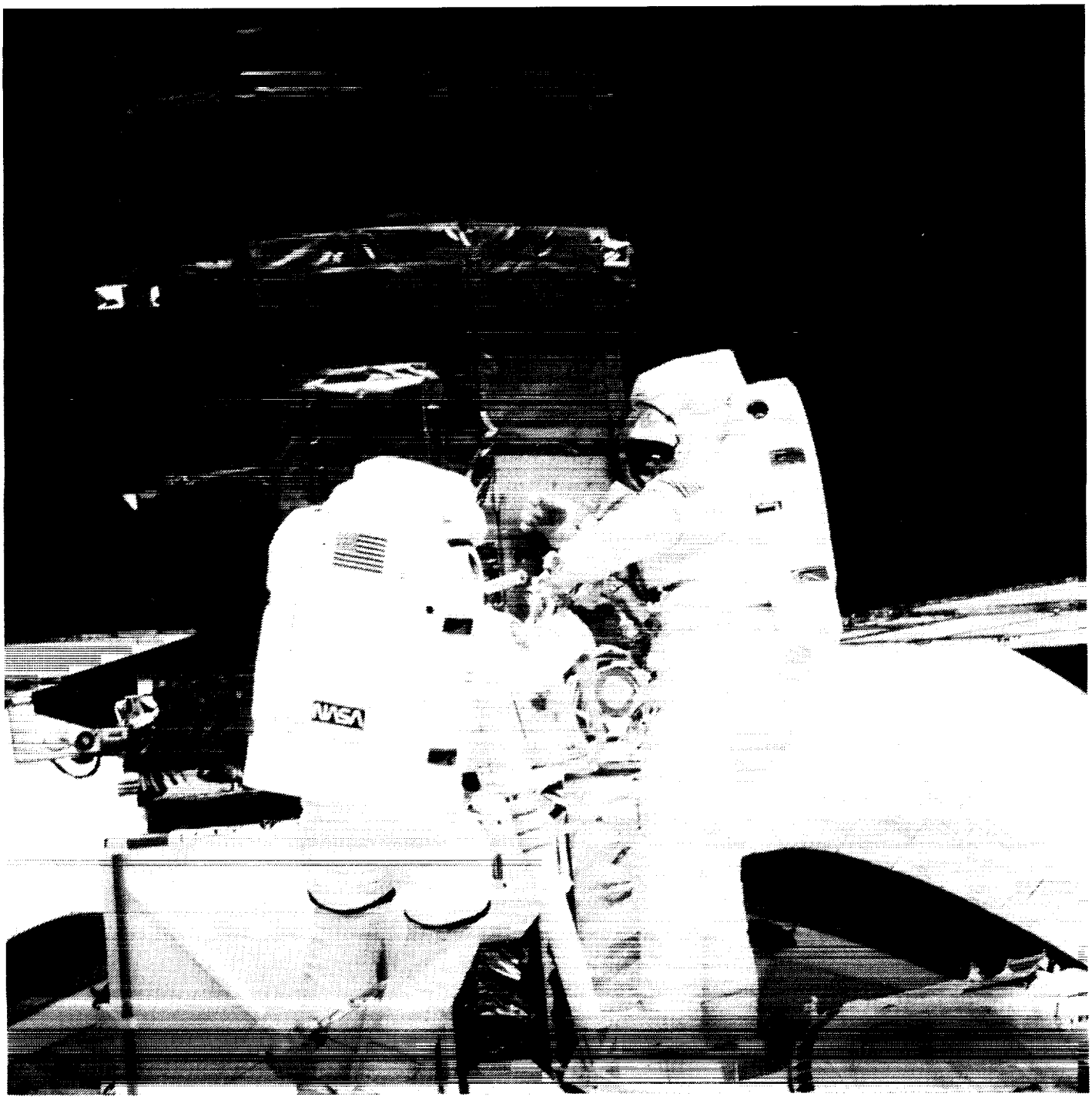

Figure 8.

Figure 9

The returned (failed) MEB after its removal from the shuttle.

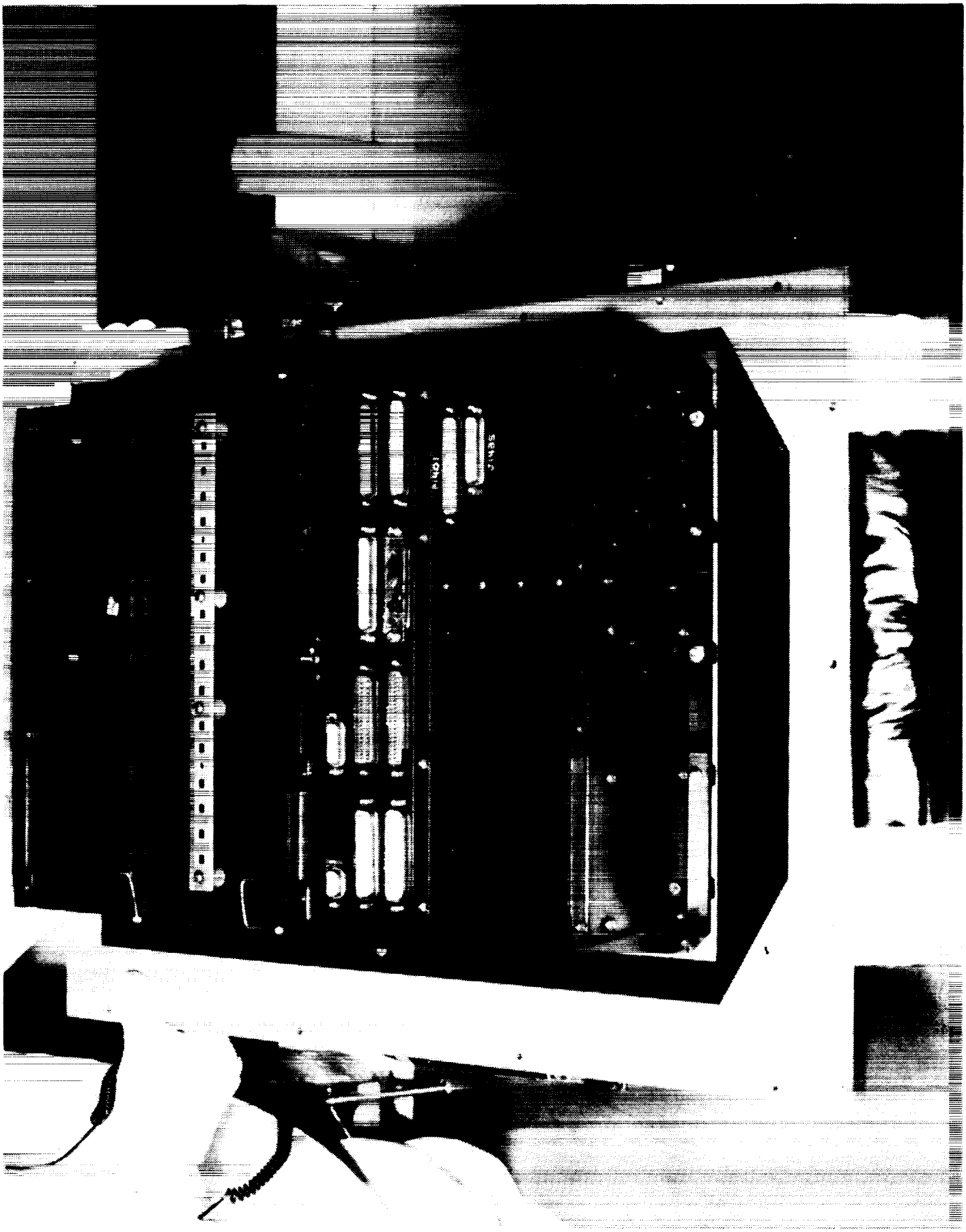

Figure 9.

Figure 10

Trouble-shooting the failed MEB in the electro-mechanical simulator (EMS). This is a high level bread board which was used to develop the original instrument, and to test the replacement MEB.

Figure 10.

Figure 11, 12

Stichweld wiring on standard boards is the component mounting method.

Figure 11.

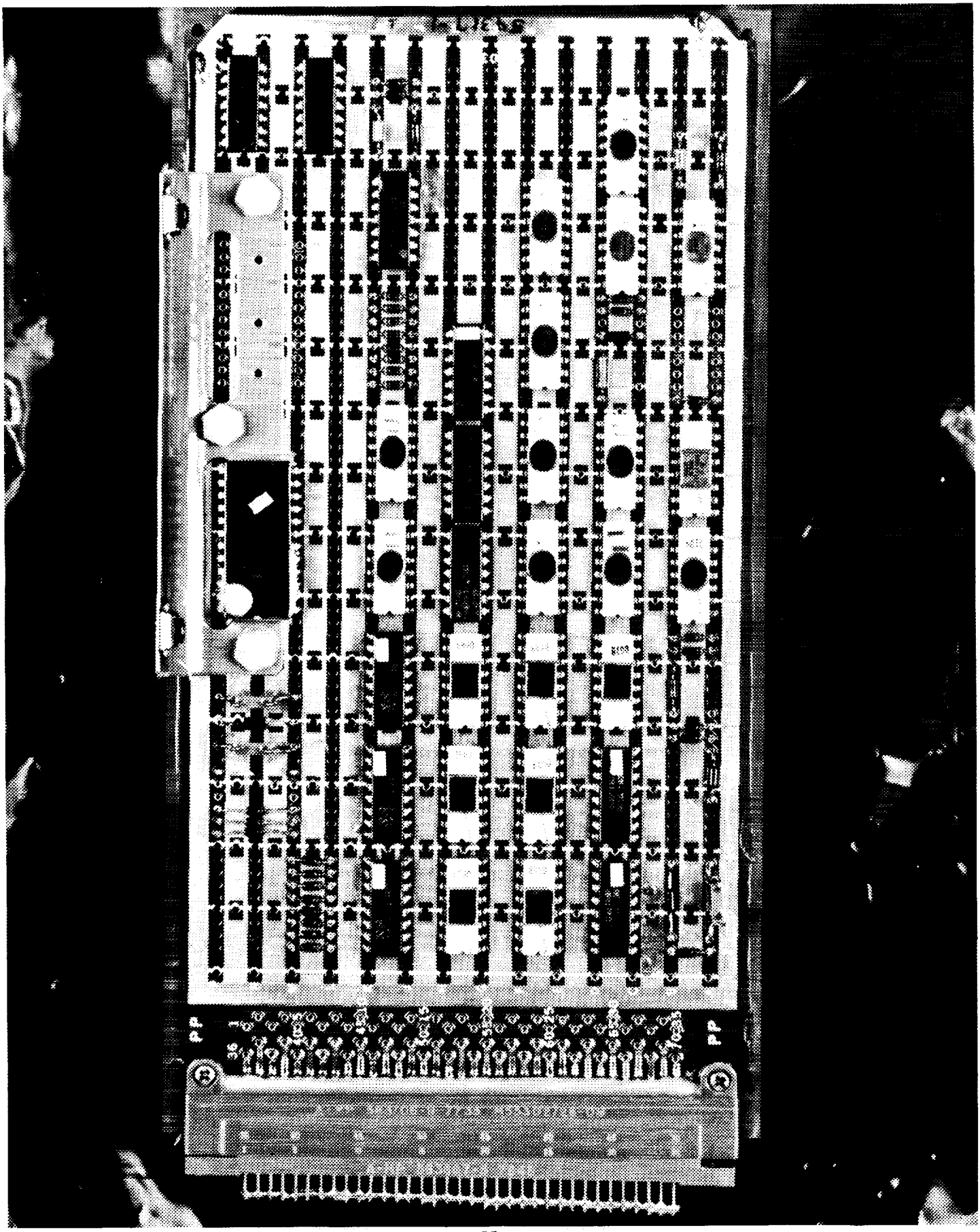

Figure 12.

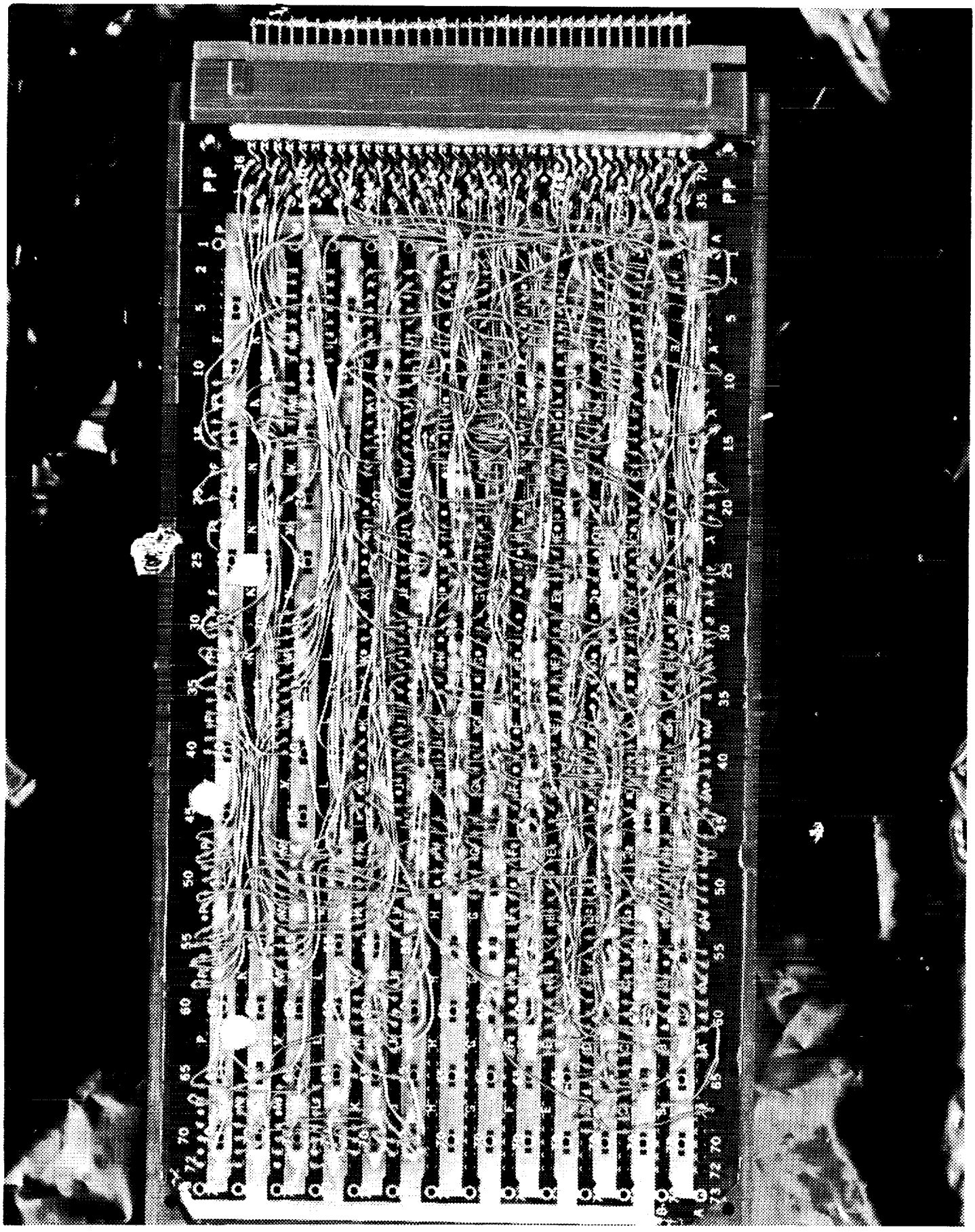

Figure 13, 14, 15

The failed MEB was restored by locating and replacing failed components one at a time. As each defective component was located, the board was turned over to Parts Analysis Branch for removal and replacement. They then analyzed the failed component while we located the next failure. The control system is highly interactive, so "live" trouble-shooting is the most effective method.

RESTORATION OF RETURNED MEB

- o ENGINEERING MODEL SIMULATOR CONNECTED THROUGH DATA INTERFACE (BCU) TO PDP 11/34 AT EOF
  - REALISTIC SIMULATION OF MEB INTERACTION WITH REAL INSTRUMENT
  - ALLOWS "LIVE" TROUBLE-SHOOTING WITH BOARDS ON EXTENDERS
  - USE COMPUTER PROGRAMS DEVELOPED TO TEST REPLACEMENT MEB
- o FAILED COMPONENTS LOCATED AND REPLACED, ONE AT A TIME
  - TERMINAL FAILURE REPAIRED FIRST
  - EXPECTED CAUSE OF FAILURE CONFIRMED (MM54C161 IN ADDRESS COUNTER OF SWEEP CONTROL SEQUENCER)
  - FAILED PART REMOVED AND NEW PART INSTALLED BY PARTS BRANCH

- READ CYCLE ON VIDICON WOULD NOT COMPLETE AT ALL

  (THIS WAS INTERMITTENT DURING FIRST MISSION)

  - FAILED MM54C161 IN ADDRESS COUNTER OF DATA CONTROL SEQUENCER
  - 2^4 BIT STUCK HIGH (SIMILAR TO SEGMENT COUNTER FAILURE)
  - PROBABLE CAUSE OF INTERMITTENT FAILURE TO COMPLETE READ CYCLE IN SEPTEMBER, 1980

- SEGMENT COUNTER FAILURE CONFIRMED AS DIAGNOSED
  - 2^8 AND 2^9 BITS STUCK HIGH
  - NO OTHER CHANGES

- SYNC SLIPS IN HOUSEKEEPING TELEMETRY
  - NOT ABLE TO DUPLICATE SLIPS IN GROUND TESTING
  - TENTATIVE DIAGNOSIS UNCONFIRMED

SUMMARY

- THREE MM54C161 IC'S (OUT OF 21 IN USE) FAILED IN ORBIT
  - FIRST FAILURE ABOUT 5 MONTHS AFTER LAUNCH
  - INTERMITTENT SECOND FAILURE BEGAN ABOUT ONE MONTH LATER
  - TERMINAL FAILURE 7 1/2 MONTHS AFTER LAUNCH
- ALL FAILURES DISCUSSED ABOVE WERE CORRECTED BY IN-ORBIT REPLACEMENT OF MEB
- ADDITIONAL PARTIAL FAILURE - "BEAM BLANKING PROBLEM"
  - NOT CORRECTED BY IN-ORBIT REPAIR
  - AFFECTS QUALITY (PHOTOMETRY) OF DATA AT ABOUT 10% LEVEL

Figure 16

An observation made with the repaired instrument. There still remains a beam-blanking problem on the vidicon which causes artifacts in the picture, e.g., the vertical bar in the center, and blackened dots of low sensitivity. These do not affect the quantity of data, but quality of the photometry is affected at about the 10 percent level. The repaired coronagraph is in continuous routine use, gathering useful information about the solar corona near the time of sunspot minimum.

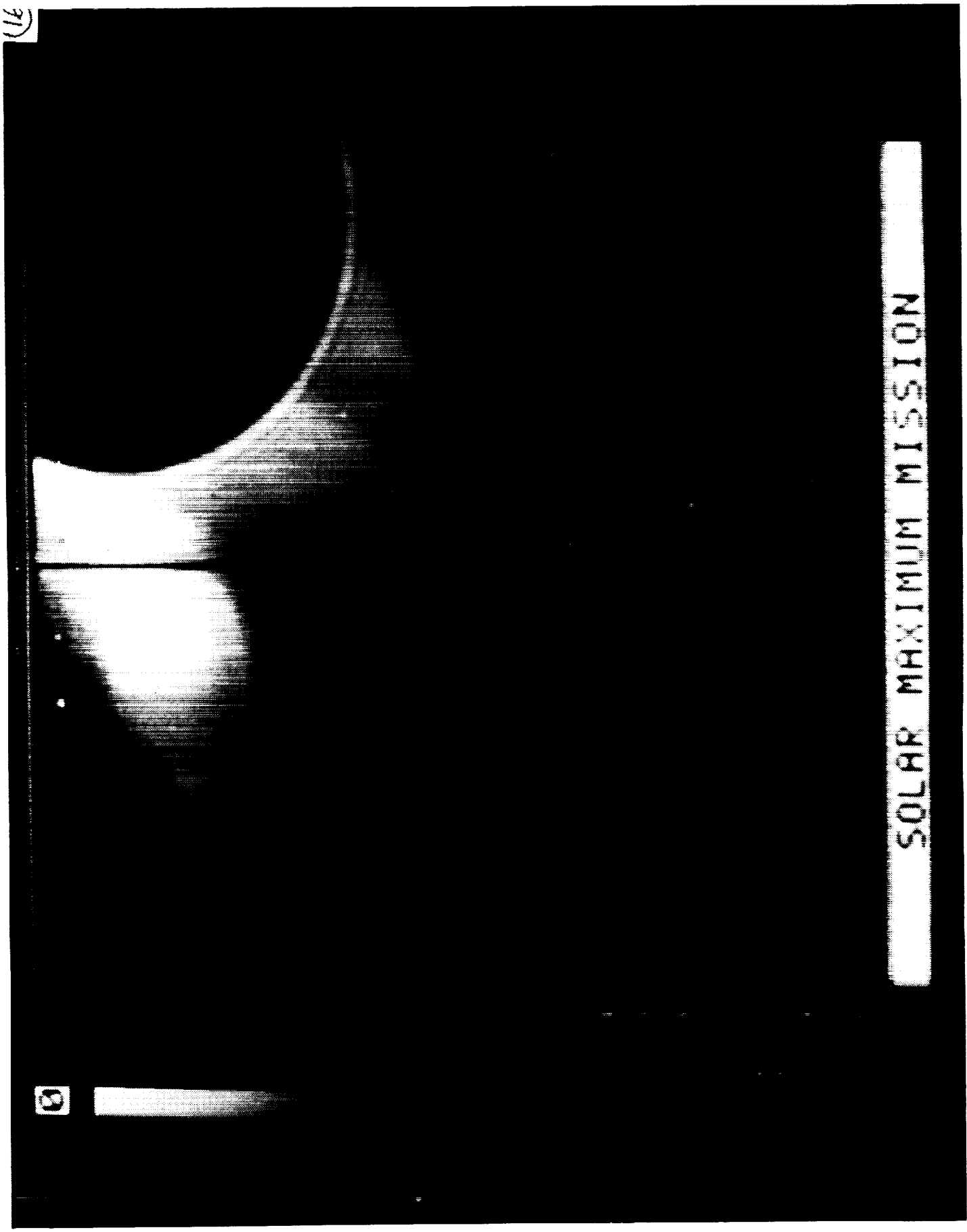

Figure 16.

GODDARD SPACE FLIGHT CENTER

FAILURE ANALYSIS REPORT

SERIAL NO. 51177
51178

MICROCIRCUIT; (1) CD4049AK, RCA, Date Code 7714, SN 37414 (1) CD4081BK, RCA, Date Code 7719, SN 33153		PROJECT: SMM SYSTEM: REQUESTER: J. Henegar
MALFUNCTION REPORT: Teledyne 10562	INCOMING INSPECTED: X YES ☐ NO ☐ UNKNOWN	INITIATED DATE: 11/16/84
PURCHASE SPECIFICATIONS: Unknown	SCREENING SPECIFICATIONS: Manufacturers	INVESTIGATOR: A. Marquez
		NASA APPROVAL: BP Baldini / 11-28-84

Two microcircuits were submitted to the GSFC Parts Analysis Laboratory for failure analysis. The parts were submitted on Teledyne Systems Inspection/Test Discrepancy Report Log No. 10562. The devices were still installed as U_2 (CD4049AK) and U_4 (CD4081BK) on assembly number 8023025 serial number 1002. The microcircuits had been tested and the leads were unsoldered from the circuit board by Teledyne. The parts were removed from the board by the failure analysis lab and the circuit board was returned to the requestor.

The microcircuit type CD4049AK functions as a COS/MOS hex inverting buffer. It is constructed using a single glassivated silicon die eutectically bonded within the cavity of a 16-pin ceramic/metal flat package.

Interconnections are accomplished using aluminum (1 mil) wire ultrasonically wedge bonded to the die metallization and the lead frame. The rectangular metal lid is attached with solder and the package is hermetically sealed.

The microcircuit type CD4081BK functions as a COS/MOS QUAD 2-INPUT AND GATE. It is constructed using a single glassivated silicon die eutectically bonded within the cavity of a 14-pin ceramic/metal flat package. Interconnections are accomplished using aluminum (1 mil) wire ultrasonically wedge bonded to the die metallization and the lead frame. The round metal lid is attached with solder and the package is hermeticaly sealed.

No irregularities were observed during external visual and radiographic examinations of the CD4049AK.

An external visual examination of the CD4081BK disclosed an indentation diagonally across the length of the metal lid. No irregularities were observed during a radiographic examination.

Pin-to-pin electrical testing of the CD4049AK indicated that pin 10 (output J) was open circuited to all other pins. No other anomalies were observed.

Functional testing of the CD4049AK showed that all of the outputs functioned normally except for pin 10. The output voltage at pin 10 was always +0.002 VDC.

Pin-to-pin electrical testing of the CD4081BK indicated that pin 7 (V_{SS}) was open circuited to all other pins. No other anomalies were observed.

Functional testing of the CD4081BK showed that all of the gates function normally if at least one input is low (+0.0 VDC).

Both devices passed Particle Impact Noise Detection and hermeticity (CD4049AK 3.8 X 10^{-8}, CD4081BK 4.0 x 10^{-8} fine and gross leak) testing.

An internal visual examination of the CD4049AK revealed fused open die metallization from pad 10 (output J). The area around the open is charred and no other damage was found. All of the interconnect wires are intact and pass a 0.5 gram bump. No other anomalies were observed.

Probe tests showed the damaged CD4049AK gate functioned normally when the open metallization was bridged.

An internal visual examination of the CD4081BK revealed fused open die metallization from pad 7 (V_{SS}). The area around the open metallization was charred and discolored. No other damage or anomalies were observed. All of the interconnect wires were intact and pass a 0.5 gram bump.

Electrical testing of the CD4081BK on the microprobe station showed that all of the gates function normally when V_{SS} (pin 7) is reconnected.

Additional electrical testing disclosed that the damage on the CD4049AK could be duplicated by applying approximately 8 VDC, positive or negative, to the output momentarily.

CONCLUSION

The failure of the two devices was confirmed. The CD4049AK failed due to a fused open die metallization track from pin 10. The fused open metallization was the result of an electrical overstress. A voltage more positive than V_{dd} or more negative than V_{SS} was applied at pin 10.

The CD4081BK failed due to a fused open die metallization track from pin 7 (V_{SS}). The fused open metallization was the result of an electrical overstress. The CD4081 is one of many commercial CMOS circuits which have been reported to exhibit latch-up. A voltage slightly more positive than V_{dd} or more negative than V_{SS} applied to an input pin is one method to initiate a latch-up condition which could overstress the V_{SS} line without additional damage to the part.

GODDARD SPACE FLIGHT CENTER

FAILURE ANALYSIS REPORT

SERIAL NO. 51179

Microcircuit; CD4017AK, RCA Date code 7425		PROJECT: SMM SYSTEM: HARDWARE REQUESTER: J. Henegar (311)
MALFUNCTION REPORT	INCOMING INSPECTED ☒YES ☐ NO ☐ UNKNOWN	INITIATED DATE: 12/10/84
PURCHASE SPECIFICATIONS: Unknown	SCREENING SPECIFICATIONS: Manufacturer's	INVESTIGATOR: A. Marquez NASA APPROVAL: G.F. Baldini 12/14/84

One RCA CD4017AK microcircuit was submitted to the GSFC Parts Analysis Laboratory for failure analysis. The device had failed while installed as U35 of the SMM/DRIRU system. The part had been intermittent with temperature and finally became a steady failure.

The RCA microcircuit type CD4017AK functions as a COS/MOS decade counter with 10 decoded outputs. It is constructed utilizing a single monolithic glassivated silicon die eutectically bonded within the cavity of a 16 pin ceramic/metal flat package. Interconnections are accomplished using aluminum (1 mil) wire ultrasonically wedge bonded to the die metallization and lead frame. The rectangular metal lid is attached with solder and the package is hermetically sealed.

No irregularities were observed during external visual and radiographic examinations.

Pin-to-pin electrical testing did not disclose any anomalies (no opens or shorts).

Functional electrical tests revealed that the device operated improperly. The counter would cycle thru three sequential counts and freeze until it was reset.

No anomalies were observed during particle impact noise detection and hermeticity (fine 3.2×10^{-8} and gross leak) testing.

An internal microscopic examination did not reveal any irregularities. All of the interconnect wires were intact and passed a 0.5 gram bump.

The glassivation was chemically removed and electrical testing indicated no change in the failure. The device was next examined in the SEM utilizing the voltage contrast analytical technique. (The counter is electrically exercised while being examined within the SEM chamber). The testing indicated that both outputs of the counters' third stage were not changing states. Testing showed that all of the correct control signals were applied to the stage.

The failed output was then examined on the microprobe station and it was determined that the output of the counters third stage was resistively short circuited to V_{SS}.

The part was examined on the SEM and an oxide defect was observed in the failed output stage. The defect was underneath the output metallization. The metallization was chemically removed revealing a defect extending into the die (V_{SS}).

CONCLUSION

The failure was confirmed. The decade counter was operating incorrectly. The failure was due to the counters third stage output being short circuited to ground. The short was thru an oxide defect underneath the output metallization. Time, temperature and a bias on the metallization eventually created a resistive path to V_{SS} causing the failure.

The defect was the result of a manufacturing irregularity during processing.

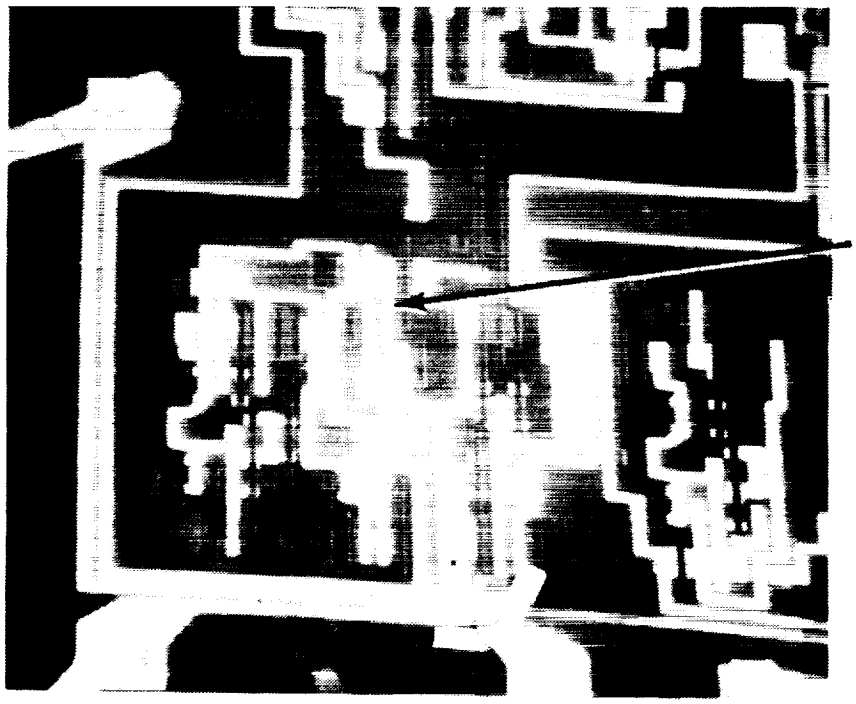

Figure 1. Photomicrograph of failed counter stage. (Light areas indicate zero volts. Dark indicates V_{DD}).

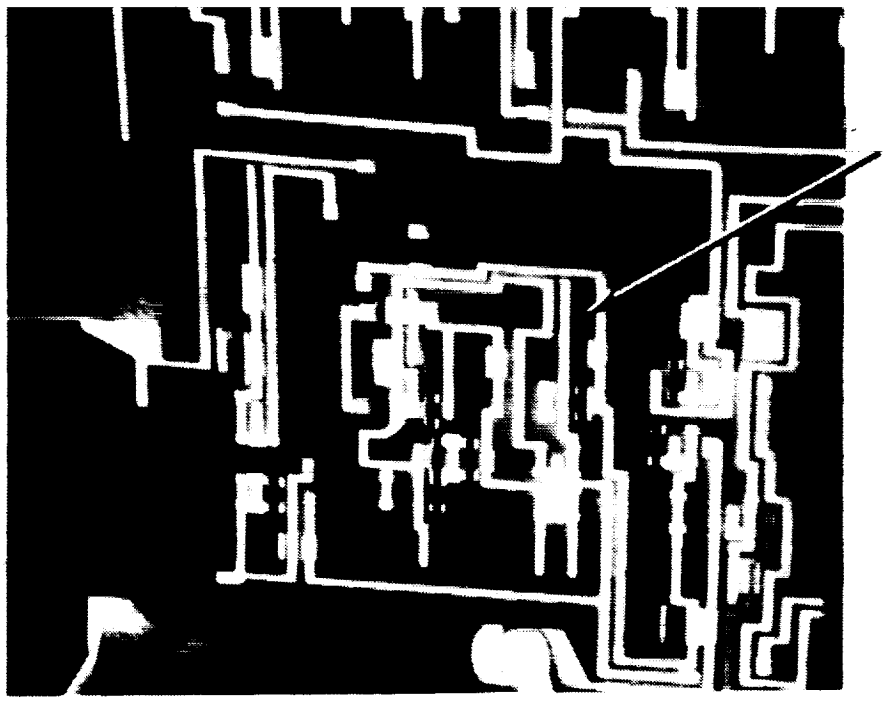

Figure 2. Photomicrograph of good counter stage.

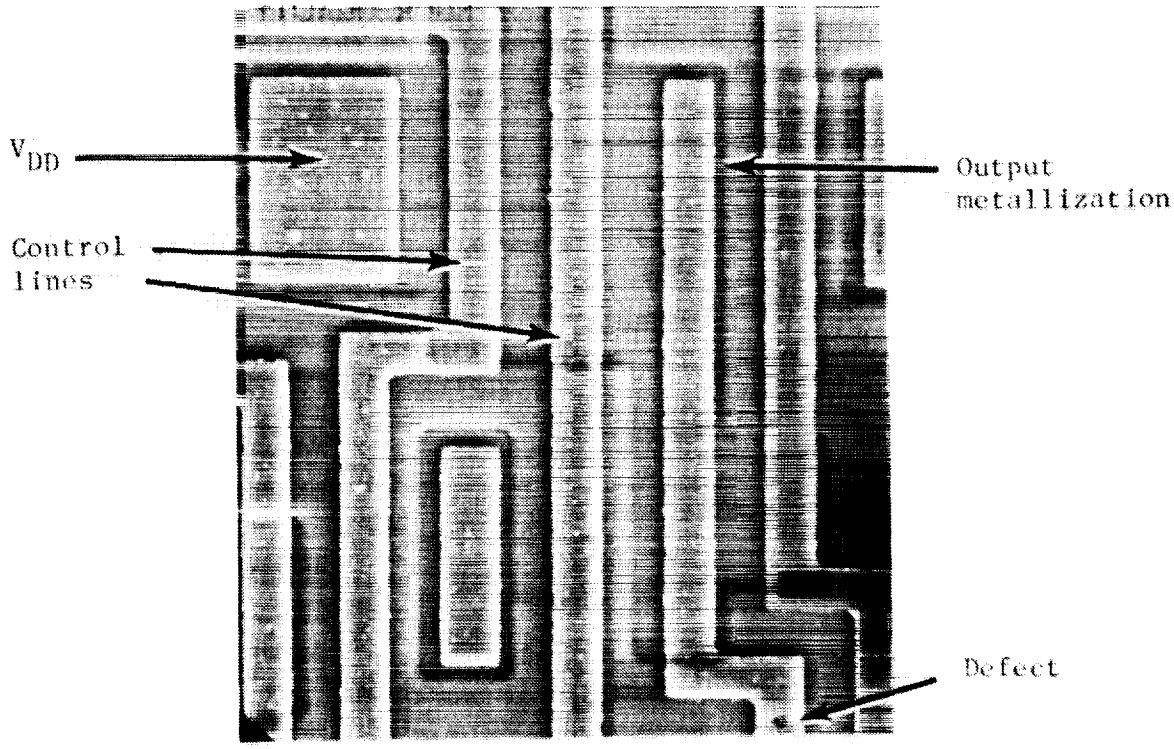

Figure 3. Photomicrograph of failed output stage. 800X

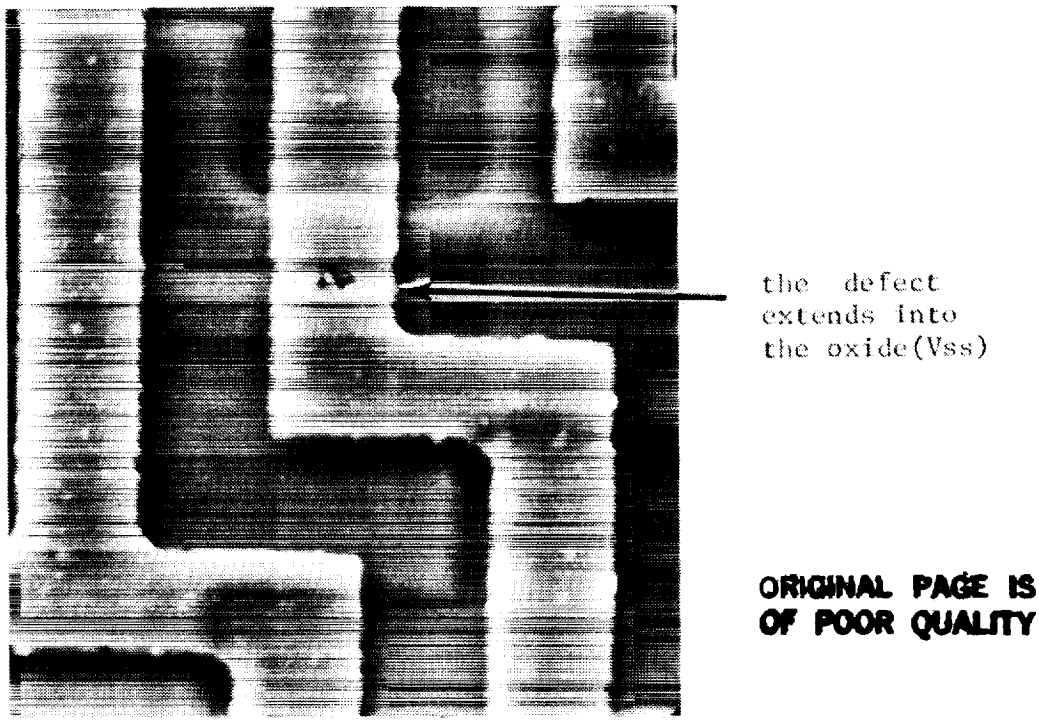

Figure 4. Photomicrograph of defect affecting output metallization. 2000X

51179

GODDARD SPACE FLIGHT CENTER

FAILURE ANALYSIS REPORT

SERIAL NO. 51230

MICROCIRCUIT (3); MM54C161J/883B, National Semiconductor, Date Code 7705, (SN 135,128,139)		PROJECT: SMM SYSTEM: Hardware REQUESTER: J. Henegar (311)
MALFUNCTION REPORT: -----	INCOMING INSPECTED: ☐ YES ☐ NO ☒ UNKNOWN	INITIATED DATE: 1/10/85
PURCHASE SPECIFICATIONS: Unknown	SCREENING SPECIFICATIONS: MIL-STD-883B	INVESTIGATOR: A. Marquez NASA APPROVAL: B F Baldwin 4/10/85

Three National Semiconductor microcircuits MM54C161J were submitted to the GSFC Parts Analysis Laboratory for failure analysis. The three parts failed while installed on circuit boards from the SMM C/P MEB. Device SN 128 was installed as U8 at location J11 (pin 1), the LSB output reportedly remained high all the time except during a $\overline{\text{CLEAR}}$. Device SN 135 was installed at location J2 (different board), all of the outputs were reportedly not switching. Device SN 139 was installed at location C46 (same board as SN 135), the first and second outputs were reportedly stuck high except with a $\overline{\text{CLEAR}}$ input signal.

The National MM54C161J devices are 4-bit, synchronous presettable up binary counters with asynchronous clear. They are constructed utilizing a single glassivated monolithic complementary MOS (CMOS) die eutectically mounted to a 16 pin dual in line lead frame. Interconnections are accomplished using aluminum (1 mil) wire ultrasonically wedge bonded to the die metallization and the lead frame. The ceramic lid and body are attached using glass frit.

An external visual examination of SN 139 showed that the ceramic lid and body had separated at the glass frit seal during removal from the board. Only a few of the leads were still attached to the body. An examination of SN 135 disclosed that pin 6 was broken flush with the package. No other anomalies were observed. An examination of SN 128 did not reveal any anomalies.

Radiographic examinations of SN 128, 135 and 139 did not disclose any additional irregularities.

Pin-to-pin electrical testing of SN 128 and SN 135 did not reveal any anomalies when the units were compared to a known good device.

Functional electrical testing of SN 128 indicated that the QA output remained high (logical 1) while the three other outputs continued counting. An appropriate input signal on the CLEAR line forced all of the outputs to a low (logical Ø). QA then returned to a high as soon as the CLEAR signal was removed.

Functional electrical testing of SN 135 disclosed that the outputs were not changing states (counting) as expected. A LOAD input signal would force the outputs, except for QA (always low), into a preselected condition but the device did not count at any time.

One device (SN 135) was unbiased baked at +150°C for 72 hours. No changes electrically were observed.

An internal visual examination of SN 139 revealed several accumulations of contamination on the die surface (see Figure 1). No other anomalies were observed. Only four interconnect wires were still connected to the die.

Pin-to-pin electrical testing of SN 139 on the probe station did not disclose any irregularities. A functional electrical test indicated that all of the outputs were always low, however, sufficient probes (12) were not available to functionally test the unit properly since some of the inputs had to be left unconnected (an undesirable condition with CMOS devices).

A SEM examination of SN 139 (with the glassivation chemically removed) disclosed several oxide defects but no evidence of an overstress condition. The contamination observed previously had been removed with the glassivation etch.

Particle impact noise detection testing of SN 128, 135 did not indicate a failure.

An internal visual examination of SN 135 revealed some surface contamination but no other anomalies. All of the bonds were well formed. All of the interconnect wires were intact. No evidence of an overstress was observed.

The glassivation was chemically removed from SN 135 and the unit was reexamined. The etch had removed the contamination and no other anomalies were observed.

Electrical testing indicated no changes in the failure mode. Testing utilizing the voltage contrast failure analysis technique on the SEM disclosed a malfunctioning transistor in the QA stage of the counter (see Figure 2). The transistor was isolated utilizing the microprobe station (see Figure 3) and testing showed a gate-to-source resistive (1K ohm) short circuit. Probe testing also indicated that the balance of the unit operated properly when the short circuit was isolated and the proper voltage level was applied at that point.

The metallization was chemically removed from SN 135. A SEM examination revealed a break in the gate oxide over the source diffussion (see Figure 4). Aluminum metallization had alloyed into the defective area. The unit was plasma etched to enhance any defects in the gate oxide (see Figure 5). An examination of the gate oxide of the failed transistor indicated the defective area extended into the source diffusion.

An internal visual examination of SN 128 disclosed some contamination but no other irregularities. All of the interconnections were intact and all of the bonds were well formed. No evidence of an overstress was observed.

The glassivation was chemically removed from SN 128. An optical examination disclosed that the etch had removed the contamination. No anomalies were observed.

Electrical tests indicated no change in the failure mode. The unit was unbias baked in a vacuum chamber at +150°C for 48 hours. No change in the failure mode was observed. The unit was examined in the SEM utilizing the voltage contrast failure analysis technique (see Figure 6). The failure was isolated to a malfunctioning transistor (see Figure 7). The transistor was isolated using the microprobe station and electrical tests indicated a resistive (750 ohms) short circuit from the gate to the source metallization (see Figure 8). Additional testing indicated that the balance of the circuit functioned properly with the correct logic applied.

The metallization was chemically removed from SN 128. A SEM examination disclosed a defect in the gate oxide (see Figure 9). Aluminum had alloyed into the defective area (see Figure 10). A plasma etch enhanced the defect and showed that it extended into the source diffusion (see Figure 11).

CONCLUSION

The failure of two of the three National MM54C161J microcircuits were confirmed. Electrical testing of SN 128 and SN 135 isolated the failures to short circuited transistors. Device SN 139 was damaged during removal from the P.C. board and therefore could not be electrically tested. The short circuits were caused when the aluminum metallization alloyed through defects in the gate oxide material. This condition formed a resistive connection to the source diffusion. No evidence of an electrical overstress was observed. The failures occurred at the weakest point in the oxide layer as a result of time, temperature and applied bias. Several oxide defects extending under the metallization were also observed in device SN 139.

A construction analysis (CA6027) of National Semiconductor MM54C161/883B microcircuits (date code 7705) dated 3/28/78 recommended that these devices not be used due to the presence of serious oxide defects in two of the four parts examined.

ADDITIONAL

A memorandum published by Wentworth O. Denoon dated 3/13/81 contained details of an investigation of 14 MM54C161J/883B CMOS counters. The parts were from the same lot suspected of failing in the X-ray Coronograph instrument on the MMS/SMM spacecraft.

"In summary, out of 14 devices tested, 3 units failed PIND tests and 6 units failed one or more of the burn-in tests. The fact that the burn-in failures recovered after an unbiased bake indicated that they contain internal ionic contamination (either on the surface of the die or in the glassivation). It is concluded that ionic contamination caused the high leakage currents observed in these devices after the burn-in, and is most probably the cause of the in-flight failures."

In a conversation with Mr. Denoon, he stated that during his testing only leakage currents were monitored and that no catastrophic failures were observed. One of the devices that had failed the burn-in was internally examined by Mr. Denoon. The examination disclosed a large amount of contamination (possibly in the glassivation). Since the devices were only marginal leakage current failures and no funds were available at the time, a failure analysis was not conducted on any of the devices.

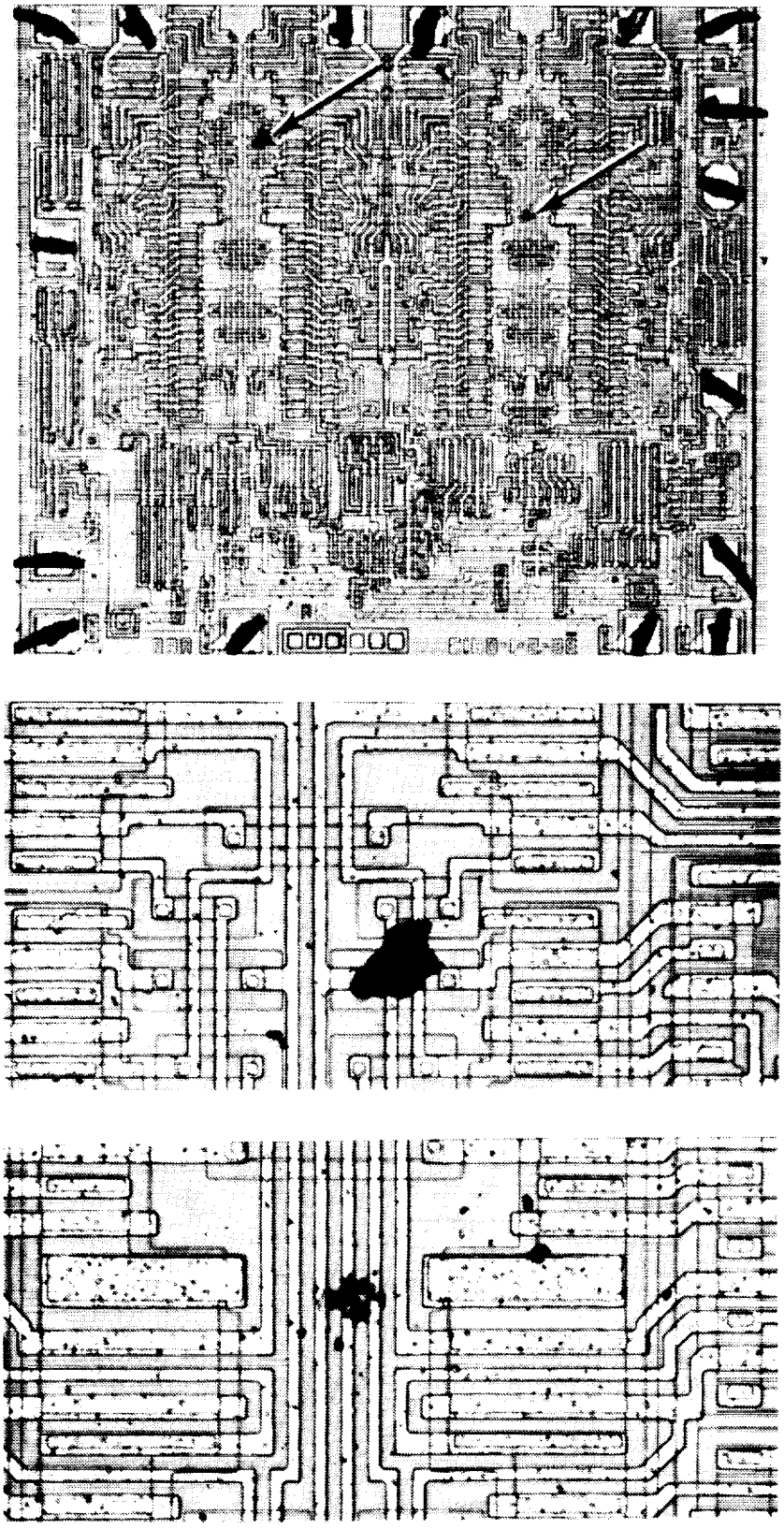

Fig. 1. Photomicrographs of die surface contamination (SN 139)

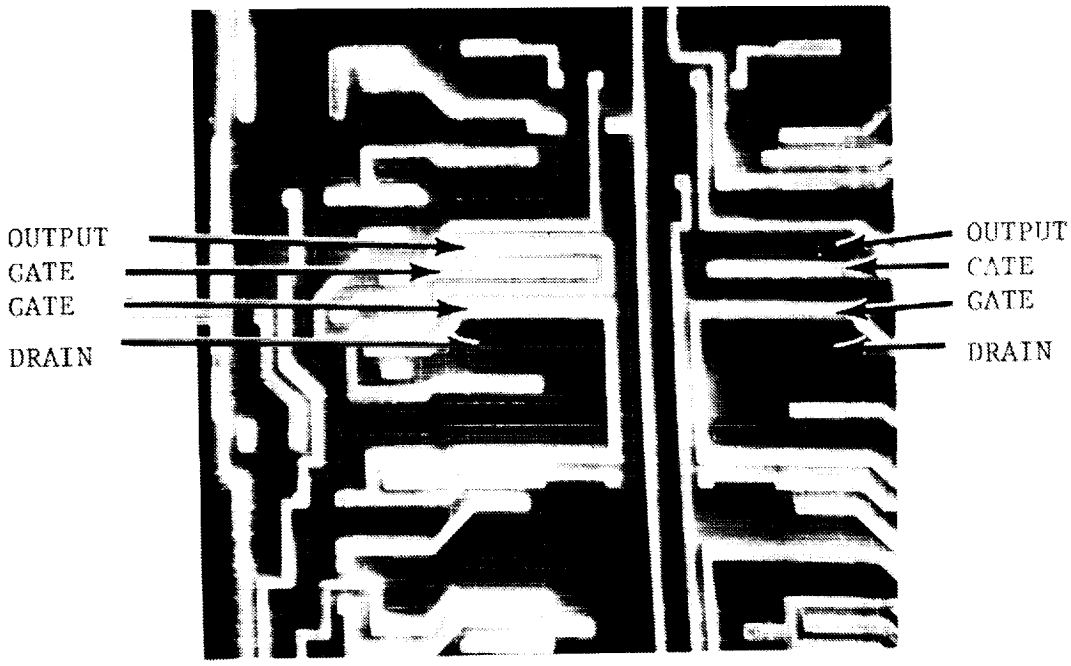

Fig. 2. SEM Micrograph of the failure utilizing Voltage Contrast. (SN 135) the A output stage (left) failed.

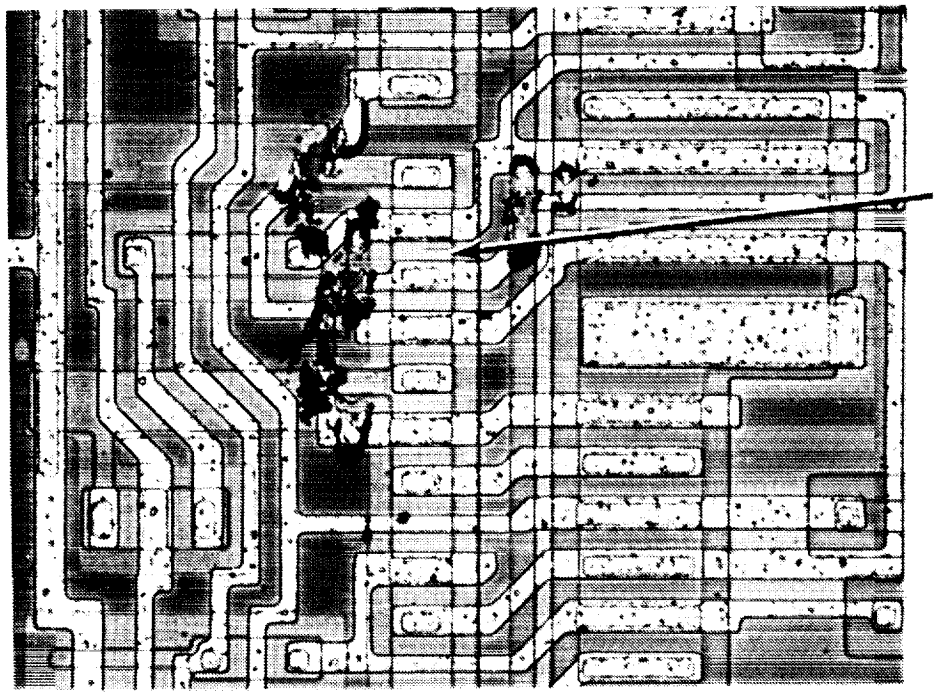

Fig. 3. Photomicrograph of the failure site isolated utilizing the microprobe station. (SN 135)

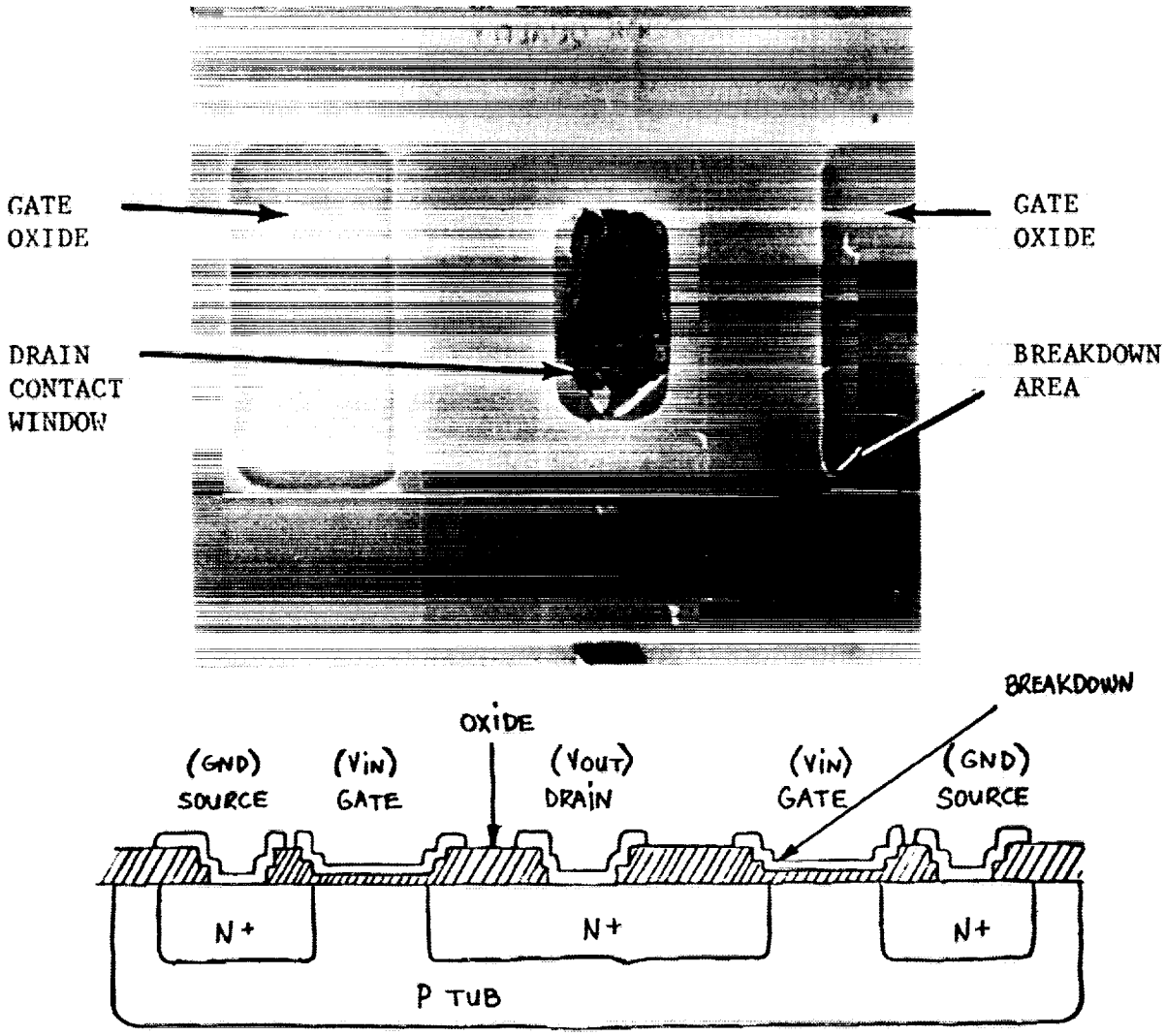

FIG 4. SEM Micrograph of the failed N-channel transistor.(SN 135)

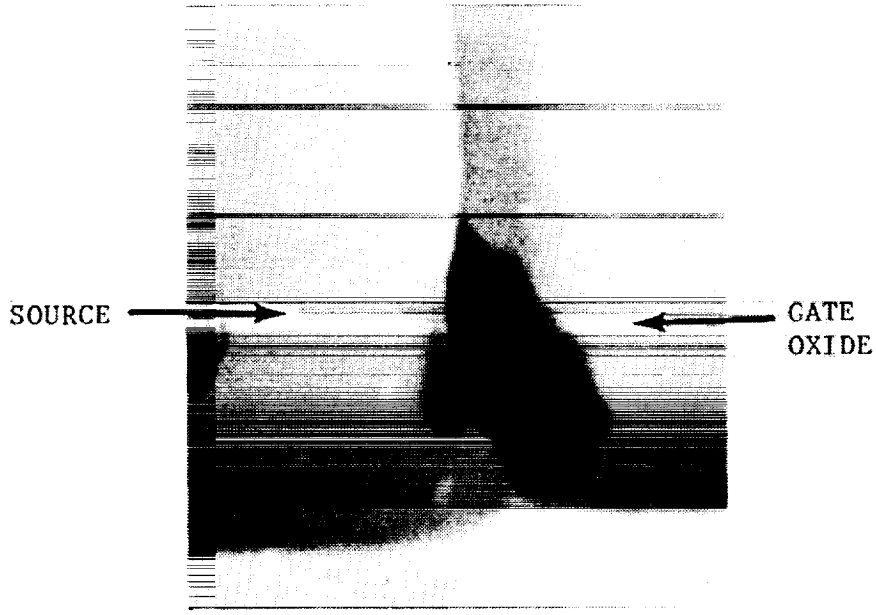

Fig. 5. Enlarged view of the breakdown area. (SN 135)

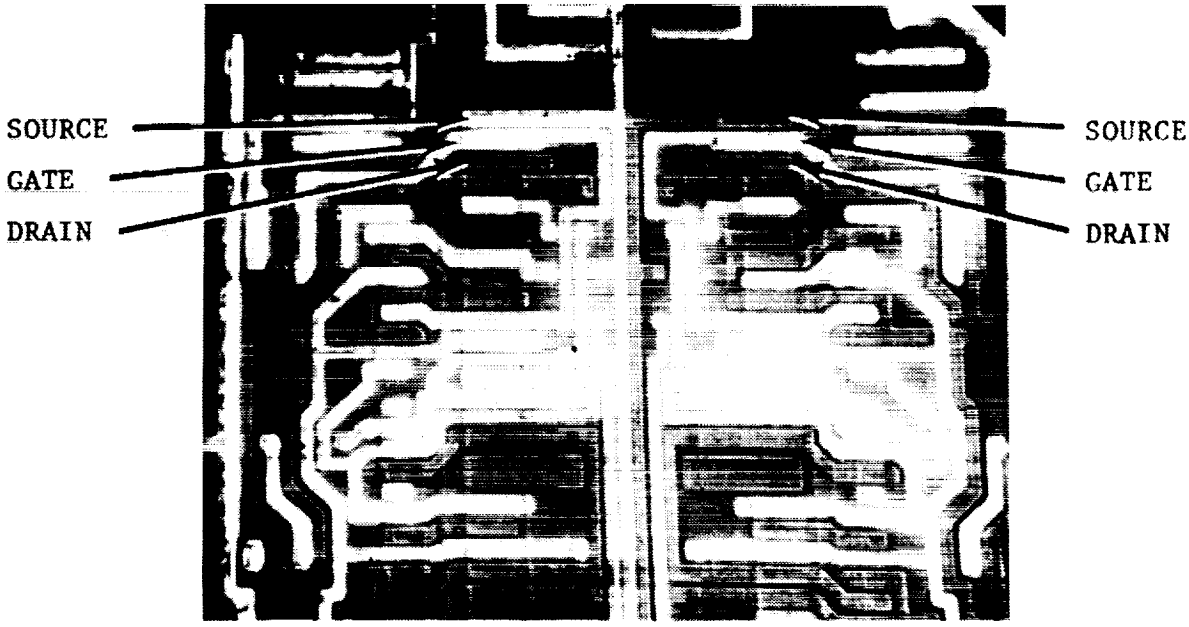

Fig. 6. SEM Micrograph of the failure utilizing Voltage Contrast. (SN 128) left is stage A (failed)

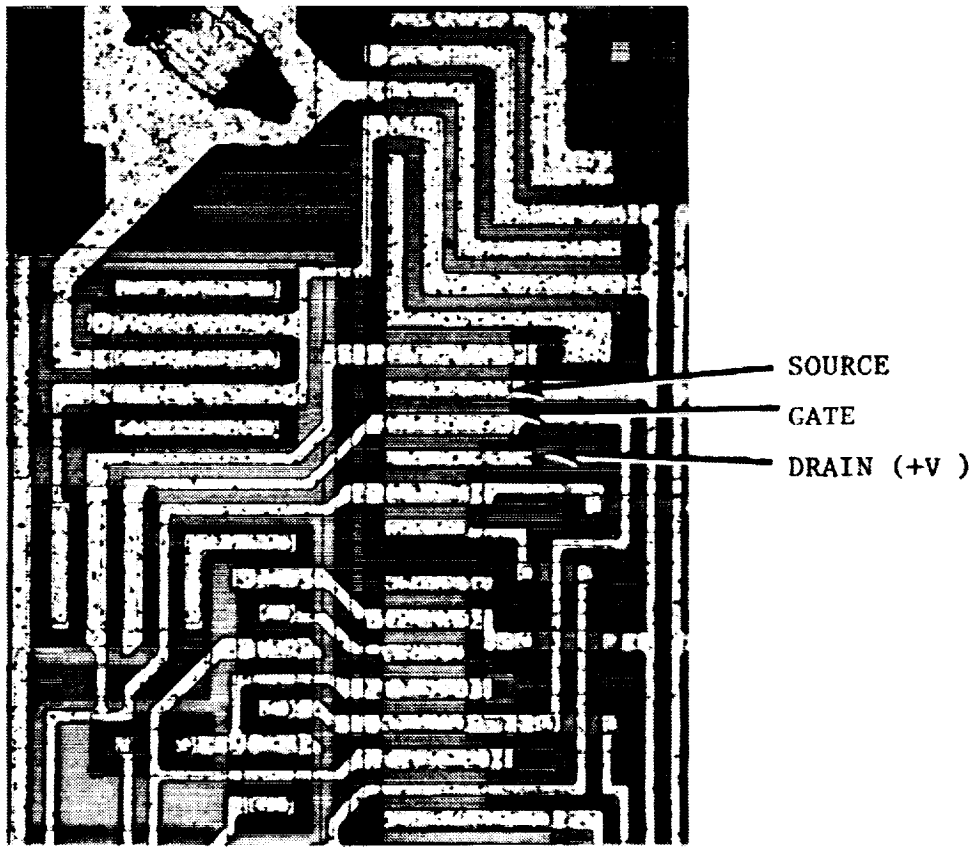

Fig. 7. Photomicrograph of the failed counter stage. (SN 128)

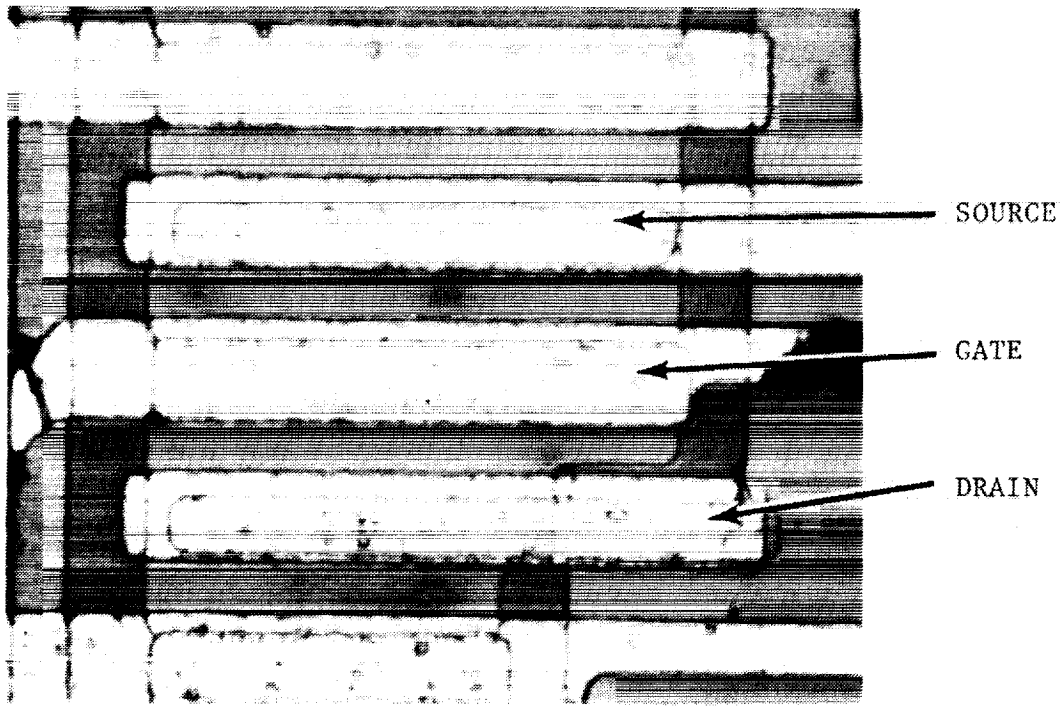

Fig. 8. Photomicrograph of the failed P-channel transistor. (SN 128)

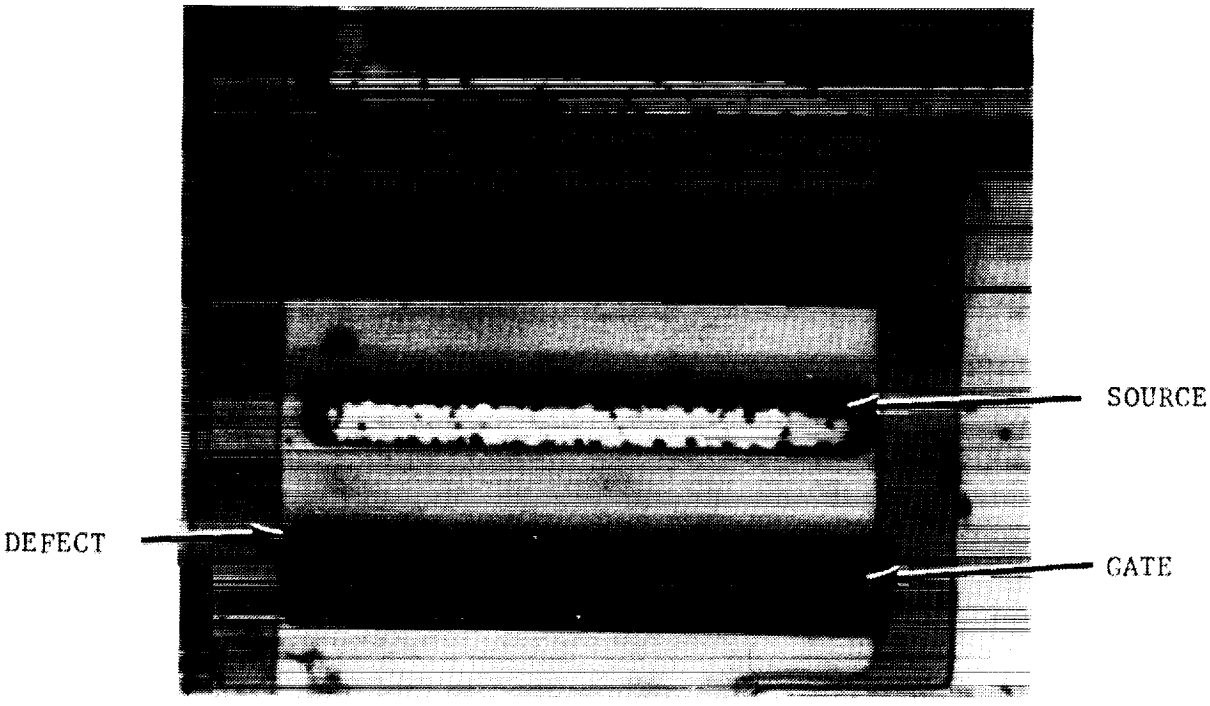

Fig. 9. SEM Micrograph of the failed area after an aluminum etch. (SN 128)

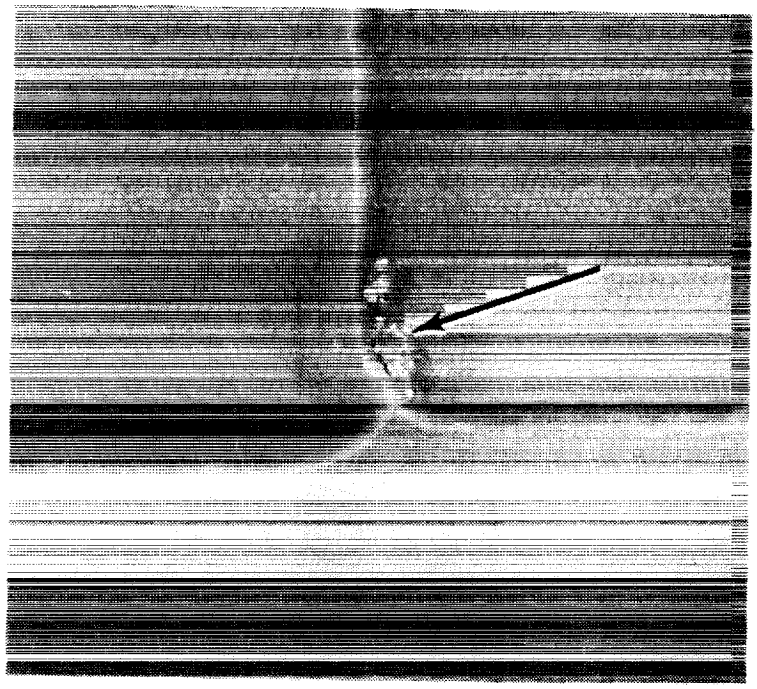

Fig. 10 SEM Micrograph of the defect in the gate oxide (SN 128)

Fig. 11. SEM Micrograph of the defect after a plasma etch was used to enhance the fault. (SN 128)

GODDARD SPACE FLIGHT CENTER

FAILURE ANALYSIS REPORT

SERIAL NO. 51490

"The information contained herein is presented for guidance of employees of the Goddard Space Flight Center. It may be altered, revised or rescinded due to subsequent developments or additional test results. These changes could be communicated internally by other Goddard publications. Notice is hereby given that this document is distributed outside of Goddard as a courtesy only to other Government agencies and contractors and is understood to be only advisory in nature. Neither the United States Government nor any person acting on behalf of the United States Government assumes any liability resulting from the use of the information contained herein."

MICROCIRCUIT (1); MM54C161J/883B, National, Date Code 7705, SN 154

PROJECT: SMM

SYSTEM: MEB

REQUESTER: R. Anstead (311)

MALFUNCTION REPORT	INCOMING INSPECTED	INITIATED DATE
---	☐ YES ☐ NO ☒ UNKNOWN	5/24/85
PURCHASE SPECIFICATIONS	**SCREENING SPECIFICATIONS**	**INVESTIGATOR**
MIL-883B	Manufacturer's	A. Marquez

NASA APPROVAL: B F Baldini 6/19/85

Nine National Semiconductor MM54C161J microcircuits were removed from the MEB for a special screen. All of the nine parts had been operating properly on the MEB. The MEB is a section of the electronics recovered from the Solar Max satellite during the Solar Max Repair Mission (three other MM54C161J parts from the same date code had failed in orbit, see FA51230). Two of the parts with the screen failed initial electrical tests (SN 147 t_{PHL1}, SN 128 I_{CC2}, both marginal failures). One device SN 154 failed catastrophically after an N-channel static burn-in at +125°C for 24 hours. One part (SN 154) was submitted to the GSFC Parts Analysis Laboratory for failure analysis.

The National MM54C161J microcircuit functions as a 4-bit, synchronous precettable up binary counter with a synchronous clear. It is constructed utilizing a single glassivated monolithic complementary MOS (CMOS) die eutectically mounted to a 16 pin dual in line lead frame. Interconnections are accomplished using 1 mil aluminum wire ultrasonically wedge bonded to the die metallization and the lead frame. The ceramic lid and body are attached using glass frit.

No anomalies were observed during external visual and radiographic examinations.

Pin-to pin electrical testing did not disclose any irregularities.

Functional electrical testing revealed that the device was not functional. The Q_B (pin 13) and Q_C (pin 12) outputs were always low. A bake without bias at +150°C for 24 hours did not change the failure mode.

An internal visual examination disclosed some contamination on the die. The contamination was either lodged in the glassivation or trapped between the glassivation and the die surface. Several oxide defects which extended underneath metallization stripes were observed in the vicinity of the Q_B and Q_C circuitry. No other anomalies were observed. All of the interconnect wires were intact and all of the bonds were well formed.

The glassivation was next chemically removed. This process also removed the contamination from the die surface. No changes in the failure mode were observed.

Voltage contrast examinations in the SEM revealed a malfunctioning transistor in the Q_B and Q_C circuitry. Microprobing isolated the failure to a resistive (2K ohms) short circuit between the gate metallization and source diffusion of an internal transistor in the Q_B circuitry.

The metallization was chemically removed and a SEM examination disclosed irregularities in the gate oxide material. The device was plasma etched to enhance the failure site. A SEM examination disclosed several defective areas in the gate oxide material. The etch also enhanced the oxide defects observed during the initial internal visual examination.

CONCLUSION

The failure of the National MM54C161 microcircuit was confirmed. The device failed functionally due to a resistive (2K ohms) short circuit between the gate and the source of an internal transistor. The short circuit was due to a defect in the gate oxide material. The defect allowed a resistive path to form from the gate metallization to the source diffusion under the gate oxide material. The failure was time, temperature and bias dependent (see also FA51230 for a similar failure).

The total burn-in time, if any, of these particular devices has been questioned. The results of the burn-in (3 of 9 parts failed) and the failure of the three parts in orbit indicate a lot related problem (National Semiconductor MM54C161J/883B date code 7705). A thorough burn-in is an accepted determinant of a part's reliability. A proper burn-in will weed out weak devices and can be an indication of possible latent failures.

(This page intentionally left blank)

THE JOHNS HOPKINS UNIVERSITY
APPLIED PHYSICS LABORATORY
LAUREL, MARYLAND

SOR-85052
June 11, 1985

RADIATION EFFECTS ON SELECTED ELECTRONICS PARTS FROM THE SOLAR MAX SATELLITE

R. H. Maurer

O. M. Uy

A summary of a presentation made to the Solar Maximum Repair Mission Degradation Study Results Workshop at Goddard Space Flight Center on May 9, 1985.

THE JOHNS HOPKINS UNIVERSITY
APPLIED PHYSICS LABORATORY
LAUREL, MARYLAND

SOR-85052

RADIATION EFFECTS ON SELECTED ELECTRONICS PARTS FROM THE SOLAR MAX SATELLITE

I. Introduction

The Solar Max Satellite was launched on February 14, 1980. Problems with the Main Electronics Box (MEB) were experienced in the period from July 10 to September 30, 1980. Failure in some electronic drive circuits occurred in the Oct-Nov 1980 time frame. After these failures which temporarily curtailed the spacecraft's mission, periodic attempts to restart the satellite were made (power was turned on) until complete replacement of the MEB was carried out on the Space Shuttle mission of April 1984.

The return of the failed original MEB to earth offered an opportunity to study some electronic parts which had spent 50 months in the natural radiation environment of a low earth orbit (LEO) spacecraft. Although this particular radiation environment was judged to be a benign one, the authors felt it would be worthwhile to examine the electrical performance characteristics of selected electronic parts to see if any unexpected radiation-related degradation had occurred.

The existence of some spare parts from the same lots as the original flight parts also presented the possibility of comparing the flight parts to shelf-life controls. The latter controls could also be irradiated in an accelerated laboratory radiation environment to compare dose rate effects at approximately the same total dose. The extent of the laboratory investigations on the spares was dependent on the results seen with the flight parts. If the flight parts showed significant radiation-related degradation, it would be interesting to see what high dose rate laboratory testing would have predicted. On the other hand, if the flight parts did not show significant degradation, then the question would be whether laboratory testing would have predicted the same "null" effect.

The parts shown in Table 1 were received in late March of 1985 so that this evaluation took place after the flight parts had a year to anneal at ambient room temperatures on the ground. The evaluation was actually carried out during April and early May 1985, primarily employing Goddard Space Flight Center electrical and radiation test facilities.

Table 1

Electronic Parts Tested at GSFC - April 1985

(29 Parts Total)

	Part Manufacturer & Type	Flight Parts	Build Residual	Rebuild Residual
1.	Fairchild μA 108A(LM 108) Op Amp	7748/039	7748/026	
2.	RCA CD4034A 8-Stage Static Register	7725/3	7725/8,15 7716/3	
3.	RCA CD4001A Quad 2-Input NOR Gate	7426/23,49	7426/245,246	
4.	RCA CD4011A Quad 2-Input NAND Gate	7625/215		8144/235,236
5.	RCA CD4015A Dual 4-Stage Shift Register	7534/27		8046/34,365
6.	Harris HI-1-506A-8 16-Channel Analog Multiplexer	7802/91		8208/91,92,94
7.	TI 54LSO2 Low Power Schottky NOR Gate	7738/		8205/25,25
8.	National MM78C29 CMOS Single Ended Line Driver	7710/21		8222/206,225
9.	National MM54C151 CMOS Digital Multiplexer	7723/122		8222/134,149
		10 Flight Parts	6 Residual	13 Rebuild Residual

II. Natural Radiation Environment

The returned flight parts from the MEB spent 50 months in low earth orbit at 28.5° inclination with the altitude decaying from 310 to 265 nautical miles as flight time increased. The first year of the mission (Feb 1980-Feb 1981) was spent at solar maximum conditions with the remaining time spent at post solar maximum with the solar activity declining. The parts were under power or bias for the first 8 months and about 10% of the time thereafter when restarts of the Solar Max Satellite were attempted. Thus, one concludes that the parts were powered for about 12 out of the 50 months in orbit.

Estimates of the total dose seen by the MEB electronic parts can be made by using several documents authored by E. G. Stassinopoulos and collaborators.[1-3] The earliest document (April 1976), entitled "The Trapped Particle Environment of SMM (Solar Maximum Mission)", presented only electron and proton integral energy spectra and not radiation dose versus depth data. In addition, it used older models for the trapped protons (AP5, AP6, AP7) and trapped electrons (AE4, AE6) than those considered most valid at present.

The second document (October 1978), entitled "The ST (Space Telescope) Environment: Expected Charged Particle Radiation Levels", used the definitive[4] AP8 model for the trapped protons and the interim AEI7 model for the trapped electrons. Figure 27 of this book gives the total dose versus aluminum shield depth for a 600 kilometer (∿325 nautical miles) circular orbit with a 28.8° inclination. The epoch of the calculation was 1984 - essentially solar minimum conditions. No specific shielding configurations (sphere or slab) were considered in this work. At a shield depth of 70-75 mils of aluminum, 250 Rads(Al)/year is the predicted total dose. Even if the shield depth is as small as 40 mils of aluminum, less than 300 Rads(Al)/year are predicted. These dose values should be conservative for the Solar Max Satellite since

a) the Solar Max Mission altitude was actually 490-515 km and dose decreases with altitude at this range, and

b) for the time of Solar Max Satellite exposure at or near solar maximum conditions, the trapped proton dose is reduced compared to the same component of dose at solar minimum conditions.

From this evaluation we estimate that the 50 month total dose seen by SMM was 1040 Rads(Al) or at worst, applying a factor of two for uncertainty in the natural radiation environment models - 2080 Rads(Al).

We have also referred to a third and most recent work of Stassinopoulos and Barth ("Transport and Shielding Analysis of the Non-Equatorial Terrestrial Low Altitude Charged Particle Radiation Environment - Volume I: Solar Minimum", January 1984). Here the trapped particle models used are the same as for the Space Telescope work, but low earth orbits in the inclination ranges between 30 and 90 degrees and in the altitude range of 200-1200 kilometers were considered. In addition, up-to-date shielding codes[5,6] were used for the transport evaluation employing two simple geometries: 1) dose at the transmission surface of finite slab shields and 2) dose at the center of a solid sphere. The former geometry is the appropriate one for the SMM Main Electronics Box since this box was located on the outside of the lower half of the satellite under some thermal blankets. We note that the center of solid sphere geometry includes radiation contributions from 4π steradian exposure. In contrast, a slab geometry considers irradiation from only one side (a 2π steradian exposure) with an omnidirectional incidence and a cosine theta distribution. The cosine distribution of the particles incident on the flat slab further reduces the dose contribution at any point immediately behind the slab. Total dose calculations on a flat slab have been shown by Seltzer[7] to be reduced by a factor of 4 for protons and a factor of 10 for electrons compared to the total dose at the center of a sphere for the same shield depths in the range of 50-75 mils Al of interest to us.

Figure 44 of Stassinopoulos and Barth's work for a finite aluminum slab shield at a 30° orbit inclination predicts 225 Rads(Al) per year at a 70 mil depth and 300 Rads(Al) per year at a 40 mil depth when the doses at the maximum (575 km) and minimum (490 km) Solar Max Satellite altitudes are averaged together. This result confirms our original estimate of 250 Rads(Al)/year which includes shield depths down to 40 mils aluminum when the uncertainty factor of 2 is applied to the 50 month accumulated dose.

III. Method of Evaluation and Results

Table 1 shows the nine part types submitted to an initial electrical test at GSFC in April 1985. Only one flight part of each type was available except in the case of the CD4001A NOR gate for which we had two. Residual parts from the same date code lot as the original flight parts (designated Build Residual in Table 1) were available for only the first three part types listed in Table 1. For the remaining six part types, residual parts were available only from later date code lots purchased for the repair mission (designated Rebuild

C-2

Residual in Table 1). In all, a total of 29 electronic parts were submitted to the first set of static, dynamic, and functional electrical tests.

The results of the electrical testing showed that all parts meet or exceed the manufacturer's specification for static, dynamic, and functional electrical performance with two qualifications:

a) one of the CD4001A flight parts and the CD4015A and 54LS02 flight parts had been damaged in being removed from the flight board and would not pass a simple electrical continuity check (this reduced the number of flight part types screened to seven);

b) all of the CD4034A parts, both flight and residual, passed the D.C. parametric tests, but marginally failed the dynamic tests with transfer times of ∿770 nanoseconds compared to specified values of 750 nanoseconds.

This latter discrepancy was not considered significant and did not differentiate between flight and residual parts.

At this point we could only conclude that the flight electronic parts showed no adverse effects due to radiation because they had not degraded during Solar Max Mission or they had degraded and subsequently annealed either in orbit or on the ground since April 1984.

To test the annealing hypothesis, five residual parts of three part types were irradiated to an accumulated total dose of 2150 Rads(Si) at a dose rate of 32 Rads/hour in the Goddard Space Flight Center Cobalt 60 cell on May 3-6, 1985. The parts chosen for this laboratory analysis were

1) the two CD4001A build residual parts representing the CD4000 series CMOS devices,

2) the μA108A build residual part, an op amp representing linear devices,

3) the two MM54C151 rebuild residual parts representing a more complex CMOS device from the same family of parts as the MM54C161 thought to be responsible for the SMM failure.

The low dose rate was chosen to minimize dose rate effects between the flight and laboratory environments. The "worst case" estimated total dose was accumulated. The parts had no bias voltage applied since the corresponding flight parts had spent the majority of their time in space in this condition.

A second set of electrical measurements was made on the five spare parts after completion of laboratory radiation exposure. All five parts passed all electrical tests with the CD4001A and MM54C151 CMOS devices exhibiting no observable degradation.

The μA108A Op Amp did degrade but remained well within specified limits.

Table 2

μA108A Radiation Test Results

Electrical Parameter	Residual Pre Irradiation	Residual Post Irradiation	Flight Part	Spec.
Offset Voltage (μV)	39	86	-314	±500 Max
Bias Current (pA)	809	1260	700	2000 Max
Open Loop Voltage Gain (V/mV)	505	362	239	80 Min

We observe that the flight part and the build residual part had degraded bias currents and open loop voltage gains which were within a factor of two of each other. The flight part bias current value probably does indicate that some annealing has taken place. The flight part offset voltage would seem to be significantly worse than that of the residual part tested in the laboratory.

IV. Conclusions

1) We deduce with the help of some laboratory testing that these seven (two part types had the flight part damaged, 54LS02 and CD4015A) Solar Max Mission part types suffered no serious degradation due to the low earth orbit radiation environment.

2) Complex linear devices such as the μA108A begin to degrade at low doses and dose rates and will be susceptible to "failure" at higher altitudes and/or longer lifetimes.

3) More detailed evaluation of electronic parts in orbit awaits the CRRES mission (~1986) and the Space Station when radiation detectors actually measure the environment experienced by electronic parts which are simultaneously being monitored for electrical performance.

Acknowledgement

The authors appreciate the cooperation of Bob Anstead, Julius Hirschfeld, Bob Lee, and Wes Ousley of the NASA Goddard Space Flight Center in helping us carry out our test plan. Mr. Lee is an employee of the High Altitude Observatory. Each of these four gentlemen gave us complete, prompt, and courteous cooperation.

References

1. E. G. Stassinopoulos, "Trapped Particle Environment of SMM (Solar Maximum Mission)", GSFC document X-601-76-97, April 1976.

2. E. G. Stassinopoulos, "The ST Environment: Expected Charged Particle Radiation Levels", GSFC document X-601-78-30, October 1978.

3. E. G. Stassinopoulos and J. M. Barth, "Transport and Shielding Analysis of the Non-Equatorial Terrestrial Low Altitude Charged Particle Radiation Environment", GSFC document X-601-84-6, January 1984.

4. R. H. Maurer, private communication with Dr. J. I. Vette, November 1983.

5. S. M. Seltzer, "SHIELDOSE: A Computer Code for Space Shielding Radiation Dose Calculations", U. S. Department of Commerce, National Bureau of Standards, NBS Technical Note 1116, May 1980.

6. T. Jordan, "NOVICE: A Radiation Transport/Shielding Code", Experimental and Mathematical Physics Consultants, Report No. EMP.L82.001, January 1982.

7. S. M. Seltzer, "Electron, Electron-Bremsstrahlung and Proton Depth-Dose Data for Space-Shielding Applications", IEEE Trans. Nucl. Sci. NS-26, 4896 (1979).

RADIATION EFFECTS ON SELECTED ELECTRONIC PARTS FROM SOLAR MAX SATELLITE

R. H. Maurer
O. M. Uy
5/9/85

SOLAR MAXIMUM MISSION

- LAUNCH DATE - FEBRUARY 14, 1980
- MAIN ELECTRONICS BOX CIRCUIT FAILURES EXPERIENCED FROM JULY 10 TO SEPTEMBER 30, 1980
- FAILURE IN ELECTRONIC DRIVE CIRCUITS DURING OCT-NOV 1980
- 50 MONTHS AT 310 TO 265 N.M. ALTITUDE AND 28.5° INCLINATION
- APPROXIMATELY ONE YEAR AT SOLAR MAXIMUM CONDITIONS; REMAINING TIME POST SOLAR MAXIMUM AS SOLAR ACTIVITY DECLINES
- PARTS WERE UNDER POWER OR BIAS FOR FIRST 8 MONTHS AND ABOUT 10% OF THE TIME THEREAFTER

∴ UNDER POWER	12 MONTHS
NO POWER	38 MONTHS

ESTIMATE OF TOTAL DOSE SEEN BY PARTS DURING MISSION

- USED E. G. STASSINOPOULIS STUDY - "THE SPACE TELESCOPE ENVIRONMENT: EXPECTED CHARGED PARTICLE RADIATION LEVELS", GSFC DOCUMENT X-601-78-30, OCTOBER 1978

- FIGURE 27 OF X-601-78-30 GIVES TOTAL DOSE VERSUS SHIELD THICKNESS DEPTH FOR A 600 KM CIRCULAR ORBIT AT 28.8 DEGREES INCLINATION

- AT SHIELD DEPTH OF 70-75 MILS AL (APPROXIMATELY MAIN ELECTRONICS BOX THICKNESS PLUS THERMAL BLANKETS AND HONEYCOMB), FIGURE 27 PREDICTS 250 RADS (AL)/YEAR CIRCA 1984 (SOLAR MIN CONDITIONS)

- SHOULD BE CONSERVATIVE SINCE SOLAR MAX ALTITUDE WAS 490-575 KM AND FOR TIME OF EXPOSURE NEAR SOLAR MAX TRAPPED PROTON DOSE IS REDUCED

- THUS, FOR 50 MONTHS ESTIMATE SOLAR MAX SATELLITE SAW 1040 RADS (AL) EXPOSURE OR AT WORST USING A FACTOR OF 2 UNCERTAINTY FOR RADIATION ENVIRONMENT MODELS - 2000 RADS (AL)

ELECTRONIC PARTS TESTED AT GSFC - APRIL 1985

(29 PARTS TOTAL)

	PART MANUFACTURER & TYPE	FLIGHT PARTS	BUILD RESIDUAL	REBUILD RESIDUAL
1.	FAIRCHILD μA 108A(LM 108) OP AMP	7748/039	7748/026	
2.	RCA CD4034A 8-STAGE STATIC REGISTER	7725/3	7725/8,15 7716/3	
3.	RCA CD4001A QUAD 2-INPUT NOR GATE	7426/23,49	7426/245,246	
4.	RCA CD4011A QUAD 2-INPUT NAND GATE	7625/215		8144/235,236
5.	RCA CD4015A DUAL 4-STAGE SHIFT REGISTER	7534/27		8046/34,365
6.	HARRIS HI-1-506A-8 16-CHANNEL ANALOG MULTIPLEXER	7802/91		8208/91,92,94
7.	TI 54LS02 LOW POWER SCHOTTKY NOR GATE	7738/		8205/25,25
8.	NATIONAL MM78C29 CMOS SINGLE ENDED LINE DRIVER	7710/21		8222/206,225
9.	NATIONAL MM54C151 CMOS DIGITAL MULTIPLEXER	7723/122		8222/134,149
		10 FLIGHT PARTS	6 RESIDUAL	13 REBUILD RESIDUAL

RESULTS

ALL PARTS PASSED ALL STATIC, DYNAMIC, AND FUNCTIONAL ELECTRICAL TESTS WITH FOLLOWING QUALIFICATIONS:

A) ONE OF THE CD4001A FLIGHT PARTS AND THE CD4015A AND 54LS02 FLIGHT PARTS HAD BEEN DAMAGED IN BEING REMOVED FROM THE FLIGHT BOARD AND WOULD NOT PASS A SIMPLE ELECTRICAL CONTINUITY CHECK.

B) ALL OF THE CD4034A PARTS, BOTH FLIGHT AND RESIDUAL, PASSED THE D.C. PARAMETRIC TESTS; BUT THEY MARGINALLY FAILED THE DYNAMIC TESTS WITH TRANSFER TIMES OF ~770 NANOSECONDS COMPARED TO SPECIFIED VALUES OF 750 NANOSECONDS.

THUS, THESE ELECTRONIC PARTS SHOWED NO ADVERSE EFFECTS DUE TO RADIATION BECAUSE THEY

- HAD NOT DEGRADED

OR

- HAD DEGRADED AND ANNEALED ON THE GROUND SINCE APRIL 1984.

RADIATION EXPOSURE AT GSFC OF RESIDUAL PARTS
(MAY 3-6, 1985)

TO TEST THE ANNEALING HYPOTHESIS, FIVE RESIDUAL PARTS WERE EXPOSED TO 2150 RADS (Si) AT A DOSE RATE OF 32 RADS/HOUR IN THE GSFC COBALT 60 CELL.

- PARTS WERE THE TWO CD4001A BUILD RESIDUAL PARTS
  THE μA108A BUILD RESIDUAL PART
  THE TWO MM54C151 REBUILD RESIDUAL PARTS

- A LOW DOSE RATE WAS USED TO MINIMIZE DOSE RATE EFFECTS BETWEEN THE FLIGHT AND LABORATORY ENVIRONMENTS

- THE "WORST CASE" ESTIMATED TOTAL DOSE WAS ACCUMULATED

- PARTS HAD NO BIAS VOLTAGE APPLIED SINCE THE MAJORITY OF TIME IN SPACE WAS SPENT IN THIS CONDITION

A SECOND SET OF ELECTRICAL MEASUREMENTS WAS MADE ON THE FIVE SPARE PARTS AFTER COMPLETION OF LABORATORY RADIATION EXPOSURE. ALL FIVE PARTS PASSED ALL ELECTRICAL TESTS.

- THE CD4001A AND MM54C151 CMOS DEVICES SHOWED NO OBSERVABLE DEGRADATION
- THE μA108A OP AMP DID DEGRADE BUT REMAINED WELL WITHIN SPECIFIED LIMITS

ELECTRICAL PARAMETER	RESIDUAL PRE-IRRADIATION	RESIDUAL POST-IRRADIATION	FLIGHT PART	SPECIFICATION
OFFSET VOLTAGE (μV)	39	86	-314	±500 MAX
BIAS CURRENT (pA)	809	1260	700	2000 MAX
OPEN LOOP VOLTAGE GAIN (V/mV)	505	362	239	80 MIN

CONCLUSIONS

1) WE DEDUCE WITH THE HELP OF SOME LABORATORY TESTING THAT THESE SEVEN (TWO PART TYPES HAD THE FLIGHT PART DAMAGED, 54LS02 & CD4015A) SOLAR MAX MISSION PART TYPES SUFFERED NO SERIOUS DEGRADATION DUE TO THE LOW EARTH ORBIT RADIATION ENVIRONMENT.

2) COMPLEX LINEAR DEVICES SUCH AS THE μA108A BEGIN TO DEGRADE AT LOW DOSES AND LOW DOSE RATES AND WILL BE SUSCEPTIBLE TO "FAILURE" AT HIGHER ALTITUDES AND/OR LONGER LIFETIMES.

3) MORE DETAILED EVALUATION OF ELECTRONIC PARTS IN ORBIT AWAITS THE CRRES MISSION (~1986) AND THE SPACE STATION WHEN RADIATION DETECTORS ACTUALLY MEASURE THE ENVIRONMENT EXPERIENCED BY ELECTRONIC PARTS WHICH ARE SIMULTANEOUSLY BEING MONITORED FOR ELECTRICAL PERFORMANCE.

(This page intentionally left blank)

FAIRCHILD SPACE COMPANY

OBJECTIVE

TO CHARACTERIZE PHYSICAL PROPERTIES OF MATERIALS, LISTED BELOW AFTER FOUR (4) YEARS IN LOW EARTH ORBIT

HARDWARE RETURNED	MATERIAL EVALUATED	PHYSICAL PROPERTY OF MATERIAL TESTED
MODULE RETENSION SYSTEM PRELOAD BOLT	Ti - 6 Al - 4V	YIELD STRENGTH UTS
MAIN ELECTRONICS MODULE HONEYCOMB PANEL	EPOXY FILM ADHESIVE	PEEL STRENGTH
THERMAL LOUVERS	POLYIMIDE BLADE ADHESIVE	LAP SHEAR STRENGTH

FAIRCHILD SPACE COMPANY

MRS PRELOAD BOLT: Ti - 6AL - 4V, SOLUTION TREATED AND AGED CONDITION

FINISH: TIODIZE, TIOLUBE

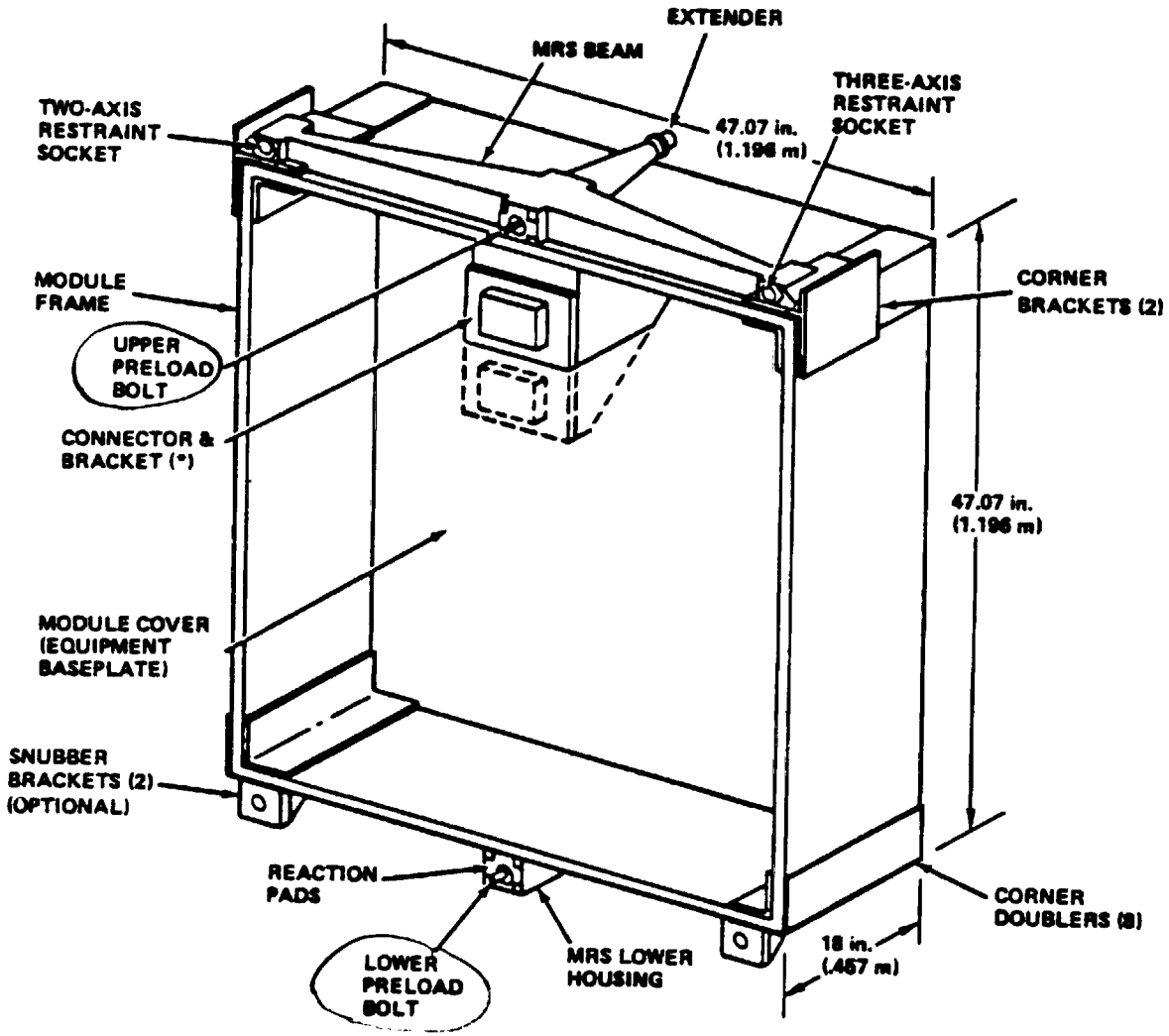

MMS MODULE STRUCTURAL ASSY

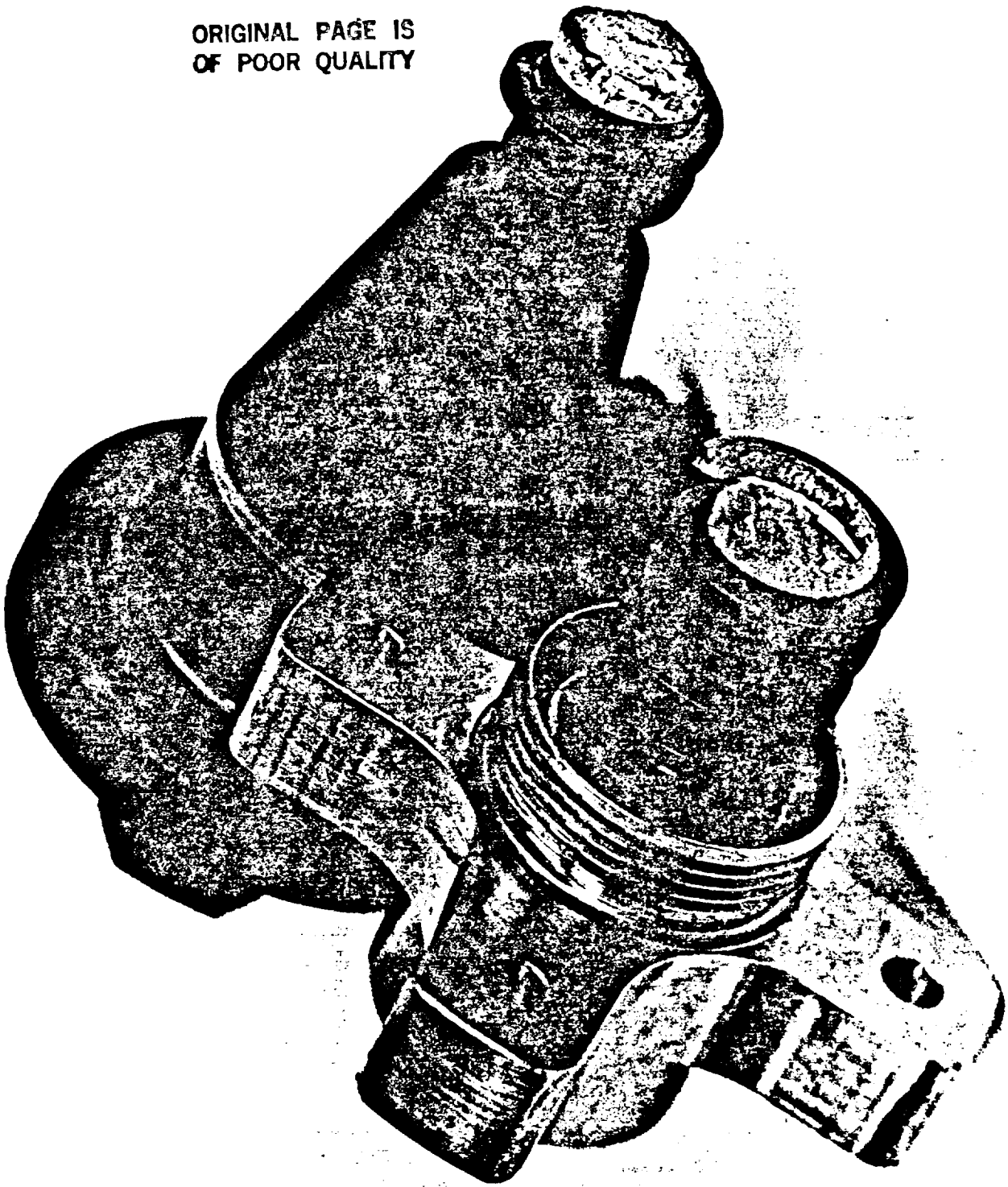

FAIRCHILD SPACE COMPANY

RESULTS OF PRELOAD BOLT EVALUATION

	TEST RESULTS					
	PROPORTIONAL LIMIT			ULTIMATE TENSILE		
	LOAD (LBS)	STRESS (KSI)	HANDBOOK STRESS (KSI)	LOAD (LBS)	STRESS KSI)	HANDBOOK STRESS (KSI)
SMM RETURNED BOLT #1	28,000	126.3	120	34,000	153.4	140
#2	29,000	130.8		35,250	157.8	
UNFLOWN MMS BOLT - CONTROL	28,000	126.3		*	*	

REMARKS: * MMS BOLT TESTED TO 32,500 LB TENSION LOAD. POST TEST INSPECTION REVEALED HAIRLINE CRACKS AT THREAD UNDERCUT DIAMETER.

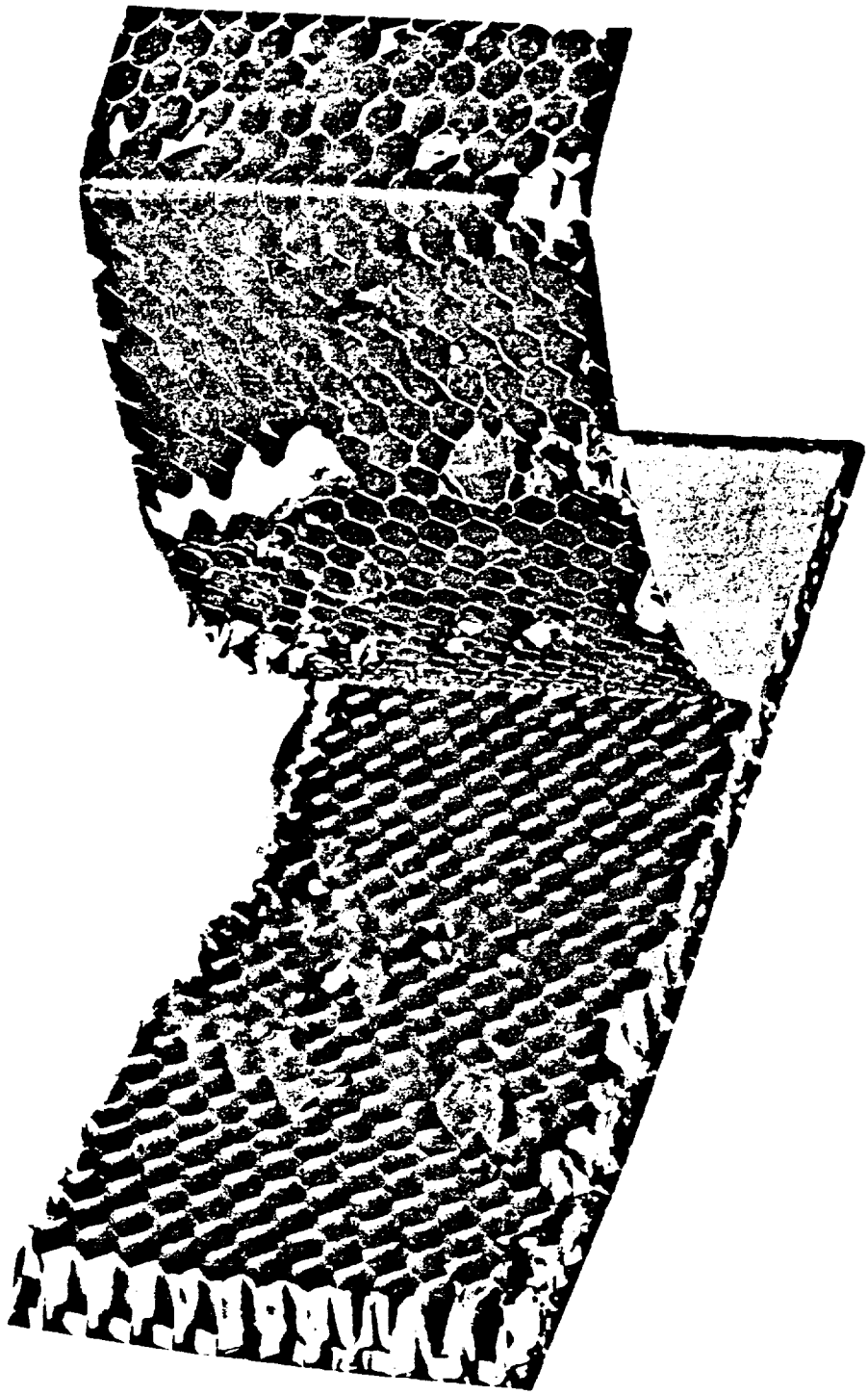

FAIRCHILD SPACE COMPANY

RESULTS OF MEM HONEYCOMB PANEL EVALUATION

	*PER DRAWING (MIL-A-25463A, TY T)	TEST SPECIMEN RESULT
INDIVIDUAL PEEL VALUE (MIN)	7. IN-LB/IN	7.2
AVERAGE PEEL VALUE (MIN)	8.5	---

CONCLUSION - NO DEGRADATION IN R.T. BOND STRENGTH OF ADHESIVE

FAIRCHILD SPACE COMPANY

SMM ACS LOUVER BLADE MATERIALS

BLADE HALVES	1100 - H18 AL
SHAFT	6061 T6 AL
ADHESIVE MATERIAL AND PROCESSING	AMERICAN CYANAMID BR34 POLYIMIDE

- o APPLIED 3-5 MIL EACH SURFACE
- o AIR DRIED 30 MINUTES
- o BAKED 30-40 MINUTES AT 220°F
- o BAKED 45 MINUTES AT 410°F
- o CLAMPED TO 45 PSI AND HEATED TO 550°F IN 30 MINUTES
- o HELD 90 MINUTES AT 550°F
- o COOLED, UNCLAMPED

LOUVER BLADE ADHESIVE

BR 34

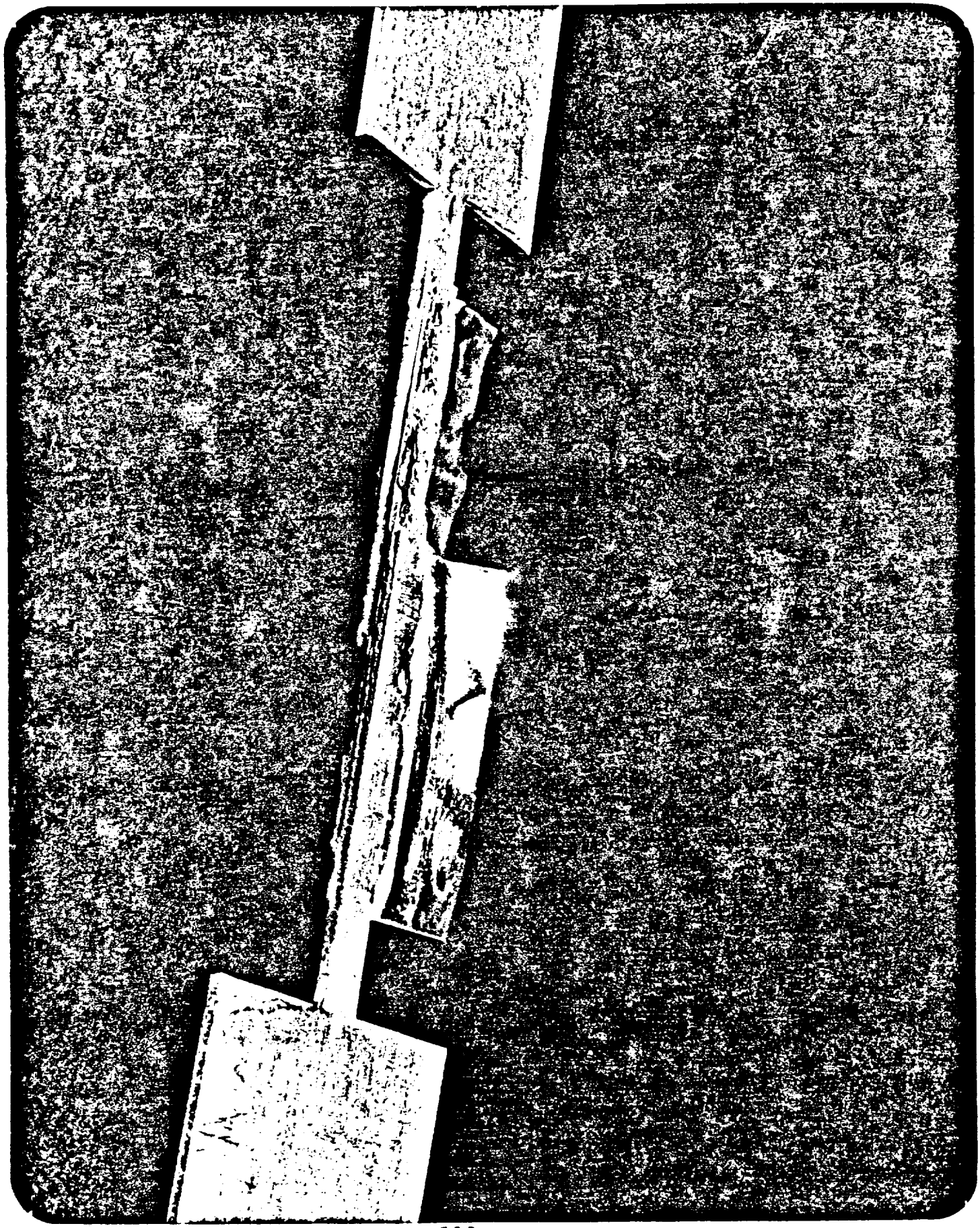

FAIRCHILD SPACE COMPANY

RESULTS OF LAP SHEAR TESTING OF LOUVER BLADE ADHESIVE

		SHEAR STRENGTH (PSI)			
CONTROL (UNFLOWN)	NO.	AVERAGE	MIN	MAX	NOMINAL
SPECIMENS	3	1420	1070	1655	1500
RETURNED (FLIGHT)					
SPECIMENS	4	525	365	750	

CHANGE IN PROPERTY (AVG): 63% REDUCTION

NOTES: o TEST SPECIMENS FABRICATED FROM BLADE EDGE MATERIAL. SPECIMENS WERE 0.375 X .125 INCH. STANDARD LAP SHEAR SPECIMENS ARE 0.5 X 1.0 INCH.

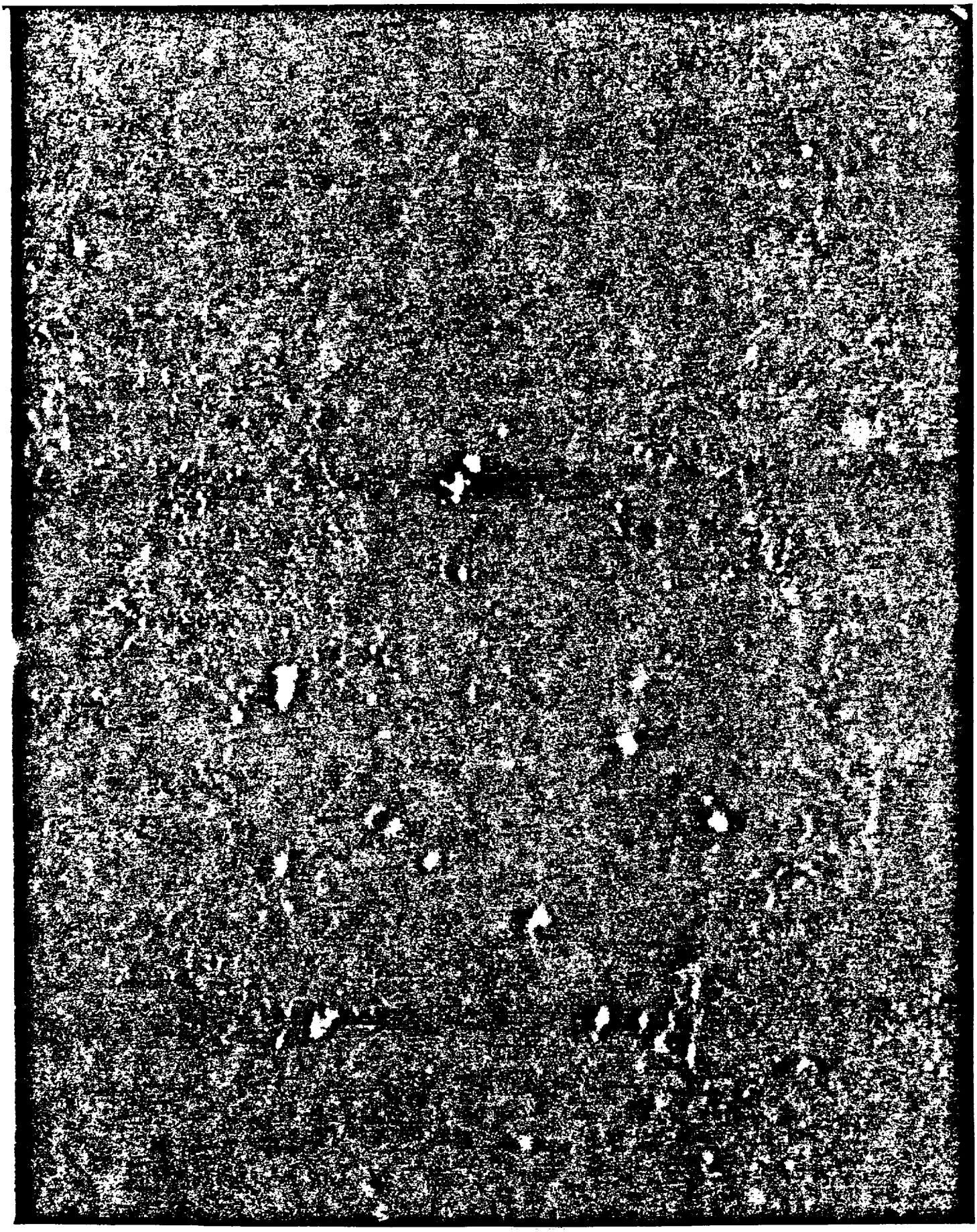

FAIRCHILD SPACE COMPANY

RED ARTIFACT PRESENCE

	FLIGHT BLADES	UNFLOWN BLADES
EDGE AREAS	BOTH SIDES OF TWO BLADES	NOT PRESENT ON ON ANY EDGE OR CENTER SHAFT OF TWO UNFLOWN BLADES
CENTER SHAFT AREAS	BOTH SIDES OF TWO BLADES	

FAIRCHILD SPACE COMPANY

BASIC CHEMISTRY OF BR34 CURING

STAGE	TEMPERATURE	PROCESS
"CURE"	350°F	o POLY-IMIDIZATION OCCURS BY CHAIN EXTENSION REACTIONS IN HIGH BOILING POINT SOLVENT SOLUTION o LOW MOLECULAR WT (H_2O), ALCOHOLS) DEVOLATILIZATION
"POST CURE"	550°F	o END OF POLYMERIZATION. PRECIPITATION OF POLYIMIDE CHAINS o DEVOLATILIZATION OF SOLVENT (NMP -

FAIRCHILD SPACE COMPANY

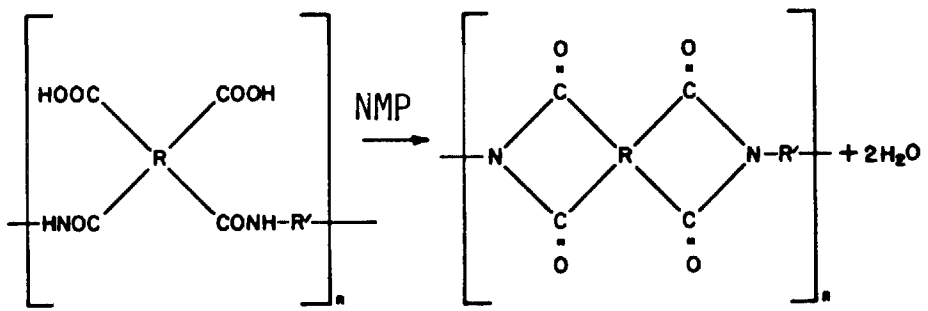

POLYAMIC ACID

POLYIMIDE

NMP = N-METHYL-2-PYRROLIDONE

THE POLYAMIC ACID IS CONVERTED TO POLYIMIDE IN THE PRESENCE OF SOLVENT, E.G., NMP.

TO OBTAIN TOUGH AND FLEXIBLE FILMS FROM THE PRODUCT AFTER MOST OF THE SOLVENT HAS EVAPORATED, IT IS NECESSARY TO COMPLETE CONVERSION TO POLYIMIDE BY HEATING TO 300 °C.

FAIRCHILD SPACE COMPANY

EVALUATION OF RED NODULES

HYPOTHESIS: RED NODULES REPRESENT REGIONS OF PURE POLYIMIDE RESIN CURED IN SPACE

- BR34 IS A MIXTURE OF POLYIMIDE RESIN, 40-60% ALUMINUM POWDER, TRACE OF As_2S_3, AND PROPRIETARY COMPOUNDS
- THE PURE POLYIMIDE RESIN IS KNOWN TO CURE INTO RED TO DARK-RED COLORS, DEPENDING UPON PROCESS VARIABLES
- ISOLATION ON NODULES IN SEM/EDAX INDICATED AL NOT PRESENT WITHIN NODULES BUT ABUNDANT IN ADJACENT AREAS AND THROUGHOUT UNFLOWN BLADE BOND LINES
- THEREFORE EVIDENCE SUGGESTS FINAL CURING IN SPACE

FAIRCHILD SPACE COMPANY

CONCLUSIONS

- o APPROXIMATELY 63% DECREASE IN ADHESIVE STRENGTH
- o FOUR PLUS YEARS IN VACUUM SERVES TO FURTHER REMOVE SOLVENT (NMP)
- o INTEGRITY OF ADHESIVE (FOR THE APPLICATION) IS UNIMPAIRED
  - SELF LIMITING PROCESS
  - MAXIMUM STRESSES WHILE IN ORBIT ARE VIRTUALLY ZERO, I.E., ALMOST NOT LOADED
  - AT 20UG'S, F_S = 72 PSI

PORTABLE INFRARED REFLECTOMETER MEASUREMENTS OF SOLAR MAX POST-FLIGHT AND SPARE PRE-FLIGHT LOUVER BLADES

FAIRCHILD SPACE COMPANY

SIDE 1

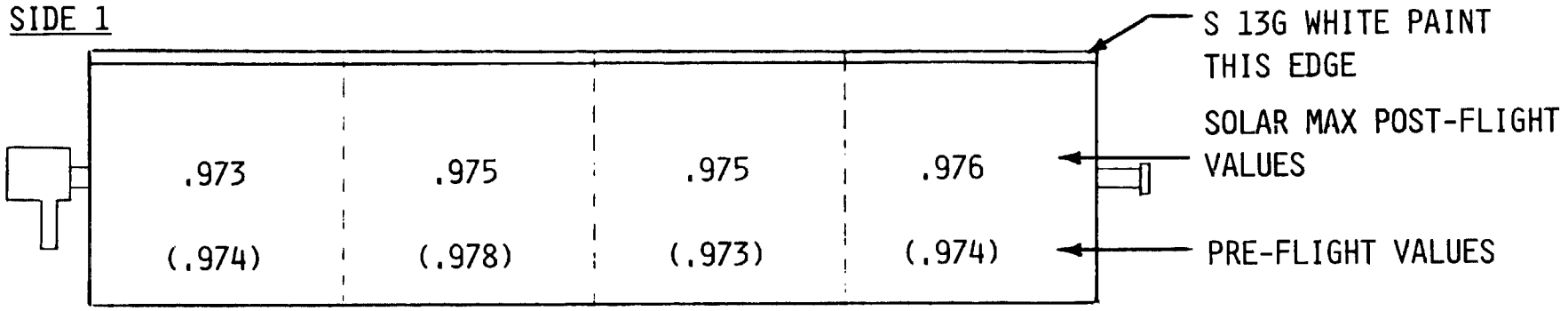

SIDE 2

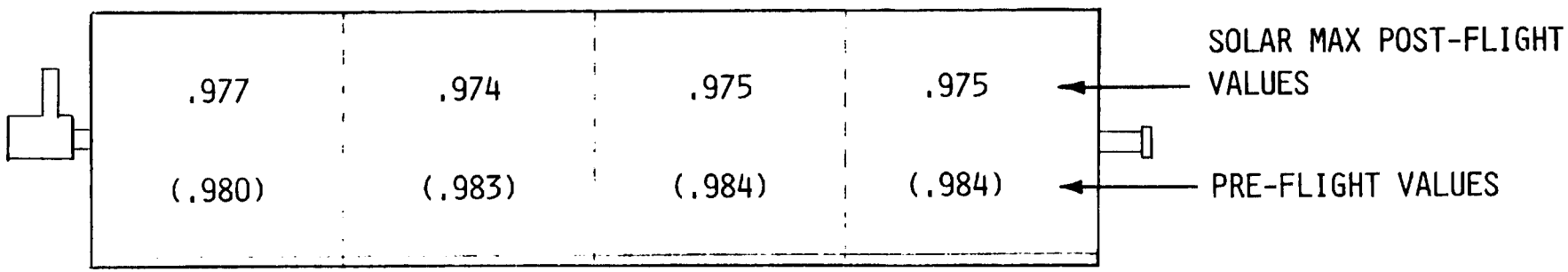

SMRM HARDWARE EVALUATION - QPA 524

- RESULTS OF EVALUATION
  - LOUVER TEMPERATURE CALIBRATION

BLADE POSITION	SPECIFICATION LIMITS (OF)	PRELAUNCH SETTINGS		POST RECOVERY SETTINGS	
		S/N003	S/N006	S/N003	S/N006
OPEN	65 ± 3.6	67.4	66.0	67.8	65.6
CLOSE	35 ± 3.6	35.0	33.0	36.5	35.6

LOUVER EFFECTIVE SOLAR ABSORPTANCE VERSUS SUN ANGLE ATS-6 TEST DATA, OSR BASEPLATE

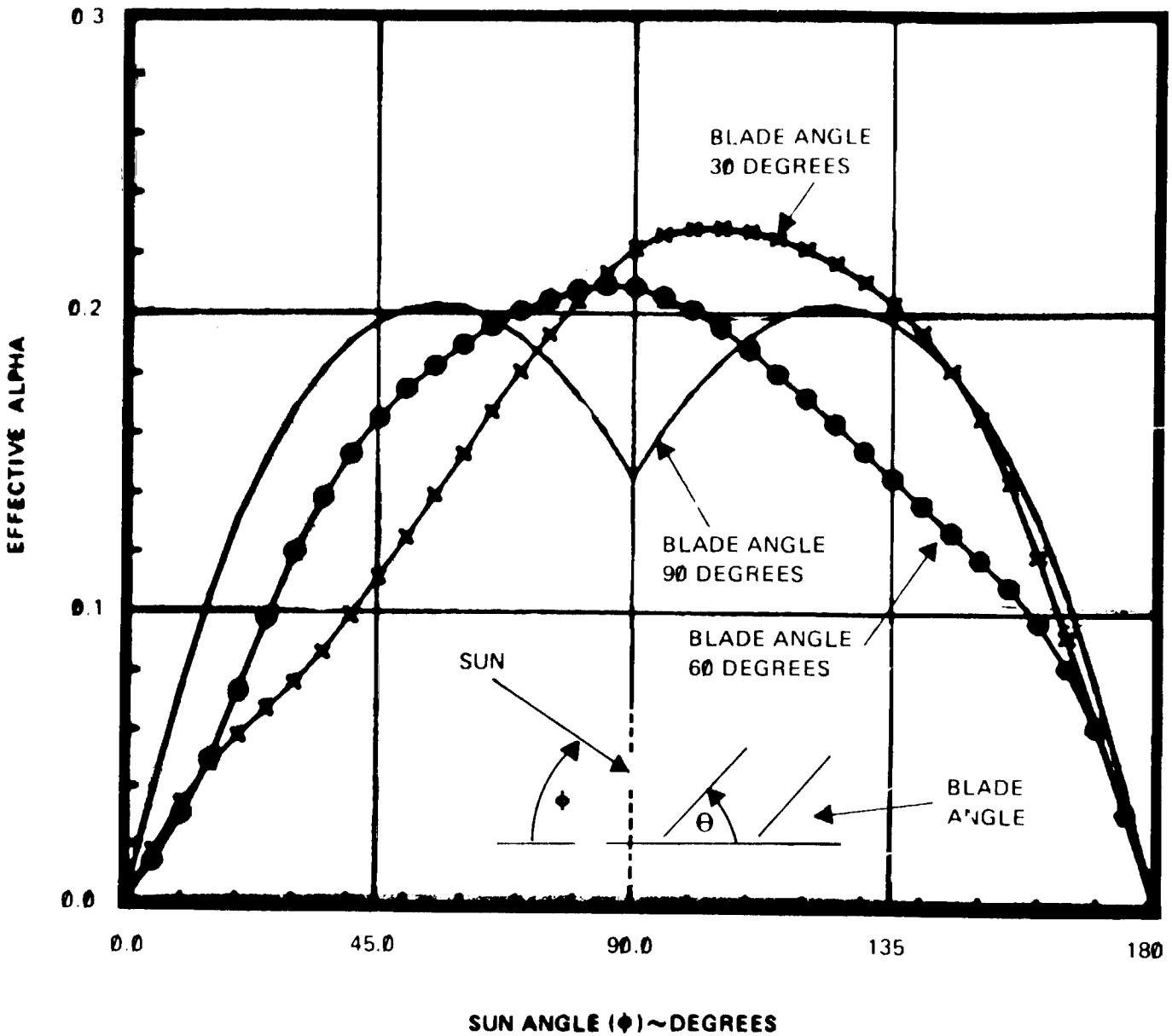

(This page intentionally left blank)

FAILURE ANALYSIS AND PERFORMANCE EVALUATION OF NASA INERTIAL REFERENCE UNIT (DRIRU II) AFTER 50 MONTHS OF ORBITAL OPERATION

K. N. Green
J. W. Ritter
D. Skinner
R. L. Van Alstine

Teledyne Systems Company
Northridge, California

The first production DRIRU II (NASA standard high performance Inertial Reference Unit) system was launched as a subsystem of the Modular Attitude Control System for the Solar Maximum Mission (SMM) spacecraft in February 1980. This hardware was retrieved during the repair of the SMM during Shuttle Flight 41-C in April 1984 and returned to Teledyne Systems Company (manufacturer) for investigation and performance measurements as directed by Goddard Space Flight Center.

A failure of one of the three gyro channels occurred approximately 6½ months after launch. The built in redundancy functioned properly, hence, the DRIRU II continued to provide the required attitude control function without performance degradation. Subsequent failure of other attitude control subsystems made the SMM a candidate for the first demonstration of the shuttle in-orbit repair capability.

This paper discusses the in-orbit DRIRU II failure scenario and the results of the analyses/tests conducted after retrieval. Comparison of this data with similar data prior to launch demonstrates the excellent stability of performance parameters achieveable with DRIRU II.

Reprinted by permission of the American Astronautical Society from Advances in the Astronautical Sciences, Guidance and Control 1985, Volume 57.

INTRODUCTION

Development of the NASA Standard High Performance Inertial Reference Unit (DRIRU II) was initiated by Teledyne Systems Company in 1976 under the direction of the Jet Propulsion Laboratory for the Goddard Space Flight Center.[1] The initial contract was for two systems, a flight system (S/N 1001) which was subsequently flown on the Solar Maximum Mission Spacecraft, and a Qualification system (S/N 1002) which was used to qualify the original design and has subsequently been used to support system design modifications associated with unique requirements of other programs using DRIRU II.

To date, a total of thirteen systems have been delivered as summarized in Table 1. Five of these systems have flown on spacecraft associated with the Solar Maximum Mission, LANDSAT, and Engineering Test Satellite (Japanese) programs, and as of January 1, 1985 have accumulated a total of approximately 237,700 gyro running hours in space (see Table 2). Two additional systems are presently being built and are planned for use on the Gamma Ray Observatory Spacecraft and a DoD program.

Failure of various subsystems aboard the Solar Max Spacecraft caused NASA to select Solar Max for the first demonstration of NASA's capability to repair spacecraft using the shuttle as an in orbit repair facility. NASA successfully demonstrated this repair capability in April 1984 when the astronauts on shuttle flight 41-C located, retrieved, repaired, and re-deployed Solar Max as a fully functional spacecraft at considerably less cost than would have been incurred if a new replacement spacecraft had been built and launched. Additionally, this Solar Max Repair Mission (SMRM) yielded the first opportunity for NASA to closely examine and analyze hardware returned to earth after being exposed to space environment for an extended period of time (50 months). The first DRIRU II system built and flown (S/N 1001) was one of the subsystems of the Modular Attitude Control System (MACS) returned for evaluation.

DRIRU II system S/N 1001 was returned to Teledyne Systems Company in September 1984 for the purpose of investigating the cause of the channel C failure that occurred approximately 6½ months into the mission and to assess the overall condition (structural integrity, materials degradation, performance, stability of parameters, etc.) of the system. The investigative effort expended to date has concluded that the Channel C failure was related to an intermittent electrical short discussed later in this paper. The physical condition of the system was excellent and revealed no apparent materials degradation. Considerable test data acquired since the system was returned has revealed no degradation in system performance when compared to data acquired prior to launch, and excellent stability of system performance parameters (scale factor, acceleration insensitive drift rate, axis alignment, etc.) as discussed in detail later in this paper.

Table 1. DRIRU II Hardware Delivery/Allocation Summary

SYSTEM SERIAL NUMBER	HARDWARE	CUSTOMER	DELIVERY DATE	PROGRAM/ALLOCATION
S/N 1001	FLIGHT UNIT	NASA/JPL	10/78	GSFC, SOLAR MAXIMUM MISSION
S/N 1002	QUALIFICATION UNIT	NASA/JPL	6/78	GSFC, LANDSAT D (SPARE)
S/N 1003	PRODUCTION UNIT	NASA/MSFC	3/79	MSFC, ANNULAR SUSPENDED POINTING SYSTEM (ASPS)
S/N 1004	PRODUCTION UNIT	NASA/JPL	9/79	GSFC, LANDSAT D
S/N 1005	PRODUCTION UNIT	NASA/JPL	11/79	GSFC, LANDSAT D
S/N 1006	PRODUCTION UNIT	NASA/JPL	12/79	GSFC, LANDSAT D
S/N 1007	PRODUCTION UNIT	NASA/JPL	1/80	SOLAR MAX
S/N 1	FLIGHT UNIT	GENERAL ELECTRIC	10/79	TOSHIBA, ETS III
S/N 2	FLIGHT UNIT	GENERAL ELECTRIC	11/79	TOSHIBA, ETS III
S/N 1008	LAB UNIT	DoD	10/81	CLASSIFIED
S/N 1015	FLIGHT UNIT	DoD	10/83	CLASSIFIED
S/N 1016	FLIGHT UNIT	DoD	12/83	CLASSIFIED
S/N 1017	FLIGHT UNIT	NASA/MSFC	4/83	OSS-3

62300-1

Table 2. DRIRU II Operation in Space

SYSTEM S/N	PROGRAM	LAUNCH DATE	GYRO OPERATING HOURS
1001	SOLAR MAX	2/14/80	89,700
1006	LANDSAT 4	7/16/82	71,300
002	ETS III	9/2/82	22,600*
1005	LANDSAT 5	3/1/84	28,500
1007	SOLAR MAX	4/6/84	25,600
TOTAL GYRO OPERATING HOURS IN SPACE ≈ 237,700			

* ONE GYRO CHANNEL OPERATING AT A TIME

62300-2

SYSTEM DESCRIPTION

DRIRU II is a self-contained, strapdown, three axis, dual redundant attitude rate sensing unit for use in spacecraft where high accuracy, high reliability and low power consumption are key requirements.[2,3] The unit contains three independent channels each of which provides two axes of output information. The three-channel inertial reference unit contains the following major elements:

a. Three two-degree-of-freedom dry tuned-gimbal gyros

b. Three independent sets of five electronic modules

c. Three independent power supplies

d. One chassis and housing assembly.

A photograph of the basic unit is shown in Fig. 1. The exploded view in Fig. 2 shows the functional organization of the previously listed major elements and the modular construction. The chassis containing the gyros, electronics and power supplies is supported by the housing through the use of four vibration isolators. This isolation system provides protection from the high mechanical inputs during payload launch and deployment and maintains the high degree of axis alignment stability required during use.

DRIRU II operates on 28 $\pm$7 VDC prime power and nominally consumes 22.5 watts. Dual range, analog rebalance loops are used with an externally supplied discrete range command for high rate tracking or low rate precision pointing. Gyro torquer self-test capability is also included. The system outputs are analog rates, digital incremental angles, clock reference and telemetry for range status, gyro temperature, motor current and regulated voltage from each of the three channels. The gyros, electronic modules and power supplies are physically described as shown in Fig. 3. Three, orthogonally mounted, two degree-of-freedom gyros and triplication of electronic modules and power supplies are used to provide full operational capability with any two of the three channels. The system sensing axes are oriented coincident with the unit's orthogonal reference axes. As the unit is modular, DRIRU II can be hardware implemented or operated with one, two or three channels.

The simplified functional block diagram for a single gyro channel shown in Fig. 4 summarizes the basic signal flow and indicates the relationship between the gyro and electronic modules.

The gyros are captured in an analog torque to balance mode with restoring currents that are proportional to the spacecraft angular rates. The voltage developed by the current passing through precision scaling resistors is then voltage-to-frequency (V/F) converted by reset integrator V/F converters. Two sets of scaling resistors are used per gyro axis to provide for the externally commandable high and low rate ranging.

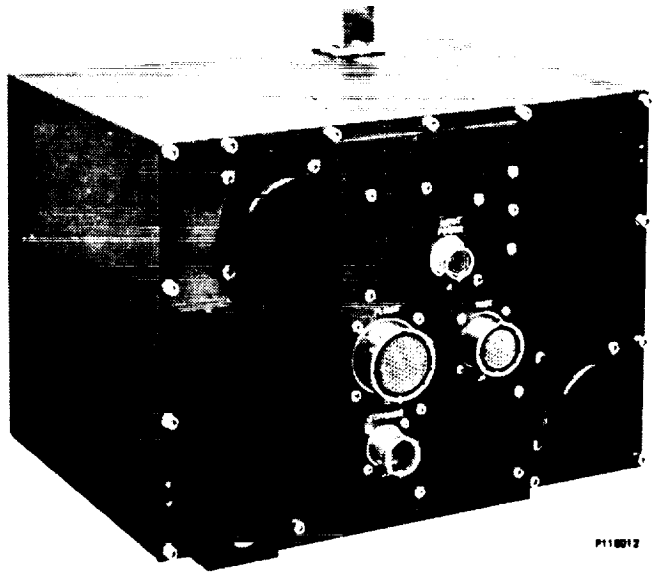

Figure 1. DRIRU II System

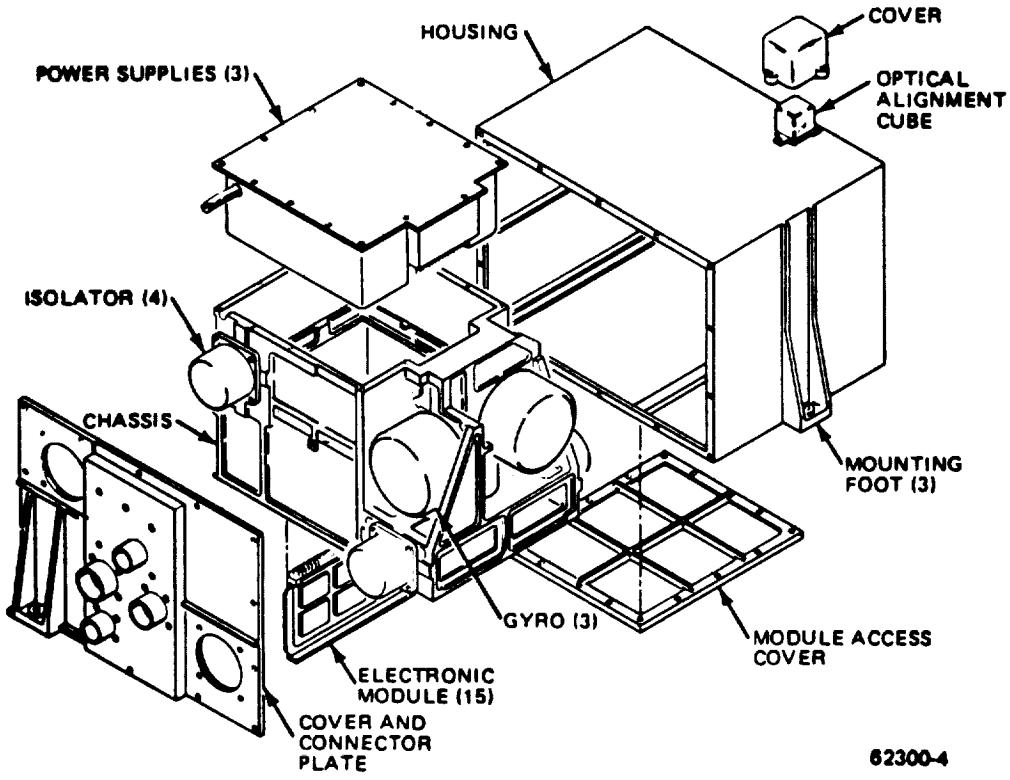

Figure 2. DRIRU II System Exploded View

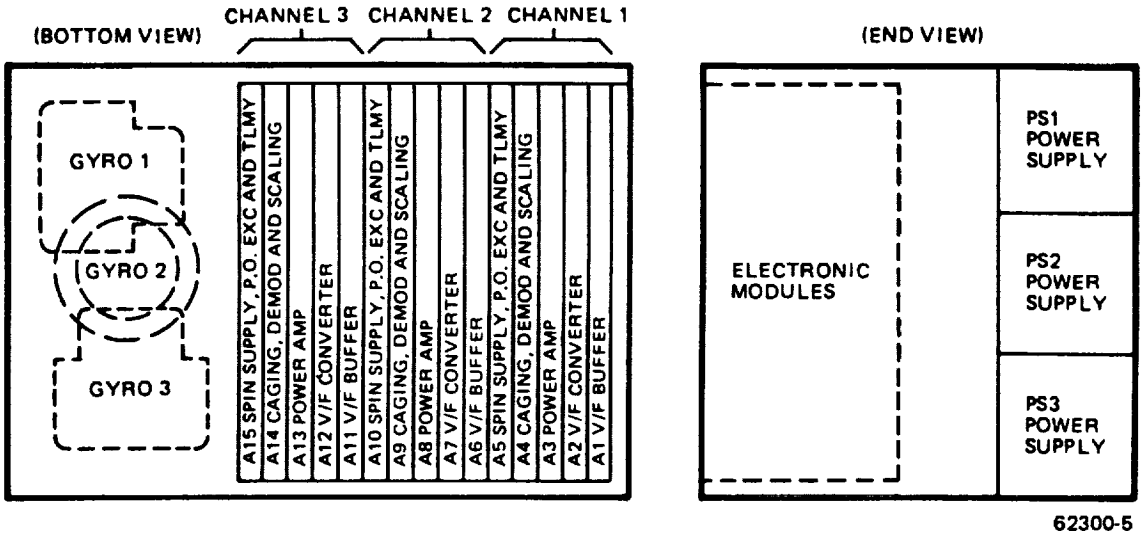

Figure 3. DRIRU II Module Arrangement

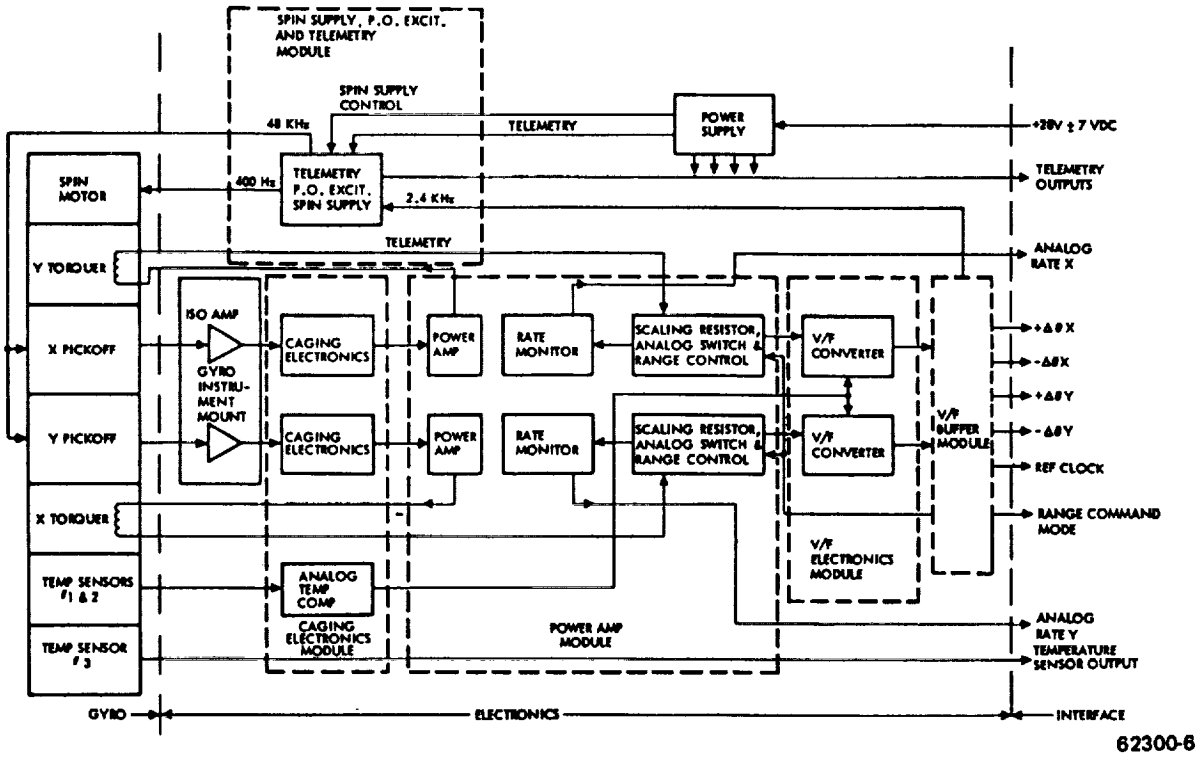

Figure 4. DRIRU II Single Channel Functional Block Diagram

The gyros used in DRIRU II are Teledyne SDG-5 Dynamically Tuned Gyros. Since the gyro performance temperature coefficients are highly linear and stable, self-contained analog temperature compensation is employed for operation over a 40°C temperature range without the need for external software compensation. No heaters or temperature control are required which significantly reduces power consumption and enhances reliability. External software compensation based on the temperature telemetry signal may be employed if operation over a broader temperature range and/or increased performance is desired.

Mechanical interface with the spacecraft is accomplished by a three point mounting on the bottom surface with orientation about the z-axis provided by alignment reference buttons, or alternatively through the use of precision mounting holes. Both the alignment reference buttons and mounting holes are related to an optical master reference cube. A fixture is available to facilitate installation of the unit in conjunction with the externally mounted optical alignment cube for boresight reference.

FLIGHT HISTORY OF S/N 1001

DRIRU II System S/N 1001 was launched into orbit aboard the Solar Maximum Mission Spacecraft on February 14, 1980. All three gyro channels operated normally until September 1, 1980 when a channel C failure was observed. That channel became inoperative and spacecraft attitude was maintained with channels A and B until retrieval in April, 1984.

Failure Scenario

The first indication of failure was the drop to near zero of the Channel C gyro motor current. This was determined from gyro motor current telemetry and Channel C 28 volt input current. After 72 seconds the motor current abruptly increased beyond telemetry saturation and subsequently the fuse in the input power line external to DRIRU II was blown. The drop of motor current is compatible with an erroneous level in the motor enable logic circuitry. The surge in motor current is compatible with the motor enabled in a static (unclocked) mode. The 28 volt MACS input current and Gyro C motor current telemetry data are shown in Fig. 5. For the purpose of illustration, minor deflections in the waveform have been omitted.

Based on these symptoms, a failure tree was created and failure analysis reports were generated by GSFC,[4] JPL[5] and Teledyne. The reports were in general agreement that the failure was most probably in the motor control logic. This conclusion was verified by troubleshooting after SMM retrieval.

In the immediate aftermath of the failure, much effort was expended to determine if the failure could have been induced by radiation. This was required because the failure occurred while in the vicinity of the South Atlantic Anomaly and was nearly coincident with unrelated memory

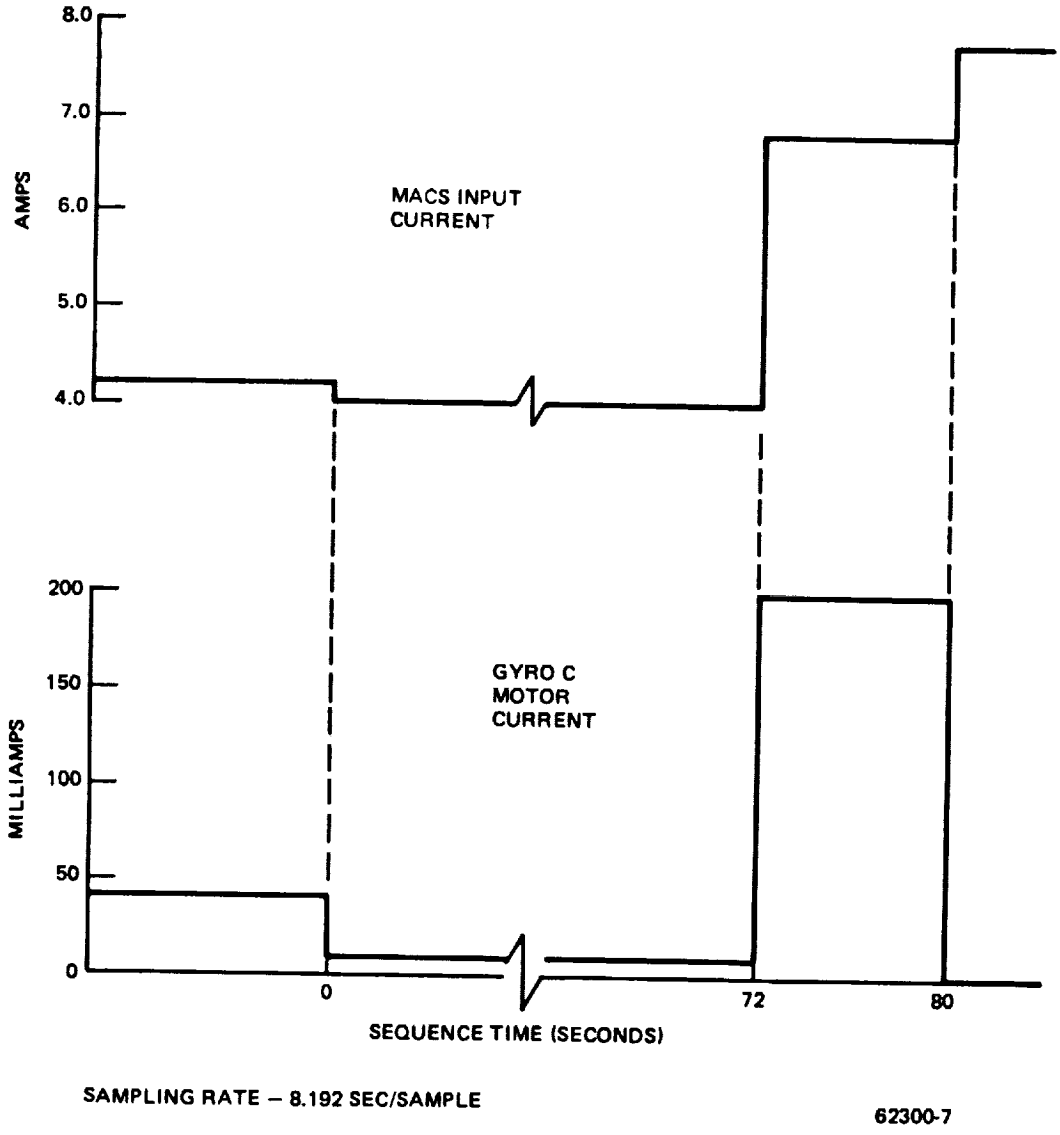

Figure 5. Failure Telemetry Data

failures elsewhere in the spacecraft that were determined to be radiation induced. Also, the suspect logic devices were CMOS, which were considered potentially sensitive to radiation. Extensive tests were performed which eventually led to the conclusion that radiation was not a probable cause of the failure. This conclusion was also verified by troubleshooting after retrieval.

POST FLIGHT EVALUATION

The unit was returned to Teledyne on 25 September 1984. Authorization was received from the Goddard Space Flight Center to proceed with evaluation of the failure and perform evaluation testing. The suspected failed module, the Channel C Spin Supply, Pickoff Excitation and

Telemetry (SSPOET) module, was removed for visual inspection and replaced with a backup module. Functional tests, including gyro spin motor functional tests, were successful on all three channels. Table 3 shows the spin motor telemetry voltages measured for each DRIRU II channel compared to original Acceptance Test data in October 1978.

Performance tests were then begun following a test plan mutually established by Teledyne and the GSFC.

System Failure Analysis

During initial stabilization at 50°C (using the substitute Channel C SSPOET module) the Channel C input current protection circuit tripped, indicating that a DRIRU II failure had occurred. This symptom was compatible with the blown fuse that occurred in orbit. Subsequent troubleshooting revealed an intermittent logic device (CD4017A) in the motor supply countdown logic on the V/F Buffer module. The original suspect SSPOET module was reinstalled and an intermittent system failure was detected characterized by loss of motor drive current. After a short period of time the intermittent failure became a hard failure. Subsequent troubleshooting revealed a failed logic device (CD4049A) on the SSPOET module. Module level testing revealed another logic device (CD4081B) with severely degraded logic threshold characteristics. The relationship of these failed components is shown in Fig. 6.

During the above troubleshooting, a strip chart recorder was used to monitor critical test points. On two occasions the +5 volt logic supply was observed to momentarily go out of tolerance on the high side. This failure mode was not caused by any of the above mentioned component failures but was considered a possible cause of one or more of those failures. To date, the cause of this +5 volt intermittent failure has not been determined. Several possible areas have been identified and further investigation will be coordinated by Teledyne and GSFC.

Table 3. DRIRU II S/N 1001 Gyro Spin Motor Current Telemetry

GYRO CHANNEL	SPIN MOTOR TELEMETRY (VOLTS DC)	
	10/78	11/84
A	1.05	0.90
B	1.05	1.10
C	1.04	1.30

SPECIFICATION REQUIREMENTS: 0.7 - 1.7 VOLTS

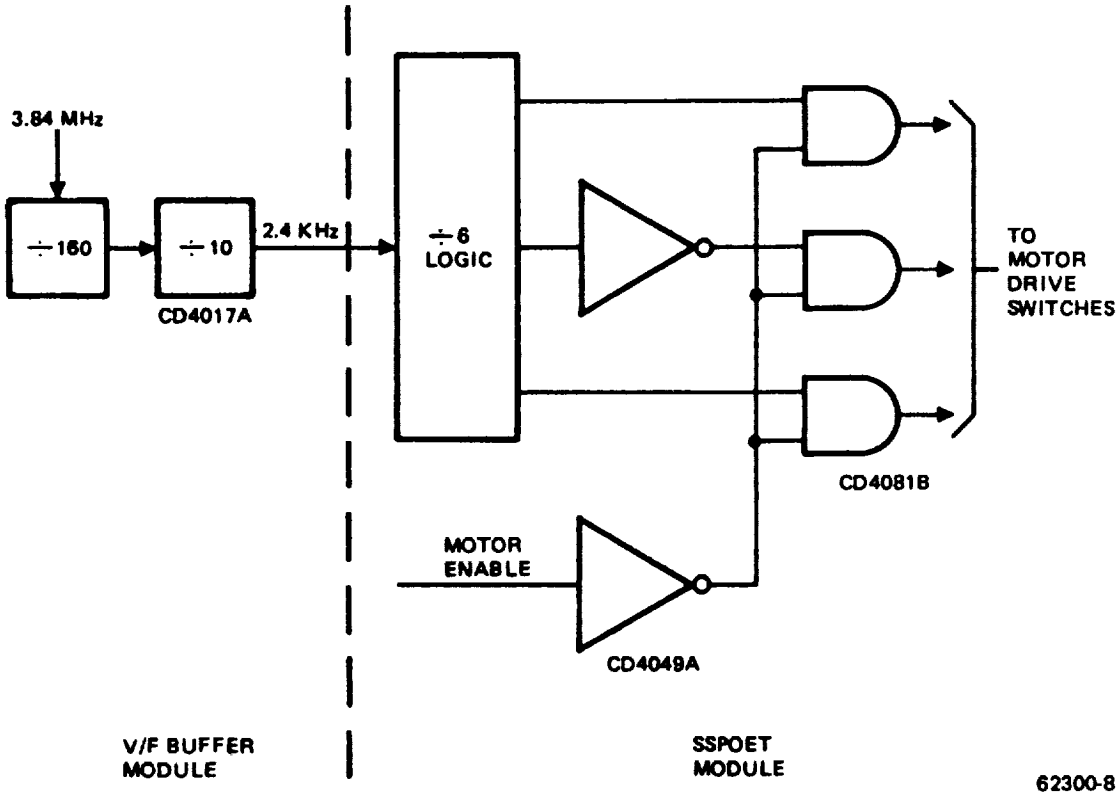

Figure 6. DRIRU II Motor Control Logic

The three failed logic devices were returned to GSFC for failure analysis.[6] The CD4049A and CD4081B exhibited obvious electrical overstress. The CD4049A had a fused output, which, at the system level, serves as an input to three pins of the CD4081B. The observed electrical overstress and the +5 volt out of tolerance condition are compatible with the application of a voltage greater than 8 volts to this node. The CD4017A did not exhibit physical signs of induced overstress but appeared to have an oxide defect that caused a resistive short between an internal die signal and ground. No scenario has been developed to relate all of the observed orbital failure symptoms solely to the defective CD4017A device. However, because the data gathered during troubleshooting indicates with a high degree of certainty that the failure was characterized by an out of tolerance logic supply voltage, it follows that the latent defect in the CD4017A could have been the most susceptible weak link. With the combination of CD4017A and CD4049A failures, all of the orbital failure symptoms have been reproduced in the laboratory.

System Performance Testing

After the two failed modules were removed for evaluation, the system was reassembled with two substitute modules for performance evaluation and

further gyro spin motor tests. Initially, only limited performance tests were planned but it was eventually decided to perform a full series of temperature tests in order to evaluate stability of scale factor and AIDR over the operating temperature range as well as to determine basic parameter repeatability with respect to as-shipped data.

The system had been initially acceptance tested in October 1978, shipped to the GSFC, then returned to Teledyne for minor modification and reshipped in early 1980. The present test series (December 1984) was designed to repeat the 1978 acceptance tests rather than the interim testing since the interim testing was limited in scope and did not provide a full data comparison base (e.g., only 66°C data were obtained, thereby precluding the comparison of temperature stability data).

The following standard DRIRU II performance tests were accomplished during the evaluation period:

a. Precision rate tests at 36°C, 50°C, and 66°C to determine scale factors, linearity and symmetry.

b. Static multiposition tests at 36°C, 50°C and 66°C to determine acceleration insensitive drift rate (AIDR).

c. Misalignment measurements for the gyro axes relative to the mounting reference axes and also the optical cube surfaces relative to the mounting reference axes.

d. Six hour AIDR stability.

e. Noise equivalent angle (NEA).

Results of the performance tests are summarized in the following paragraphs and the referenced tables and figures. Only the incremental output data were evaluated since these are the most accurate DRIRU II outputs.

1. Scale Factor Long Term Stability

Table 4 shows the scale factors measured in December 1984 compared to original acceptance test data in October 1978. All six system axes are shown for both low and high rate ranges at 50°C. Note that average absolute changes over the 74 month period were 229 ppm and 271 ppm for the low and high ranges, respectively. Channel C was the largest contributor by far to these averages. For Channels A and B, the corresponding average low and high range changes are only 58 and 142 PPM, respectively. Concern about significant scale factor changes due to gyro torquer magnet aging effects are not borne out by these data. Even assuming that the worst case Channel C change is all due to magnet aging, this would show an average rate of change over the six year period of approximately 100 ppm per year. Channels A and B show no discernible aging characteristics.

Table 4. DRIRU II S/N 1001 74 Month Scale Factor Stability

GYRO CHANNEL	AXIS	LOW RANGE DEVIATION FROM NOMINAL (PPM)			HIGH RANGE DEVIATION FROM NOMINAL (PPM)		
		10/78	12/84	CHANGE	10/78	12/84	CHANGE
A	X_1	+2349	+2480	+131	−916	−698	+218
	Z_1	−484	−569	−85	−735	−872	−137
B	X_2	+14	+18	+4	−561	−526	+35
	Y_1	+1112	+1124	+12	−1138	−970	+168
C	Y_2	+30	−573	−603	−593	−1215	−622
	Z_2	−1261	−1726	−465	−2251	−2697	−446
MEAN				−168			−131
STD. DEVIATION				295			340
AVERAGE ABSOLUTE CHANGE				229			271

SPECIFICATION REQUIREMENTS:

ABSOLUTE VALUES WITHIN ± 5000 PPM OF NOM.
ENVIRONMENTAL STABILITY < ± 100 PPM (LOW)
LONG TERM STABILITY (30 DAY) < ± 50 PPM (LOW)
< ± 200 PPM (HIGH)

62300-9

These data show that careful temperature stabilization techniques used on the samarium cobalt gyro torquer magnets can produce excellent long term performance characteristics.

2. Scale Factor Linearity

Table 5 shows scale factor linearity data measured in October 1978 and December 1984. Only low range measurements are required by the acceptance test procedure. Note that the average non-linearity measured in 1984 is less than half the original data (36 ppm vs. 78 ppm). This reflects an improvement in test technique rather than improvement in actual linearity. Non-linearity is defined as the worst case deviation of the scale factor determined from data acquired at input rates of ±.03, ±.06 and ±.09 degrees per second.

3. Scale Factor Asymmetry

Scale factory Asymmetry measurements are shown in Table 6. Again, the improvement in test techniques is shown dramatically in the data

Table 5. DRIRU II S/N 1001 Scale Factor Linearity

GYRO CHANNEL	AXIS	LINEARITY (PPM) LOW RANGE	
		10/78	12/84
A	X_1	78	36
	Z_1	103	40
B	X_2	84	34
	Y_1	58	26
C	Y_2	71	39
	Z_2	75	43
AVERAGE		78	36

SPECIFICATION REQUIREMENT: < 100 PPM

62300-10

Table 6. DRIRU II S/N 1001 Scale Factor Asymmetry

GYRO CHANNEL	AXIS	ASYMMETRY (PPM) LOW RANGE		ASYMMETRY (PPM) HIGH RANGE	
		10/78	12/84	10/78	12/84
A	X_1	5	4	17	7
	Z_1	17	1	14	3
B	X_2	26	5	10	0
	Y_1	45	7	7	2
C	Y_2	33	5	14	6
	Z_2	4	3	33	4
AVERAGE		22	4	16	4

SPECIFICATION REQUIREMENT: <50 PPM LOW RANGE ONLY

62300-11

for both low and high rate ranges. The most recent data, averaging 4 ppm, are within the accuracy of scale factor determination.

4. Scale Factor Temperature Stability

Since DRIRU II is not temperature controlled, internal temperature compensation circuitry is used to correct the basic system level temperature sensitivities (primarily gyro related). To evaluate the

adequacy of the compensation circuitry, scale factor is measured at three temperatures - 36°C, 50°C and 66°C. Table 7 shows the peak to peak variations over those temperatures for the six axes. Note that in all but one case the variations were lower for the retest data as compared to the original data. As before, this is due to improved test techniques.

5. AIDR Long Term Stability

Long term stability of Acceleration Insensitive Drift Rate (AIDR) is shown in Table 8. For low range, the average absolute change was 0.0051 arc sec/sec (o/hr). Only one axis out of six showed a change greater than 0.01 arc sec/sec. These stability values show exceptional DRIRU II performance especially in view of the current Teledyne specification (document 7516544) limit of 0.02 arc sec/sec for 30 days of continuous operation in a benign environment plus an additional 0.03 arc sec/sec instability allowance over launch environments. For high range, the changes were only slightly worse, averaging 0.0147 arc sec/sec. The difference between the two ranges is mainly due to the coarse scaling of the high range, 0.8 arc sec/pulse vs. 0.05 arc sec/pulse for low range.

6. AIDR Short Term Stability

Stability of AIDR under benign conditions is measured over a six hour period using ten minute averages. Peak-to-peak variations of these ten minute averages are recorded as six hour stability. Table 9 summarizes the peak-to-peak variation of each of the six axes for pre- and post-flight testing. All data are within specification limits (0.003 arc sec/sec) except Z2 axis which is associated with channel C. The cause for this out of tolerance condition may be the high temperature sensitivity of the Z2 axis as discussed below.

7. AIDR Temperature Stability

AIDR is measured at the same three temperatures as used for scale factor testing. Results of these tests are shown in Table 10. The specification requirement is specified as an equation including linear and second order terms involving temperature deviations from a 50°C reference point. To simplify the comparison of test data, a specification limit of 0.083 arc sec/sec peak to peak was calculated from this equation using the two end points, 36°C and 66°C. As can be seen one of the six axes exceeds this limit, axis Z2. However, as the table indicates, this same axis was out of tolerance when initially delivered (a waiver was approved by GSFC) and the retest data is very close to the original number. Current production units benefit from refinements in compensation techniques, thereby eliminating similar out of tolerance conditions on more recent and current systems.

Table 7. DRIRU II S/N 1001 Scale Factor Temperature Stability

GYRO CHANNEL	AXIS	PK-PK CHANGE (PPM) OVER 30°C LOW RANGE	
		10/78	12/84
A	X_1	110	98
	Z_1	213	80
B	X_2	133	60
	Y_1	157	223
C	Y_2	227	195
	Z_2	93	61

NOTE: TESTS WERE CONDUCTED AT +36°C, +50°C AND +66°C. THE TABULATED VALUES ARE PEAK TO PEAK SCALE FACTOR CHANGES OVER THE THREE TEMPERATURES.

SPECIFICATION REQUIREMENT: 200 PPM PK-PK.

62300-12

Table 8. DRIRU II S/N 1001 74 Month AIDR Stability

GYRO CHANNEL	AXIS	LOW RANGE (ARC SEC/SEC)			HIGH RANGE (ARC SEC/SEC)		
		10/78	12/84	CHANGE	10/78	12/84	CHANGE
A	X_1	−.1669	−.1518	+.0151	−.3489	−.3447	+.0045
	Z_1	−.3615	−.3562	+.0053	−.3084	−.2913	+.0171
B	X_2	−.1148	−.1146	+.0002	−.1619	−.1607	+.0039
	Y_1	+.3830	+.3780	−.0050	+.4241	+.4403	+.0162
C	Y_2	−.1729	−.1712	+.0017	−.2192	−.2033	+.0159
	Z_2	+.2481	+.2450	−.0031	+.4186	+.3853	−.0333
MEAN				+.0024			+.0041
STD DEVIATION				.0072			.0193
AVERAGE ABSOLUTE CHANGE				.0051			.0147

SPECIFICATIONS REQUIREMENTS:

ABSOLUTE VALUE	< 2.0 ARC SEC/SEC
ENVIRONMENTAL STABILITY	< .03 ARC SEC/SEC (LOW)
LONG TERM STABILITY (30 DAY)	< .02 ARC SEC/SEC (LOW) < .03 ARC SEC/SEC (HIGH)

62300-13

Table 9. DRIRU II S/N 1001 AIDR Short Term Stability (Low Range)

GYRO CHANNEL	AXIS	6 HOUR DRIFT STABILITY (ARC SEC/SEC PK-PK)	
		10/78	12/84
A	X_1	.0016	.0012
	Z_1	.0024	.0014
B	X_2	.0018	.0023
	Y_1	.0017	.0018
C	Y_2	.0022	.0027
	Z_2	.0022	.0045

62300-14

SPECIFICATION REQUIREMENT: < .003 ARC SEC/SEC PK-PK (LOW RANGE ONLY)

Table 10. DRIRU II S/N 1001 AIDR Temperature Stability

GYRO CHANNEL	AXIS	PK-PK CHANGE (ARC SEC/SEC) OVER 30°C LOW RANGE	
		10/78	12/84
A	X_1	.0604	.0517
	Z_1	.0381	.0245
B	X_2	.0481	.0318
	Y_1	.0234	.0049
C	Y_2	.0261	.0285
	Z_2	.1957*	.1912

62300-15

NOTE: TESTS WERE CONDUCTED AT +36°C, +50°C AND +66°C. THE TABULATED VALUES ARE PEAK TO PEAK AIDR CHANGES OVER THE THREE TEMPERATURES.

SPECIFICATION REQUIREMENT: .083 ARC SEC/SEC

*UNIT WAS INITIALLY DELIVERED WITH AN APPROVED WAIVER FOR Z2 AXIS

8. Gyro Axes Alignment Stability

Two types of measurable axis alignments are important to DRIRU II - alignment of the gyro input axes to the external mounting surfaces and alignment of the optical reference cube to the external mounting surfaces. Stabilities of these alignments are important, particularly the stabilities of the gyro axes through launch environments and over extended time periods. Table 11 shows the twelve measured alignment terms (two for each gyro axis) for the original acceptance data and the post retrieval data. Average absolute change was 7.7 arc sec. These terms include misalignments within the gyros, across the shock isolators, and within the DRIRU II housing and chassis structures. Also included are remount uncertainties and test errors. The concern held by some that an elastomeric isolation system cannot provide good mechanical stability is dispelled by these data. In order to show the consistency of the measurements, the recorded changes were regrouped

Table 11. DRIRU II S/N 1001 74 Month Gyro Axis Alignment Stability

GYRO CHANNEL	TERM*	GYRO AXIS ALIGNMENT (ARC SECONDS)		CHANGE (ARC SEC) (74 MONTHS)
		10/78	12/84	
A	X_1Y	−65	−74	−9
	X_1Z	+74	+80	+6
	Z_1X	−17	−19	−2
	Z_1Y	−101	−109	−8
B	X_2Y	−45	−58	−13
	X_2Z	+29	+33	+4
	Y_1X	+9	+14	+5
	Y_1Z	+90	+101	+11
C	Y_2X	+79	+96	+17
	Y_2Z	+142	+149	+7
	Z_2X	−34	−37	−3
	Z_2Y	−132	−141	−9
MEAN STANDARD DEVIATION AVERAGE ABSOLUTE CHANGE				−0.3 8.9 7.7

62300-16

*NOTE: TERM INDICATES GYRO AXIS MISALIGNMENT TOWARD DESIGNATED IRU MOUNTING REFERENCE AXIS.

SPECIFICATION REQUIREMENTS: ABSOLUTE VALUES < 300 ARC SEC
STABILITY (ACROSS LAUNCH ENV.) < 20 ARC SEC

by system axis rather than by gyro axis and are retabulated in Table 12. Note here that each group of four misalignment terms correspond to one direction of rotation about a given DRIRU II reference axis. The extremely good correlation within each group indicates that accurate measurements of angular position change of the instrument cluster (three gyros mounted on a rigid body) were made and that the changes are apparently due mostly to DRIRU II structural movement (including isolators) rather than individual gyro axes.

9. Optical Cube Alignment Stability

Another type of alignment of importance, but only for the purpose of insuring accurate installation of DRIRU II in the spacecraft, is the relationship of the optical cube mounted on the top surface of the unit to the DRIRU II mechanical mounting surfaces. This alignment is measured optically by the Teledyne Metrology Department and is independent of any error sources internal to DRIRU II. Table 13 shows the results of these measurements for pre- and post-flight data. Worst case change was 19 arc sec over 74 months, compared to a 20 arc sec specification limit over the launch environments.

Table 12. DRIRU II S/N 1001 74 Month Axis Alignment Stability

SYSTEM REF AXIS	TERM	CHANGE (ARC SEC)	MEAN (ARC SEC)	STD. DEV. (ARC SEC)
X	Y_1Z	+11		
	Y_2Z	+7	+8.8	1.7
	$-Z_1Y$	+8		
	$-Z_2Y$	+9		
Y	$-X_1Z$	−6		
	$-X_2Z$	−4	−3.8	1.7
	Z_1X	−2		
	Z_2X	−3		
Z	X_1Y	−9		
	X_2Y	−13	−11.0	5.2
	$-Y_1X$	−5		
	$-Y_2X$	−17		

62300-17

NOTE: EACH GROUP OF FOUR TERMS ARE THE FOUR GYRO INPUT AXIS MISALIGNMENTS ABOUT A GIVEN DRIRU II MOUNTING REFERENCE AXIS. SIGNS INDICATE POSITIVE OR NEGATIVE ROTATION ABOUT THAT REFERENCE AXIS ACCORDING TO THE RIGHT HAND RULE.

Table 13. DRIRU II S/N 1001 74 Month Optical Reference Stability

REF AXIS	OPTICAL ALIGNMENT (ARC SECONDS)		CHANGE (ARC SEC) (74 MONTHS)
	10/78	12/84	
X	+42	+58	+16
Y	+256	+253	-3
Z	−9	+10	+19

62300-18

NOTE: ALIGNMENT TERMS ARE FOR A GIVEN OPTICAL CUBE REFERENCE SURFACE MEASURED WITH RESPECT TO THE CORRESPONDING DRIRU II MOUNTING REFERENCE AXES.

SPECIFICATION REQUIREMENTS: ABSOLUTE VALUES < 300 ARC SEC
STABILITY (ACROSS LAUNCH ENV.) < 20 ARC SEC

This requirement for stability over launch environment is imposed only to assure stability over pre-launch spacecraft integration testing and handling.

10. Noise Equivalent Angle (NEA)

Noise Equivalent Angle is a means of specifying the output noise performance of the DRIRU II by accumulating continuous 200 msec samples of incremental output data over a period of time generally 30 or 60 minutes. These data are analyzed to determine the peak-to-peak variation in equivalent angular output after the best fit slope (drift rate) is removed from the data record. A typical graphical representation of NEA data is shown in Fig. 7 for one axis tested during the post retrieval evaluation. Table 14 shows the peak-to-peak NEA for this axis tabulated along with data for the other axes. All are within the 1.0 arc sec peak-to-peak specification limit even though the testing encompassed a 60 minute period rather than the 30 minute period presently specified.

Gyro Disassembly Investigation

As a third phase of the post-retrieval evaluation, GSFC authorized the disassembly and inspection of one of the three gyros. Motor evaluation tests conducted during system testing indicated that normal operating parameters (i.e., sync time, start and run current levels, motor telemetry) were all within specification. Additional testing, specifically motor milliwatt traces, was accomplished to determine which of the two gyros that had been operating continuously during the orbital period (Channels A and B) showed greater signs of degradation. The gyro from Channel B was selected because the variations in milliwatt trace were larger.

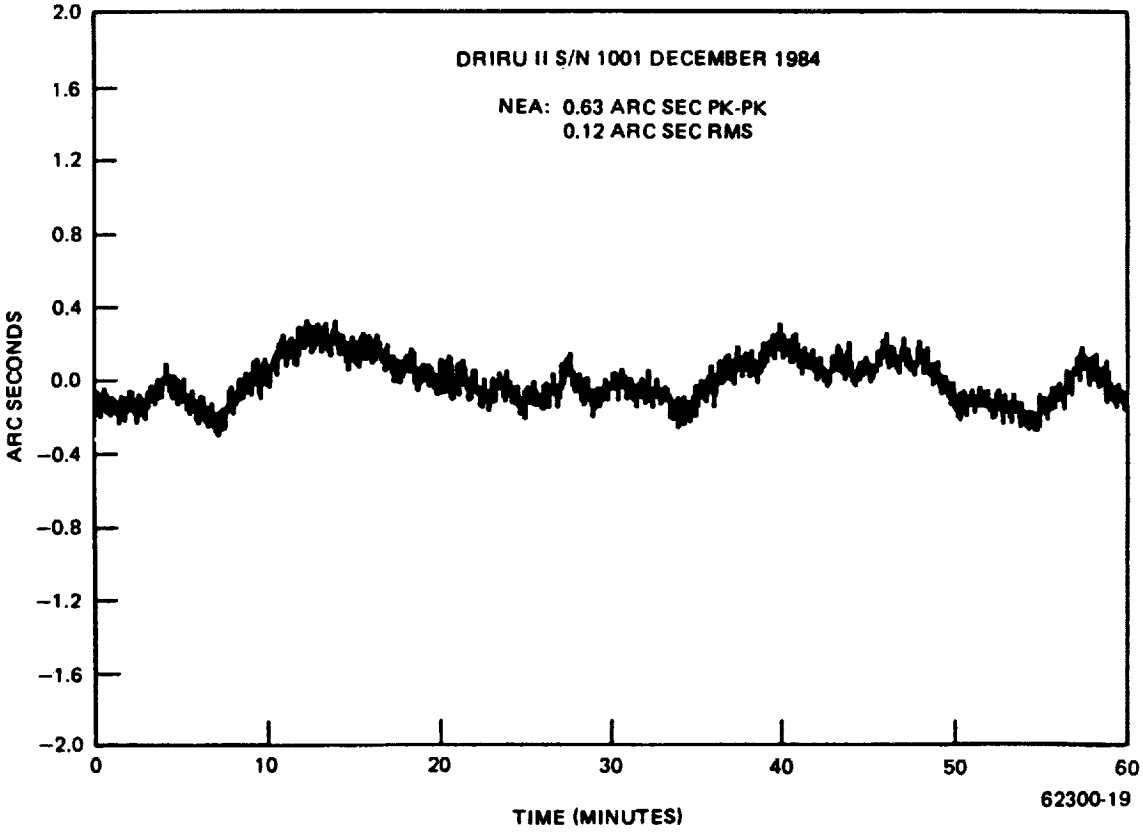

Figure 7. DRIRU II S/N 1001 Typical Noise Equivalent Angle (NEA) (X2 Axis)

Table 14. DRIRU II S/N 1001 Noise Equivalent Angle (Low Range)

GYRO CHANNEL	AXIS	NEA (ARC SEC PK-PK)	
		10/78	12/84
A	X_1	.86	.75
	Z_1	.93	.61
B	X_2	1.05	.63
	Y_1	.82	.89
C	Y_2	.87	.80
	Z_2	.83	.98

SPECIFICATION REQUIREMENT: <1.0 ARC SEC PK-PK OVER 30 MINUTES (LOW RANGE ONLY)

NOTE: THE ABOVE TESTS WERE CONDUCTED OVER A 60 MINUTE PERIOD

62300-20

This gyro (S/N 094) was disassembled in the presence of GSFC personnel and all parts and subassemblies were carefully inspected. Particular attention was paid to the condition of the ball bearings. Although evaluation has not yet been completed, the disassembly effort yields the following observations.

The bearing races, balls and retainers showed no excessive wear. The races exhibited minor ball tracking which would be normal for extended bearing life (over 40,000 hours). The balls were free of banding or other signs of abnormal wear. The phenolic retainers appeared normal with no evidence of ball pocket damage or overheating. However, there was evidence of lubricant deterioration in the bearings. This appeared as a dark colored, viscous residue mainly in the ball tracks and the retainer ball pockets. One bearing showed significant amounts of this residue with minimal oil remaining. The other bearing exhibited a small quantity of oil and contained small amounts of the residue. Samples of the residue and all bearing parts were returned to GSFC for further analysis, cleaning, and detailed inspection of surface finishes, material condition, retainer retention characteristics, etc. The results of these investigations were not available at the time of this writing.

Other subassemblies and piece parts in the gyro were also visually examined. No evidence of failure or degradation was found except for the incidence of small spots of white substance attached to non-contact surfaces of the rubber contact ring which is part of the rotor limit stop. This part has also been sent to GSFC for analysis.

CONCLUSIONS

Based on the failure analysis, inspections and performance testing performed on DRIRU II S/N 1001 and its subassemblies, the following conclusions can be made:

1. All evidence to date indicates that the Channel C failure was most probably caused by an intermittent electrical "short" between the +5 volt logic supply and a higher voltage level.

2. Two of the three failed logic devices were induced failures consistent with an overvoltage on the +5V terminal. The third device exhibited a latent internal defect causing a signal to ground short.

3. There is no evidence of system performance degradation due to the operational and other environments encountered.

4. The system exhibited excellent long term stability of performance parameters across the launch, orbital operation and retrieval environments over a 74 month period.

5. There was no measurable degradation of the shock/vibration isolators as evidenced by the excellent alignment stability measured over the 74 month period.

6. There was no evidence of structural or mechanical changes and no apparent outgassing or degradation of exposed materials in DRIRU II.

7. Gyro ball bearings showed no detectable damage to raceways, balls or retainers, but the bearing lubricant had begun to experience deterioration.

8. There was no evidence of other gyro subassembly degradation except for the presence of small amounts of a white substance (to be analyzed) adhering to the limit stop rubber contact ring.

REFERENCES

1. Ritter, J. W. and Irvine, R. B., "DRIRU II - Standard High Accuracy Inertial Reference Unit for Spacecraft Through the 1980's," Presented at the 34th Annual Meeting of the Institute of Navigation, Arlington, Virginia, June 1978.

2. Irvine, R.B. and Ritter, J.W., "DRIRU II - The NASA Standard High Performance Inertial Reference Unit," Paper presented at the Rocky Mountain Guidance and Control Conference of the American Astronautical Society, February 1979.

3. Green, K.N., Oshika, E.M. and Van Alstine, R.L. "Spectral Noise Performance of a High Accuracy Dry Tuned Gyroscope and the NASA Standard Redundant Dry Rotor Inertial Reference Unit (DRIRU II)," Paper presented at the Ninth Biennial Guidance Test Symposium, Holloman AFB, New Mexico, October 1979.

4. Goddard Space Flight Center Document, SMM/MMS Anomaly Investigation, February 1981.

5. Jet Propulsion Laboratory Document No. 900-983, Solar Maximum Mission Final Report of the DRIRU II Anomaly Team for the C Channel Failure, March 11, 1981.

6. Goddard Space Flight Center, Failure Analysis Report Serial No. 51177/51178, November 16, 1984.

Analysis of DRIRU Bearings and Lubricant from Solar Max Repair Mission

by

Joanne M. Uber
NASA/Goddard Space Flight Center
Greenbelt, Maryland

INTRODUCTION

The Solar Max Repair Mission (SMRM) by shuttle astronauts in April 1984, returned to Earth the Delta Redundant Inertial Reference Unit II (DRIRU II) from the Solar Max satellite. The DRIRU II included three gyroscopes as shown in Figure 1. The gyroscope, S/N 094, in position 2 was disassembled by Teledyne Systems personnel of Northridge, California, and the bearings were returned to Goddard space Flight Center (GSFC) for examination. The Solar Max satellite had been in orbit for 4 years with the bearings running continuously at 6000 rpm. See Table I for the gyroscope design parameters.

CONCLUSIONS

The ball bearings--S/N B40 and S/N B58--showed little wear, had sufficient remaining lubricant and had run successfully for over 4 years. As a result of these findings, the bearings should have lasted their predicted life of 5 years with no problems.

OBSERVATIONS

The gyro, as shown in Figure 2, contained two thrust bearings made by Barden stamped SR4HX18. The lower bearing was stenciled with S/N B40 and the upper bearing was stenciled with S/N B58.

Teledyne Systems supplied two new bearings, S/N E2 and S/N D55, for comparison with the gyro bearings removed from Solar Max. Figure 3 shows a disassembled new Barden thrust bearing, stamped SR4HX360, presently used by Teledyne Systems in their gyroscopes.

Removal of the case and the hystersis ring, Figure 2, allowed examination of B40 while still in the gyro. The bearing had numerous particles clinging to the bearing parts, as shown in Figure 4. After removing B40 from the gyro, the bearing parts left an oil trail in the Petri dish--evidence that the bearing was lubricated. Bearing B58 could not be examined in the gyroscope. On removal we found that B58 had fewer particles and was well lubricated as it too left an oil trail in its Petri dish.

Both bearings were rinsed first with alcohol and then chloroform and the debris was collected. Typical debris particles are shown in Figure 5. The particles ranged in color from yellow-red to black. A particle count of each bearing's debris showed that B40 contained over 500 particles and B58 contained only 150 particles. Figure 6 shows the histograms of the counts. X-ray spectroscopy using Energy Dispersive Analysis of X-rays (EDAX) showed that the debris particles consisted primarily of iron and chromium. A similar analysis showed that the bearing material was 440C stainless steel.

The retainers are a phenolic material which is porous and is used as an oil reservoir. Wash samples were taken from each retainer and an Infrared Analysis (IR) was run to confirm the type of lubricant in the bearings. The retainers contained an aliphatic hydrocarbon lubricant as shown by the lower IR curve in Figure 7. Teledyne Systems stated that the bearings were lubricated with KG-80 which is an aliphatic hydrocarbon and its IR curve as shown in Figure 7 is consistent with the oil samples removed from the retainers.

One of the new bearings, S/N E2, was disassembled and parts from it were compared to the used bearings to evaluate the wear. Figure 8 shows the inner races of all 3 bearings; note that the two used inner races show double wear tracks, which can be caused by a step or a sudden change in load. Mr. John Ritter of Teledyne Systems stated that it is not unusual for gyro bearings to exhibit double wear tracks. SEM photos, shown in Figure 9, of the inner races of E2 and B40 show that E2 is smooth while the wear area of B40 is filled with tiny pits and scratch-like deformations. Figure 10 shows the SEM photos of two balls. The E2 ball's surface is smooth while the B40 ball has numerous tiny pits. B58 had an appearance similar to but less pronounced than that of B40 since B58 had less wear than B40 (150 particles as compared to 500 particles). These tiny pits on the surface of B40 and B58 are the origination of the wear particles described above.

TABLE I

Summary of Design Parameters for the Strapdown Gyro

GENERAL	
Weight	< 2.3 Lbs.
Size	3" Dia. x 3" Long
Torque Required for 1°/hr. Rate	5 Dyne-Cm/$^{\circ}$/Hr.
Figure of Merit	300
g-Capability	150 G's
ROTOR	
Mass of Rotor	260 GMS
Polar Moment of Rotor	1600 GM-CM^2
Angular Momentum @ 100 RPS	1 x 10^6 GM-CM^2/SEC
SUSPENSION	
Number of Gimbals	3
Mass of Gimbals and Weights	33 GMS
TORQUER	
Maximum flux density in inner/outer flux rings	4.5 kilo gauss
Average field flux density of air gap	3.0 kilo gauss
Nominal torquer scale factor	160°/hr/ma
Nominal power required for 100°/sec rate (about one axis)	40 watts
BALANCING/TUNING ADJUSTABILITY	
Tuned frequency adjustability	$\pm$6 Hz (Mech.)
Axis separation adjustment	$\pm$.002 In. Minimum
Axial adjustment of rotor "GG"	$\pm$.003 In. Minimum
Radial adjustment of rotor "GG"	.005 In. Minimum
STRUCTURAL	
Minimum low axial frequency (15° CA)	650 Hz
Nominal low torsional frequency (15° CA)	425 Hz

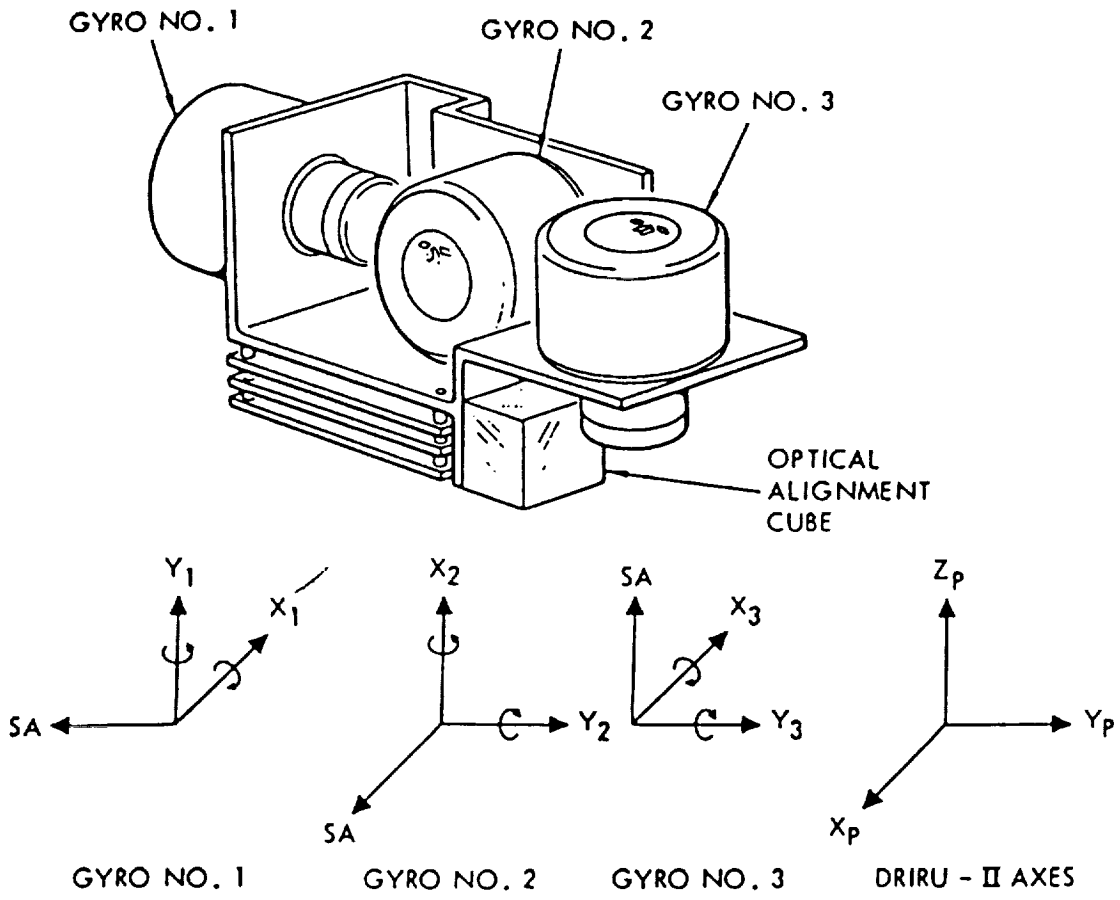

Figure 1. Exploded View of Gyros and Instrument Mount Snowing Gyro Axes Orientation.

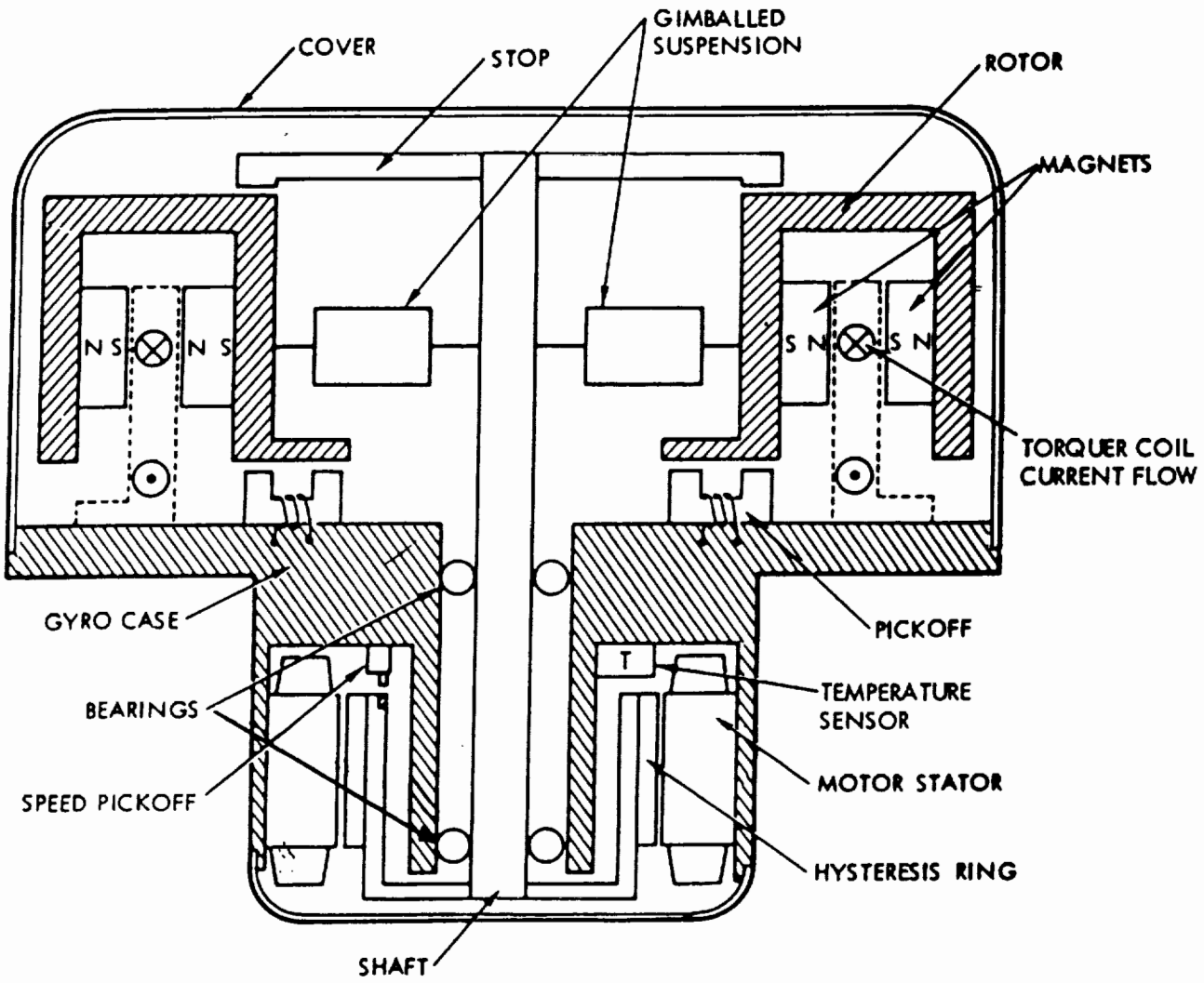

Figure 2. Schematic Cross-Section of the Strapdown Gyro

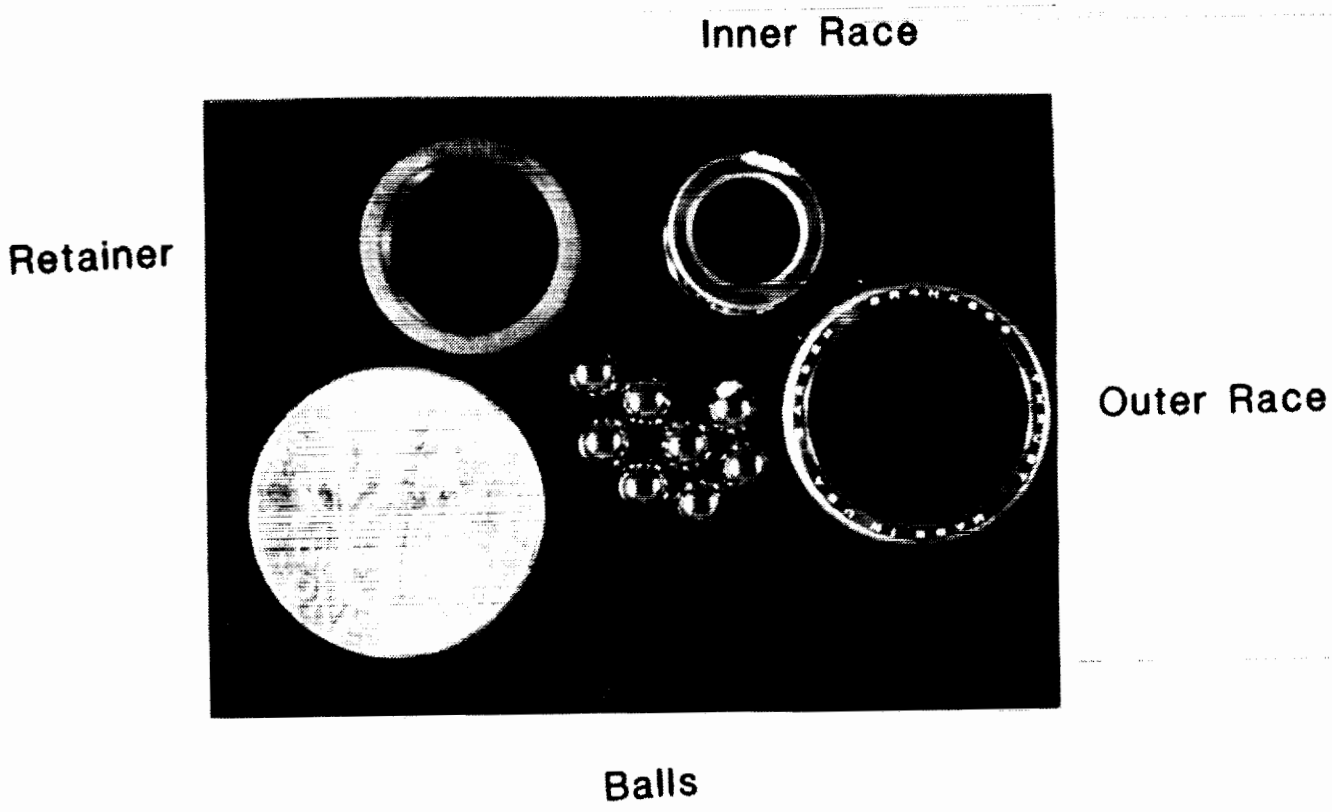

Figure 3. Disassembled new gyroscope bearing E2 shown with dime to indicate size.

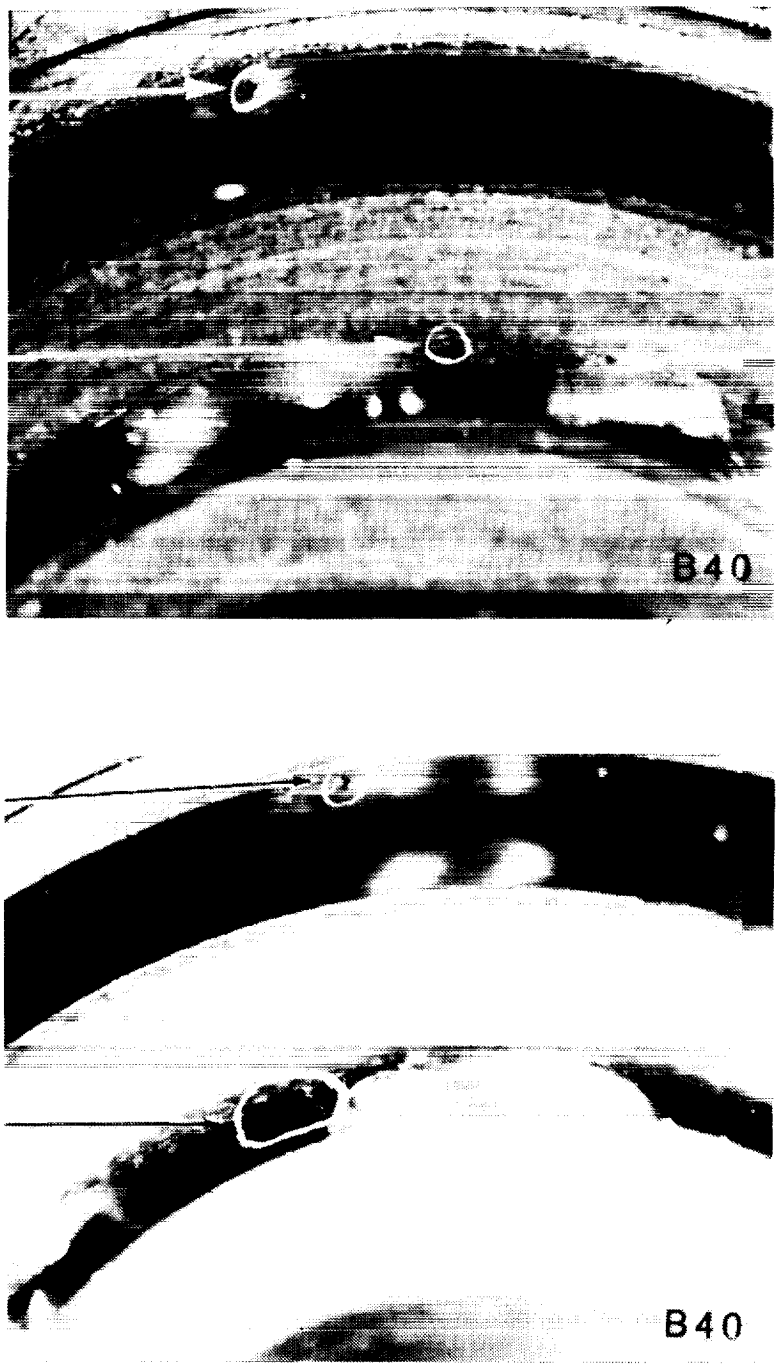

Figure 4. Typical particles observed clinging to B40 while still in gyroscope., 20×.

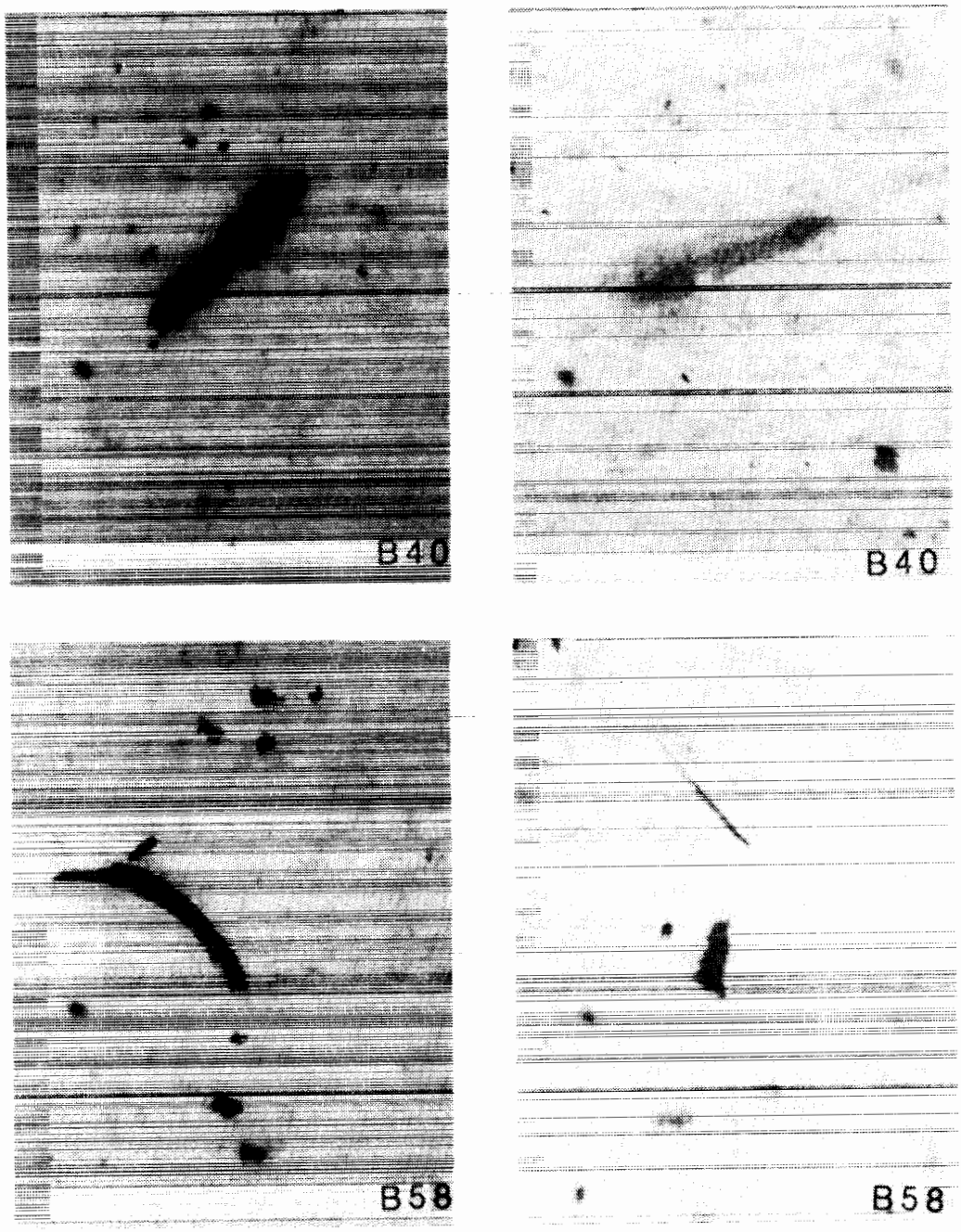

Figure 5. Typical particles collected off of B40, top, and B58, bottom. 56×.

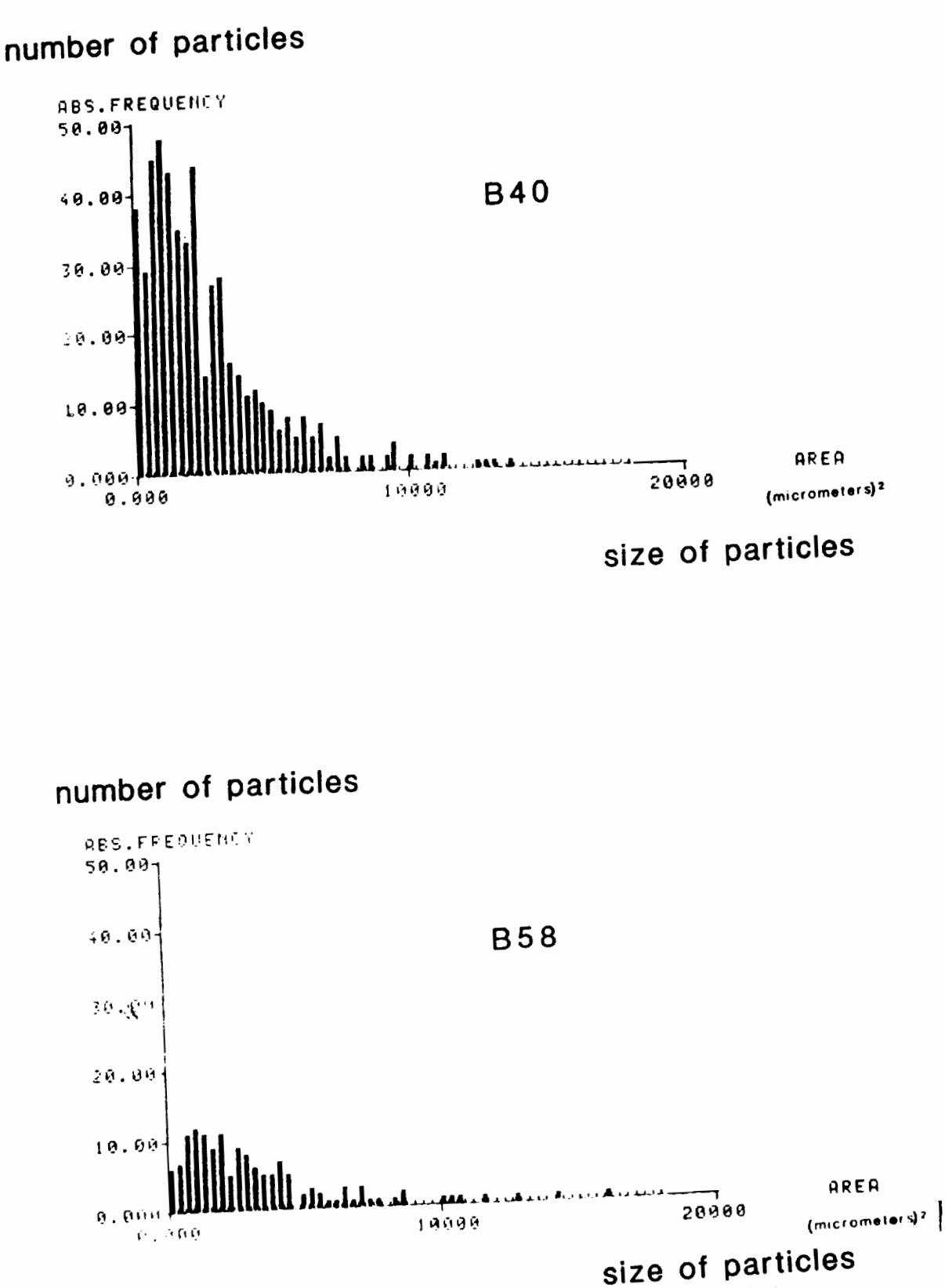

Figure 6. Histograms of particle count of debris--B40, top graph, and B58, bottom graph.

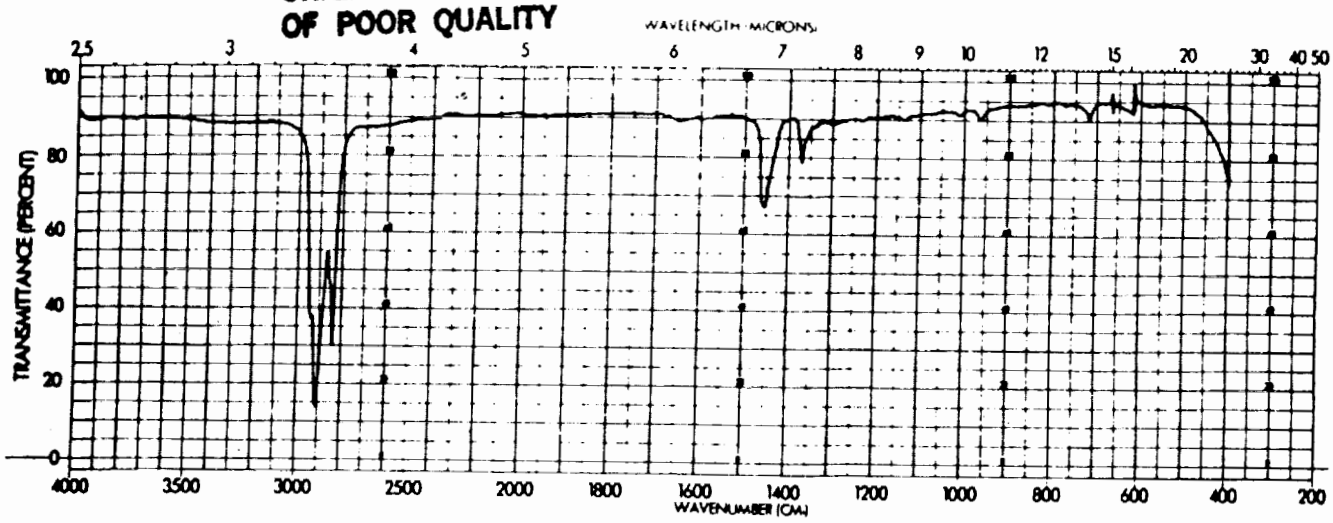

KG-80 oil.

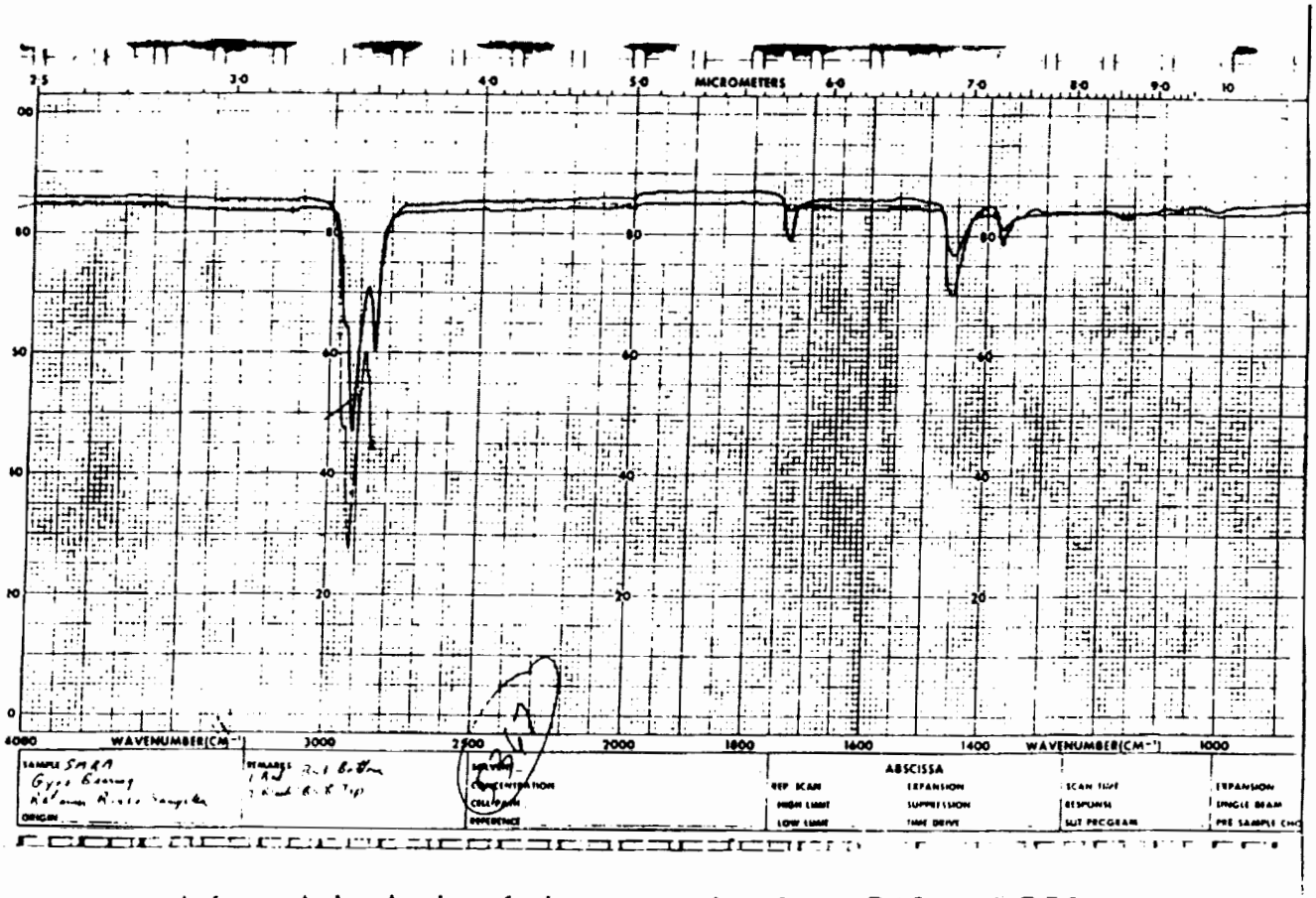

Infrared Analysis of rinse samples from B40 and B58

Figure 7. Infrared Analysis of alleged gyroscope lubricant, KG-80, top curve, and actual lubricant in B40 and B58, bottom curves. All three are aliphatic hydrocarbon lubricants.

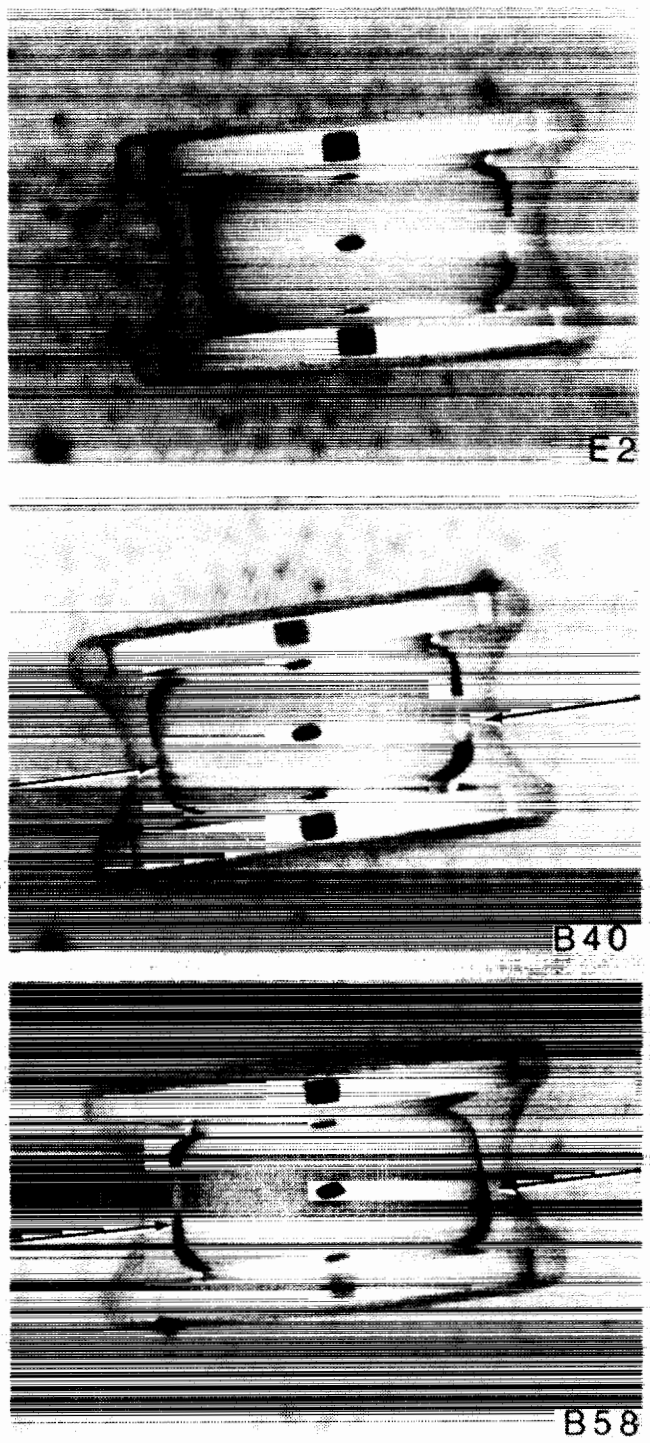

Figure 8. Inner races of bearings—top to bottom—E2, B40, B58. Note double wear tracks indicated by arrows on B40 and B58. 7.5×.

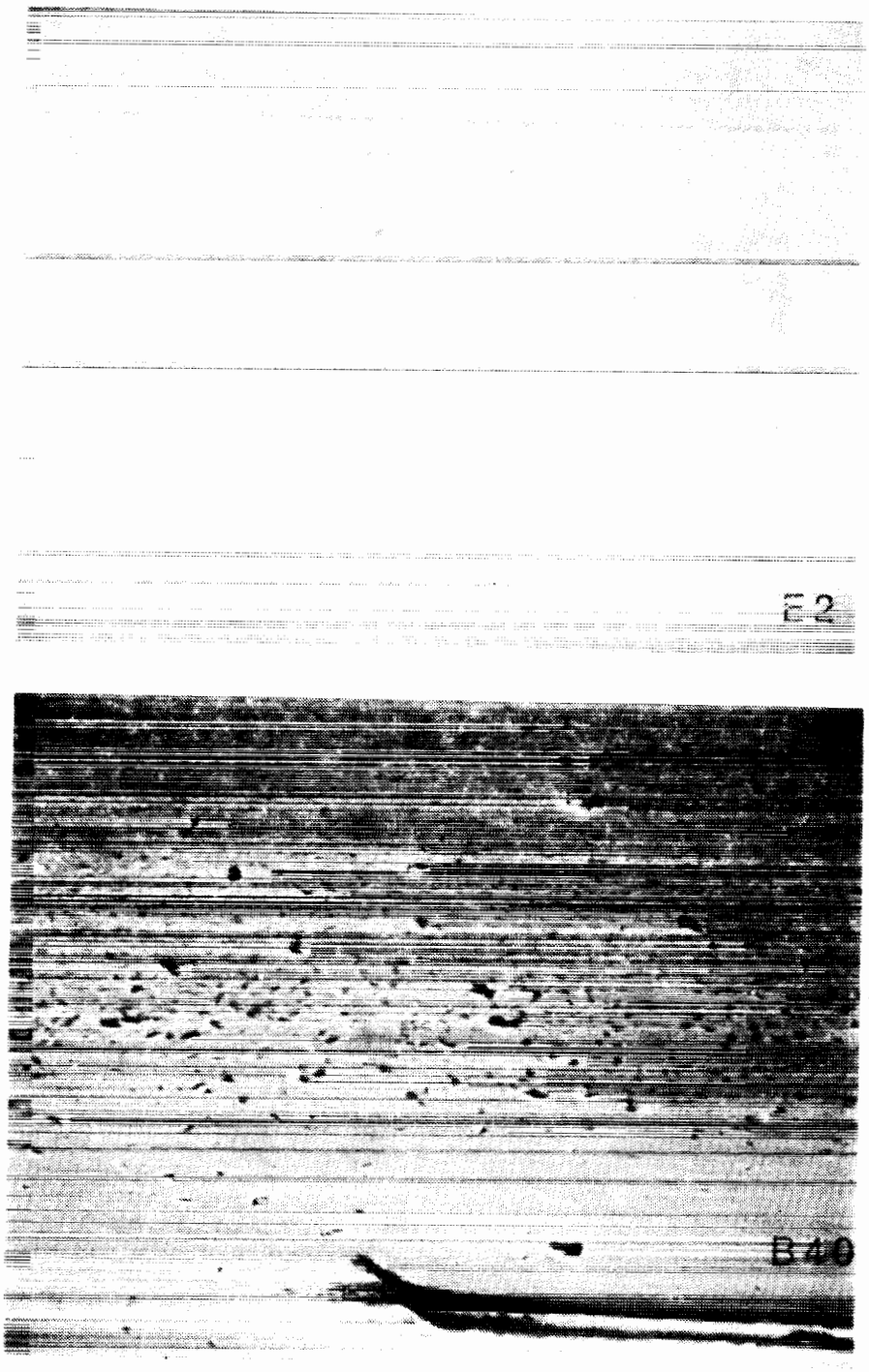

Figure 9. SEM photos of innter race of E2, top, and wear area of B40, bottom. 1250×.

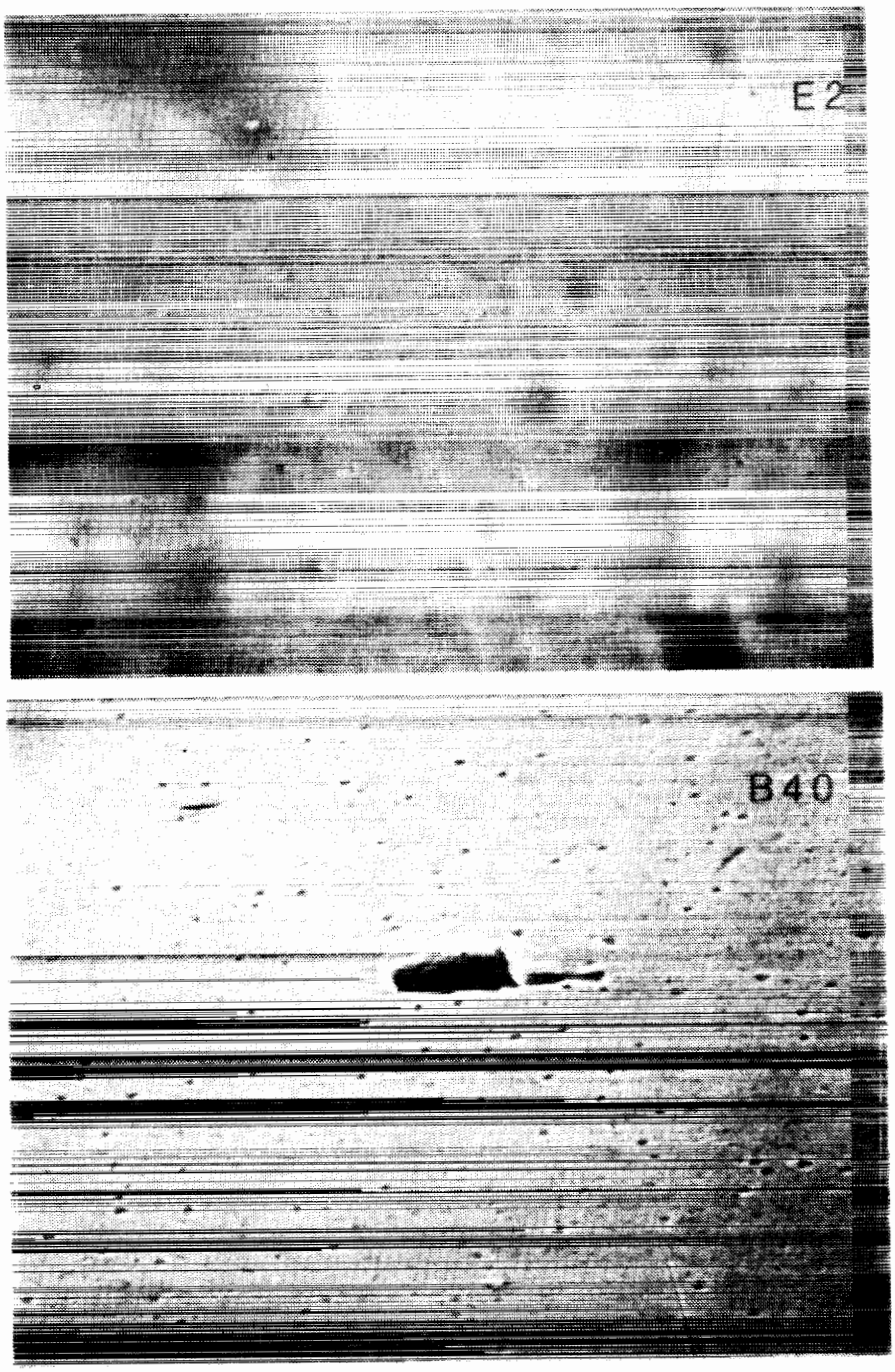

Figure 10. SEM photos of balls from E2, top, and B40, bottom. Note "large" pit is 115 square micrometers. 1250×.

(This page intentionally left blank)

MACS RIU SN23 EVALUATION

FAIRCHILD SPACE COMPANY

- LOCATED IN MACS MODULE "B" SIDE
- OPERATED IN "OFF" MODE DURING FLIGHT
  - POWER SUPPLY ON
  - BUS TRANSCEIVER ON
- VERIFIED OPERATIONAL PRIOR TO LAUNCH, FEBRUARY 1980
- VERIFIED OPERATIONAL POST SMRM, APRIL 1984
- ENGINEERING EVALUATION PERFORMED DECEMBER 1984 - APRIL 1985
- RIU #23 MEETS ALL SPECS OVER QUAL TEMPERATURE RANGE
- NO DEGRADATION OBSERVED

FAIRCHILD SPACE COMPANY

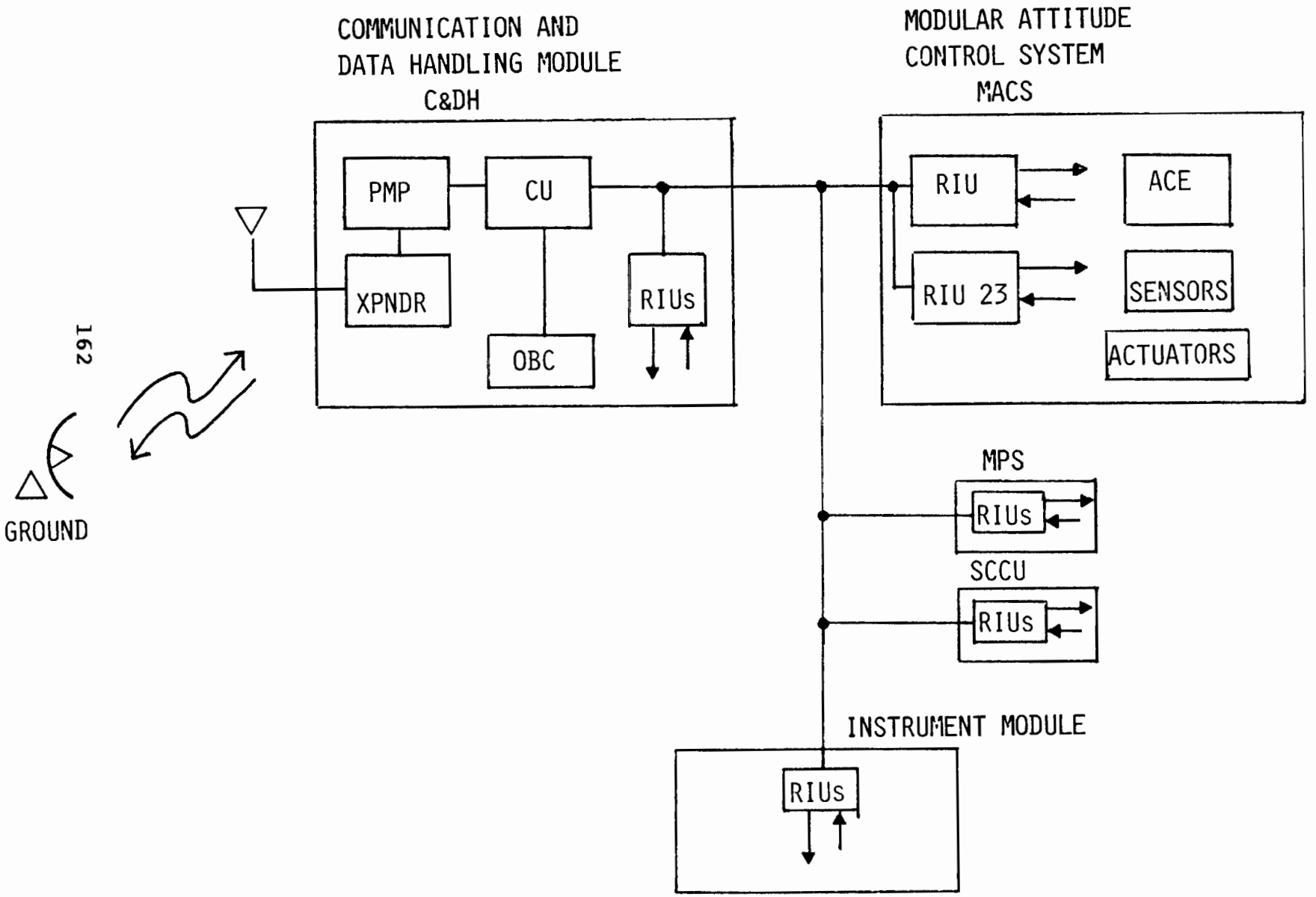

POST FLIGHT ENGINEERING EVALUATION

VISUAL INSPECTION	NO VISUAL DEGRADATION
AMBIENT PERFORMANCE	
AUTOMATED "GO - NOGO"	PASSED
READ AND RECORD PARAMETERS	ALL PARAMETERS WITHIN SPEC
ENVIRONMENTAL PERFORMANCE	
AMBIENT PERFORMANCE "GO - NOGO"	PASSED, RETORQUED CONNECTOR MOUNTING LUG
AMBIENT PERFORMANCE "GO - NOGO"	PASSED
COLD -20°C (QUAL LIMIT)	
2 HOUR SOAK	
PERFORMANCE "GO - NOGO"	PASSED
READ AND RECORD	ALL PARAMETERS WITHIN SPEC
HOT +60°C (QUAL LIMIT)	
2 HOUR SOAK	
PERFORMANCE "GO - NOGO"	PASSED
READ AND RECORD	ALL PARAMETERS WITHIN SPEC
AMBIENT	
PERFORMANCE "GO - NOGO"	PASSED
READ AND RECORD	ALL PARAMETERS WITHIN SPEC
INTERNAL VISUAL INSPECTION	NO VISUAL DEGRADATION

RIU ANALOG TO DIGITAL CONVERSION CIRCUITRY

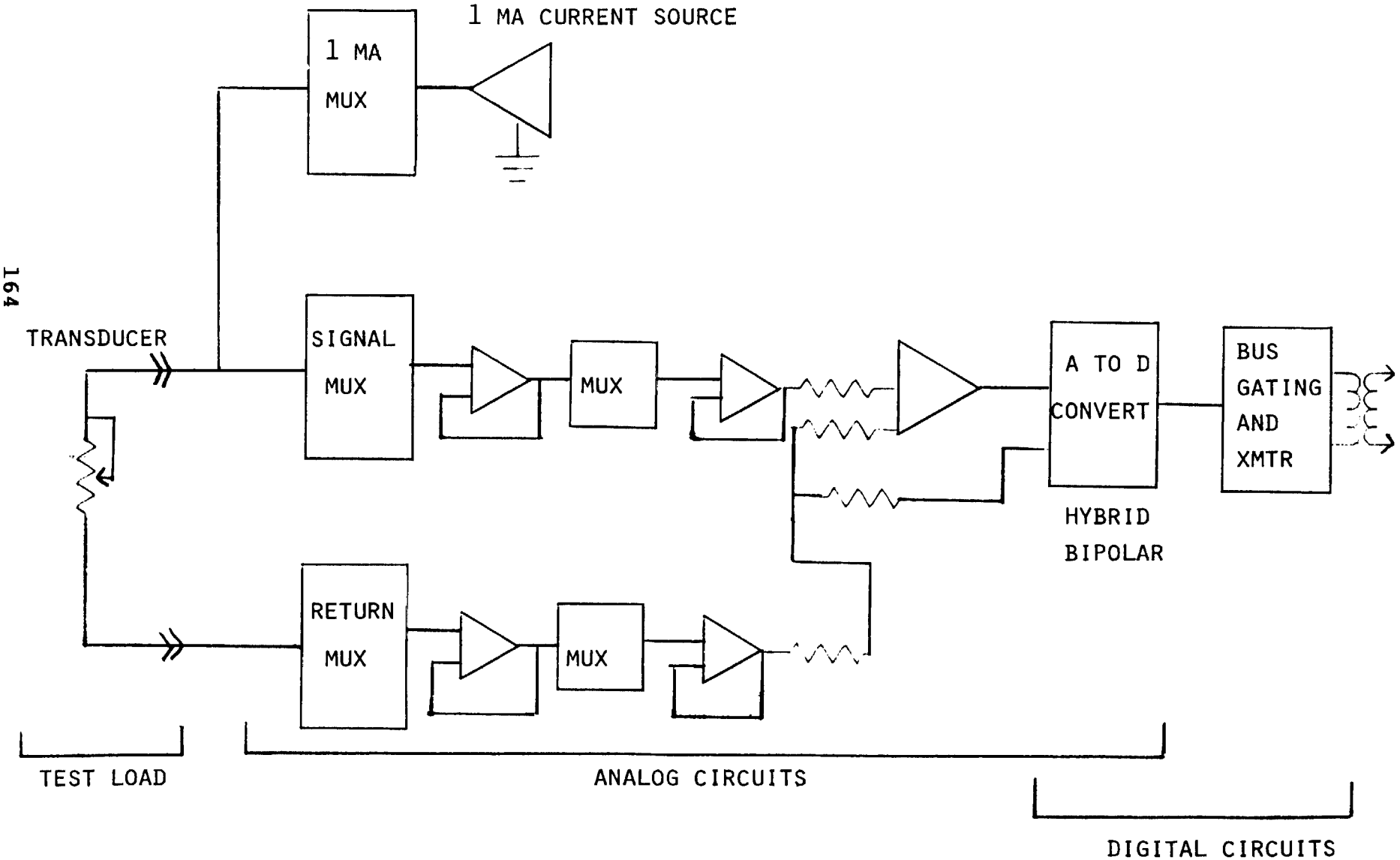

FAIRCHILD SPACE COMPANY

ANALOG TO DIGITAL CONVERTER ACTIVE ANALOG LINEARITY

		PRELAUNCH	POST SMM FLIGHT	SPEC ± 10mV
AMBIENT		12	6	10
		1274	1266	1270
		2554	2551	2550
		5089	5091	5090
COLD	-10°C	9	6	10
		1271	1265	1270
		2553	2553	2550
		5085	5091	5090
	-20°C			
HOT	+50°C	10	6	10
		1271	1267	1270
		2558	2554	2550
		5088	5093	5090
	+60°C			

FAIRCHILD SPACE COMPANY

ANALOG TO DIGITAL CONVERTER PASSIVE ANALOG LINEARITY

		PRELAUNCH		POST SMM FLIGHT	SPEC ± 10mV
AMBIENT		13		10	10
		171		170	170
		2544		2536	2540
COLD	-10°C	9	-20°C	7	10
		169		171	170
		2550		2544	2540
HOT	+50°C	10	+60°C	8	10
		170		168	170
		2538		2543	2540

FAIRCHILD SPACE COMPANY

READ AND RECORD PARAMETERS

PULSE COMMAND

- CURRENT
- PULSE WIDTH

SERIAL DIGITAL COMMAND

A TO D LINEARITY

SERIAL DIGITAL TELEMETRY

POWER DISSIPATION

PHASE LOCK LOOP

SUMMARY

NO VISIBLE DEGRADATION

READ AND RECORD PARAMETERS WITHIN SPECIFICATION,
SOME "BETTER" THAN PRELAUNCH

NO DEGRADATION DUE TO ON-ORBIT ENVIRONMENT PRECLUDES
REUSE OF RIU

CONSIDER ORBITING RIU'S FOR 4 YEARS PRIOR TO LAUNCH.

THE FOLLOWING IS AN EXCERPT FROM THE REPORT "POSTFLIGHT EVALUATION OF THE SOLAR MAXIMUM SPACECRAFT MAGNETOMETERS." THE COMPLETE REPORT MAY BE OBTAINED FROM THE SATELLITE SERVICING PROJECT LIBRARY, (#408-01643), GODDARD SPACE FLIGHT CENTER.

POSTFLIGHT EVALUATION OF THE SOLAR MAXIMUM SPACECRAFT MAGNETOMETERS

PREPARED BY

Warren D. Dunham
Schonstedt Instrument Company
1775 Wiehle Avenue
Reston, VA 22090

April 8, 1985

TABLE OF CONTENTS

SOLAR MAXIMUM THREE AXIS MAGNETOMETER (TAM)

Manufactured by: SCHONSTEDT INSTRUMENT COMPANY
RESTON, VIRGINIA

Administrative contact: Charles R. Upton
Technical contact: Warren D. Dunham

Solar Maximum Mission spacecraft was launched February 14, 1980 from Cape Kennedy. Attached to one side of the spacecraft was the Modular Attitude Control System (MACS), manufactured by General Electric. Two Schonstedt magnetometers were located within the MACS module.

Although primarily used as a backup attitude determination system during the Solar Maximum Repair Mission, the magnetometers were instrumental in stabilizing the spacecraft. The spacecraft became unstable when retrieval operations were initiated. The "B." or "BDOT" program was transmitted to the spacecraft control unit, and the outputs of one magnetometer were used in coordination with the spacecraft torqueing bars to stabilize Solar Maximum.

In October of 1984 the Solar Maximum magnetometers were returned to Schonstedt Instrument Company for postflight analysis. One magnetometer, designated the primary unit, was utilized by the attitude and control system as required. The other magnetometer served as a backup unit in the event the primary magnetometer failed. No malfunctions occurred with the primary magnetometer, so the backup magnetometer was never employed.

When these magnetometers were returned to Schonstedt Instrument Company, they were subjected to the same electrical performance tests that they experienced prior to delivery to General Electric. In both instances the magnetometer performance was exceptional. Postflight test data nearly duplicated preflight test data.

MAGNETOMETER SERIAL NUMBER 16851

	SENSITIVITY	ZERO
(1) Maximum Variation	.44 Percent	.010 Volts
(2) Average Variation	-.11 Percent	-.003 Volts

(3)	Standard Deviation	.17 Percent	.004 Volts
(4)	Specification Limit	1.00 Percent	.010 Volts
	SUMMARY	In Spec.	In Spec.

MAGNETOMETER SERIAL NUMBER 16852

		SENSITIVITY	ZERO
(1)	Maximum Variation	.86 Percent	.009 Volts
(2)	Average Variation	.09 Percent	-.001 Volts
(3)	Standard Deviation	.33 Percent	.004 Volts
(4)	Specification limit	1.00 Percent	.010 Volts
	SUMMARY	In Spec.	In Spec.

Postflight testing revealed that both magnetometers still satisfied the original specification requirements (G.E. Specification number SVS-9675).

(1) Even though the sensor orthogonality measurements are still within the original magnetometer specification limits, it is believed that the sensor alignment angles recorded during postflight testing should be used for data evaluation. In the seven years since the Solar Maximum magnetometers were manufactured, the ability to accurately calibrate the sensor alignment fixture has been improved. Since the magnetometer sensor is a rigid, encapsulated assembly, it is doubtful that there has been any change in the sensor alignment. The apparent variation in alignment is due strictly to an inability seven years ago, to accurately measure the misalignment error of the old alignment fixture.

(2) The indicated improvement in magnetometer efficiency is misleading. This particular test is poorly defined in the original acceptance test procedure and is not easily repeatable as defined. The acceptance test procedure states that the magnetometer current will be measured with all outputs in saturation. However, the magnetometer power consumption is not symmetrical. The negative supply current is derived from the magnetometer drive circuitry with a typical efficiency of less than fifty percent. This means that there is a potential fifty percent variation in each signal channel operating current depending upon whether it is in negative or positive saturation. Moreover, since each channel incorporates output limiting

diodes, the magnitude of saturation is also critical. This test should be performed with the magnetometer sensor in a shield. Only when the magnetometer sensor is in a controlled environment can we obtain repeatable current measurements.

Retesting of the Solar Maximum magnetometers consisted of rerunning the preflight ATP with the exception of the random vibration test. The ATP tests are listed below.

1. Electrical performance @ Room Temperature and 28 VDC
2. Electrical performance @ Room Temperature and 24.5 VDC
3. Electrical performance @ Room Temperature and 31.5 VDC
4. Output Ripple
5. Output Noise
6. Electrical performance @ -10 Degrees Centigrade
7. Electrical performance @ +61 Degrees Centigrade
8. Orthogonality
9. Insulation Resistance

A tabulation summary of the magnetometer test results, including the variations between preflight and postflight data, is attached to this report.

Appendix A contains the preflight and postflight test results for Magnetometer Serial Number 36851, and Appendix B contains the preflight and postflight test results for Magnetometer Serial Number 36852.

Nearly seven years have passed since these magnetometers were manufactured and the preflight tests performed. Subsequent to the acceptance tests the magnetometers were subjected to the physical stresses of launch and the spaceflight environment for almost three and a half years. Considering the elapsed time, the variation between preflight test data and postflight test data is trivial.

SCHONSTEDT INSTRUMENT COMPANY
RESTON, VIRGINIA 22102

MAGNETOMETER S/N: 18991
MODEL # SAM-63C-5

Test	Axis	Output	SENSITIVITY Initial (Volts/Gauss)	SENSITIVITY Postflight (Volts/Gauss)	SENSITIVITY Delta (%)	ZERO Initial (Volts)	ZERO Postflight (Volts)	ZERO Delta (Volts)
2	X	ACE	-10.011	-10.015	0.04	0.001	0.005	0.004
RT		RIUA	2.503	2.503	0.00	2.500	2.493	-0.007
		RIUB	2.507	2.508	0.04	2.499	2.492	-0.007
	Y	ACE	-10.016	-10.015	-0.01	0.001	0.002	0.001
		RIUA	2.507	2.507	0.00	2.499	2.493	-0.006
		RIUB	2.513	2.513	0.00	2.498	2.491	-0.007
	Z	ACE	-10.008	-10.005	-0.03	0.002	0.006	0.004
		RIUA	2.510	2.509	-0.04	2.497	2.490	-0.007
		RIUB	2.505	2.504	-0.04	2.499	2.492	-0.007
17	X	ACE	-10.056	-10.015	-0.41	0.007	0.003	-0.004
HOT		RIUA	2.514	2.503	-0.44	2.501	2.497	-0.004
		RIUB	2.523	2.512	-0.44	2.503	2.498	-0.005
	Y	ACE	-10.010	-10.021	0.11	-0.003	0.002	0.005
		RIUA	2.505	2.507	0.08	2.505	2.497	-0.008
		RIUB	2.515	2.517	0.08	2.505	2.497	-0.008
	Z	ACE	-10.033	-9.998	-0.35	-0.005	0.005	0.010
		RIUA	2.514	2.506	-0.32	2.502	2.494	-0.008
		RIUB	2.513	2.505	-0.32	2.506	2.498	-0.008
18	X	ACE	-10.024	-10.022	-0.02	-0.006	0.004	0.010
COLD		RIUA	2.508	2.505	-0.12	2.490	2.488	-0.002
		RIUB	2.507	2.505	-0.08	2.488	2.485	-0.003
	Y	ACE	-10.022	-10.021	-0.01	-0.003	0.002	0.005
		RIUA	2.510	2.509	-0.04	2.490	2.486	-0.004
		RIUB	2.511	2.511	0.00	2.489	2.485	-0.004
	Z	ACE	-10.016	-9.997	-0.19	0.001	0.002	0.001
		RIUA	2.514	2.507	-0.28	2.490	2.485	-0.005
		RIUB	2.503	2.499	-0.16	2.491	2.486	-0.005

TEST #24 - ALIGNMENT (Degrees)

Axis	Initial	Postflight	Delta	Spec. Limit	Summary
X	0.03	0.16	0.13	0.25	In Spec
Y	0.02	0.07	0.05	0.25	In Spec
Z	0.02	0.16	0.14	0.25	In Spec

TEST # 5 - CURRENT DRAIN (Milliamperes)

Initial	Postflight	Delta	Spec. Limit	Summary
42.0	38.9	-3.1	60	In Spec

SCHONSTEDT INSTRUMENT COMPANY
RESTON, VIRGINIA 22102

MAGNETOMETER S/N: 16851
MODEL # SAM-63C-5

DATA SUMMARY

Number	SENSITIVITY Initial (Volts/Gauss)	SENSITIVITY Postflight (Volts/Gauss)	Delta (%)	ZERO Initial (Volts)	ZERO Postflight (Volts)	Delta (Volts)
1	-10.011	-10.015	0.04	0.001	0.005	0.004
2	2.503	2.503	0.00	2.500	2.493	-0.007
3	2.507	2.508	0.04	2.499	2.492	-0.007
4	-10.016	-10.015	-0.01	0.001	0.002	0.001
5	2.507	2.507	0.00	2.499	2.493	-0.006
6	2.513	2.513	0.00	2.498	2.491	-0.007
7	-10.008	-10.005	-0.03	0.002	0.006	0.004
8	2.510	2.509	-0.04	2.497	2.490	-0.007
9	2.505	2.504	-0.04	2.499	2.492	-0.007
10	-10.056	-10.015	-0.41	0.007	0.003	-0.004
11	2.514	2.503	-0.44	2.501	2.497	-0.004
12	2.523	2.512	-0.44	2.503	2.498	-0.005
13	-10.010	-10.021	0.11	-0.003	0.002	0.005
14	2.505	2.507	0.08	2.505	2.497	-0.008
15	2.515	2.517	0.08	2.505	2.497	-0.008
16	-10.033	-9.998	-0.35	-0.005	0.005	0.010
17	2.514	2.506	-0.32	2.502	2.494	-0.008
18	2.513	2.505	-0.32	2.506	2.498	-0.008
19	-10.024	-10.022	-0.02	-0.006	0.004	0.010
20	2.508	2.505	-0.12	2.490	2.488	-0.002
21	2.507	2.505	-0.08	2.488	2.485	-0.003
22	-10.022	-10.021	-0.01	-0.003	0.002	0.005
23	2.510	2.509	-0.04	2.490	2.486	-0.004
24	2.511	2.511	0.00	2.489	2.485	-0.004
25	-10.016	-9.997	-0.19	0.001	0.002	0.001
26	2.514	2.507	-0.28	2.490	2.485	-0.005
27	2.503	2.499	-0.16	2.491	2.486	-0.005

	SENSITIVITY Variation (Percent)		ZERO Variation (Volts)	
	Maximum	0.44	Maximum	0.010
	Average	-0.11	Average	-0.003
	Dstd.	0.17	Dstd.	0.005
	Spec limit	1.00	Spec limit	0.010
	SUMMARY	In Spec.	SUMMARY	In Spec

SCHONSTEDT INSTRUMENT COMPANY
RESTON, VIRGINIA 22102

MAGNETOMETER S/N: 16852
MODEL # SAM-63C-5

Test	Axis	Output	SENSITIVITY Initial (Volts/Gauss)	SENSITIVITY Postflight (Volts/Gauss)	SENSITIVITY Delta (%)	ZERO Initial (Volts)	ZERO Postflight (Volts)	ZERO Delta (Volts)
2 RT	X	ACE	-10.001	-10.007	0.06	0.003	0.003	0.000
		RIUA	2.501	2.506	0.20	2.497	2.493	-0.004
		RIUB	2.508	2.510	0.08	2.503	2.499	-0.004
	Y	-10.0	-10.024	-10.015	-0.09	0.001	0.002	0.001
		RIUA	2.507	2.507	0.00	2.504	2.495	-0.009
		RIUB	2.499	2.501	0.08	2.500	2.499	-0.001
	Z	ACE	-10.019	-10.015	-0.04	0.002	0.004	0.002
		RIUA	2.502	2.500	-0.08	2.499	2.494	-0.005
		RIUB	2.502	2.500	-0.08	2.499	2.494	-0.005
17 HOT	X	ACE	-9.995	-10.007	0.12	-0.002	0.003	0.005
		RIUA	2.493	2.507	0.56	2.503	2.498	-0.005
		RIUB	2.501	2.513	0.48	2.510	2.504	-0.006
	Y	ACE	-9.931	-10.017	0.86	-0.001	0.002	0.003
		RIUA	2.485	2.506	0.84	2.505	2.500	-0.005
		RIUB	2.480	2.500	0.80	2.509	2.504	-0.005
	Z	ACE	-10.031	-10.008	-0.23	0.001	0.004	0.003
		RIUA	2.506	2.499	-0.28	2.502	2.497	-0.005
		RIUB	2.509	2.502	-0.28	2.504	2.499	-0.005
18 COLD	X	ACE	-10.013	-10.012	-0.01	-0.003	0.003	0.006
		RIUA	2.508	2.507	-0.04	2.491	2.490	-0.001
		RIUB	2.507	2.507	0.00	2.493	2.496	0.003
	Y	ACE	-10.027	-10.028	0.01	0.000	0.002	0.002
		RIUA	2.510	2.510	0.00	2.493	2.492	-0.001
		RIUB	2.501	2.501	0.00	2.498	2.496	-0.002
	Z	ACE	-10.029	-10.010	-0.19	-0.001	0.003	0.004
		RIUA	2.505	2.499	-0.24	2.494	2.492	-0.002
		RIUB	2.500	2.496	-0.16	2.493	2.491	-0.002

TEST #24 - ALIGNMENT (Degrees)

Axis	Initial	Postflight	Delta	Spec. Limit	Summary
X	0.03	0.16	0.13	0.25	In Spec
Y	0.02	0.07	0.05	0.25	In Spec
Z	0.02	0.16	0.14	0.25	In Spec

TEST # 5 - CURRENT DRAIN (Milliamperes)

Initial	Postflight	Delta	Spec. Limit	Summary
42.0	38.9	-3.1	60	In Spec

SCHONSTEDT INSTRUMENT COMPANY
RESTON, VIRGINIA 22102

MAGNETOMETER S/N: 16852
MODEL # SAM-63C-5

DATA SUMMARY

Number	SENSITIVITY Initial (Volts/Gauss)	SENSITIVITY Postflight (Volts/Gauss)	Delta (%)	ZERO Initial (Volts)	ZERO Postflight (Volts)	Delta (Volts)
1	-10.001	-10.007	0.06	0.003	0.003	0.000
2	2.501	2.506	0.20	2.497	2.493	-0.004
3	2.508	2.510	0.08	2.503	2.499	-0.004
4	-10.024	-10.015	-0.09	0.001	0.002	0.001
5	2.507	2.507	0.00	2.504	2.495	-0.009
6	2.499	2.501	0.08	2.500	2.499	-0.001
7	-10.019	-10.015	-0.04	0.002	0.004	0.002
8	2.502	2.500	-0.08	2.499	2.494	-0.005
9	2.502	2.500	-0.08	2.499	2.494	-0.005
10	-9.995	-10.007	0.12	-0.002	0.003	0.005
11	2.493	2.507	0.56	2.503	2.498	-0.005
12	2.501	2.513	0.48	2.510	2.504	-0.006
13	-9.931	-10.017	0.86	-0.001	0.002	0.003
14	2.485	2.506	0.84	2.505	2.500	-0.005
15	2.480	2.500	0.80	2.509	2.504	-0.005
16	-10.031	-10.008	-0.23	0.001	0.004	0.003
17	2.506	2.499	-0.28	2.502	2.497	-0.005
18	2.509	2.502	-0.28	2.504	2.499	-0.005
19	-10.013	-10.012	-0.01	-0.003	0.003	0.006
20	2.508	2.507	-0.04	2.491	2.490	-0.001
21	2.507	2.507	0.00	2.493	2.496	0.003
22	-10.027	-10.028	0.01	0.000	0.002	0.002
23	2.510	2.510	0.00	2.493	2.492	-0.001
24	2.501	2.501	0.00	2.498	2.496	-0.002
25	-10.029	-10.010	-0.19	-0.001	0.003	0.004
26	2.505	2.499	-0.24	2.494	2.492	-0.002
27	2.500	2.496	-0.16	2.493	2.491	-0.002

	SENSITIVITY Variation (Percent)		ZERO Variation (Volts)	
	Maximum	0.86	Maximum	0.009
	Average	0.09	Average	-0.001
	Datd.	0.33	Datd.	0.004
	Spec limit	1.00	Spec limit	0.010
	SUMMARY	In Spec.	SUMMARY	In Spec

SPERRY CORPORATION
FLIGHT SYSTEMS
P O BOX 21111
PHOENIX, ARIZONA 85036
TELEPHONE (602) 869-2311

SOLAR MAXIMUM MISSION

POST FLIGHT PERFORMANCE ANALYSES

OF

STANDARD REACTION WHEELS

S/N's 102, 103, 104, AND 105

PREPARED FOR

NATIONAL AERONAUTICS AND SPACE ADMINISTRATION

GODDARD SPACE FLIGHT CENTER

GREENBELT, MARYLAND 20771

SUMMARY

This report documents the Post Flight Analysis of the returned Solar Maximum Mission Standard Reaction Wheels, S/N's 102, 103, 104, and 105. The report presents a comparison between "as delivered" and post flight reaction wheel performance results. Included in the report is the teardown and lubrication weight analysis of RWA S/N 103.

Prepared By: Terrence J. Brandell Approved By: C Lutter

TABLE OF CONTENTS

LIST OF ILLUSTRATIONS

1.0 INTRODUCTION

On 24 January 1985, the four Solar Maximum Mission Reaction Wheels, S/N 102 through 105 were returned to Sperry for post flight analysis. The analysis consisted of visual examination, preliminary electrical checks, performance testing at ambient, hot and cold temperature environments, and internal pressure measurements. Based on the performance test results and past utilization in space, one reaction wheel was selected for teardown to study lubricant distribution, bearing and reservoir lube loss, bearing raceway condition and visual examination of conformal coating, soldering, and other internal features.

2.0 BACKGROUND

On 24 January 1985 the four Reaction Wheel Assemblies of the Solar Maximum Mission (SMM) were received from Goddard Space Flight Center on a loan basis for purposes of post flight analysis of the units. The four Reaction Wheels, S/N's 102, 103, 104, and 105 were fabricated at Sperry Flight Systems and delivered to G.E. in late 1978. The flight units were launched into space in February 1980 and after several months into the mission encountered electrical interface problems resulting in power loss to the Reaction Wheels. The Reaction Wheels were retrieved from the satellite and returned to earth in April 1984. The resultant accumulated space operation hours and reaction wheel utilization is presented in Figure 2.0.

3.0 VISUAL INSPECTION OF RECEIVED UNITS

The Reaction Wheels were receive on 24 January 1985 and found packaged separately in wooden crates which all appeared in normal condition with crate bands in place. The crates were opened one at a time and the units examined. All the flight units in general were in good condition. Each housing revealed a white paste on the mounting pads believed to be conductive contact paste. The housing for flight unit S/N 103, contained an approximate 1/4" length dent on the housing cover's outer edge approximately 130 CCW from the connector when viewing down on the unit. The dent had apparently been previously touched up with bits of the touchup paint chipped away exposing the base metal. All I.D. plates appeared in good condition. Connectors and pins for each unit were in good condition, with pins straight and knick free, however, small metallic debris was located on the connector grommet for RWA S/N 103. Other unit's grommets were clean.

S/N	Operational Hrs. @ Sperry	Operational Hrs. @ G.E. (est.)	Actual Space Hours (est.)	Total Hours (est)	Space Utilization and Comments
102	213	500	6500	7212	Reaction Wheel utilized in Pitch Attitude Control
103	233	500	6000	6733	Reaction Wheel utilized in Roll Attitude Control and also experienced a no-load/ overtemperature (60 C) condition for approximately 3 hours due to a control software problem
104	199	500	1000	1699	Reaction Wheel utilized in Skew Attitude Control
105	203	500	6500	7203	Reaction Wheel utilized in Yaw Attitude Control

Table 2.0

RWA Space Utilization

4.0 PRELIMINARY ELECTRICAL TESTING

Following visual examination of the flight units, preliminary electrical tests: continuity, bonding, and isolation were conducted. Two units were within the acceptance test limits of 0.0025 ohms. The actual bonding resistances recorded for RWA's S/N 102 and 103 were 0.0040 and 0.0051, respectively. These bonding resistances were not considered excessive and all RWA's proceeded to pressure transducer electrical measurements. The pressure transducer measurements revealed internal pressures far below atmospheric for all units therefore indicating that the vacuum seal was still present. The RWA's proceeded to power run-up for initial coastdown drag torques.

5.0 PRELIMINARY REACTION WHEEL RUN-UP/COASTDOWN

Initial power run-up and coastdown was completed on RWA's S/N's 102 throught 105 with coastdown torque vs. wheel speed presented in Figure 5.0. The drag torque curves show S/N's 102, 103, and 105 to be near identical at 2000 RPM (1.5 - 1.6 oz-in) and decreasing uniformly. The coastdown drag torque curve for RWA S/N 104 presents a lower drag torque curve than S/N's 102, 103, and 105 at 2000 RPM (1.20 oz-in) decreasing to zero speed. The drag torques of all units confirmed the presence of low internal housing pressures suitable for start of performance testing.

6.0 PERFORMANCE TESTING

Performance test was conducted using the Manual Test Console (MTC) Data Acquisition System, T337084. This system only monitors and records the reaction wheel inputs and outputs but serves no control function. Original acceptance testing on S/N's 102 through 105 was conducted using the Automatic Test System (ATS) which automatically ran the performance test defined by the operator and recorded input and output data. Subtle differences will be noticed between data outputs due to the equipment and interfaces utilized but will overall maintain performance test tolerances specified in the associated test procedure. The performance tests conducted are presented in Figure 6.0 and are identical to the original tests performed with the following differences noted:

A. Hot and cold testing was conducted without a Thermal Vacuum Chamber thus not providing a total space environment. Performance results would be identical since the unit is sealed.

B. Steady state speed test range for the MTC was within +25 RPM of 1200, 2160 RPM. Speed test range for the ATS was +5 RPM.

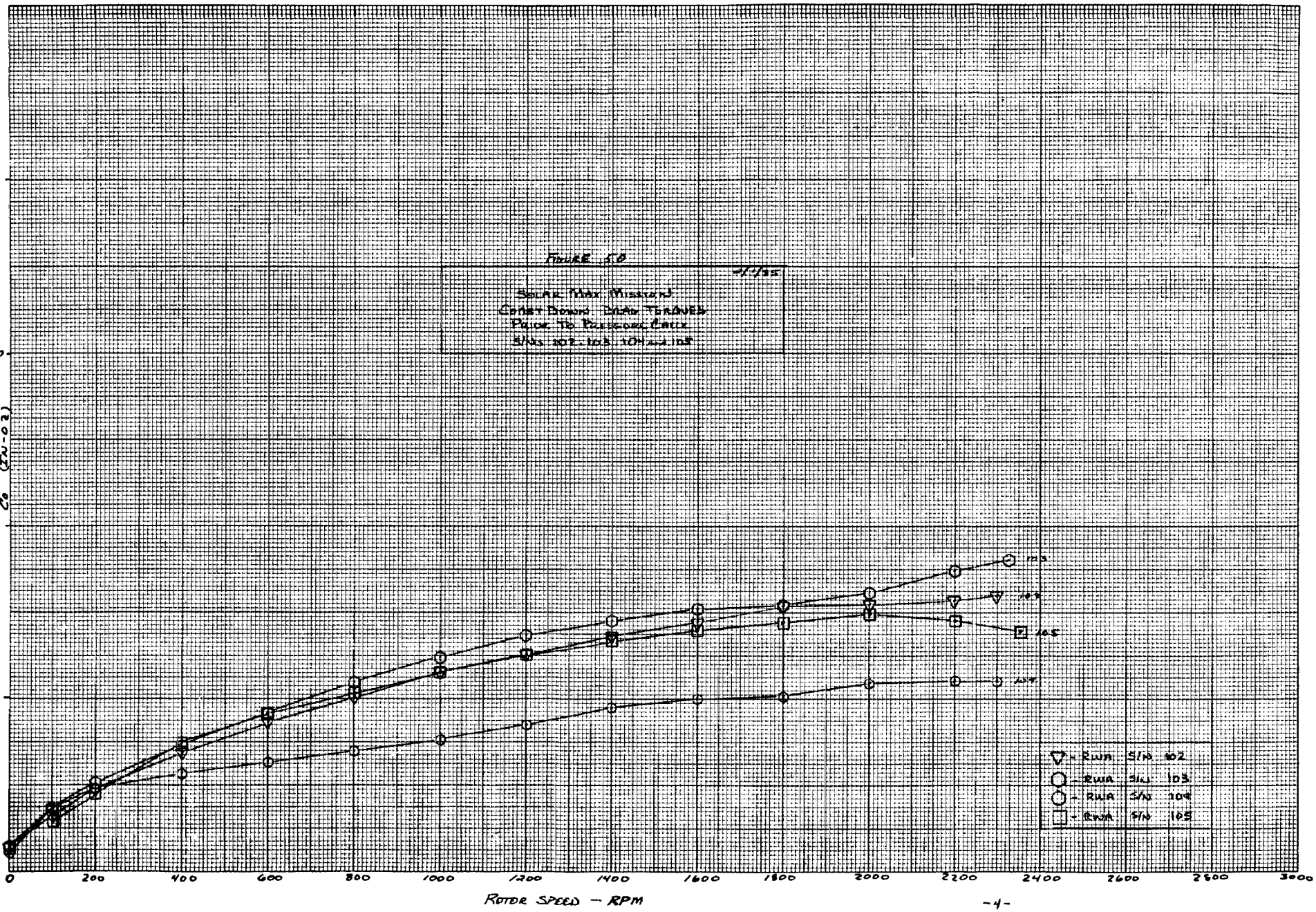

Paragraph	Test
5.3.3, 5.3.6	Reaction Torque - Acceleration/Deceleration - 24/33 Volts - CW/CCW
5.3.4, 5.3.8	Momentum - Steady State - CW/CCW
5.3.3, 5.3.6, 5.3.7, 5.3.10	Peak Power - 24/33 Volts - CW/CCW
5.3.13, 5.3.12, 5.3.15, 5.3.16	Steady State Power - CW/CCW
5.3.13, 5.3.17	Drag Torque - CW/CCW
5.3.13, 5.3.17	Rundown Time - CW/CCW
5.3.14, 5.3.18	Breakaway Torque - CW/CCW
5.3.19	Torque Noise

Table 6.0

Performance Tests Conducted @ Ambient,
40 C and 0 C Temperature Environment

C-3

C. High speed drag torque measurements occurs at 2000 RPM for the MTC vs. 2160 RPM for the ATS.

D. Torque and power "requirements" for 33 volt acceleration and deceleration tests are not a part of the MTC System; the present programs do not require 33 volt testing. The test results, however, indicate successful completion with all requirements met and are noted as such on the appropriate data sheets.

E. Motor power measurement techniques currently utilized on the MTC are more accurate than previous testing on the ATS system which derived power measurements via calibrated scaling techniques. Power is currently measured using a Yokagawa Digital Power Meter, Model Type 2503, which typically results in a lower, more accurate reading as shown by the lower power measurements recorded in this Post Flight Analysis when compared to as delivered power measurements.

A Solar Max Test Data Summary comparing "as delivered" test data to past flight test data is presented in figures 6.1 through 6.4 for RWA S/N's 102, 103, 104, and 105.

6.1 AMBIENT PERFORMANCE FUNCTIONALS

Flight units S/N's 102, 103, 104, and 105 were initially tested at ambient room temperature environment and successfully passed all tests with reasonable margin except torque noise. The RWA's exceeded the allowable position error of 1.5 0-pk for the 12 minute torque noise test at +500 RPM with a 0.1 rad/sec high pass filter. Reference Figure 6.5. These torque noise results are comparable to the Final Acceptance Test (as delivered) results of S/N's 102 through 105. The RWA's were retested for torque noise with a 0.3 rad/sec high pass filter and passed with similar results to the as-delivered RWA torque noise data.

Bearing performance of the RWA's is presented in Figure 6.6 representing bearing drag torque at 1200 and 2160 RPM rotor speed. The drag torque values reveal RWA's S/N's 102 and 103 performance to be similar to as delivered performances. RWA S/N 105 demonstrated an overall increase in drag torques in comparison to as-delivered performance data: 0.0081 - 0.0092 N-M (as retested) vs. 0.0066 - 0.0065 N-M (as delivered). RWA S/N 104 however, demonstrated an overall decreases in drag torques: 0.0058 - 0.0074 N-M (as retested) vs. 0.0074 - 0.0104 N-M (as delivered).

Figure 6.7 presents steady state power measurements at 1200 and 2160 RPM for RWA S/N's 102, 103, 104, and 105. The graph demonstrates decrease steady state power requirements for all RWA's than when previously delivered.

SOLAR MAX
TEST DATA SUMMARY
FLIGHT UNIT SERIAL NUMBER 102

TEST		TEST REQUIREMENTS		FINAL AMBIENT PERFORMANCE TEST AUG 1978	AMBIENT PERFORMANCE TEST FEB 1985	HOT THERMAL VACUUM TEST 40°C JULY 1978	HOT THERMAL TEST 40°C FEB 1985	COLD THERMAL VACUUM TEST 0°C JULY 1978	COLD THERMAL TEST 0°C FEB 1985
REACTION TORQUE 24V	ACCELERATION	225 RPM	>.15 N-M	.194	.184	.197	.186	.182	.169
		1200 RPM		.178	.181	176	.175	.180	180
	DECELERATION	225 RPM	>.15 N-M	.191	.188	.187	.189	.185	.183
		1200 RPM		.171	169	.173	.168	.168	.161
REACTION TORQUE 33V	ACCELERATION	225 RPM	>.30 N-M	.409	.371	N/A	.376	N/A	.360
		1200 RPM		.349	.349		.346		.362
	DECELERATION	225 RPM	>.30 N-M	.374	.370	N/A	.370	N/A	.355
		1200 RPM		.337	.332		.333		.317
MOMENTUM (24V)		STEADY STATE	20 N-M-S	21.7	21.4	21.8	21.4	21.8	21.4
PEAK POWER 24V	ACCELERATION	225 RPM	<75 WATTS	69.85	67.60	70.47	67.40	70.60	64.60
		1200 RPM		63.84	67.40	65.18	66.00	65.18	66.60
	DECELERATION	225 RPM	<75 WATTS	70.72	68.00	71.70	68.60	71.15	64.40
		1200 RPM		69.18	62.40	70 52	63.80	69.28	58.20
PEAK POWER 33V	ACCELERATION	225 RPM	<150 watts	137.96	135.60	N/A	136.40	N/A	130.4
		1200 RPM		121.06	131.60		128.00		130.2
	DECELERATION	225 RPM	<150 WATTS	137.36	135.60	N/A	136.40	N/A	128.4
		1200 RPM		135.16	135.40		128.00		117.6
STEADY STATE POWER		1200 RPM	<5 watts	3.45	2.28	3.02	1.18	4.46	1.66
		2160 RPM	<10 watts	6.89	5.23	6.46	3.38	7.30	5.15
DRAG TORQUE		1200 RPM	N/A	.0078	.0083	0062	.0065	.0107	.0095
		2160 RPM		.0100	.0100	.0084	.0086	.0111	0120
COAST DOWN TIME (MIN)		1200 RPM ↓ 0 RPM	N/A	41.2	43.0	59.2	60.0	28.5	27.1
BREAKAWAY TORQUE		CW	<.003 N-M	.0011	.0016	.0016	.0020	0015	.0019
		CCW		.0013	.0017	.0011	.0016	0014	0016
TORQUE NOISE		50 RPM	<1.5 DEG. (3.0° P-P)	CCW 1.084	CW 2.4° CCW 1.3°	N/A	N/A	N/A	N/A
		500 RPM		CCW 3.495	CW 4.0° CCW 4.2°				

SOLAR MAX
TEST DATA SUMMARY
FLIGHT UNIT SERIAL NUMBER 103

TEST		TEST REQUIREMENTS		FINAL AMBIENT PERFORMANCE TEST AUG 1978	AMBIENT PERFORMANCE TEST FEB 1985	HOT THERMAL VACUUM TEST 40°C JULY 1978	HOT THERMAL TEST 40°C FEB 1985	COLD THERMAL VACUUM TEST 0°C JULY 1978	COLD THERMAL TEST 0°C FEB 1985
REACTION TORQUE 24V	ACCELERATION	225 RPM	>.15 N-M	.182	.173	.196	.180	.187	.166
		1200 RPM		.178	.170	.173	.170	.178	.165
	DECELERATION	225 RPM	>.15 N-M	.185	.148	.185	.178	.185	.175
		1200 RPM		.166	.158	.171	.162	.166	.160
REACTION TORQUE 33V	ACCELERATION	225 RPM	>.30 N-M	.390	.345	N/A	.361	N/A	.340
		1200 RPM		.350	.336		.335		.345
	DECELERATION	225 RPM	>.30 N-M	.342	.347	N/A	.355	N/A	.341
		1200 RPM		.326	.302		.320		.306
MOMENTUM (24V)		STEADY STATE	20 N-M-S	21.7	20.8	21.7	20.7	21.9	20.6
PEAK POWER 24V	ACCELERATION	225 RPM	<75 WATTS	69.62	65.80	69.83	68.00	70.30	65.00
		1200 RPM		64.03	66.00	62.97	67.20	64.68	67.60
	DECELERATION	225 RPM	<75 WATTS	70.49	64.80	70.94	66.80	70.77	63.20
		1200 RPM		68.64	59.20	69.79	61.20	68.68	56.80
PEAK POWER 33V	ACCELERATION	225 RPM	<150 watts	133.75	130.00	N/A	135.40	N/A	129.60
		1200 RPM		119.21	128.00		129.20		130.00
	DECELERATION	225 RPM	<150 WATTS	136.42	130.60	N/A	135.20	N/A	127.60
		1200 RPM		133.92	123.00		125.80		116.40
STEADY STATE POWER		1200 RPM	<5 watts	3.14	3.36	3.28	2.04	3.55	4.17
		2160 RPM	<10 watts	6.07	5.48	7.01	4.40	5.59	4.80
DRAG TORQUE		1200 RPM	N/A	.0063	.0092	.0068	.0066	.0080	.0119
		2160 RPM		.0084	.0103	.0097	.0073	.0080	.0118
COAST DOWN TIME (MIN)		1200 RPM ↓ 0 RPM	N/A	43.4	39.52	52.0	55.0	29.9	23.5
BREAKAWAY TORQUE		CW	<.003 N-M	.0009	.0019	.0014	.0013	.0015	.0015
		CCW		.0013	.0021	.0011	.0014	.0014	.0018
TORQUE NOISE		50 RPM	<1.5 DEG.	CCW 1.36	CW 1.9 CCW 2.6	N/A	N/A	N/A	N/A
		500 RPM		CCW 33.6	CW 4.2 CCW 4.2				

SOLAR MAX
TEST DATA SUMMARY
FLIGHT UNIT SERIAL NUMBER 104

TEST		TEST REQUIREMENTS		FINAL AMBIENT PERFORMANCE TEST	AMBIENT PERFORMANCE TEST	HOT THERMAL VACUUM TEST 40°C	HOT THERMAL TEST 40°C	COLD THERMAL VACUUM TEST 0°C	COLD THERMAL TEST 0°C
				AUG. 1978	FEB 1985	JULY 1978	FEB 1985	JULY 1978	FEB 1985
REACTION TORQUE 24V	ACCELERATION	225 RPM	>.15 N-M	.197	.183	.191	.184	.183	.172
		1200 RPM		.180	.183	.179	.174	.185	.182
	DECELERTION	225 RPM	>.15 N-M	.196	.187	.192	.186	.186	.184
		1200 RPM		.173	.164	.172	.167	.164	.162
REACTION TORQUE 33V	ACCELERATION	225 RPM	>.30 N-M	.387	.371	N/A	.375	N/A	.362
		1200 RPM		.352	.387		.366		.365
	DECELERATION	225 RPM	>.30 N-M	.351	.365	N/A	.370	N/A	.358
		1200 RPM		.336	.320		.329		.315
MOMENTUM (24V)		STEADY STATE	20 N-M-S	21.7	21.5	21.9	21.4	21.8	21.4
PEAK POWER 24V	ACCELERATION	225 RPM	< 75 WATTS	71.3	67.00	69.85	66.80	69.65	64.80
		1200 RPM		64.7	67.20	63.00	65.40	64.78	67.40
	DECELERATION	225 RPM	< 75 WATTS	72.04	66.80	71.02	67.20	69.78	64.20
		1200 RPM		70.55	60.60	69.84	61.80	67.24	57.60
PEAK POWER 33V	ACCELERATION	225 RPM	< 150 watts	136.12	133.40	N/A	135.20	N/A	130.60
		1200 RPM		120.86	131.00		130.20		131.60
	DECELERATION	225 RPM	< 150 WATTS	141.41	133.00	N/A	136.00	N/A	129.60
		1200 RPM		134.69	122.80		126.40		118.00
STEADY STATE POWER		1200 RPM	< 5 watts	3.38	1.34	2.65	1.50	3.39	2.09
		2160 RPM	< 10 watts	7.01	3.41	5.40	3.55	5.85	3.60
DRAG TORQUE		1200 RPM	N/A	.0074	.0058	.0052	.0049	.0075	.0081
		2160 RPM		.0104	.0074	.0074	.0071	.0093	.0089
COAST DOWN TIME (MIN)		1200 RPM ↓ 0 RPM	N/A	45.9	49.6	56.1	68.7	32.4	31.3
BREAKAWAY TORQUE		CW	< .003 N-M	.0008	.0017	.0009	.0015	.0009	.0015
		CCW		.0014	.0010	.0007	.0016	.0010	.0018
TORQUE NOISE		50 RPM	< 11.5 DEG.	CCW 1.07°	CW 2.0° CCW 2.2°	N/A	N/A	N/A	N/A
		500 RPM		CCW 6.86°	CW 7.8° CCW 5.6°				

SOLAR MAX
TEST DATA SUMMARY
FLIGHT UNIT SERIAL NUMBER 105

TEST		TEST REQUIREMENTS		FINAL AMBIENT PERFORMANCE TEST	AMBIENT PERFORMANCE TEST	HOT THERMAL VACUUM TEST 40°C	HOT THERMAL TEST 40°C	COLD THERMAL VACUUM TEST 0°C	COLD THERMAL TEST 0°C
				AUG 1978	FEB 1985	JULY 1978	FEB 1985	JULY 1978	FEB 1985
REACTION TORQUE 24V	ACCELERATION	225 RPM	>.15 N-M	.193	.185	.189	.187	.175	.164
		1200 RPM		.177	.177	.175	.177	.180	.177
	DECELERATION	225 RPM	>.15 N-M	.190	.180	.186	.183	.176	.180
		1200 RPM		.167	.163	.167	.161	.159	.162
REACTION TORQUE 33V	ACCELERATION	225 RPM	>.30 N-M	.376	.360	N/A	.345	N/A	.349
		1200 RPM		.349	.362		.343		.344
	DECELERATION	225 RPM	>.30 N-M	.363	.354	N/A	.347	N/A	.345
		1200 RPM		.332	.313		.310		.307
MOMENTUM (24V)		STEADY STATE	20 N-M-S	21.8	21.4	21.8	21.4	21.8	21.3
PEAK POWER 24V	ACCELERATION	225 RPM	<75 WATTS	70.11	67.60	69.63	68.00	68.47	64.00
		1200 RPM		63.75	66.20	62.78	66.20	64.36	66.60
	DECELERATION	225 RPM	<75 WATTS	71.14	65.00	70.26	66.60	68.62	63.00
		1200 RPM		68.90	59.60	68.77	61.60	65.96	56.60
PEAK POWER 33V	ACCELERATION	225 RPM	<150 watts	134.73	131.60	N/A	126.80	N/A	127.60
		1200 RPM		120.56	128.00		121.40		128.40
	DECELERATION	225 RPM	<150 WATTS	137.33	129.80	N/A	127.20	N/A	125.40
		1200 RPM		133.70	120.40		118.80		114.40
STEADY STATE POWER		1200 RPM	<5 watts	3.09	1.32	2.86	2.42	3.86	2.93
		2160 RPM	<10 watts	5.83	4.95	6.20	3.64	5.75	5.19
DRAG TORQUE		1200 RPM	N/A	.0066	.0081	.0058	.0064	.0090	.0099
		2160 RPM		.0065	.0099	.0081	.0077	.0087	.0102
COAST DOWN TIME (MIN)		1200 RPM ↓ 0 RPM	N/A	42.2	40.3	56.4	56.1	34.8	27.4
BREAKAWAY TORQUE		CW	<.003 N-M	.0016	.0019	.0015	.0022	.0026	.0038
		CCW		.0012	.0018	.0010	.0016	.0014	.0038
TORQUE NOISE		50 RPM	<1.5 DEG.	CCW 1.302°	CW 2.5° CCW 1.60	N/A	N/A	N/A	N/A
		500 RPM		CCW 5.674°	CW 3.9° CCW 3.9°				

ORIGINAL PAGE IS
OF POOR QUALITY

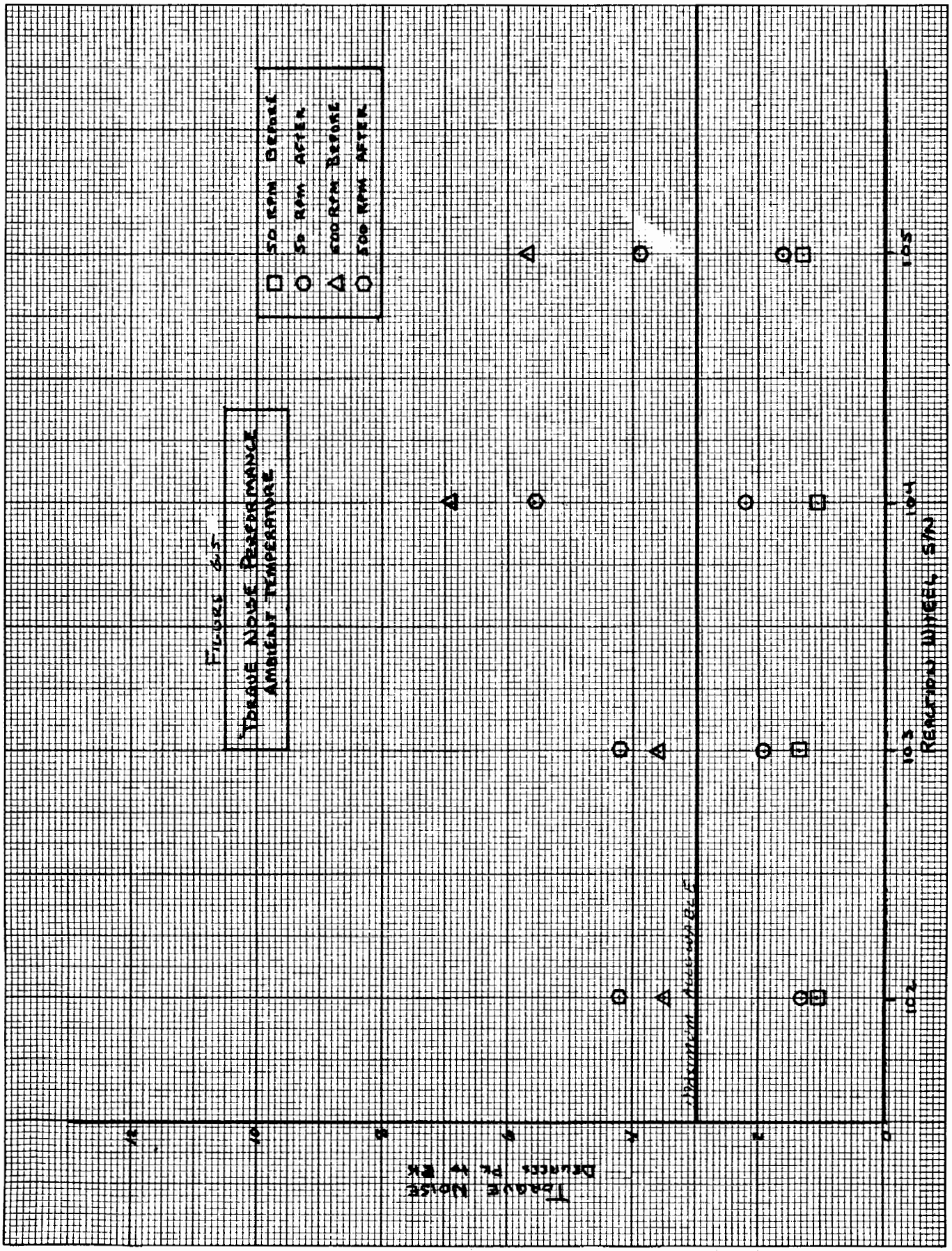

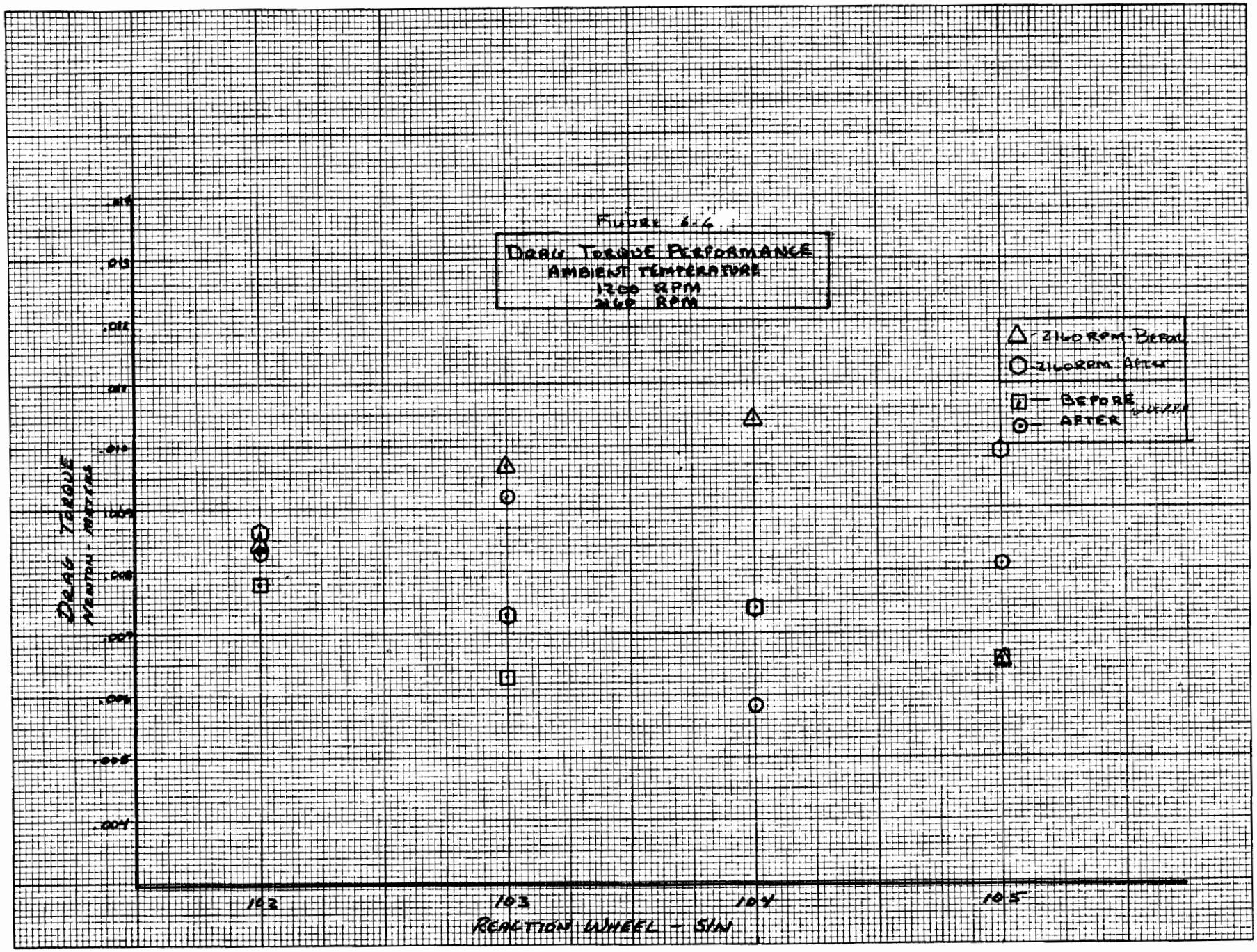
FIGURE 6-6
DRAG TORQUE PERFORMANCE
AMBIENT TEMPERATURE
1200 RPM
2160 RPM
2160 RPM - BEFORE
2160 RPM - AFTER
BEFORE
AFTER
DRAG TORQUE
NEWTON - METERS
.014
.012
.010
.008
.006
.004
102
103
104
105
REACTION WHEEL - SIN

ORIGINAL PAGE IS
OF POOR QUALITY

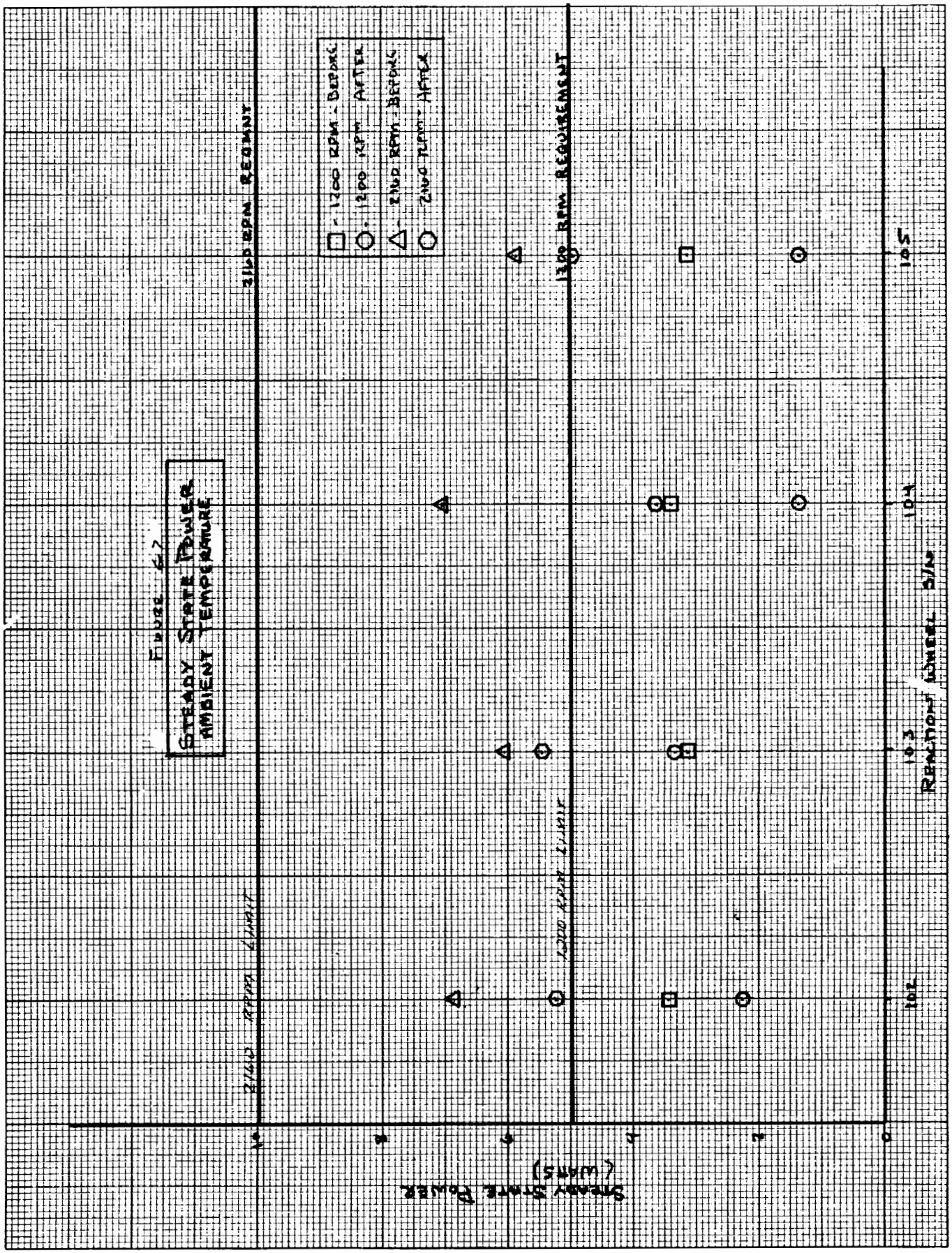

ORIGINAL PAGE IS
OF POOR QUALITY

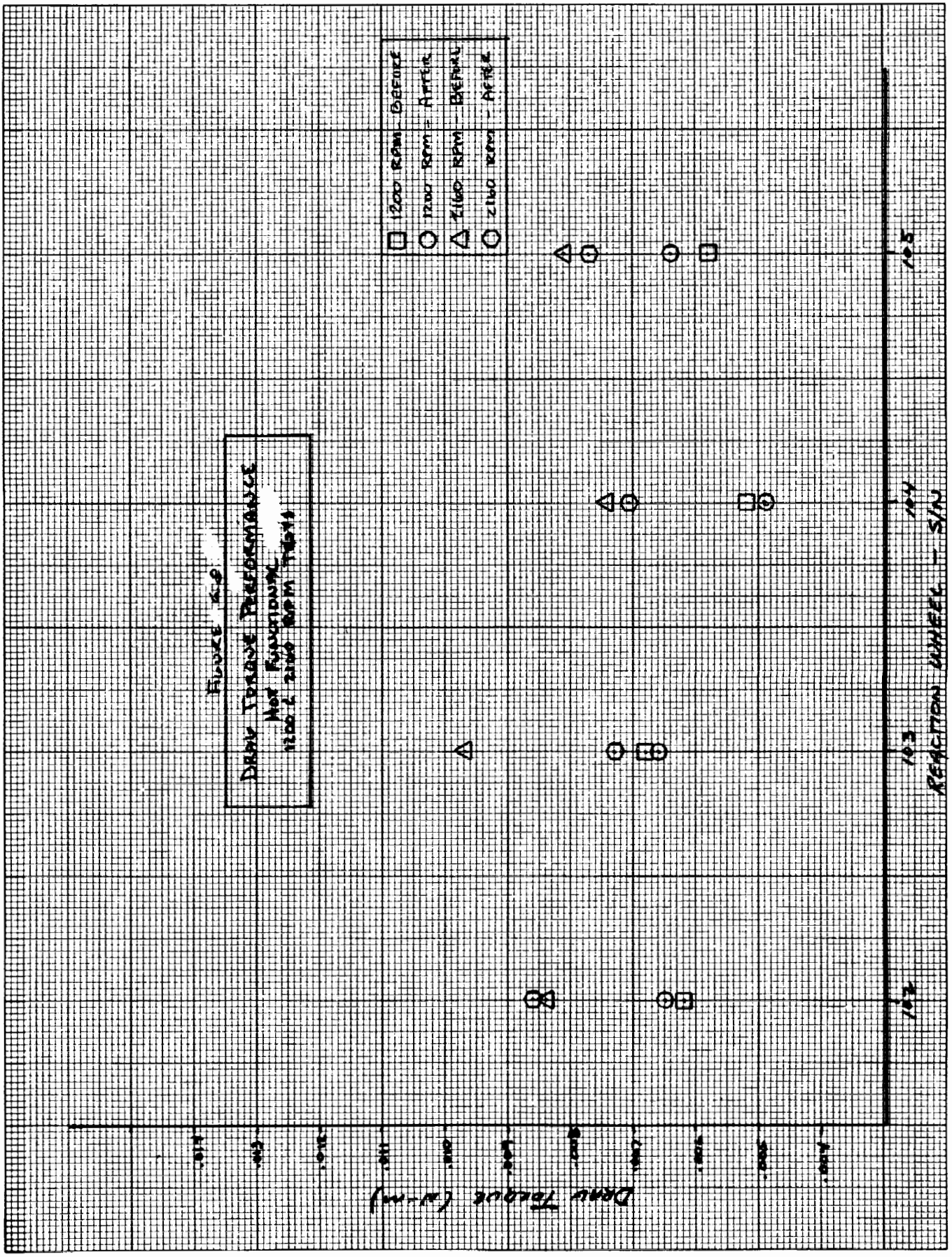

6.2 HOT FUNCTIONAL TESTING

Following ambient performance testing the RWA's were bought up to 40 C for hot functional testing. Note: These functional tests were not conducted with a vacuum environment as previosly tested. RWA's S/N 102, 103, 104, and 105 all successfully passed hot functional testing.

Bearing performances of the RWA's is presented in Figure 6.8 representing bearing drag torques at 1200 and 2160 RPM rotor speed. The graph reveals S/N's 102, 104, and 105 drag torques to be slightly decreased from as delivered. RWA S/N 103 demonstrates similar performance to as delivered at 1200 RPM and a noticeable decrease in drag torque at 2160 RPM.

Figure 6.9 presents steady state power measurements at 1200 and 2160 RPM for RWA S/N's 102, 103, 104, and 105. The graph demonstrates decreased power requirements for all RWA's with the most noticeable decreases occuring at the higher rotor speed 2160 RPM.

6.3 COLD FUNCTIONAL TESTING

Following hot functional testing the RWA's were brought down to 0 C for cold functional testing. Note: These functional tests were not conducted with a vacuum environment as previously tested. RWA's S/N's 102, 103, 104, and 105 all successfully passed cold functional testing.

Bearing performance of the RWA's is presented in Figure 6.10 representing drag torque at 1200 and 2160 RPM rotor speeds. RWA S/N 102 demonstrates a slight decrease in bearing drag torque. RWA S/N's 104 and 105 demonstrate similar drag torque performance as previously delivered. RWA S/N 103 demonstrates an increase in drag torque at both speeds: 0.019 and 0.018 N-M vs. 0.008 N-M as delivered.

Figure 6.11 presents steady state power measurements at 1200 and 2160 RPM for RWA S/N's 102, 103, 104, and 105. The graph demonstrates decreased power requirements for RWA S/N's 102, 104, and 105 and similar power requirements for RWA S/N 103 as previously delivered.

6.4 INTERNAL PRESSURE MEASUREMENT

Following performance testing, RWA S/N's 102, 103, 104, and 105 were measured for internal pressure. Figure 6.12 demonstrates that all RWA's maintained a good vacuum over the life of the mission.

FIGURE 6.4
STEADY STATE POWER
HOT TEMPERATURE

ORIGINAL PAGE IS
OF POOR QUALITY

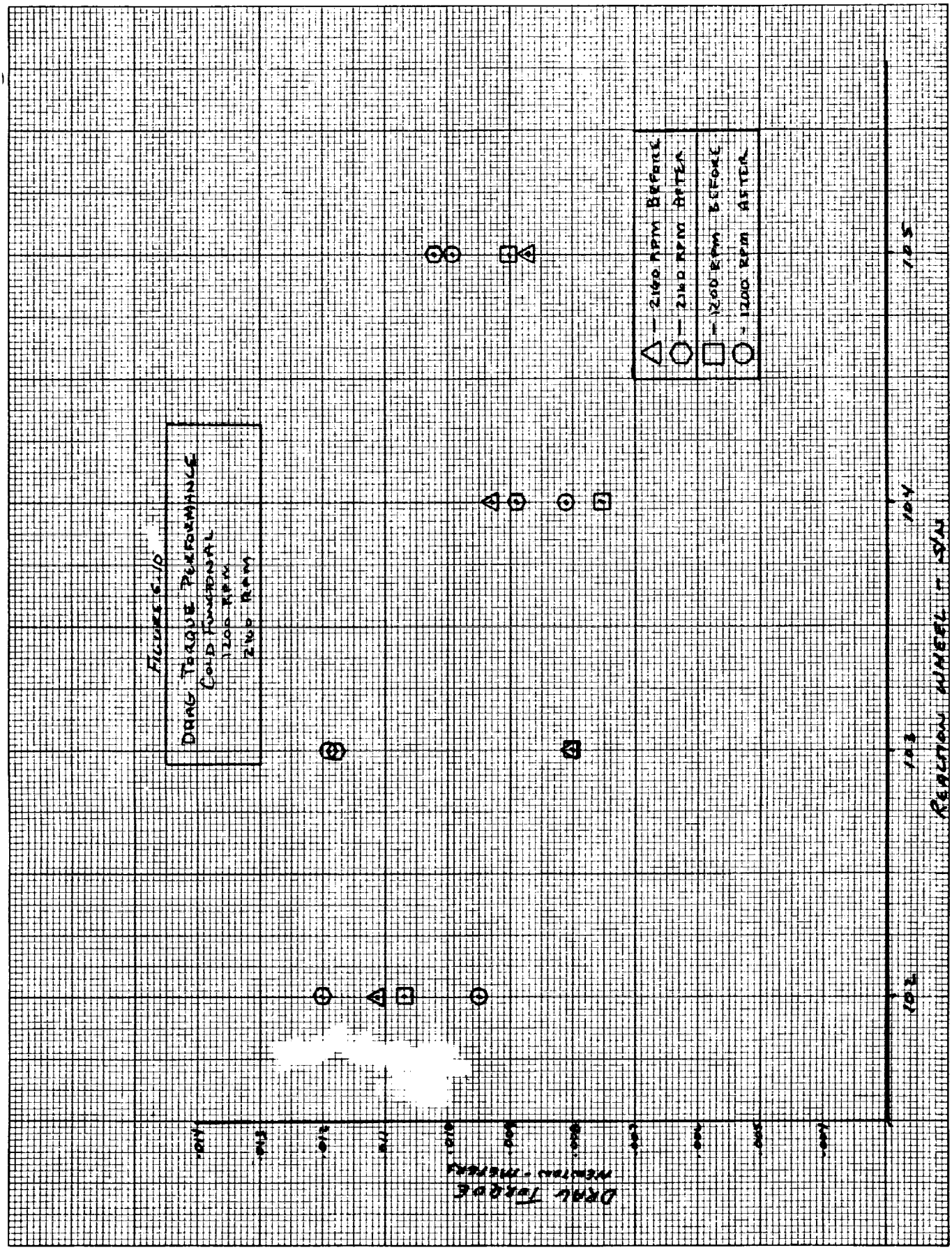

FIGURE 6.10

ORIGINAL PAGE IS
OF POOR QUALITY

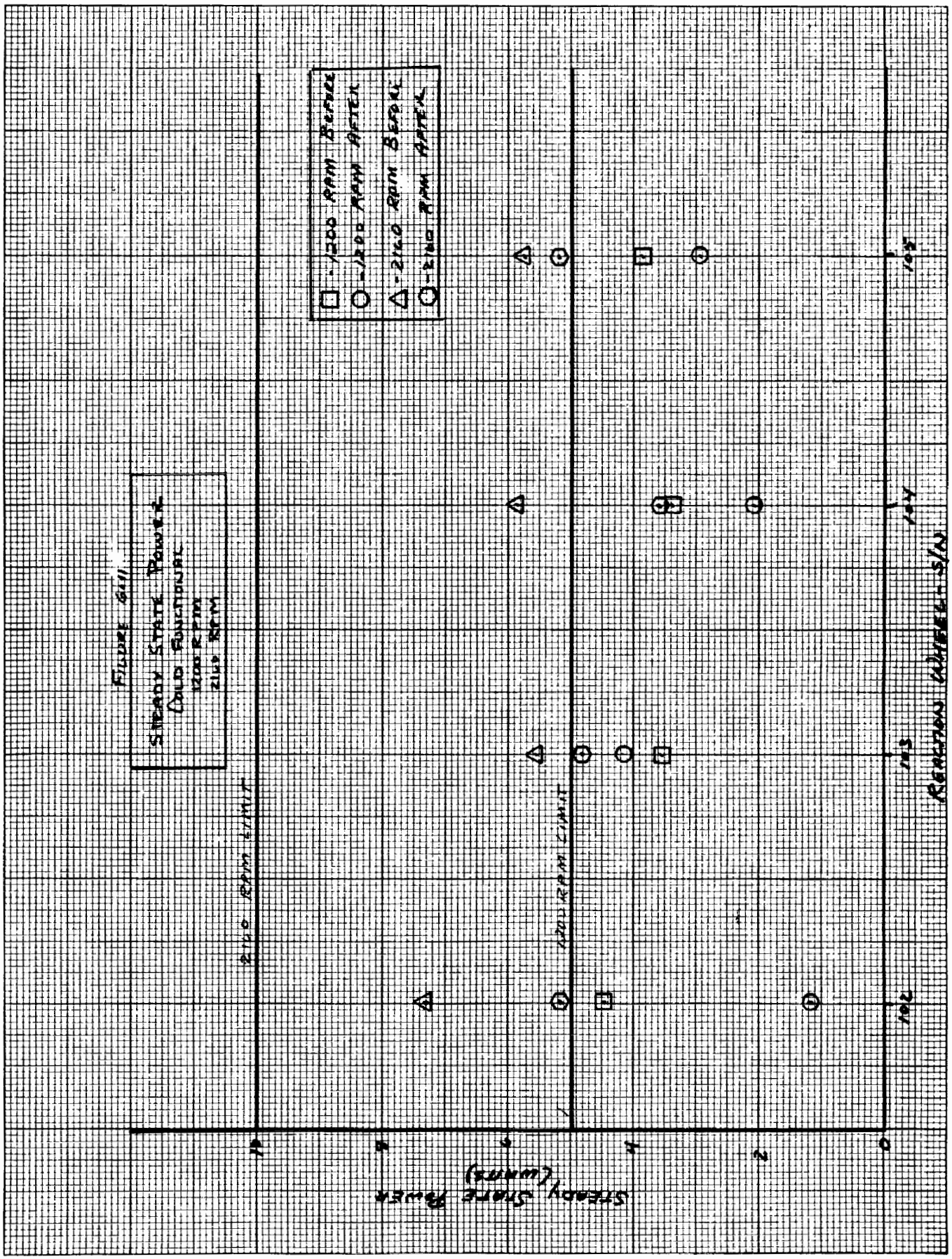

RWA S/N	Pressure Internal, N
102	1400
103	1000
104	1500
105	1900

Table 6.12

7.0 REACTION WHEEL ASSEMBLY S/N TEARDOWN

Reaction Wheel S/N 103 was selected for teardown due to its slightly deteriorated performance coupled with the no-load speed/ overtemperature incident as previously stated in section 2.0.

Internal visual investigation revealed an "as-new" assembly appearance with shiny metallic surfaces, sound solder joints and conformal coatings without any signs of deterioration. Rotor/ bearing disassembly revealed the floating bearing cartridge with an exterior oil film as applied at initial installation. All bearing assembly component adhesive stakes and Loctite bondings were intact.

An investigation package including contamination wipes, oil and grease samples, and photographs of the major points of interest were submitted to NASA, Goddard Space Center for analysis, reference Figure 7.0. The wipes were taken at each major RWA surface and submitted for lubricant/contamination analysis. Rotor bearings and reservoirs were weighed for a lubricant loss/gain investigation and submitted to NASA with one of the two bearing pairs (fixed bearing) disassembled for bearing surface wear analysis.

Figure 7.1 presents the lubricant weight analysis of the floating and fixed bearing assemblies. The analysis indicates an oil depletion in both floating and fixed outboard bearings but increased oil weights in the inboard bearings of both cartridge bearing assemblies.

All bearing reservoirs demonstrated an oil weight loss, as expected. In general, the floating bearing system indicated a higher lubricant loss than the fixed bearing system, 10% vs. 7.1%, respectively. Figure 7.2 represents actual bearing system lubricant loss for S/N 103 as compared with predicted bearing system lubrication losses for the standard Reaction Wheel at 67 C and 32 C operating temperatures.

REACTION WHEEL, S/N 103

TEARDOWN

INVESTIGATION PACKAGE

CONTENTS

1. Wipe - Floating Cartridge, Externally
2. Wipe - Web, Floating Cartridge Side
3. Wipe - Web, Fixed Cartridge Side
4. Wipe - Cover, Housing
5. Wipe - Case, Housing
6. Wipe - Evacuation Valve/O-Ring Location
7. Wipe - Bore, Case, Floating Cartridge Side
8. Wipe - Inboard Retainer, Fixed Bearing
9. Wipes - Non Used, Control Group, Quantity 3
10. O-Ring, Case/Cover
11. Bearing, Floating Outboard
12. Bearing, Floating Inboard
13. Reservoir, Floating Outboard
14. Reservoir, Floating Inboard
15. Sample, Apiezon H Grease
16. Sample, SRG-60 Oil
17. Negative - Case, View Connector @ 270
18. Negative - Case, View Connector @ 360
19. Negative - Cover
20. Negative - Rotor, Floating Cartridge Side
21. Negative - Rotor, Fixed Cartridge Side
22. Negative - Floating Cartridge - Inboard View
23. Negative - Floating Cartridge - Outboard View
24. Bearing - Fixed - Outboard Disassembled
25. Bearing - Fixed - Inboard Disassembled

Table 7.0

BEARING LUBRICATION WEIGHT ANALYSIS

RWA S/N 103

LOCATION	BEFORE WEIGHT (grams)	AFTER WEIGHT (grams)	% LUBE LOSS/GAIN
Floating Bearing Cartridge Assembly	3.1328	2.8201	-10.0
- Bearing Inbd/	.0330	.0369	+11.8
- Bearing Outbd.	.0298	.0232	- 7.8
- Reserv. Inbd.	1.1800	1.0200	-13.6
- Reserv. Outbd.	1.8900	1.7400	- 7.9
Fixed Bearing Cartridge Assembly	3.2449	3.0134	- 7.1
- Bearing Inbd.	.0292	.0328	+12.3
- Bearing Outbd.	.0257	.0206	-19.8
- Reserv. Inbd.	1.2700	1.2500	- 1.6
- Reserv. Outbd.	1.9200	1.7100	-10.9

TABLE 7.1

ORIGINAL PAGE IS
OF POOR QUALITY

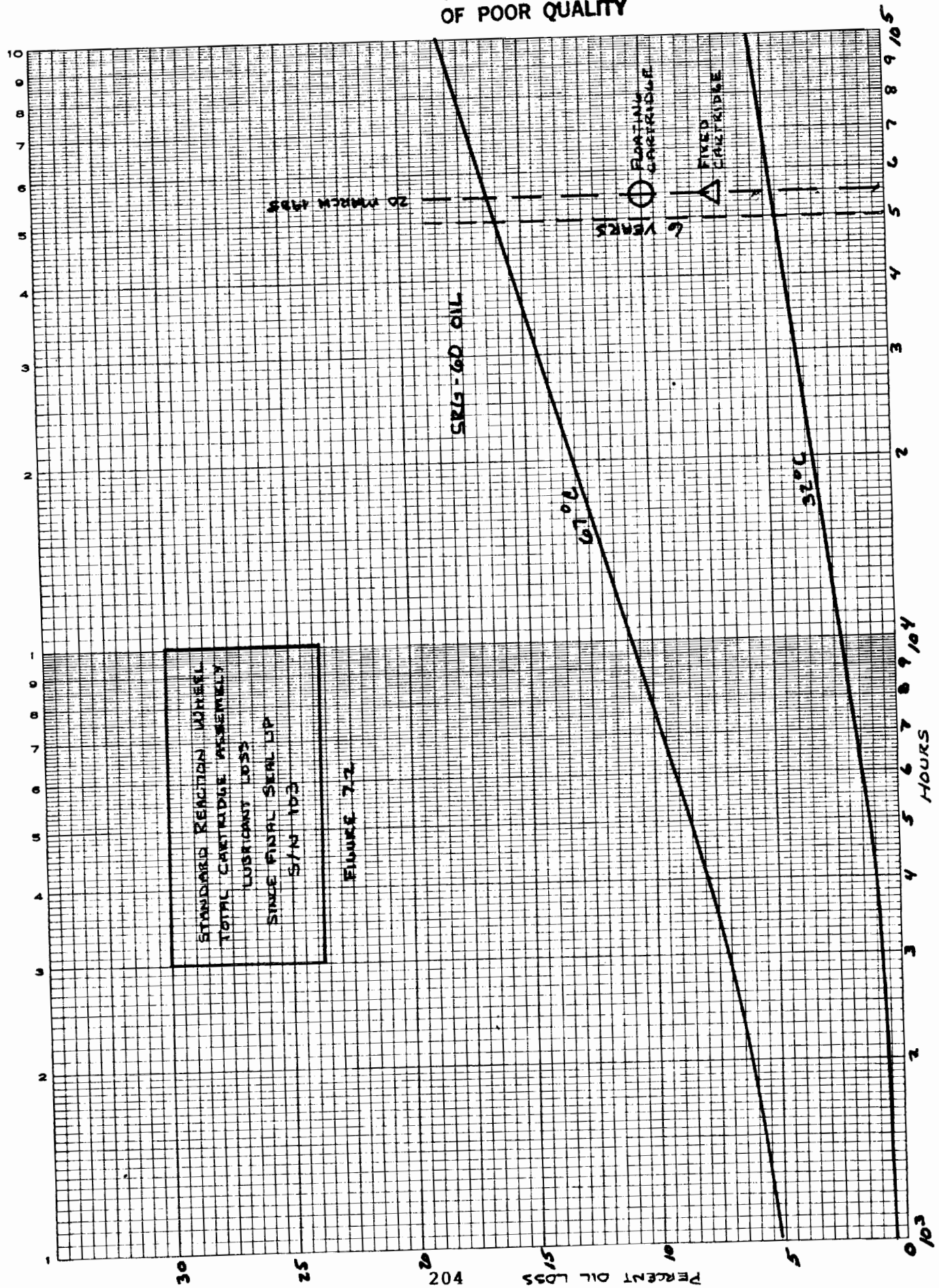

FIGURE 7.2

8.0 CONCLUSION

The returned Solar Maximum Mission Reaction Wheels, S/N 102, 103, 104, and 105 were visually examined externally upon receipt and found to be in good condition.

Preliminary electrical testing was satisfactorily completed with the only discrepancy being connector shell bonding values slightly above the requirements on two units, S/N 102 and 103 but were not considered excessive.

Overall performance testing results of RWA S/N 102 through 105 demonstrated successful completion of each performance test requirement at ambient, 40 C and 0 C temperature environments with exception to the 500 RPM torque noise tests. As previously delivered, torque noise exceeded 3.0 peak to peak deviation for all RWA's using a 0.1 rad/sec filter. The RWA's subsequently met the torque noise requirements using a 0.3 rad/sec filter as previously delivered.

Individual performance results indicated that RW S/N 104 demonstrated decreased bearing drag torques and extended coast down times. RWA S/N's 102 and 105 demonstrated similar performance results as previously delivered with only slight negligeable performance alterations. RWA S/N 103, though successfully completing all test requirements, demonstrated the most performance difference which included a 45% increase in drag torques and reduced coast down time.

Teardown analysis of RWA S/N 103 revealed an "as new" appearance of the internal components and surfaces. The lubrication analysis showed a greater lubrication loss in the floating cartridge system than the fixed cartridge system. An investigation package including contamination wipes, lubricant samples, photographs of items of importance and bearing components was sent to NASA, Goddard Space Center for analysis.

(This page intentionally left blank)

Post Flight Analysis of NASA Standard Star Trackers Recovered from the Solar Maximum Mission

by

P. Newman
NASA/Goddard Space Flight Center
Greenbelt, Maryland

The objective of the Satellite Servicing Project is to analyze the flight hardware returned after the SMM repair mission to determine the effects of 4 years in space. The NASA Standard Star Tracker would have been a good candidate for such analysis because it is moderately complex and had a very elaborate calibration during the acceptance procedure. However, the recovery process extensively damaged the cathode of the image dissector detector making proper operation of the tracker and a comparison with pre-flight characteristics impossible. Otherwise, the tracker functioned nominally during testing at the GSFC and at the Kennedy Space Center.

Background

The two SMM Standard Star Trackers, S/N001 and S/N002, were the first trackers built under the NASA Standard program. Of the two trackers, S/N002, was tested to qualification levels. Because of the model changes, the production and test of the new trackers was a very difficult process. Many problems surfaced because of a low position on the learning curve. The situation was further aggravated by the tight schedule required to meet the flight integration deadline.

The trackers performed flawlessly during the SMM. However, because of inconsistencies in the flight data, some questions arose about the position calibration and alignment. The inconsistencies were attributed partly to a new calibration method and partly to the paucity of flight data. (The specific scientific nature of the SMM was not conductive to a proper engineering test of the trackers).

During the period from the spacecraft failure to just prior to recovery, the trackers were used occasionally, but were always adequately protected by the shutter. At the time of the grappling attempt, the trackers and the shutter were powered off. They remained in this condition until recovery.

Testing

The first post flight tracker testing took place at the Kennedy Space Center as part of the MACS testing. The test used a hood that had several simulated stars in various parts of the tracker field of view. Part of the tracker test connector was accessible so that wave shapes could be observed during the test.

The tracker was still in a flight interface condition (command and data terminals connected to the flight RIU). Except for two anomalies, the tracker performed nominally.

The first anomaly was that the tracker did not track a star in certain locations of its field of view. Rotating the stimulus slightly, corrected the problem. The preliminary conclusion was that some regions in the tracker field of view lacked light sensitivity. This was observed in both trackers.

Our project test engineers at KSC were not able to see any physical defects by looking into the tracker lens because the light shade prevented them from getting sufficiently close to avoid the effects of a large image magnification.

Prior to the MACS disassembly at the GSFC, the author and the current BASD project manager inspected the trackers. The thermal insulation and the light shades had been removed. It was possible to get within a few inches of the lens surface. A number of tracks crossing from one side of the cathode to the other were observed in each tracker. The thin film cathode normally has a characteristic interference color depending on the illumination, but the tracks showed an absence of color. The attached photographs show the condition of the cathodes. In addition, it was observed that the lens of S/N001 had some sort of debris on the outer surface.

To further examine the characteristics of the "tracks" under more controlled conditions, a test set was borrowed from the vendor and used with a special collimator in a tracker laboratory at the GSFC. The test set was not completely functional so that some of the tests made at the KSC could not be duplicated (digital data). But enough capability remained to demonstrate that the tracks on the cathode were indeed insensitive regions. To perform the test, the tracker sensitivity threshold was set at its minimum (5.7m) and the star (about 2m) was moved around until it was acquired. The collimator star was then moved in small increments by means of a micrometer controlled optical wedge. Eventually star magnitude output decreased until the tracker lost track (signal from star too weak to track). Moving the star further in small increments (slowly since the search has a 10 sec cycle) reacquired the star and the star magnitude analog signal increased to its original value.

The debris on the surface of the lens of tracker S/N001 was found to be peelings from the MgF lens coating. A low power binocular microscope examination indicated a rather extensive amount of deterioration over the entire lens with large pieces of flaking or peeling in an annular region about 1 cm from the edge.

Looking at the "tracks" on S/N001 one can notice a track that starts near the middle of the field. A possible explanation is that the tracker was looking at the sun at sunrise or sunset. A pair of tracks in S/N002 starting close to the edge are a little more difficult to explain. These tracks also appear to be

slightly thinner. This suggests that the sun was moving across the surface at a higher angular velocity. Since the edge of the cathode is in close proximity to a metallic seal, the thermal conductivity at the edge could be responsible for the starting point being away from the edge. It turns out that it is possible for the spacecraft to acquire large amounts of angular momentum for certain orbits due to the varied effect of the gravity gradient torque and thus change the angular velocity.

Refurbishment

Since the remainder of the tracker appears to function close to the nominal specifications, it has been suggested that the tracker could be repaired by installing a new tube. This turns out to be a very complex and costly process because the tube replacement must be accomplished in reverse order of fabrication.

To give the tracker long term stability, the tube is bonded to the back of the lens in one of the very first steps of the tracker assembly. This means removing all the components and subassemblies, the harness and the connectors, the coils and the shields together with harness staking. Then, after replacing the tube and perhaps the focus and deflection coils if they do not survive disassembly, the rest of the tracker can be reassembled. The entire disassembly procedure is extremely risky. It is likely that damage will be done to a component and that the defect will not be discovered until far long in the test process. For example, nicking a high voltage lead is likely to produce a corona discharge the first time the tracker is under vacuum.

In addition, most of the boards are built up with cordwood modules. Virtually no spares exist. Modules containing CMOS and certain types of amplifiers are usually more sensitive to radiation. They would have to be checked and replaced if their characteristics exceed tolerances. It would be difficult to even assess changes in these components since parts in the cordwood modules are not easily accessible.

Finally, acceptance tests of the restored tracker would require considerable effort since test facilties are no longer available for analog trackers. All vendor's test facilities have been converted for testing the digital standard tracker and are not compatible with the analog standard tracker.

The cost consequences of the above factors as well as our past experiences with malfunction and repair of the analog tracker indicate that the likely restoration costs would be almost as high as those of a new digital tracker. Since restoration of the tracker does not appear to be cost effective, it is not recommended.

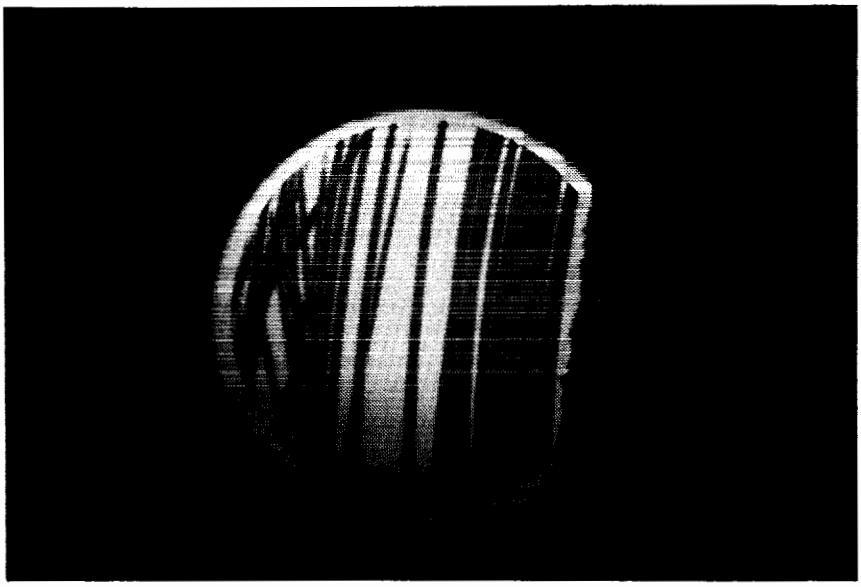

Photo cathode of Standard Star Tracker S/N 002 showing damage caused by the sun during SMM recovery. Lines are regions where heat from the solar image evaporated the cathode material resulting in regions of no sensitivity.

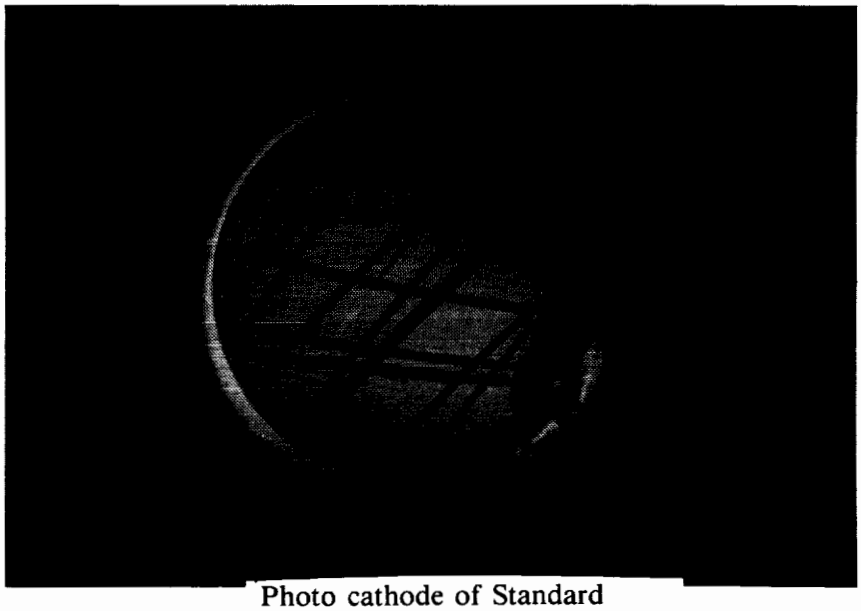

Photo cathode of Standard Star Tracker S/N 001 showing damage caused by the sun during SMM recovery. Lines are regions where heat from the solar image evaporated the cathode material resulting in regions of no sensitivity.

RESULTS OF EXAMINATION OF MATERIALS FROM THE SOLAR MAXIMUM RECOVERY MISSION

BY

John J. Park

Materials Control and Applications Branch
NASA Goddard Space Flight Center
Greenbelt, MD 20771

ABSTRACT

Four years and two months in space at 310 nautical miles orbit has produced different effects on Kapton, silver/Teflon, and on aluminum. Kapton, a polyimide, lost up to 31% in thickness, though other locations showed much less loss. The degradation of silver/Teflon was drastic but very localized, due perhaps to the formation of silver oxide, Ag_2O, through cracks in the protective Inconel layer which exposed the silver to the oxygen atom environment. Penetrations of thin aluminum sheet in the form of thermal louvers and also of the thermal blanket material due to unknown particles were unexpected, making the debris a potentially serious problem because of the threat of damage to components.

INTRODUCTION

The repair mission for the Solar Maximum Mission (SMM) satellite in April 1984 was very successful in replacing certain components which had failed early in the mission. The removal and replacement of the Main Elctronics Box (MEB) and of thermal blanket from the MEB and the recovery of the thermal louvers from the Attitude Control System (ACS), provided many components for evaluation of the effect of operating time and of the space environment on these components.

The SMM was intended to be sun-seeking, being launched in Febraury 1980 and maneuvered to look at the sun continuously. After about nine months, a suspected electronic failure resulted in the need to spin-stabilize the SMM for the remaining lifetime until the repair mission. The spin rate was 1°/second and the satellite had a wobble of ±15° about the sun.

Kapton from the Attitude Control System

Thermal blankets were used on all four sides of the ACS which was attached to the structure. On the left side as one faces the thermal louvers, portions of thermal blanket had covered the Power Supply Unit (PSU) fuse box and also the Ground Support Equipment (GSE) test connector (Figure 1). These pieces were adhered with a Velcro strip and also were taped at the edges using Kapton tape.

The PSU fuse box cover was an 11-3/4 inches x 9-3/4 inches rectangle. The surface had been relatively smooth and had been taped at the edges to the remaining thermal blanket. A one-square-inch circular area was cut from places near the front (toward the louvers) and from the rear, and these pieces were from areas approximately 8 inches between the centers of the circles.

The GSE test connector cover was approximately 7-7/8 inches by 7-1/2 inches. Two discs were cut from this cover, each of 1 square inch area and with the centers approximately 4-1/8 inches apart. As Figure 1 shows, the cover would not have been flat but had a raised center due to the projection of the circular test connector. The appearance of the Kapton was non-uniform, the front area having a matte finish and an area at the rear being shiny and unaffected.

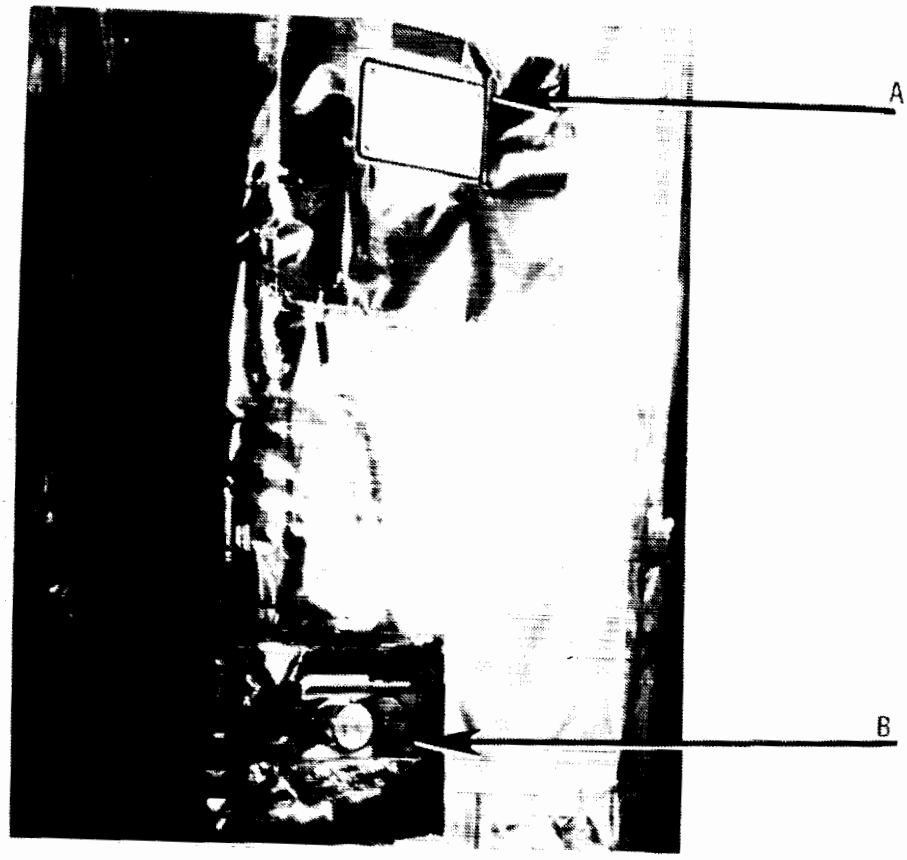

Figure 1. View of left side of ACS showing areas once covered by Kapton blankets, 'A' being the Power Supply Unit, and 'B' being the Ground Support Equipment connector.

Weight-loss measurements of these circular discs showed drastic differences due to location. By using the weight of the bottom layer of Kapton as a reference, which was found to the relatively uniform from weighing separate pieces, the actual loss of Kapton could be determined.

The results for the weight loss measurements are as follows:

PSU Fuse Box Cover	Loss
Front	31.4%
Rear	3.51%
GSE Test Connector Cover	
Front	7.4%
Rear	0.54%

The weight difference for the PSU fuse box Kapton cover was unexpected because of the relatively uniform appearance of the whole cover. On re-examining the location of the cover and of the ACS on the spacecraft, it appears that the rear part of the ACS was closest to the structure and perhaps was thus shielded, which could account for the difference. Also, the weight loss results for the GSA test connector cover further demonstrated the effect of shielding. As mentioned earlier, this cover was not flat but was raised near the center by the projection of the circular test connector. Thus, the low loss of 0.54% of exposed but shielded Kapton shows how great the difference can be. Thus, some directionability of the environmental flow must cause an increase in weight loss.

Silver/Teflon Film

Strips of "silver/Teflon" film had been applied to the edges of the ACS frame for thermal control reasons. The silver/Teflon film is a vapor-deposited layer of silver on Teflon, and a layer of Inconel is deposited over the silver to protect it from terrestrial reactions. The film is typically used with the silver surface exposed to space, with the silver visible through the transparent Teflon. However, at the top and bottom of the ACS, the film had been adhered at the edges to a U-shaped channel support which resulted in the Inconel being exposed to space. It was observed that the long strip of silver/Teflon on the bottom of the ACS had separated in at least three places (Figure 2).

The result of exposing the Inconel in this way was the apparent removal of the vapor deposited metals (Figure 2) in a narrow strip of approximately 1/3 of the total width of deposited metal. The width of the total exposed surface was about 2-1/4 inches and the eroded surface, though non-uniform and irregular, was about 3/4 inch, or about 1/3 of the total exposed surface's width. In addition, the separations in the Teflon film ran essentially to the edges where the film was adhered to the U-channel which kept the film from coming loose.

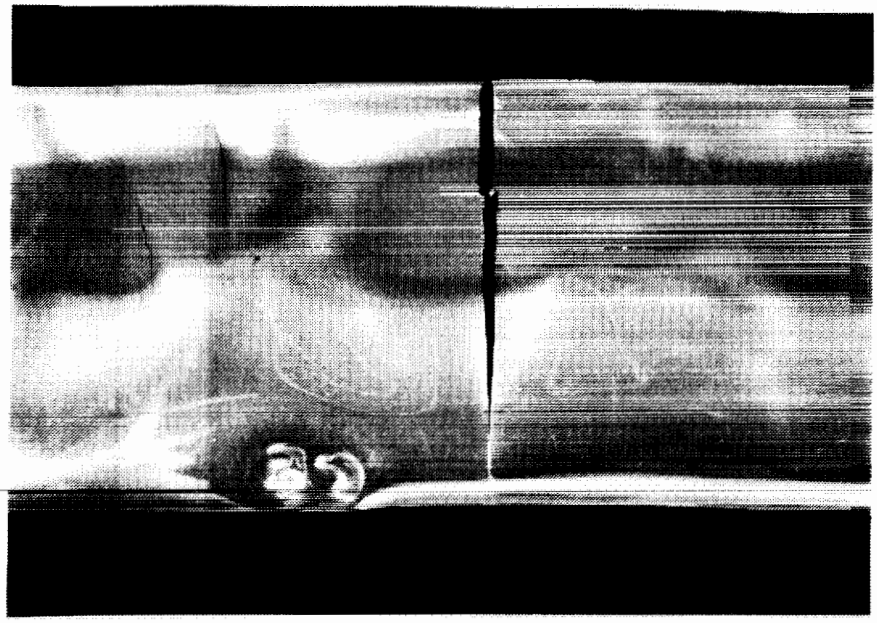

Figure 2. Silver/Teflon film showing area having lost deposited metallic films, from bottom (B2) of ACS, with separation running across the short dimension of the film.

The Inconel surface was examined in the Scanning Electron Microscope. The surface was unusual, as indicated by views in Figure 3. Deposits of an unknown compound appeared to be growing from cracks in the Inconel. As the pictures demonstrate, the deposits became more prevalent nearer to the darker area and certain small areas had curled edges (Figure 3D) nearest to the black, eroded area. In the blackened area, surface charging occurs, indicating lack of metallic film.

The surface deposits on the Inconel surface were collected and analyzed by X-ray diffraction. The results clearly indicated that silver oxide, Ag_2O was present in the samples, along with Teflon and silver. Other data from fluorescence analysis (EDAX) indicated the presence of nickel, chromium, and iron from the Inconel, plus fluorine from the Teflon. Consequently, we can conclude that silver oxide can be formed through cracks in the Inconel surface.

The size of the silver/Teflon film was sufficient to permit tensile testing of various areas to determine other effects of the erosion (Figure 4). Samples were cut from various areas: one was cut along the eroded area so that this whole sample was eroded (identified as Black), another at 90° to this direction so that the narrow waist of the sample was within the eroded area (identified as Half/Half), and the third sample was cut from the least eroded area to simulate the best unreacted film (identified as Shiny). As expected, the strength results demonstrate an effect of loss of metallic film.

Table I

Tensile Strengths of Eroded Ag/Teflon Film

Sample	Max.Load	Elongation
1. Shiny	1.7 lb	125%
2. Half/Half	1.1 lb	50%
3. Black	1.1 lb	Zero

A. Far from eroded area, 320X

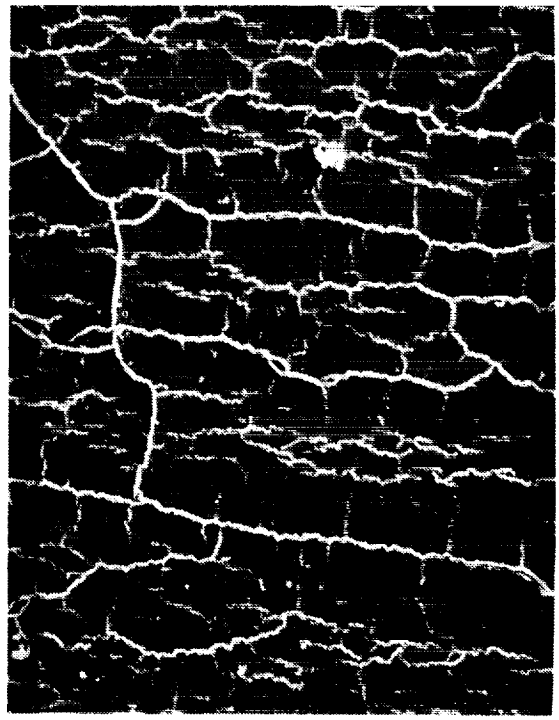

B. Closer to eroded area, 320X

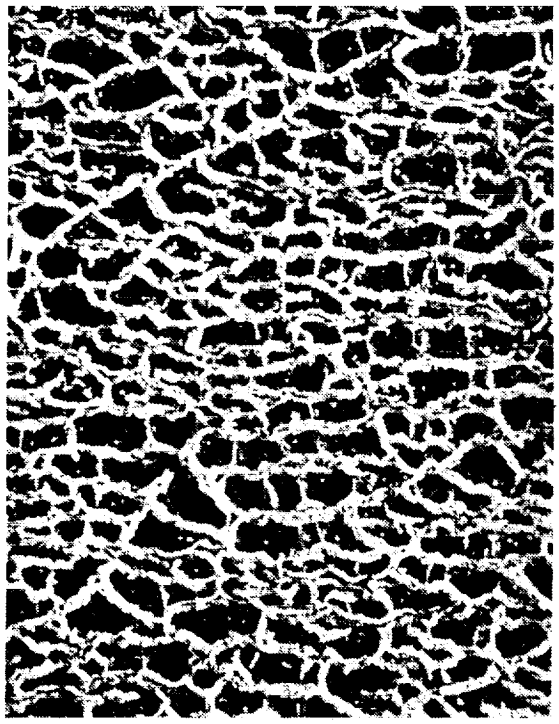

C. Near eroded area, 320X

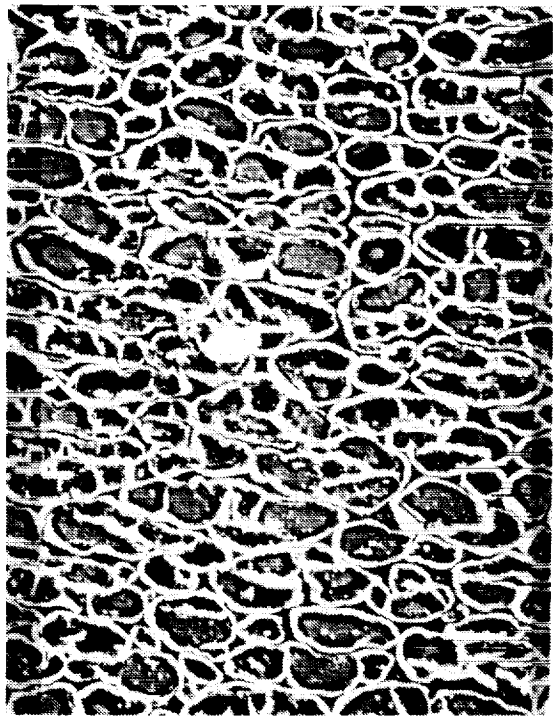

D. Nearest eroded area, 320X

Figure 3. Scanning Electron Microscope images of Inconel surface, showing "grain boundaries" of Ag_20.

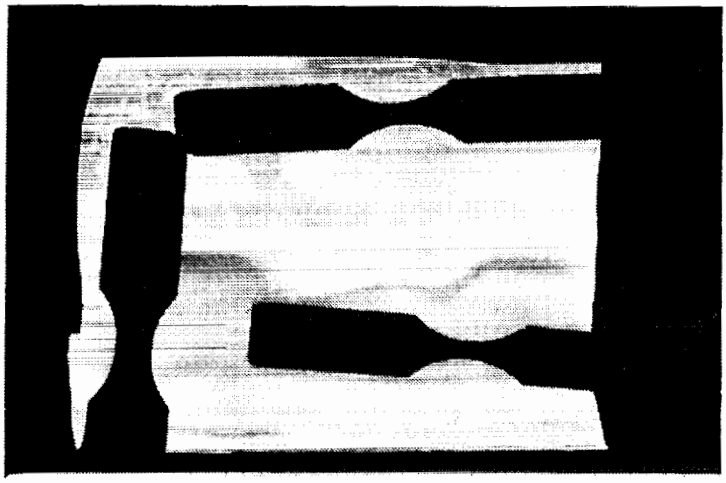

Figure 4. Silver/Teflon showing areas die-cut for tensile testing. Note right hand edge, which was one actual separation in the film.

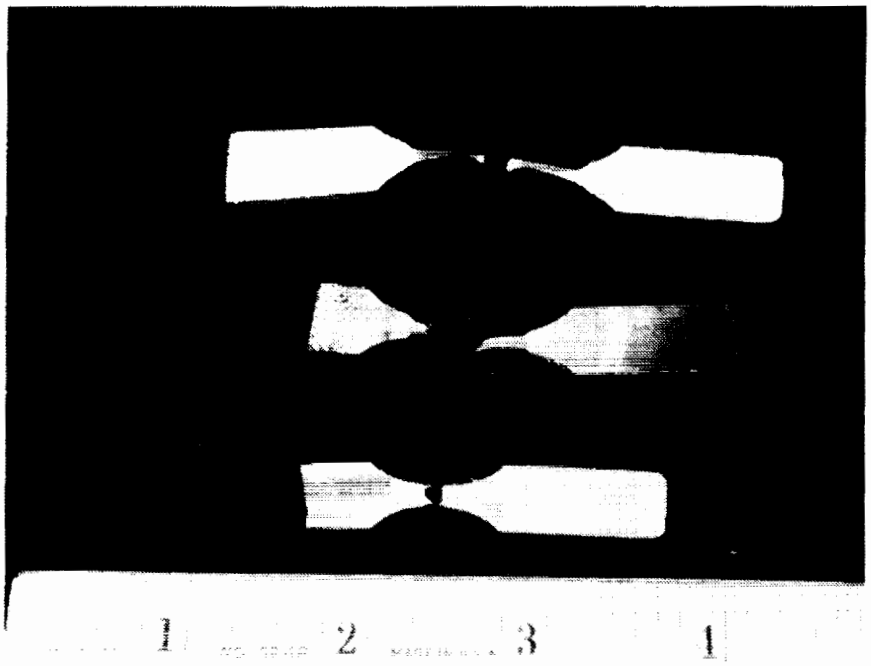

Figure 5. Tensile specimens from the ACS silver/Teflon, showing differences in elongation at room temperature.

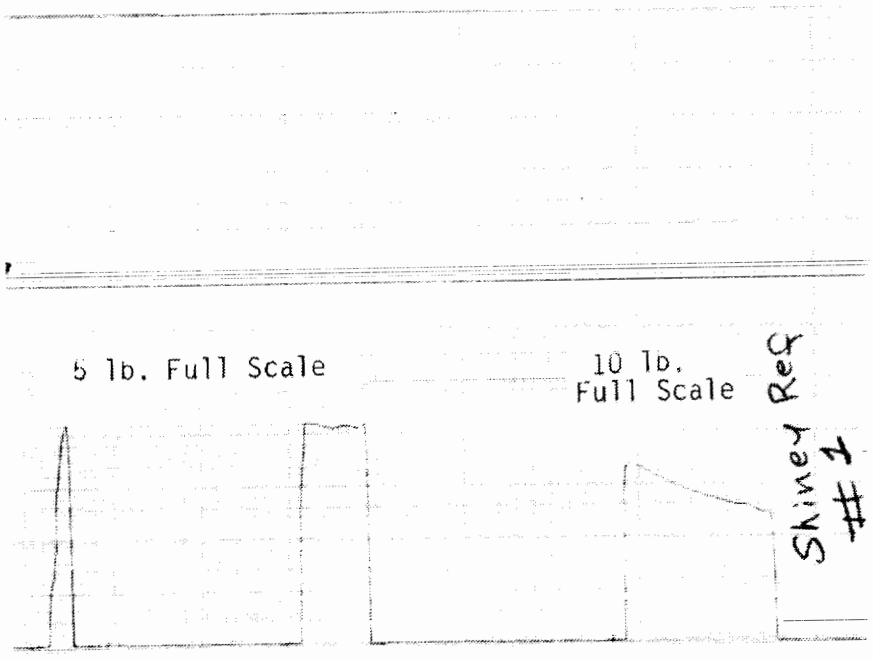

Figure 6. Tensile test results for ACS silver/Teflon film.

Figures 5 and 6 demonstrate the differences in elongation and the break of the Black sample indicates a possible reason for the separation in the exposed silver/Teflon film. Note that the Black and the Half/Half were cut to be 90° different in orientation in the eroded area. Thus, the abrupt failure of the Black is in the direction that the film actually separated. Thus, thermal change and the resultant expansion and shrinkage would apply a tension load in the same direction as for the Black specimen tensile test. The very low elongation for this film, at room temperature, indicates that the eroded areas have no ductility even though the 1.1 lb breaking load is the same as that for the Half/Half specimen.

Tensile testing of unexposed siler/Teflon samples show that elongation is much greater than for the space-exposed film, even though the breaking loads are similar. Specimens were cut from an elongated piece of film, three in the "long" dimension and three more at 90° to that first direction, in order to emphasize any directionality. The average breaking load of the "long" dimension was 1.73 lb and the elongation was 210%; the breaking load for the samples in the 90° dimension averaged 1.75 lb and the elongation was 225%.

MEB Thermal Blanket

The thermal blanket was approximately 30 inches square and composed of an outer layer of three mil Kapton, aluminized on one side, plus layers of aluminized Mylar separated by Dacron mesh, between the Kapton. The Kapton surface faced out for both sides of the thermal blanket, which was attached to the MEB by Velcro areas sewn to the blanket. This construction provided a reference material for comparison purposes, a material that had been in space for the four years but with the side next to the MEB not being open to the ambient atmosphere.

The appearance of the space-exposed Kapton was drastically different than the original Kapton. The space-exposed Kapton was dull, rather than shiny, and had a matter finish rather than the original smooth surface. In addition, there were "wipe" marks on the blanket, as if it had been cleaned at some time before launch (Figure 7).

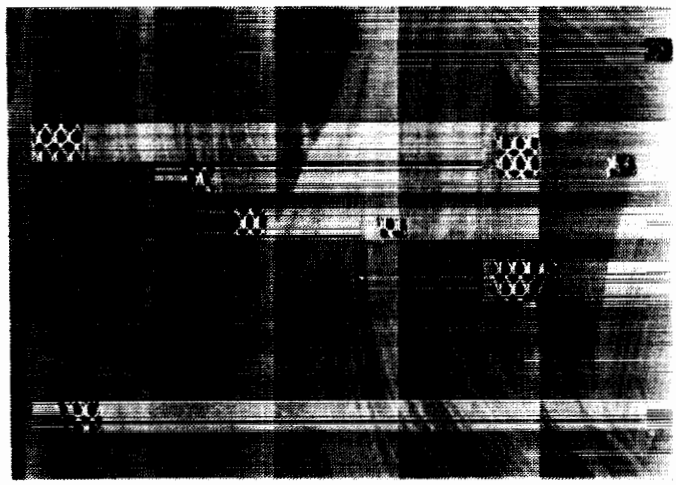

Figure 7. Wiping marks left on MEB Kapton thermal blanket. Holes were made for examination of penetrations by JSC personnel.

The change in the Kapton surface can be demonstrated by measurements for the Bidirectional Reflectance Distribution Function. The enclosed graph, Figure 8, shows the comparisons of the MEB Kapton and the ACS Kapton with the standard barium sulfate surface. As demonstrated in the graph, the changes due to the space exposure result in a diffuse surface, as can be observed visually, also.

Another unusual feature of the MEB blanket was the appearance of what was an unusual pattern of light spots or reflections. Upon examining the back of the outer Kapton layer, it was noted that the aluminum deposit had been rubbed off, making it appear that there had been holes in the Kapton. By comparing the rubbed pattern with the knots (Figure 9) of the Dacron mesh in the thermal blanket, one can demonstrate how the pattern occurred.

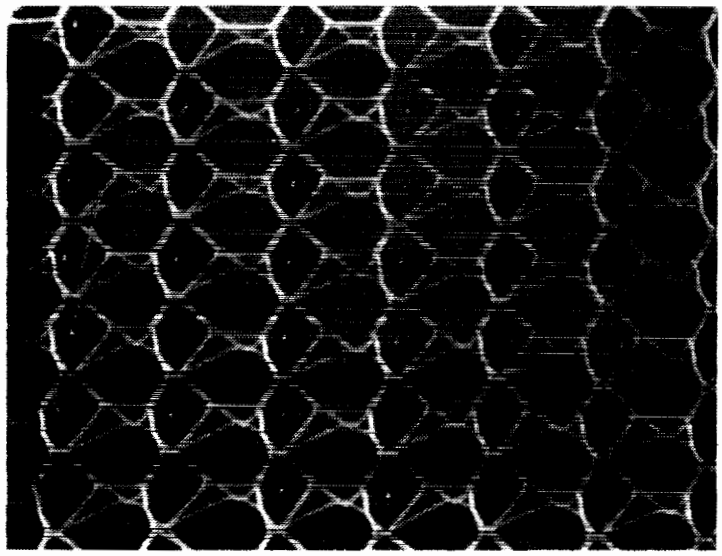

Figure 9. Back-lighted MEB Kapton showing lighted areas adjacent to knots in the Dacron mech, demonstrating how the deposited alulminum was removed.

The micrographs in Figure 9 show how the removed aluminum and the knots make a pattern which matched. More than likely, the abrasion resulted from the treatment of the MEB blanket which had been removed by the astronauts and then folded and stored in a case for return to Earth.

A small piece of Kapton had been cut from an area below the ACS but also in an area which presumably was the most exposed to the space environment. This almost square piece was measured as 0.817 x 0.808 inches. Because there was no direct comparison piece, it was necessary to use as comparisons the weights and densities of non-flight pieces of Kapton. The calculations indicated a weight loss of 41% after the 4 years and 2 months in space. It is estimated that these calculations have a maximum error of 5%, due mainly to the dimensional measuring methods.

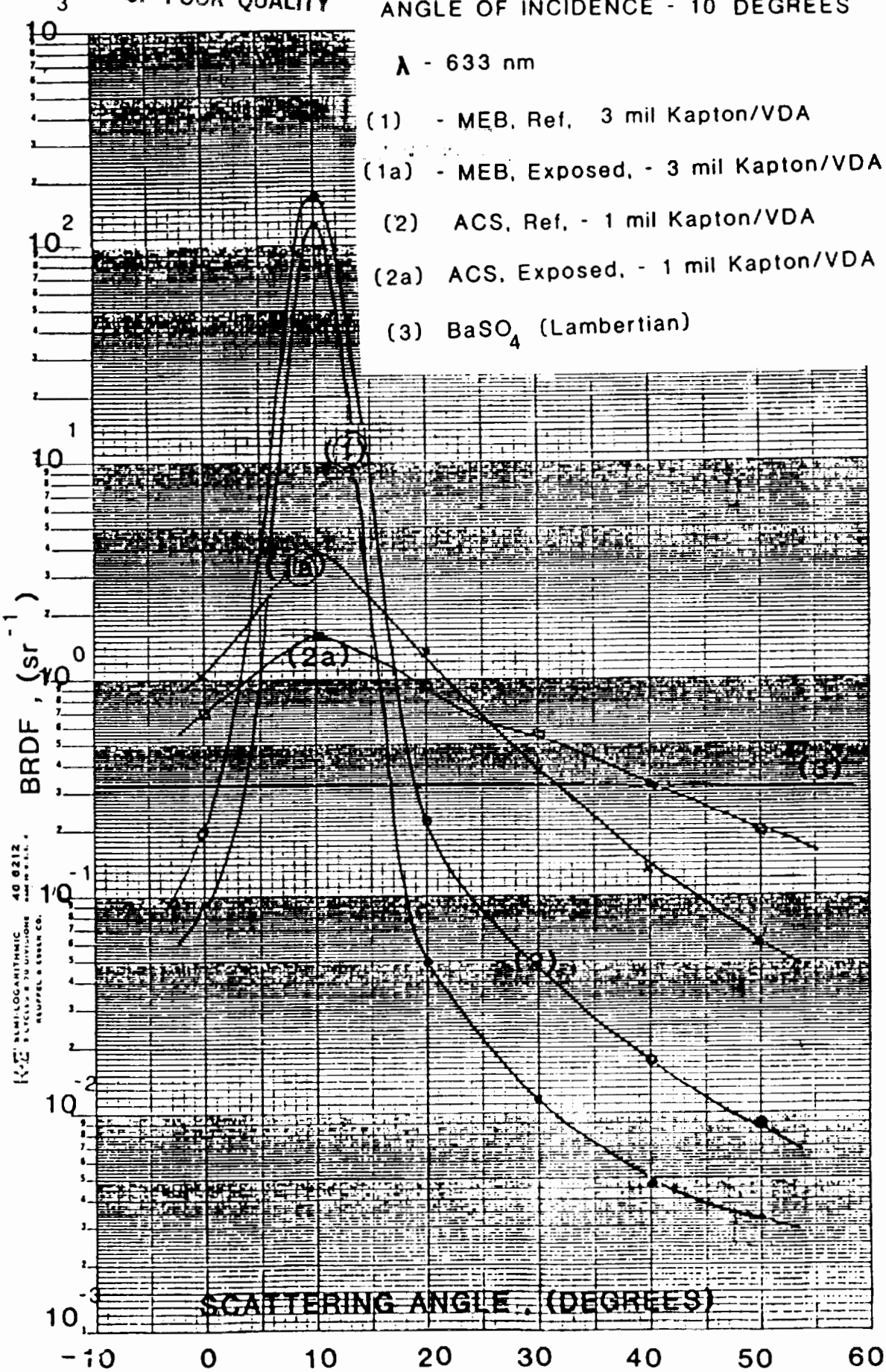

Figure 8. Bidirectional Reflectance Distribution Function Data for Exposed Kapton Film.

Penetrations

Visual examination of the thermal blanket around a Star Tracker indicated that some unknown particle had penetrated the blanket completely. In fact, it was possible to feel a slight depression in the aluminum shield for the Star Tracker and to observe with reflected light a slightly disturbed area of the black paint on the aluminum cover where the projectile had hit.

Removal of the thermal blanket permitted a closer examination of the penetration. Pictures of the front Kapton surface (Figure 10) showed a circular hole. Measurements indicated that it was an elongated hole, being 0.054 inch diameter and 0.110 inches long. The back Kapton surface also had a hole, being larger, elongated, and with a slightly torn surface (Figure 11).

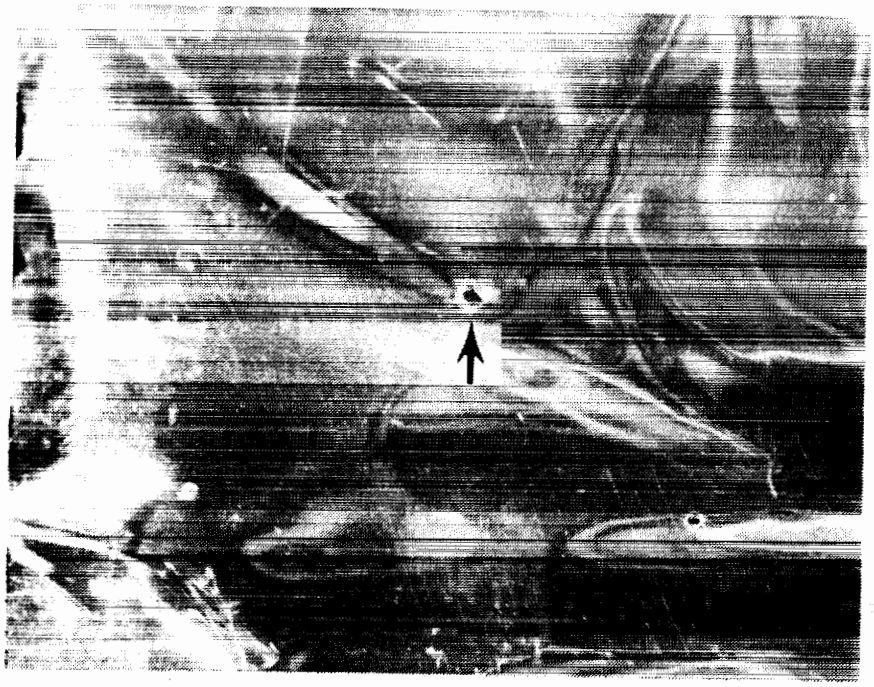

Figure 10. Penetration through front side of Kapton thermal blanket which protected the Star Tracker.

Figure 11. Penetration through rear Kapton layer of thermal blanket.

Upon further examination of the Kapton blanket material one could note numerous penetrations of the outer layer of Kapton, many of which went through the back layer of Kapton.

Members of the Geology Branch at Johnson Space Center had been analyzing micrometeorites for a number of years and had studied impacts on Skylab windows. Arrangements were made for these Branch members to examine all the exposed Kapton materials and to count and categorize these holes. In addition, they intended to analyze any particles found and to determine their origins, whether from micrometeorites or from other "orbital debris."

To emphasize the problems of orbital debris, examination of the thermal louvers from the ACS showed many penetrations of the thin aluminum sheet. These louvers are formed of two polished aluminum sheets, having a central spine, and being 10" long and 2" wide. Examples of the pentrations are shown in Figure 12. These penetrations were observed on at least 44 of the total of 84 louvers.

The existence of these penetrations raises the problem of "orbital debris," a phenomenon which is highlighted by the examples provided here. With the recovery of the SMM components through the use of the re-usable Shuttle, the surfaces of the MEB are providing much information on the numbers and types of particles floating around in space. However, many exposed optical lenses and other critical surfaces could be damaged by these particles, which is an occurrence which cannot be planned for. The data from the MEB and ACS will provide much information on the problem, which will be useful for future experimenters and designers.

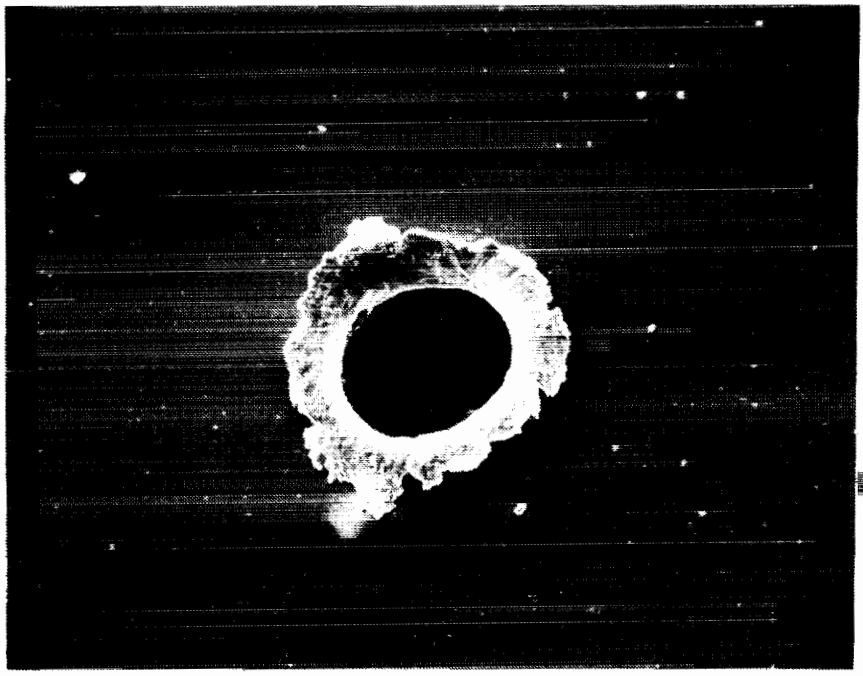

40X

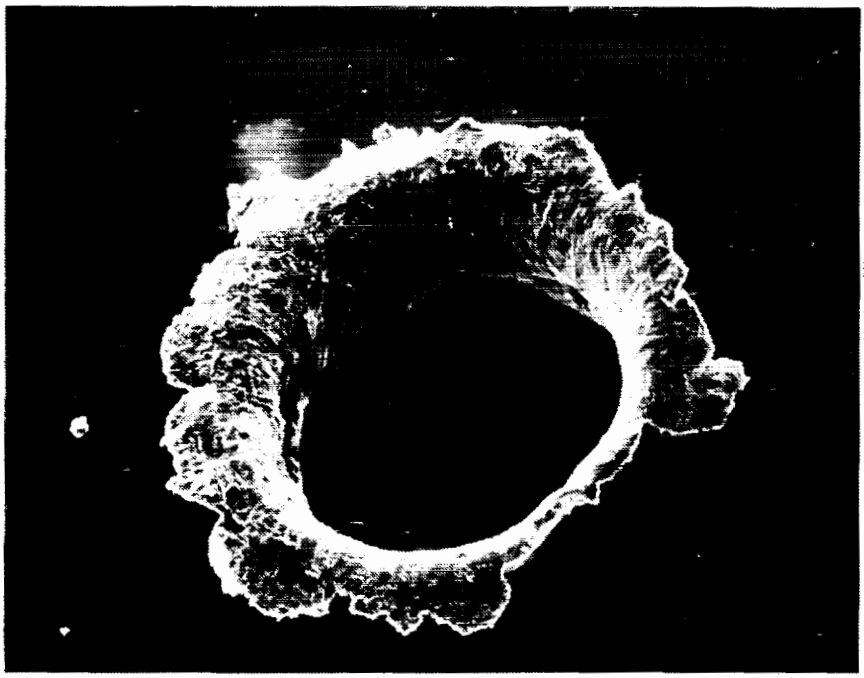

80X

Figure 12. Penetration through 0.15 mm thick aluminum of thermal louver.

Discussion

The existence of Ag_2O, along with the known atmosphere containing the O atoms, leads to a possible mechanism for the loss of the deposited metals of the silver/Teflon film. A reference book*, indicates that Ag_2O decomposes at 300°C but that the peroxide, Ag_2O_2, decomposes at >100°C. Through cracks in the Inconel, the reaction of silver and oxygen occurs, as determined by X-ray diffraction; with an atmosphere richest in oxygen atoms, the formation of Ag_2O_2 and its decomposition at a relatively low temperature as sunlight heats the narrow area of Inconel, seems to be a reasonable occurrence. Repeated formation and decomposition of the silver compounds eventually could lead to flaking (Figures 3C,D) and loss of metallic layers.

Conclusions

The recovery of the Solar Maximum Mission components has demonstrated the significant effects from 4-1/6 years in low earth orbit upon polymeric materials. The loss of Kapton has been measured as much as 31.4%, but it was as low as 0.54% for thermal blanket material on the same side of the ACS but shielded differently from a direct impingement of reactive constituents. One piece of Kapton receiving more exposure lost 41%. The drastic changes in silver/Teflon film were unexpected, but a possible reaction mechanism of the formation of Ag_2O and of Ag_2O_2, coupled with a postulated thermal cycling effect, could explain the reason for loss of metallic film. A major concern for future flights arises from the collection of much space debris and the resultant penetrations through thermal blankets and through thin aluminum sheet.

Acknowledgments

Many members of the Materials Control and Applications Branch provided support, which is deeply appreciated: Walter Viehmann for Bidirectional Reflectance Distribution Function measurements; Brad Parker for Scanning Electron Microscopy; Tom Robinson for X-ray diffraction analysis; Bill Campbell for weighing specimens; Jim Wall for tensile testing; and Diane Kolos for metallography.

*Handbook of Chemistry and Physics, The Chemical Rubber Co., 50th Edition (1969), p. B-155.

(This page intentionally left blank)

STUDIES OF EROSION OF SOLAR MAX SAMPLES OF KAPTON AND TEFLON*

R.M. Fristrom, R. C. Benson, C. B. Bargeron, T. E. Phillips, C. E. Vest, C. H. Hoshall, F. G. Satkiewicz and O. M. Uy
The Johnson Hopkins University Applied Physics Laboratory

I. INTRODUCTION

The Solar Max satellite was repaired during the third Shuttle mission and the replaced pieces were returned to earth. This material was exhibited and discussed in a meeting at NASA Goddard in June 1984. Subsequently portions of the material were repleased to interested groups for examination. Applied Physics Laboratory/Johns Hopkins University (APL/JHU) received three samples: Fig. 1. (1) A 100 mm x 100 mm section of the protective blanket composite, (2) a 30 mm x 40 mm section of the silver-coated Teflon which had been shaded, and (3) a 20 mm x 40 mm section of silver-coated Teflon, portions of which had been exposed to the sun.

Our original plans were to compare externally exposed samples with unexposed material and with virgin materials using laboratory simulated exposures to low presure oxygen atoms and high velocity oxygen atoms. It was not feasible to complete all of the proposed measurements (RC-RCS-043, Nov. 26, 1984), but Table I lists the tests which were completed. The high energy oxygen atom beam apparatus was not operational in time to use on tests. The Auger electron spectroscopic measurements were abandoned because we felt the surface was compromised by the lengthy exposure to the atmosphere so that reliable information could not be obtained. In the future if such a sample becomes available, it would be useful to have it stored in a controlled environment (e.g., dry nitrogen) to minimize surface contamination prior to analysis.

The sample was of interest because its condition sheds light on the erosiveness of the near space environment. This is relevant to the design of long-lived satellites. The sample represents material behavior in near earth space in contrast to the more distant lunar samples from the Apollo mission and the information from the Viking Mars expedition. A shuttle experiment is scheduled to expose selected samples, but these exposure times will be short compared with that of our sample which was exposed for over two years. It was hoped that examination would provide clues as to the identity of erosive

*To be presented at SMRM Degradation Studies Workshop, NASA Goddard, May 9-10, 1985

processes and the responsible species. Interest centered around oxygen atoms which are ubiquitous at these altitudes and are known to erode some metal surfaces, particularly osmium. We also searched for clues implicating other species. The materials available were three polymers and aluminum metal films. The polymers were Kapton (outer envelope), Dacron (the netting), and aluminized Mylar (inner layers).

II. DIAGNOSTICS

In the effort to detect exposure effects on the polymer samples, three diagnostic methods were employed: (1) Optical microscopy (OM); (2) Scanning electron microscopy (SEM); and (3) Fourier transform infrared spectroscopy (FTIR).

Optical microscopy was used to survey the surfaces at low magnifications and a x5 mosaic of the Kapton and Teflon samples was prepared. After the survey, areas were selected for more detailed study and examined at magnifications up to x400 using a conventional metallographic microscope. The scanning electron microscope was an ETEC Autoscan with auxiliary X-ray elemental analysis. Magnifications up to x3800 were employed. Some stereoscopic images were produced by angling the sample. Infrared spectra between 800 and 2200 wave numbers were recorded. This is a spectral region often used to characterize polymers. It would be expected to change if the materials were fundamentally altered. Film spectra were obtained by pressing the material against a KRS-5 ATR crystal.

Two types of simulation were attempted. The first was a flow containing low energy oxygen atoms. Oxygen atoms at about two percent level at a pressure of 0.5 torr were passed over the samples for three hours. The second simulation was bombardment with 3000 volt Ar ions in an ion bombardment mass spectrometer.

III. OBSERVATIONS

The results are of two types: examination and simulation. Examination included various studies of exposed surfaces, and simulations were laboratory exposures of unexposed samples and virgin materials. The tests are listed in Table I. Four types of material were examined: (1) Aluminized Kapton; (2) Nylon netting; (3) Aluminized Mylar; and (4) Silver-coated Teflon. The materials were available from exposed areas and from protected areas. They will be discussed in order.

(1) Kapton: The outer skin and backing were of aluminized Kapton with the polymer surface facing outward from the sandwich. The front surface of the material appeared to be "gold coated". The yellow color is due to the Kapton, and the metallic appearance is due to the back surface mirror behavior of the aluminum coating. The back surface was mirror bright aluminum. In exposed areas the Kapton was a

dull yellow. By contrast it was mirror bright where the material was protected by assembly tape and on the back side of the "sandwich" which was in relatively close contact with the satellite surface and hence not directly exposed to the outer environment.

The superficial erosion which formed a hazy surface on the outward facing film was examined using scanning electron microscopic (SEM) pictures of the surface under high magnification (up to 3.8×10^3). The micrographs suggest a chemical type of etching, producing a wavelike pattern which is presumably due to the inherent microstructure of the polymer (Figs. 2, 3). Several raised lines were also etched out, suggesting lines of stress in the polymer (Fig. 3). No contaminant elements above atomic number 9 were detected; this is the lower limit of our EDAX system.

In addition to the normal breathing hole, backlighting of the Kapton showed several apparent pinholes. No evidence was observed on the underlying Mylar sheet, suggesting any impacting material was volatilized. They were of the order of 0.1 mm diameter and were circular. Many scratches were observable under backlighting, suggesting rough handling at some point. More extensive studies with the scanning electron microscope (SEM) showed that these apparent pinholes were imperfections in the aluminum backing of the Kapton rather than impact holes. However, optical and electron microscopic observations of both the Kapton and Teflon samples show a number of other areas that do appear to be a result of impacts. Examples are shown in Figs. 3, 5, 6. However, none of these show true penetration and none of them show residue of any element above atomic number 9 (the lower limit of our EDAX system). This does not rule out impacts by ice or carbonaceous particles but it does rule out the iron family type of meteorite unless one wishes to postulate a "clean hit".

Fourier transform infrared spectroscopy was performed in the hope of detecting changes in the polymer structure. The spectra were obtained by pressing the Kapton samples against the KRS-5 ATR crystal. As can be seen in Fig. 5, no significant differences were observed in the exposed Kapton sample as compared with the "matched unexposed sample". Scanning electron micrographs of exposed and unexposed Kapton are shown in Fig. 2. It is apparent that the exposed surface is rather rough, resulting in a visually dull surface as compared to the shiny unexposd surface. Thus, in the case of Kapton, the main effect of exposure seems to be a roughening or etching of the surface due to ablation with the residual polymer structure essentially unchanged.

(2) Separation Net. No etching of the separation (apparently nylon) was observed under optical microscopy. Special attention was made to compare the small section exposed by

the breathing hole in the Kapton outer film with more protected areas.

(3) Aluminum-Coated Mylar Inner Films. The inner films of the blanket were inspected visually using an optical microscope up to 400 power. No erosion was apparent. Particular attention was paid to comparing the area exposed through the breathing hole in the Kapton outer film with more protected areas.

(4) Silver-Coated Teflon (Figs. 6, 7, 8). The sample of silver-coating of the Teflon appears to be severely eroded in the area exposed to sunlight. At x5 magnification, however, it can be seen that a few islands of silver remain in the eroded area and that there is a density gradient at the boundary.

On the Teflon material, many degradation cracks were found in the illuminated area where the "silver coating" is not visible (see Fig. 4). There is residual silver in this area as indicated by the X-ray analysis, but it is minor.

Under the 400 power optical microscope, the impacts appear visually as circular, often but not always surrounded by a bright ring. The impression is similar to flash pictures of water droplet impacts or lunar craters. Although these impact points are clearly visible optically, we were unable to locate them with the scanning electron microscope.

IV. SIMULATIONS

To test the cause of the erosion, we subjected a sample of the unetched Kapton to a low pressure oxygen atom discharge (a microwave discharge in molecular oxygen was used at 0.5 torr with about 2% conversion to oxygen atoms). Part of the sample was illuminated by the microwave discharge which is rich in ultraviolet, and part of the sample was shaded. After a three-hour exposure no apparent erosion was observed in either the illuminated or unilluminated portions. To test the possible role of high energy ions, a sample of virgin Kaption was exposed to a 3 keV argon ion beam under high vacuum conditions. A similar etching was observed on this sample.

A test of the uneroded silver-Teflon sheet in a low pressure oxygen atom discharge (0.5 terr ~ 2% 0 atoms, room temperature) showed a strong attack on the coating. After fifteen minutes the material took on the black velvet appearance of colloidally dispersed metal similar to the "platinum black" of hydrogen electrodes. Attack was more rapid where the material was illuminated by the ultraviolet radiation from the discharge, but even completely shaded material showed some attack after three hours. Silver oxide is a grey-black material which if finely divided would have a black velvet appearance.

V. CONCLUSIONS

A. The etching of the Kapton is superficial, affecting a layer less than a tenth of a micron as indicated by the stero SER pictures and the persistence of 100 micron fibers produced in punching out the breathing holes. Further evidence is the lack of any change in the infrared signature of the polymer.

B. The etching of the Kapton is probably due to high energy impacts rather than attack by thermal oxygen atoms. The evidence for this is the resistance of the material to laboratory 0 atoms both in the dark and with UV illumination. By contrast, 3 keV Argon ions produced a similar etching. Possible candidates are "orbiting" atoms and other excited molecules which could impact with twice the satellite velocity. Cosmic ray ions and submicron meteorites are also possible high energy ablators.

C. Thermal oxygen atoms are apparently not a factor in materials attack at this altitude since laboratory oxygen atoms showed no attack of the Kapton; yet the exposed satellite surface was attacked. By contrast, 0 atoms strongly attacked the silvered Teflon in a manner different from that observed on the exposed satellite material which was only eroded in the dark.

D. Both aluminized Mylar and the nylon net materials of the blanket were resistant to the agent which etched the Kapton. This observation is substantiated by the absence of visible attack of these materials in the area under the breathing hole where they are exposed to the same environment as the Kapton.

E. There is evidence suggesting impacts by micrometeorites, but they were not large enough to penetrate the Kapton blanket and left no residue of elements above atomic number 9 which is the lower limit of our instrument. This suggests that they were micrometeorites but that they were small and either icy or carbonaceous.

ACKNOWLEDGEMENT: This work was supported by the U. S. Naval Sea Systems Command under Contract N00024-85-C-5301.

Table I

APL/JHU Program to Study Solar Max Returned Samples

	SAMPLE		Optical Microscopy	Scanning Electron Microscopy	Low Energy O Atom Bombardment	Ion Bombardment	Fourier Transform Infrared Spectroscopy
13A	Al-Kapton	Front Etched	C	C			C
		Front Impact	C	C			
		Front Breathing Hole	C				
		Front Pin Hole	C				
		Back (Overall)	C	C			
	Aluminized Mylar	Behind Breathing Hole	C				
		Overall	C				
	Net	Separation Net	C				
	Silvered Teflon	Cleared Area	C	C			
		Boundary	C	C			
		Impacts	C	C			
		Impacts ($+y_2$)	C	C	C		
Virgin Composition		Kapton	C	C	C		C
		Nylon Net	C				
		Aluminized Mylar	C				
		Silvered Teflon	C		C		

C = Completed

LIST OF FIGURES

SOLAR MAX RETURNED MATERIAL
OVERALL VIEWS

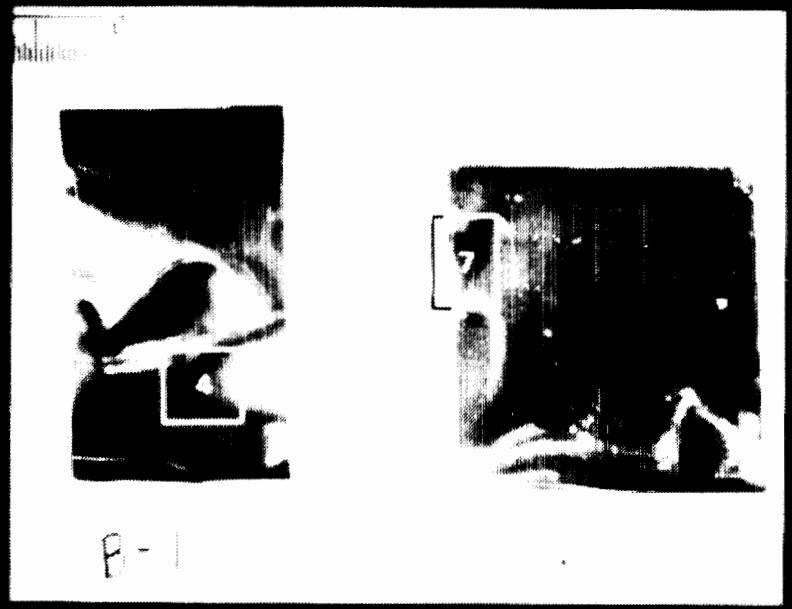

TWO SILVER COATED TEFLON PIECES
B1 AND Y2

KAPTON BLANKET ASSEMBLY
13 A

Fig. 1. Overall view of APL/JHU Solar Max Returned Materials (SMRM)

SCANNING ELECTRON MICROGRAPHS OF SOLAR MAX KAPTON SHOWING THE ROUGHENED SURFACE OF THE EXPOSED KAPTON. MAGNIFICATION = 2000

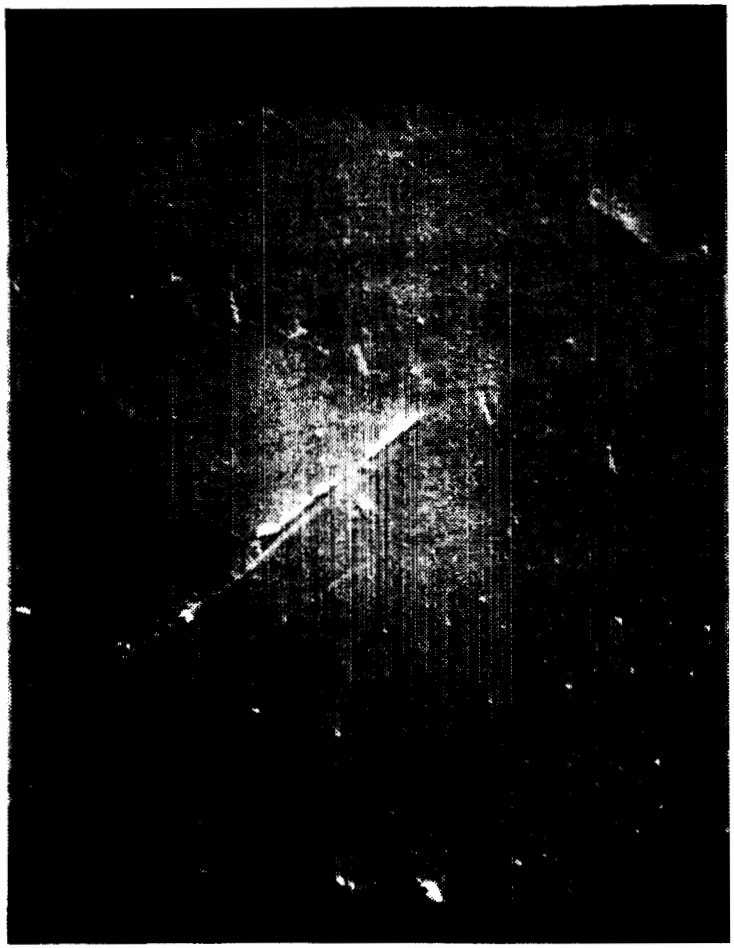

Unexposed Kapton

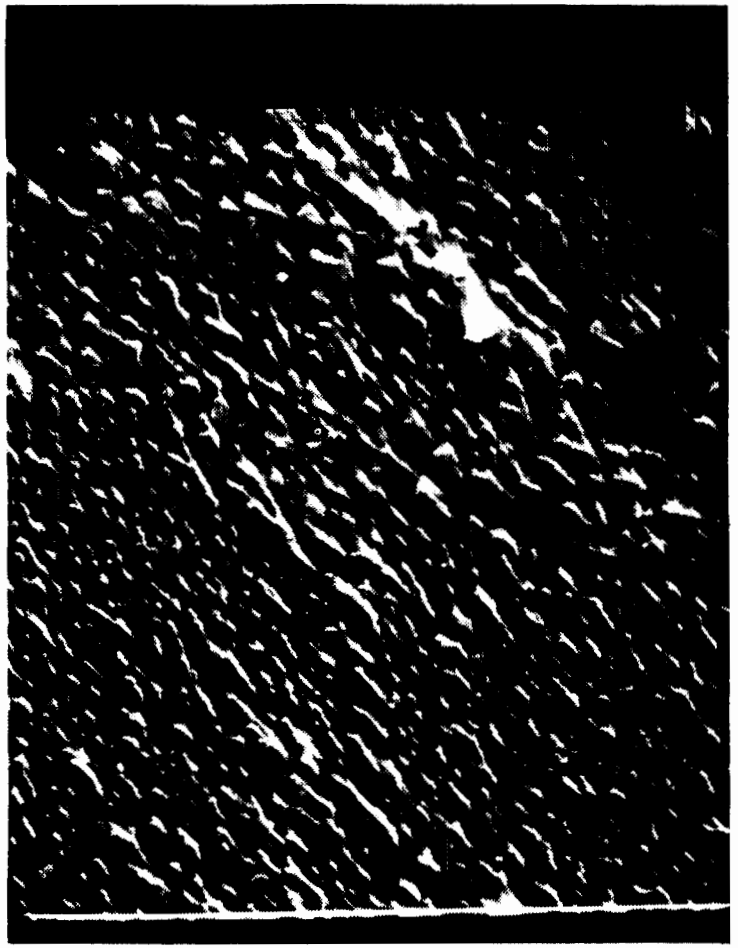

Exposed Kapton

Fig. 2 Comparison of exposed and unexposed surfaces of Kapton

SOLAR MAX RETURNED MATERIAL
SCANNING ELECTRON MICROSCOPE PICTURES

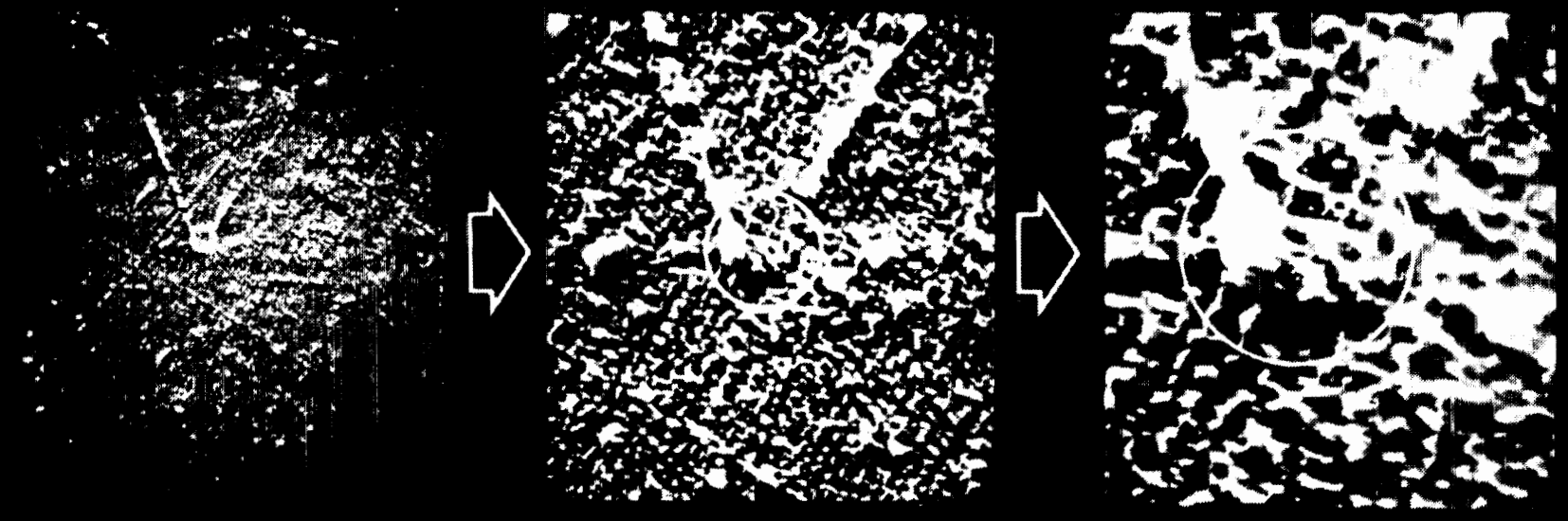

Fig. 3 SEM pictures of exposed Kapton under various magnifications

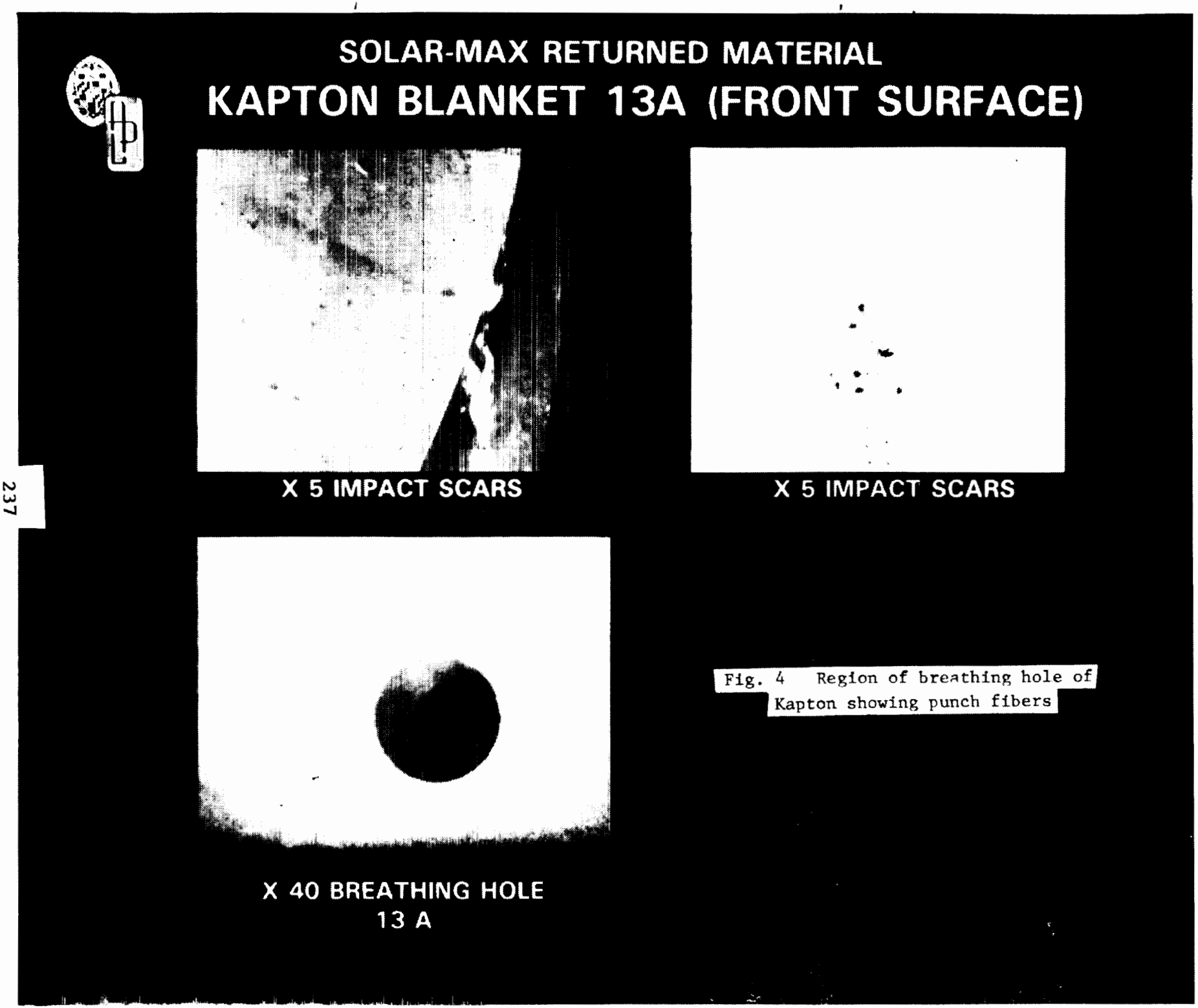

Fig. 4 Region of breathing hole of Kapton showing punch fibers

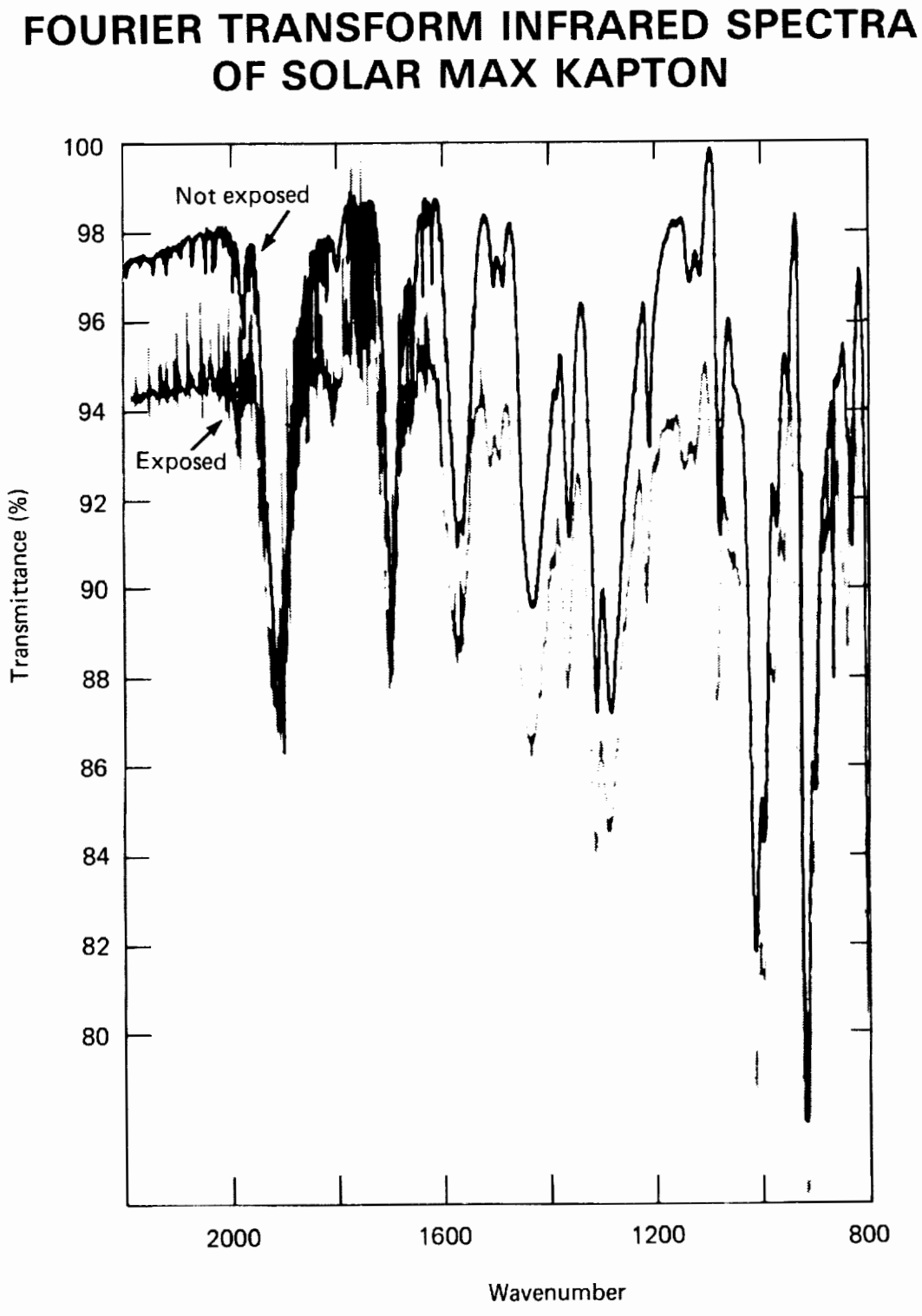

Fig. 5 Comparison of FTIR spectra of exposed and unexposed Kapton

SOLAR-MAX RETURNED MATERIAL
SILVER COATED TEFLON

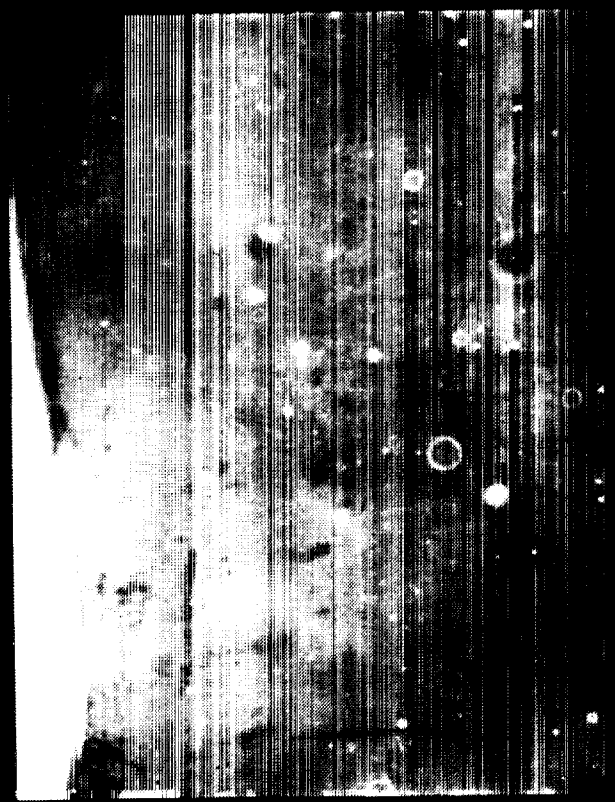

X 5 IMPACT SCARS

X 5 LIGHT ASSISTED EROSION

Fig. 6 Light-assisted erosion boundary

OPTICAL MICROGRAPH OF SOLAR MAX SILVER-COATED TEFLON THAT HAD BEEN ILLUMINATED BY THE SUN DURING ORBIT

MAGNIFICATION = 200

Silver-coated Teflon

Fig. 7 Magnified light-eroded Teflon surface

EXAMPLES OF APPARENT IMPACTS ON SOLAR MAX KAPTON AND SILVER-COATED TEFLON

Silver-coated Teflon

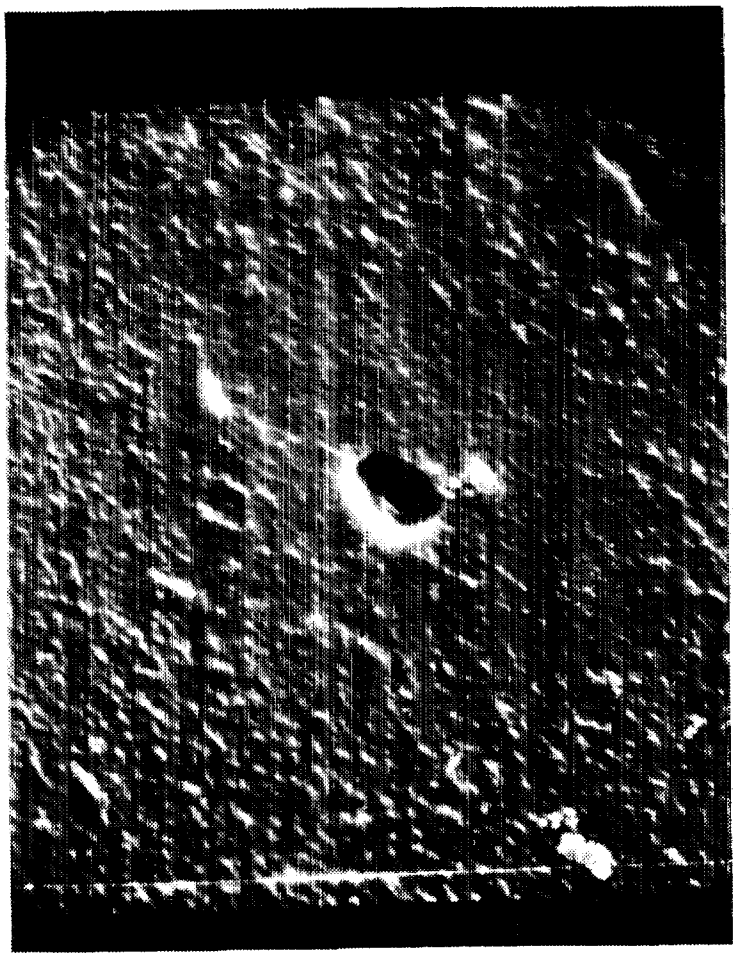

Kapton

Fig. 8 ESR pictures of apparent impact areas. A - Kapton, B - Teflon

(This page intentionally left blank)

ANALYSIS OF MICROMETEORITE MATERIAL CAPTURED BY THE SOLAR MAX SATELLITE;

L.S. Schramm[1], D.S. McKay[2], H.A. Zook[2], G.A. Robinson[1]; [1]Lockheed/EMSCO, 2400 Nasa Rd. 1, Houston, TX 77058; [2]NASA/Johnson Space Center, Houston, TX 77058

The Solar Maximum satellite, launched Feb. 14, 1980, was retrieved and repaired April 10, 1984, after being subjected for four years and 55 days to impacts by micrometeorites and Earth-orbiting space debris. A companion abstract (1) describes in detail the nature of the returned parts, the size distribution of the hundreds of impact craters found, and the chemical groupings of the material found at impact sites. We restrict ourselves here to the chemical variety and physical condition of particles associated with two particular impact structures in the insulation blanket of the main electronics box, named M-19-280 and M-Q-355.

A JSM-35CF scanning electron microscope (SEM) equipped with a PGT System IV energy dispersive x-ray analyzer (EDXA) was used to determine morphology and chemistry of impacted areas and associated particles. The thermal blanket consists of 17 layers of aluminized Kapton and Mylar plastic films each separated by a thin dacron net. For both M-19-280 and M-Q-355, a single circular penetration hole, 280 micrometers and 355 micrometers in diameter, respectively, with a raised rim was produced in the 75 micrometer thick first (outer) layer of the insulation blanket. The affected area on the second layer of M-19-280 consists of a ring of tiny (1 to 30 micrometer) holes and craters surrounding a central roughed up area approximately 5 millimeters in diameter; that of M-Q-355 consists of a wedge-shaped pattern of craters and concentrically elongated holes approximately 2 millimeters wide with a large elongated hole at the apex. These patterns are similar to those formed in the capture cell technique described by McDonnell (2,3). For both impacts, the projectile was apparently disrupted by the impact with the outer layer. The disrupted projectile sprayed inward in a cone-shaped pattern which then interacted with the second layer, producing the observed features. Some of the projectile material and/or material from the first layer also penetrated through the second layer, but most did not.

Particles were analyzed on the front (impacted) side of Layer 2 of both craters and the back (exiting) side of Layer 1 of M-19-280. Particles were chosen at random and represent only a fraction of the entire population available. Approximately three-fourths of the particles analyzed were fragments or melt droplets of Kapton. However, 210 non-Kapton particles of variable composition were analyzed (Table 1). These particles range from .5 to 5 micrometers in diameter; most are about 1 micrometer. They range from spherical droplets to globular shapes to rare irregular fragments. The most abundant particles are predominately magnesium, silicon and iron (MSF) in composition. The next most abundant particles are of aluminum composition. Aluminum, also present in most EDXA spectra, probably derives in large part from the thermal blanket aluminum coatings. The third most common particles contain mainly iron, sulfur, and nickel (FSN). In M-Q-355, FSN particles dominated; no MSF particles were found (Table 1).

The MSF and FSN particle EDXA data were reduced, using standards and the BSAM program from PGT; this program corrects for x-ray fluorescence and absorption, but not particle size and shape. Because of variable particle size, it was necessary to normalize the data to 100%. In Figure 1, atomic ratios of Mg, Si, and Fe for 100 individual MSF particles from M-19-280 are shown as well as ratios for a 'chondritic' micrometeorite in the stratospheric dust collection published by Brownlee (4), for ordinary L chondrites (5), and

for the Allende carbonaceous chondrite (6). The MSF particles are clearly close to chondritic in composition. The major difference between the MSF particles and chondritic material seems to be higher Mg and lower Fe and Si. We suggest that most of these particles have been fractionated by volatilization of Fe and possibly Si during partial or complete melting after impact with Layer 1. Some evidence for this is found in EDXA spectra of broad areas of the textured region of Layer 2 which show small Fe and possibly Si peaks not present elsewhere on the Kapton; a thin vapor coating is apparently present. Another possible explanation for lower iron (and sulfur) in our analyzed silicate particles compared to bulk chondrites is that some of the iron (and sulfur) from the bulk projectile is in the associated FSN particles also found in M-19-280. For both impact structures, the FSN particles have approximately stoichiometric (Fe,Ni)S proportions. The 21 analyzed FSN particles in M-Q-355 contain an average of 6.8 wt.% (±3.4 wt.%) Ni; the 12 analyzed particles in M-19-280 contain an average of 0.7 wt.% (±0.2 wt.%) Ni. We conclude that M-19-280 and M-Q-355 were formed by micrometeorite impact. MSF particles in M-19-280 are probably residue of a chondritic micrometeorite; FSN particles in M-Q-355 are residue of an iron-nickel sulfide micrometeorite.

While our examination of the returned Solar Max hardware is still in a preliminary stage, it seems clear that the insulation blankets have inadvertently acted as micrometeorite capture devices similar to the capture cells designed for that purpose (2,3). These results should encourage further experiments to capture micrometeorites in space and to capture cometary dust during comet rendezvous and flyby missions.

Table 1. Composition of non-Kapton particles in Solar Max craters.

Particle Type by Most Abundant Elements	No. in M-19-280	No. in M-Q-355
Mg,Si,Fe (MSF)	100	-
Fe,S,Ni (FSN)	12	21
Al	46	8
K,Cl	4	-
Fe,Cr,Ni	3	-
Na,Cl	3	-
Al,Si	3	-
Ca	3	-
S	2	-
Ba,S	1	1
Zn	1	-
Mg,Ca	-	1
	178	32

Figure 1. Mg-Si-Fe atom ratio distribution for MSF particles in M-19-280 and for other chondritic meteorites.

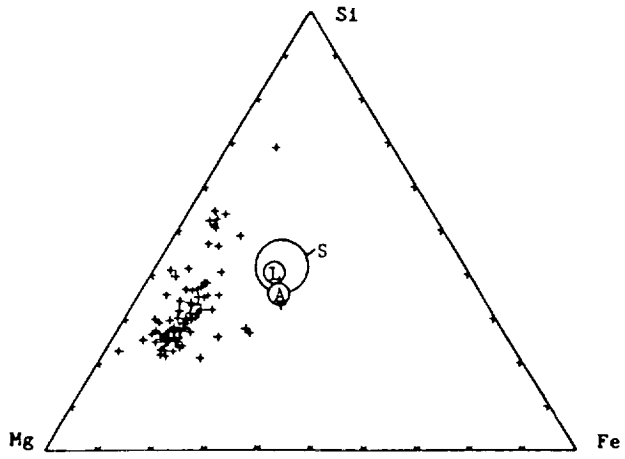

+ = M-19-280 MSF particles
S = majority of submicron grains from stratospheric micrometeorite SP56A (4)
L = average of ordinary L chondrites (5)
A = Allende carbonaceous chondrite (6)

(1) Kessler, D.J. et al. (1985) This vol. (2) McDonnell, J.A.M. et al. (1984) Nature, 309, p. 237-240. (3) McDonnell, J.A.M. et al. (1983), Lunar and Planet. Sci. XIV, p. 475-476. (4) Brownlee, D.L. (1984) Lunar and Planet. Sci. XV, p. 94-95. (5) Dodd, R.T. (1981) Meteorites: A Petrologic-Chemical Analysis, Cambridge University Press, p. 19. (6) Clarke, R.S. et al. (1970) Smithsonian Contributions to the Earth Sciences, 5, p. 45.

EXAMINATION OF RETURNED SOLAR-MAX SURFACES FOR IMPACTING ORBITAL DEBRIS AND METEOROIDS.

D.J. Kessler, H.A. Zook, A. E. Potter, D.S. McKay (NASA/JSC, Houston, TX 77058), U.S. Clanton (Dept. of Energy, P.O. Box 14100, Las Vegas, NV, 89114), J.L. Warren, L.A. Watts (Northrop, P.O. Box 34416, Houston, TX 77234), R.A. Schultz (Purdue Univ., Dept. of Geosciences, West Lafayette, IN 47907), L.S. Schramm, S.J. Wentworth, and G.A. Robinson (Lockheed, 1830 NASA Rd. 1, Houston, TX 77058).

Previous theoretical studies (1) predicted that in certain regions of earth orbit, the man-made earth orbiting debris environment will soon exceed the interplanetary meteoroid environment for sizes smaller than 1 cm. Recent analyses of impact measurements obtained from Explorer 46 (2), Skylab experiment S-149 (3), The Apollo/Skylab windows (4), and the STS 7 Shuttle window (where a 2mm high-velocity impact crater was found to contain titanium with a trace of aluminum) suggest that a significant orbital debris population already exists in earth orbit (5). However, these experiments had either short exposure times, no conclusive technique to differentiate debris from meteoroids, or an altitude or time of flight where a lesser amount of debris would be expected. The surfaces returned from the repaired Solar Max Mission (SMM) by STS 41-C on April 12, 1984, offered an excellent opportunity to examine both the debris and meteoroid environments.

Solar Max was launched on February 14, 1980, into a near circular orbit at 570 km altitude, and an inclination of 28.5°. By April 10, 1984, the orbit had decayed to 500 km and SMM was captured for repair in the shuttle payload bay, after nearly 50 months of exposure to space. The returned surfaces included about 1.5 sq.met. of thermal insulation material and 1.0 sq. met. of aluminum thermal control louvers. The thermal insulation consisted of 17 layers of alumized kapton or mylar, each separated by a dacron net, and the louvers consisted of 2 layers of heavy aluminum foil separated by about 3 mm. These types of surfaces offer excellent opportunities to obtain chemistry of impacting particles.

To date, approximately 0.7 sq. met. of the thermal insulation and 0.05 sq. met of the aluminum louvers have been mapped by optical microscope for crater diameters larger than 40 microns. Smaller craters were recorded in some cases; however, smaller craters are increasingly difficult to recognize optically. In addition, atomic oxygen has eroded up to 20 microns of the exposed kapton surfaces(6), removing the older and smaller craters. Figure 1 shows the crater size distribution found on 3 different kapton surfaces. Craters larger in diameter than about 100 microns found on the initial 75 micron thick Kapton first sheet on the MEB (Main Electronics Box) blanket are actually holes and constitute perforations through that blanket. Similarly, 70 micron craters form complete holes through the initial 50 micron thick first sheet of thermal blankets #6 and #9. About 160 craters were found to have penetrated these surfaces. Based on very limited calibration data, this is a factor of 2 to 5 above what would be expected from the meteoroid flux alone.

The chemical study of these craters is only in the initial stages. About 250 chemical spectra have been recorded of particles observed in or around impact pits or in the debris pattern found on the second layer beneath impact holes in the outer layer. Chemistry is obtained via a PGT 4000 Energy Dispersive Spectrometer on a JEOL JSC-35CF Scanning Electron Microscope (SEM).

The following populations have been found to date in impact sites on these blankets:

EXAMINATION OF SOLAR-MAX SURFACES

Kessler, D.J. et. al.

Meteoritic material-characterized mainly by particles or droplets composed primarily of Si, Mg, Fe, Ca, and Al, or less often, iron-nickel sulphides. A more detailed analysis of the meteoritic component is given in (7).

Paint particles - Characterized by titanium and zinc, whose oxides form pigments for white thermal paints. The chemistry of these particles also includes potassium, silicon, aluminum, and chlorine. Potassium silicate is used as a "binder" to cement the pigment grains together. Aluminum is apparently used for pigmentation. The source of the chlorine in these particles is not yet understood. It is not yet clear whether the paint particles have impacted at high or at low velocity. This may become understood when the aluminum louvers are examined in detail.

Aluminum droplets-For these craters, only aluminum droplets are observed in the ejecta on the second sheet. The ejecta patterns observed on the second sheet are well spread out and are composed of finely divided particles or droplets. These impacts are most likely caused by man-made space debris.

Waste particles-This single impact went through three layers of the blanket. Chemistry was Na, K, Cl, P and minor amounts of sulphur. Sodium and potassium chlorides, sulphur, and minor amounts of phosphates are consistent with urine residue. This particle was almost certainly an ice particle from the Shuttle waste management system.

The Solar Max thermal blankets (and louvers) represent a very valuable resource of information about the near-Earth impacting particle population. The chemistry found within most of the craters is consistent with an origin other than meteoroids. Because of the many different sources of particles, some time is required before the chemically different populations can be quantitatively separated into clearly recognized origins.

References: 1. Kessler, D.J. and Cour-Palais B.G.(1978) JGR, 83, 2637. 2. Kessler D.J.(1984) IAU Colloquium 85, in press. 3. Hallgren D.S. and Hemenway C.L. (1976) Lecture Notes in Physics, 270. 4. Clanton U.S., Zook H.A., Schultz R.A. (1980) Proc. 11th Lunar Planet. Sci. Conf., 2261. 5. Kessler D.J. Advances in Space Research 1984,(1984) in press. 6. Park, J.J. (1985) NASA/GSFC, personal communication, and verified by authors. 7. Schramm L.S., McKay D.S., Zook H.A., Wentworth S.J., Robinson G.A., Warren J.L. (1985) LPSC XVI, this volume.

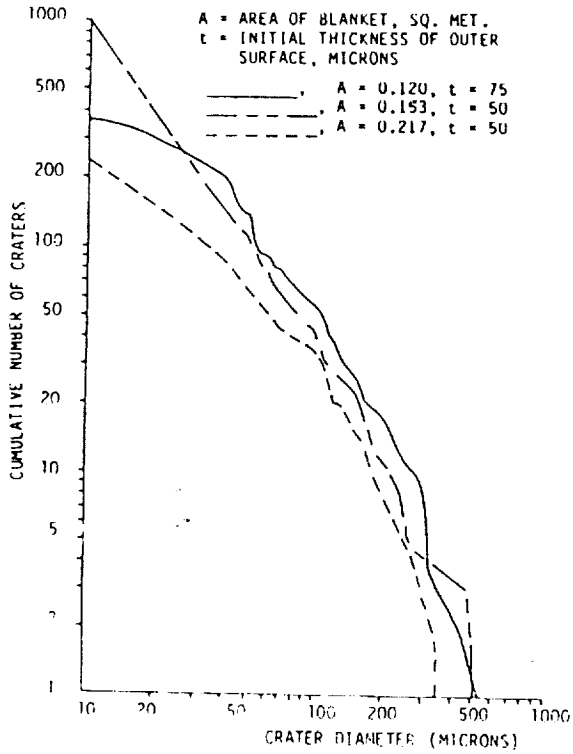

FIGURE 1. COMPOSITE OF CUMULATIVE SIZE PLOTS FOR SOLAR MAX MEB, 9, and 6 BLANKETS

A Preliminary Report on the Study of the Impact Sites and Particles of the Solar Maximum Satellite Thermal Blanket

by

Herbert A. Zook
NASA, Lyndon B. Johnson Space Center
Houston, Texas

This constitutes a preliminary report of our work as of December 6, 1984, on examining the impact pits in, or penetrations through, the thermal blanket of the Solar Maximum Satellite.

To date, the three largest pieces of the thermal blanket have been optically scanned with a total surface area of about one half square meter. Over 1500 impact sites of all sizes, including 432 impacts larger than 40 microns in diameter have been documented. The scanning has missed about 40% of the craters from 40 to 50 microns in diameter but only a few larger than about 60 microns. Many more craters that have been recorded are below the 40 micron pit diameter.

Craters larger in diameter than about 100 microns found on the 75 micron thick Kapton first sheet of the MEB (Main Electronics Box) blanket are actually holes and constitute perforations through that blanket. Similarly, 70 micron craters usually constitute holes through the 50 micron thick first sheet of thermal blankets #6 and #9. Table 1 represents a summary of the impact pit populations that have been found. Tables 2, 3, and 4 represent a more detailed breakout of the data in Table 1.

Figures 1, 4, and 7 represent cumulative curves (number of holes, or craters, larger than a given diameter) on a log (number) versus log (crater diameter) relation. Figure 10 summarizes these three curves. The other figures represent differential plots of the same data.

The chemical study of these craters is only in the initial stages. About 250 chemical spectra of particles observed in or around impact pits, or in the debris pattern found on the second layer in those cases where there is a hole in the first layer, have been recorded. Chemistry is obtained via Energy Dispersive X-ray analyses on a JEOL JSC-35CF Scanning Electron Microscope (SEM).

The following populations have been found to date in impact sites on these blankets:

1. Meteoritic material - Characterized mainly by particles or droplets composed primarily of Si, Mg, Fe, Ca, and Al, or, less often, of iron-nickel sulphides. Other chemical combinations, such as calcium-aluminum oxides,

also appear but more rarely. That the latter combinations are also of meteoritic origin is surmised from their association, in a single impact site, with the other chemistries cited above.

2. Paint particles - Characterized by titanium and zinc, whose oxides form pigments for white thermal paints. The chemistry of these particles also includes potassium, silicon, aluminum, and chlorine. Potassium silicate is used as a "binder" to cement the pigment grains together. Aluminum is apparently used for pigmentation. The source of the chlorine in these particles has not yet been determined. We do not know yet whether the paint particles have impacted at high or at low velocity. We hope that when there is a chance to look at the aluminum louvers, a decision on this question may be made.

3. Aluminum droplets - Only aluminum droplets have been observed in the ejecta on the second sheet. The ejecta patterns that have been observed on the second sheet are well spread out and are composed of finely divided particles or droplets. These impacts are maybe caused by man-made space debris.

4. Waste particle - This single impact particle went through three layers of the blanket. Chemistry was Na, K, Cl, P and minor amounts of sulphur. Sodium and potassium chlorides with minor amount of phosphates are consistent with urine residue. We suspect that this particle is an ice particle from the waste management system.

5. Tungsten-Bismuth - This single impact particle went entirely through the thermal blanket. GSFC had cut out this hole and sent it to Dr. Uel Clanton who was still here at that time. Dr. Clanton found traces of Tungsten and Bismuth around the rim area of some of the examined penetrations (or holes) in the deeper layers due to this impact. We do not have any good ideas as to the source for this particle.

The Solar Max thermal blankets (and louvers) represent a very valuable resource of information about the near-Earth impacting particle population. Because of the many different sources of the particles, it is still going to require some time before the chemically different populations are quantitatively separated into clearly recognized origins. To do this quantitative separation, a large amount of data will be needed on each population. This means that, although quite a few impact sites have been found, some populations will probably not be as well represented as others. Therefore, it would be very desirable to analyze as many blankets as possible to gain information on the chemically less represented populations.

The SEM analysis work is presently led by Dr. David McKay. This effort constitutes nearly all the remaining studies to be done on the available thermal blankets.

Table 1

Summary of number craters (or holes) found that were larger than a stated diameter on each of three different thermal blankets from the Solar Max Satellite.

	MEB	#9	#6	Totals
Total Number	362	236	969	1567
Number with D> 40	200	87	145	432
Number with D>80	68	40	53	161
Number with D>100	55	35	43	133
Number with D>120	39	21	28	88
Number with D>160	23	14	18	55
Number with D>200	18	8	10	36
Number with d>300	8	3	3	14
Area (cm^2)	1198	2170	1529	4897

Table 2

Solar Max MEB Blanket

Total area scanned = 1198 cm^2

Total number of impacts = 363

Impacts/cm^2 = 0.317

Impact Size, μm	Number of Occurrences
<40	162
40	52
45	9
50	43
55	2
60	12
65	2
70	12
80	9
90	4
100	7
110	8
115	1
120	7
130	3
140	3
150	3
160	3
170	1
195	1
200	3
210	1
220	2
240	1
250	1
280	2
300	4
320	1
355	1
440	1
520	1

Table 3

Solar Max Blanket 9

Total area scanned = 2170 cm^2

Total number of impacts = 232

Impacts/cm^2 = 0.117

Impact Size, μm	Number of Occurrences
<40	145
40	23
50	13
60	8
70	3
80	3
90	2
100	7
110	7
120	1
130	2
140	3
150	1
160	2
170	2
180	1
190	1
200	2
230	1
250	1
280	1
300	1
320	1
350	1

Table 4

Solar Max Blanket 6

Total area scanned =1529 cm^2
Total number of impacts = 969
Impacts/cm^2 = 0.566

Impact Size, μm	Number of Occurrences
<40	824
40	26
45	3
50	38
60	18
70	7
80	8
90	2
100	12
110	3
120	2
130	1
140	2
150	5
160	2
170	3
180	3
220	1
230	1
240	1
250	2
260	2
480	1
500	2

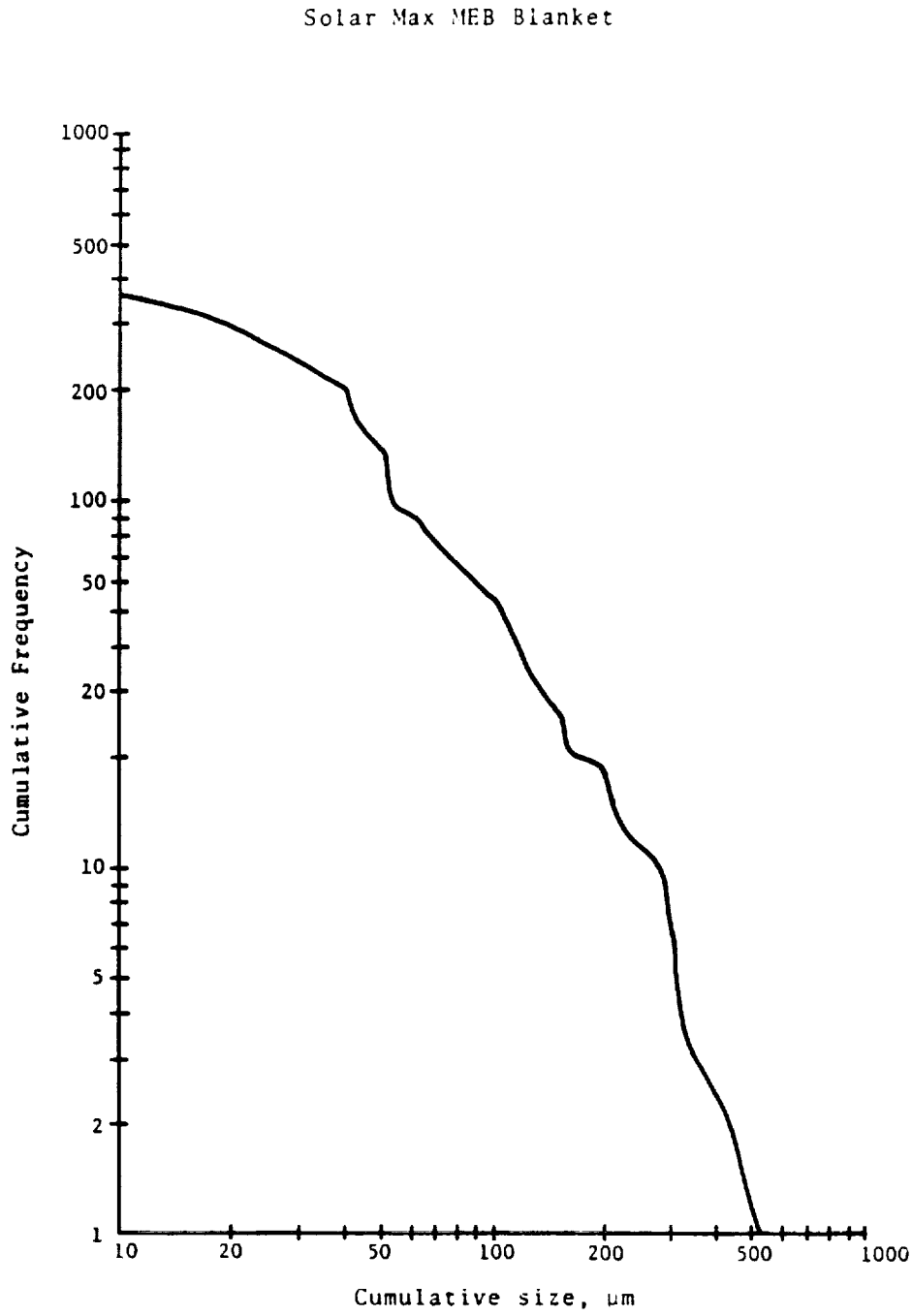

Figure 1. Cumulative Number of Craters (or holes) Whose Diameter Exceeds a Certain Size, MEB

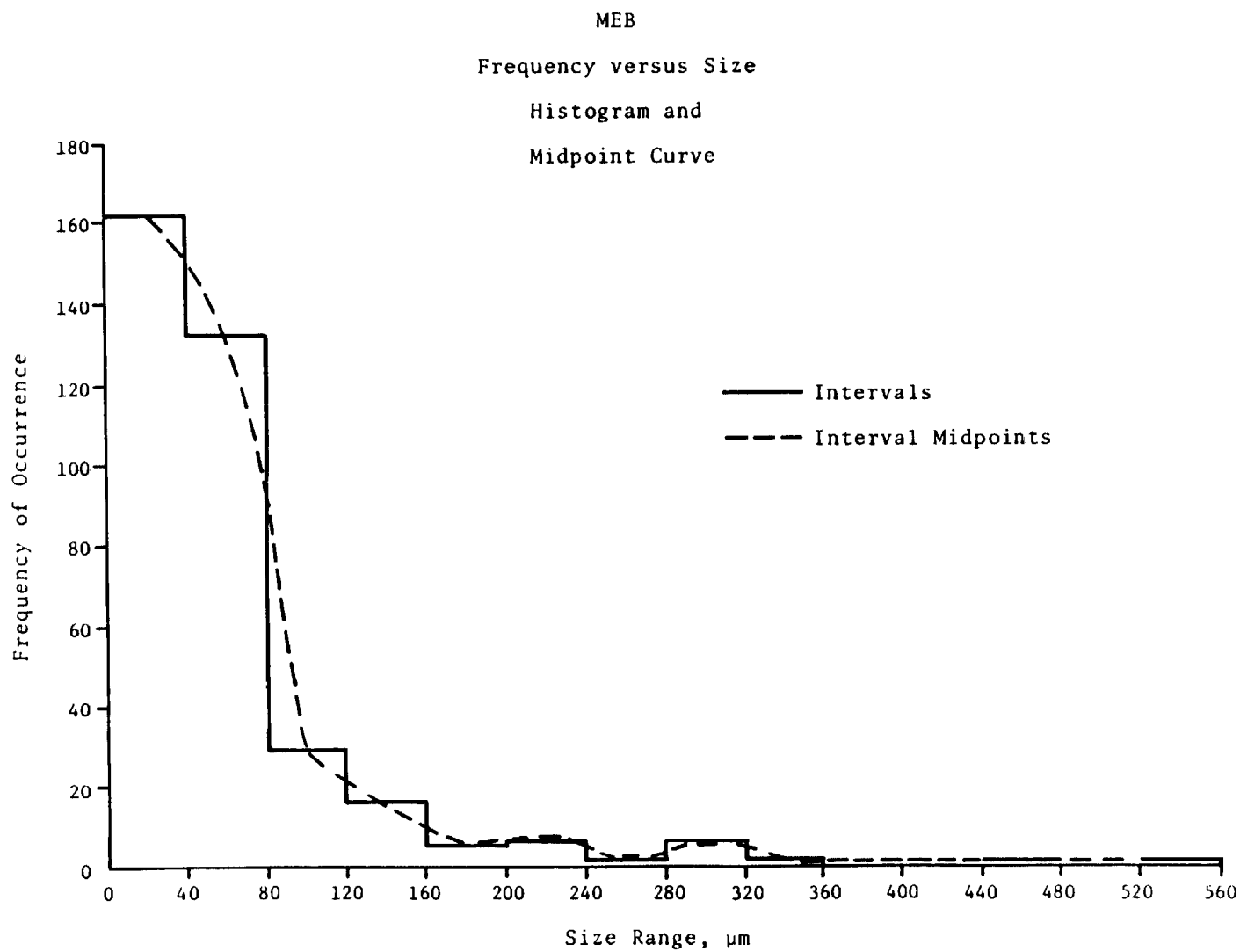

Figure 2. Frequency Versus Size Histogram and Midpoint Curve, MEB

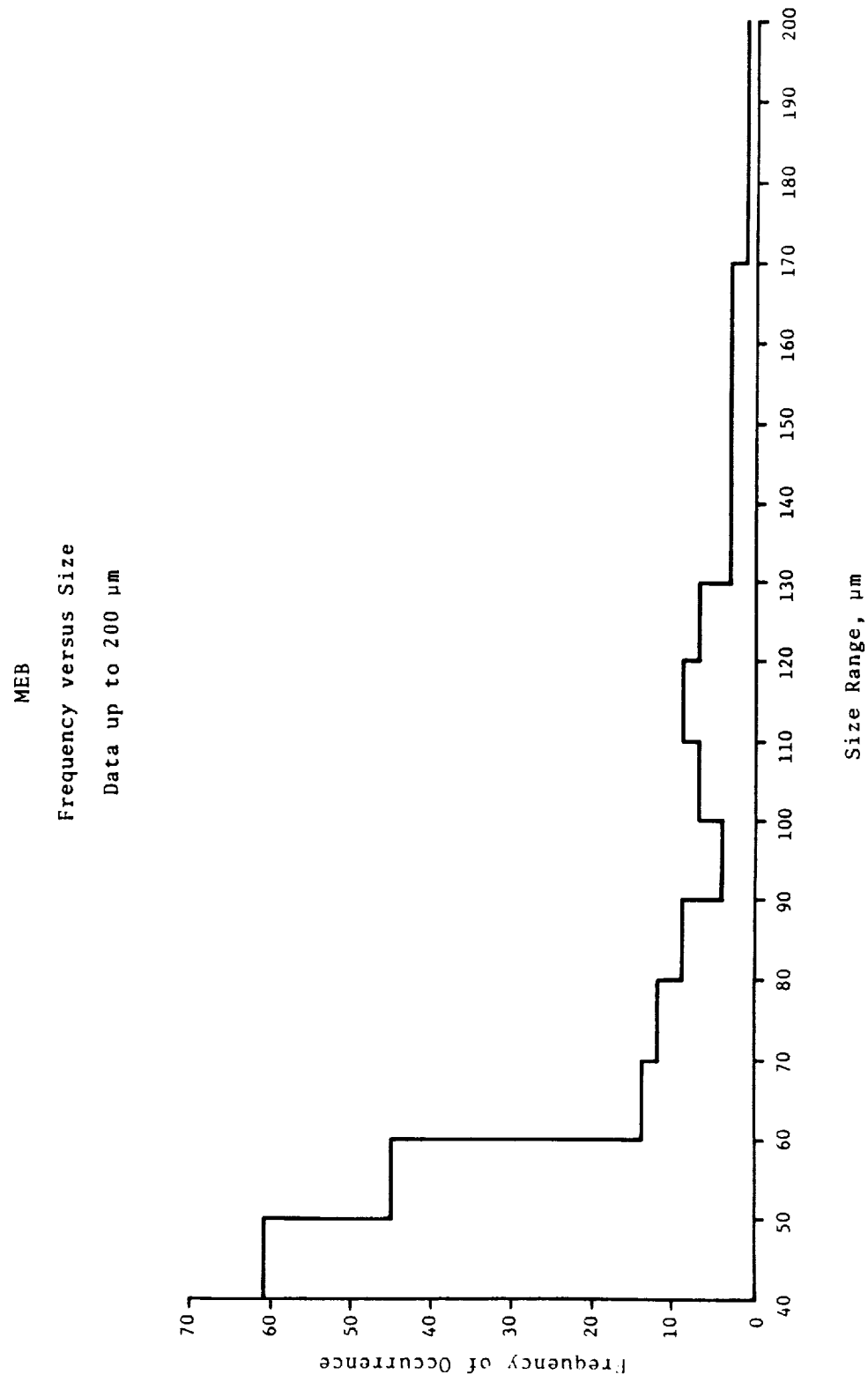

Figure 3. Frequency Versus Size Data up to 200 μm, MEB

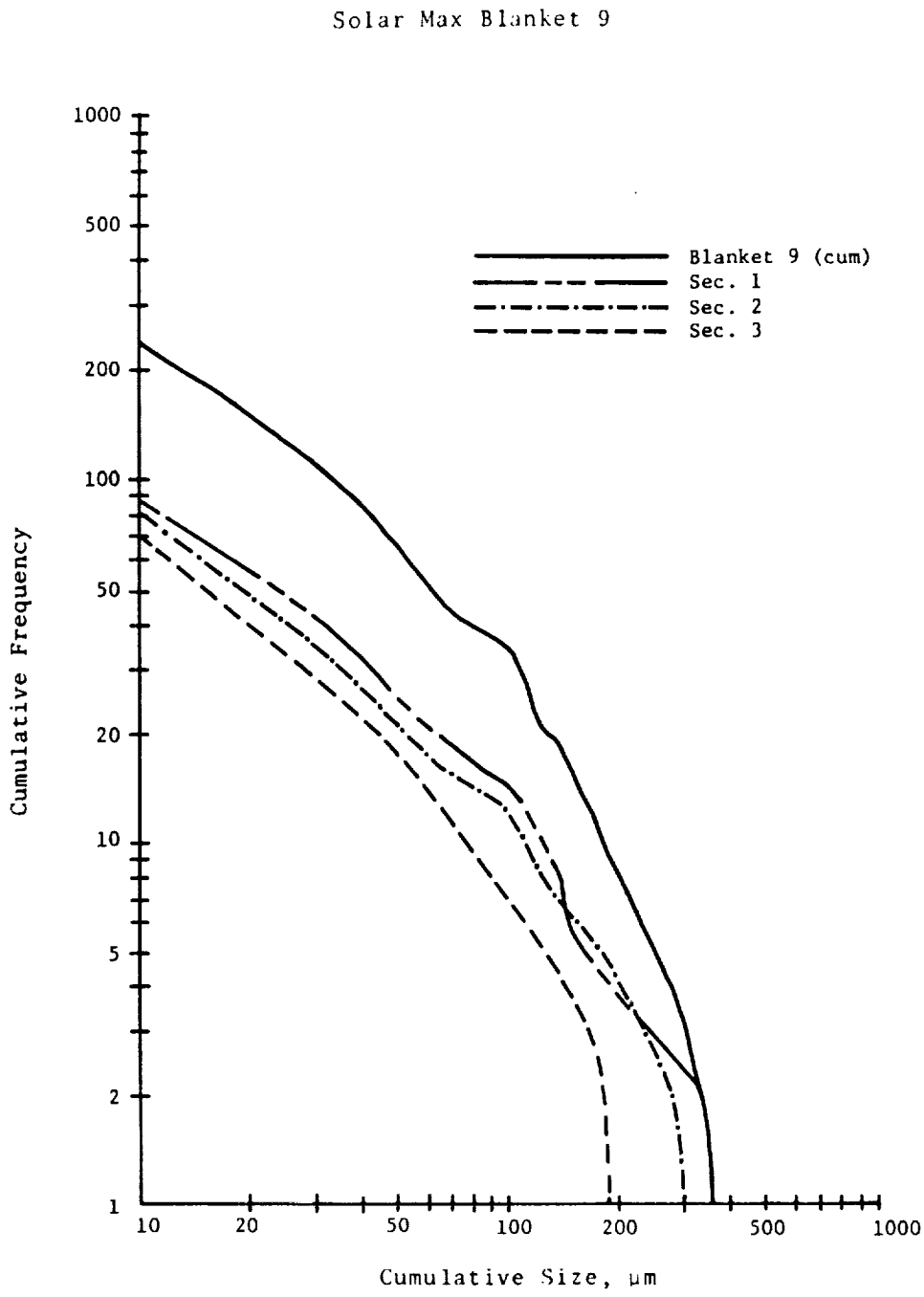

Figure 4. Cumulative Frequency v. Size, Blanket 9

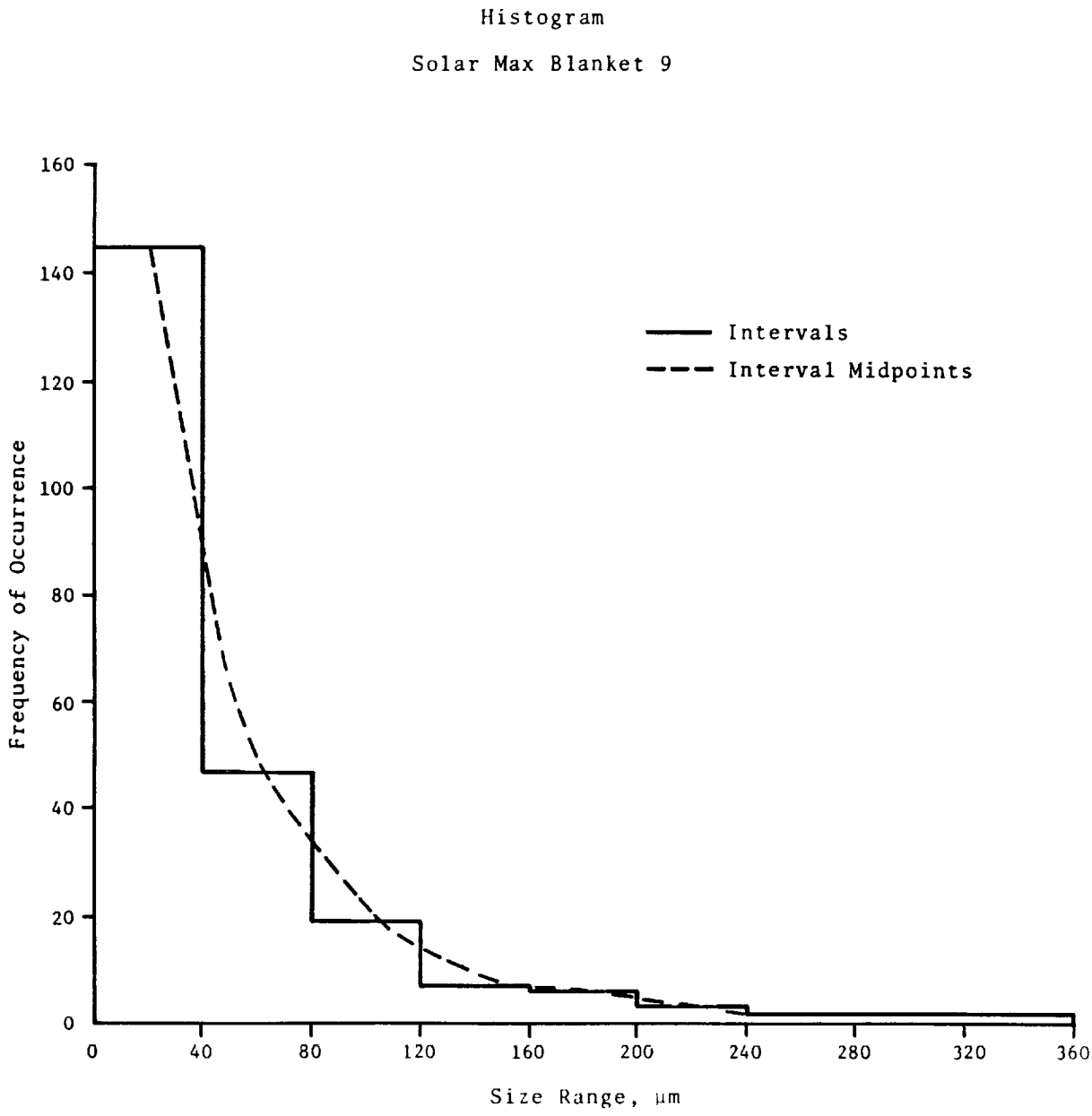

Figure 5. Frequency of Occurrence v. Size, Blanket 9

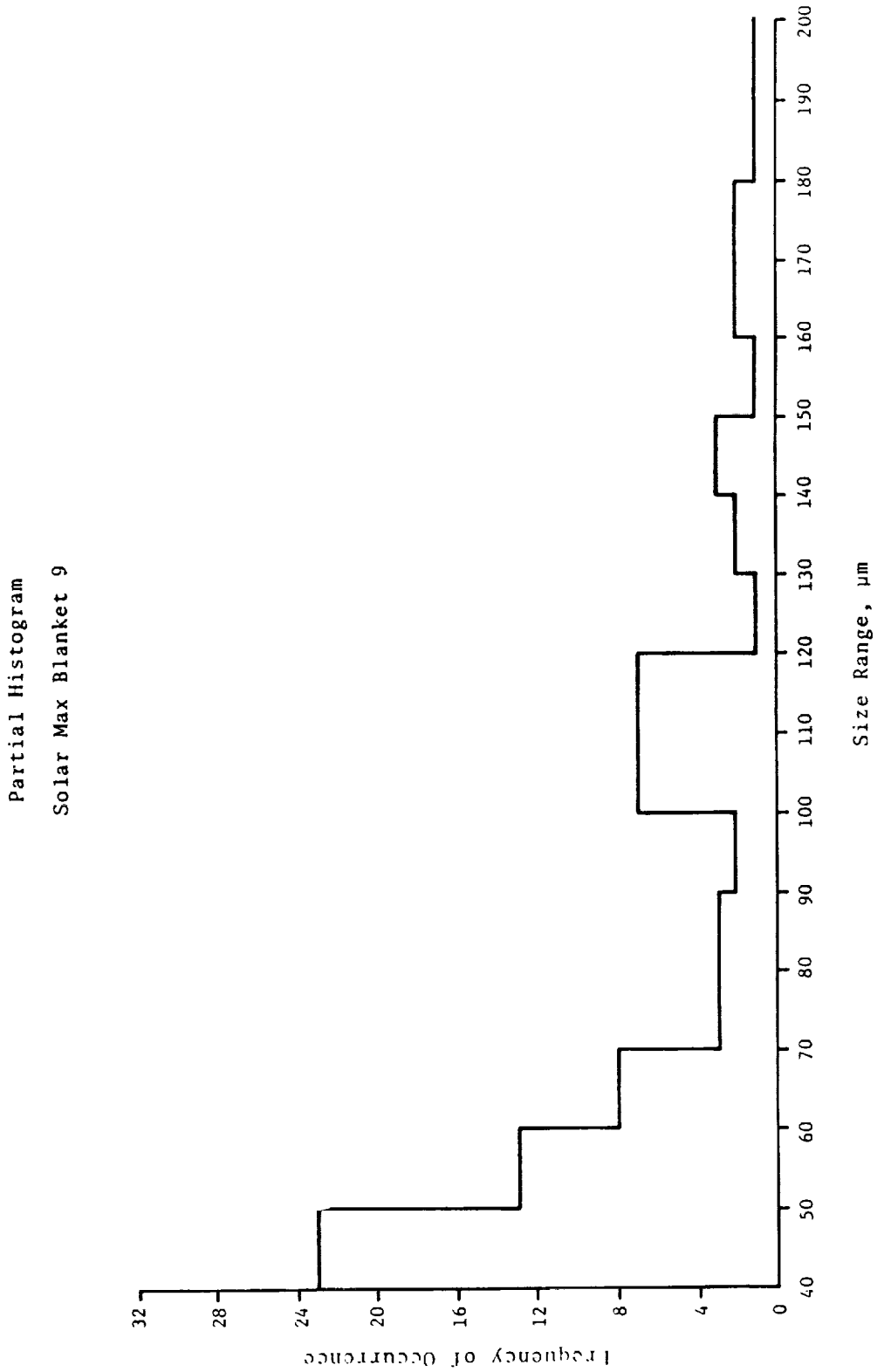

Figure 6. Partial Histogram; Frequency of Occurence v. Size, Blanket 9

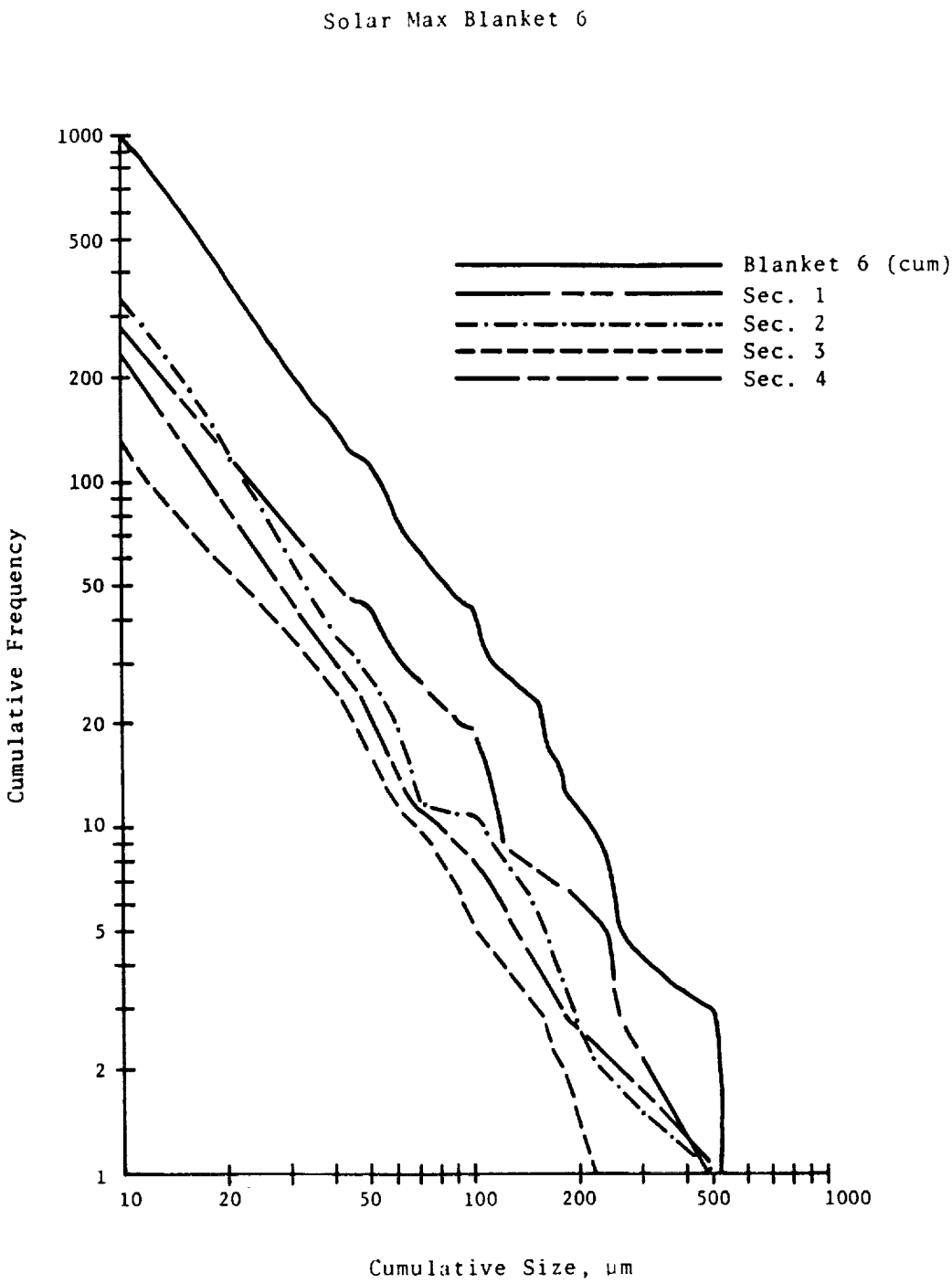

Figure 7. Cumulative Frequency v. Size, Blanket 6

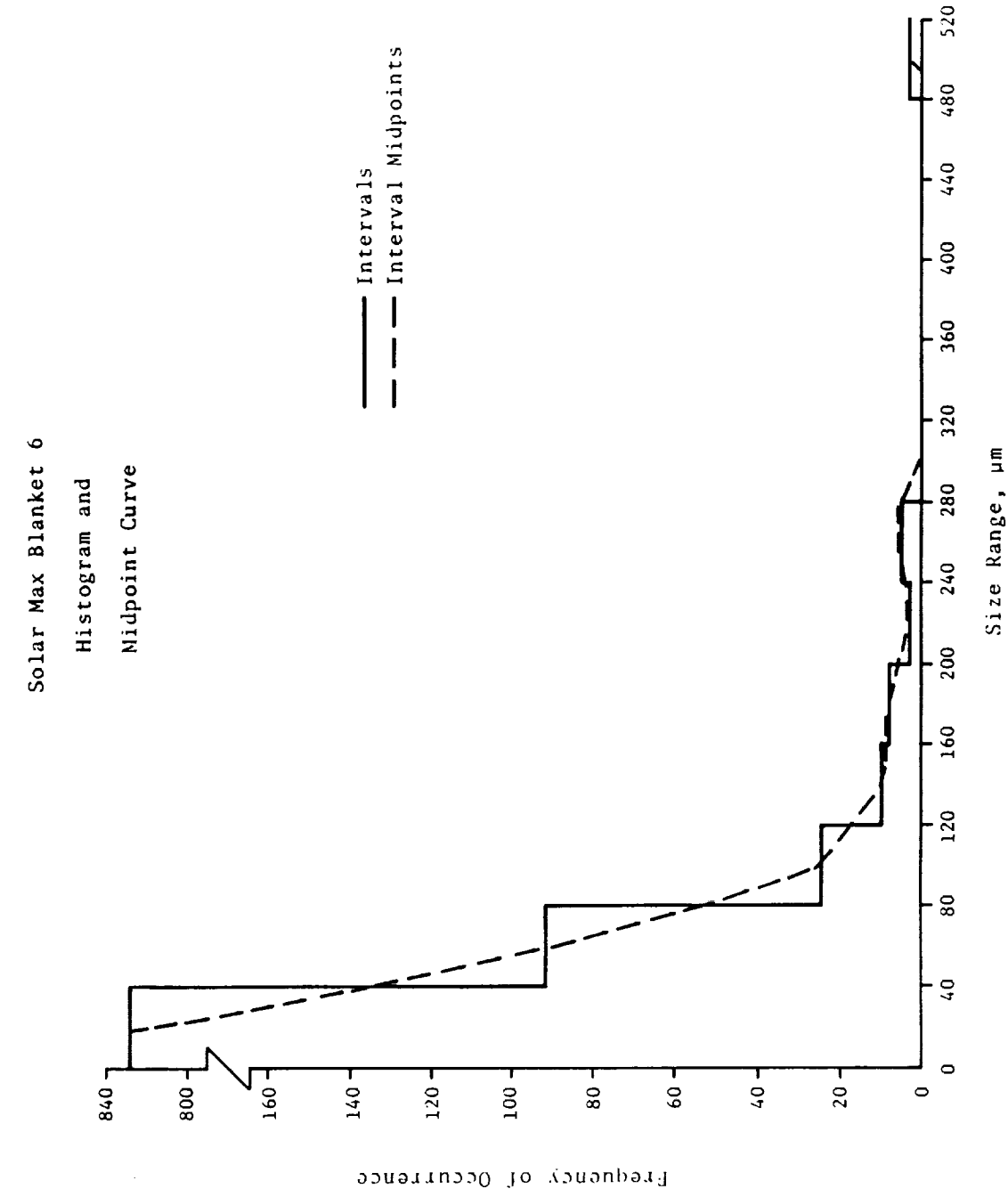

Figure 8. Frequency of Occurrence v. Size, Blanket 6

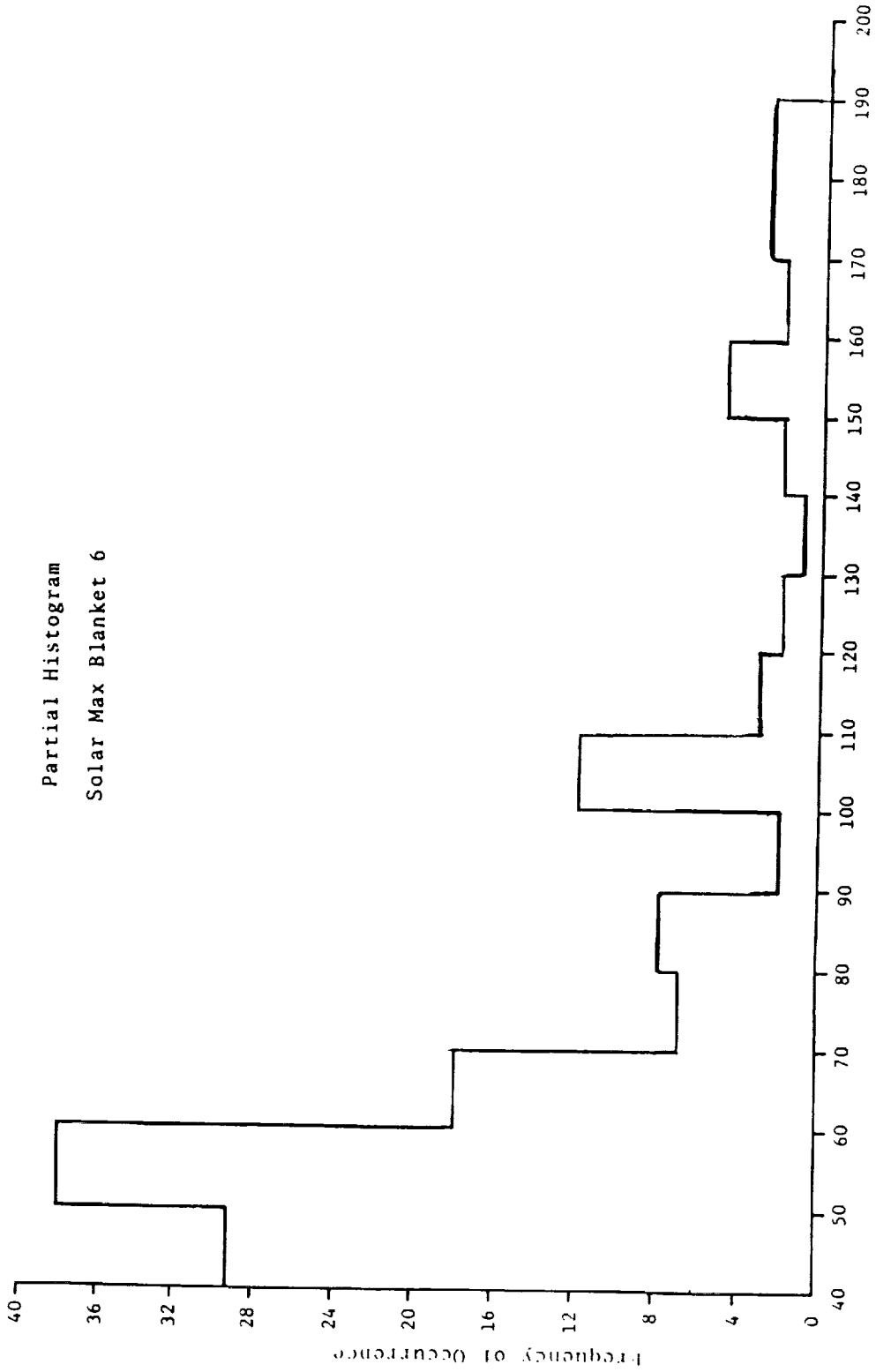

Figure 9. Frequency of Occurrence v. Size, Partial Histogram, Blanket 6

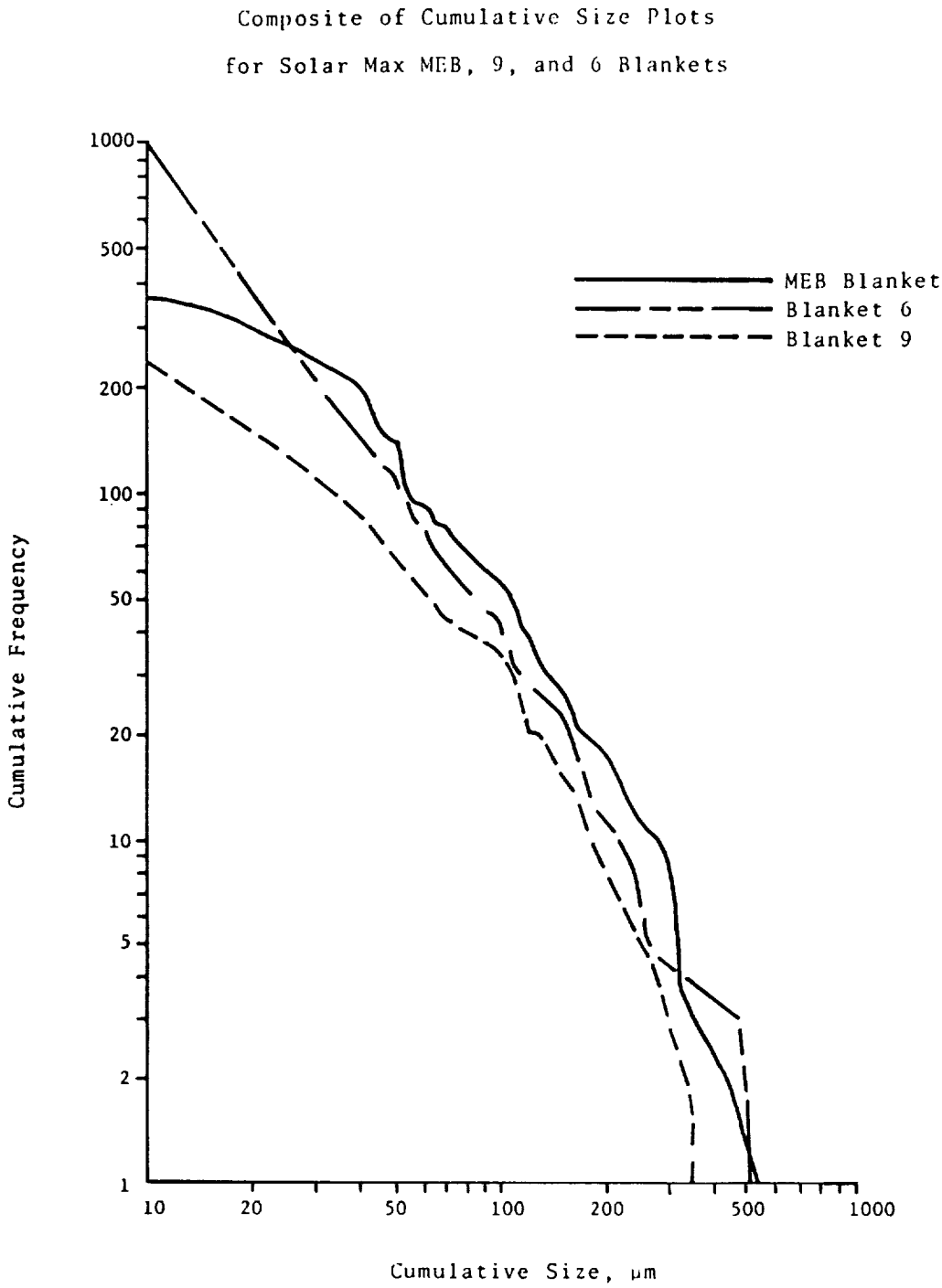

Figure 10. Composite of Cumulative Frequency v. Size for Solar Max MEB, Blanket 9 and 6

(This page intentionally left blank)

N87-14388

SSM ATOMIC OXYGEN REACTIONS ON KAPTON AND SILVERIZED TEFLON

Roger Linton and Ann Whitaker

Surface morphology studies at MSFC using Scanning Electron Microscopy on Kapton and Inconel silver coated teflon material samples retrieved from the Solar Maximum Mission spacecraft revealed significant changes attributed to orbital atomic oxygen - induced reactions. The Kapton recession observed on the aluminized Kapton material samples appeared equivalent in nature with that observed on previous Space Shuttle LEO missions, as expected, based on the comparable mission fluence levels of atomic oxygen (balancing reduced flux levels for the higher SMM orbital altitude with the extended 4-year lifetime). SSM teflon-taped material samples, coated on the back side with films of Inconel-protected, silver were observed degraded on both sides; visibly severe reactions on the back side (Inconel/silver) produced total blackening, generally restricted to areas, or strips, of the tape with a narrow, direct view-factor of the external orbital environment. High magnification S.E.M. views provided evidence of near total silver reaction, flaking, and subsequent erosion of the underlying teflon itself.

MSFC received nine material samples retrieved and cut from thermal-blankets of the SMM spacecraft, including four pieces of Inconel-silver coated FEP teflon and 5 pieces of multi-layer aluminized Kapton blankets (Figures 1 and 2). In Figure 1, the two teflon samples on the left, labeled Samples A and B, are shown viewing the coated back-side, indicating the localized (dark) regions of reaction previously referred to. In Figure 2, the single Kapton sample from the SMM Main Electronics Box (M.E.B.) wrapping shows the pattern of a deliberate ethyl alcohol wipe presumably performed prior to the original launch. No particular analysis has been undertaken at MSFC of the pinholes and/or potential micrometeoroid/debris impact holes observed in these photos of the Kapton samples. The visible diffussiveness of the exposed Kapton samples in these two unmagnified views is attributable mainly to atomic-oxygen induced reaction (pitting, erosion) and, possibly, univestated contamination.

For the purposes of this report, only three of the extensive S.E.M. photographs, (ranging to 20,000 X magnification) illustrating the basic reactions observed, are included pending more detailed investigation by various analytical techniques. For either the Kapton or teflon materials, unexposed (control) samples provide featureless, unrelieved photographic views at all of the S.E.M. magnifications used. Fig. 3 provides magnified views of an eroded Kapton sample from the SSM Attitude Control Systems (A.C.S.) module. Figure 4 provides views of the eroded backside (inconel/silver) coated area of a teflon sample on

the A.C.S. louver structure, showing only shreds of the metallic coating left and the bristle-like reacted pattern of the underlying teflon. For comparison, Figure 5 provides evidence of similar teflon reaction on the teflon exposed side of the sample.

Figure 1.

Figure 2.

ORIGINAL PAGE IS
OF POOR QUALITY

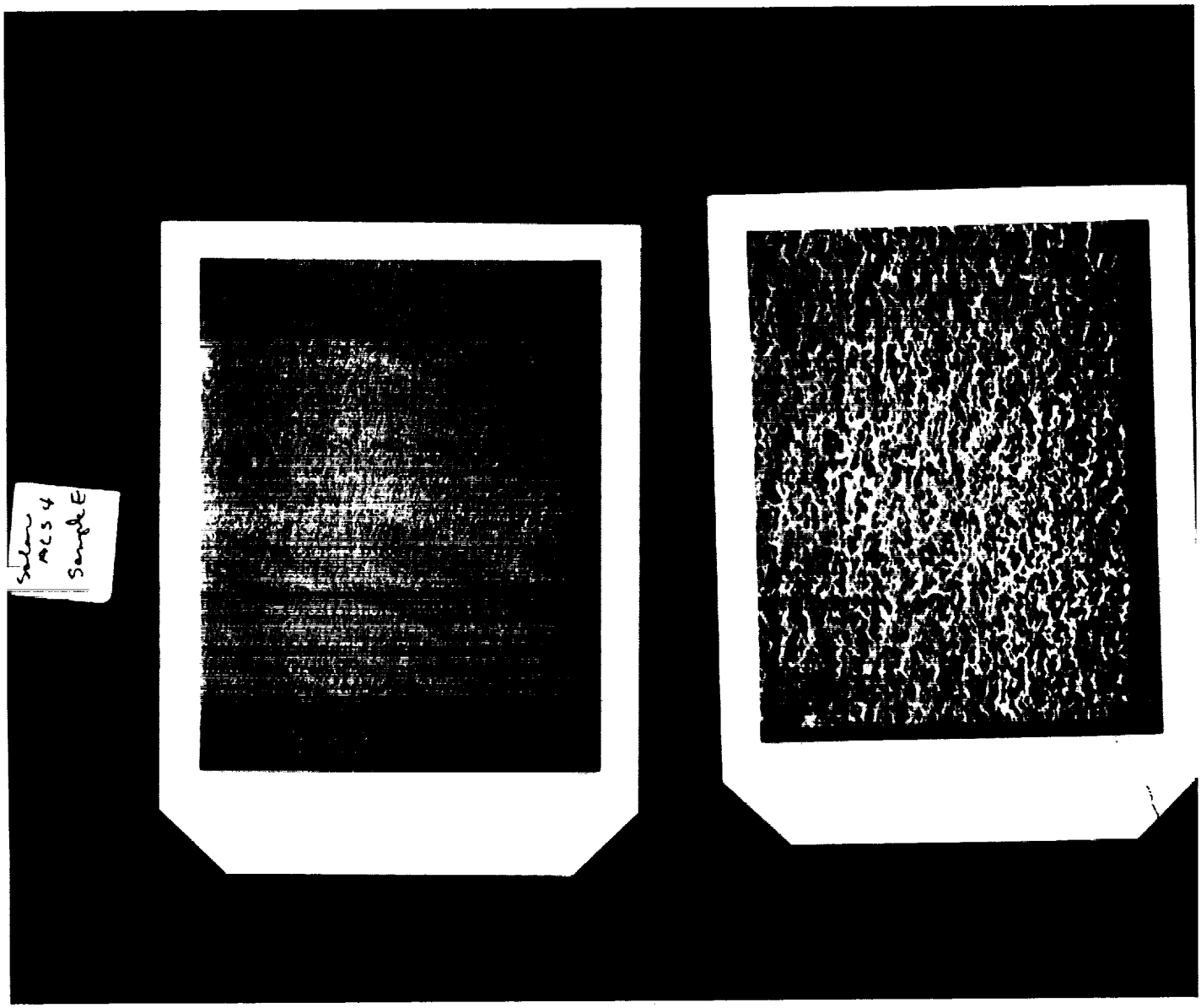

Figure 3.

Figure 4.

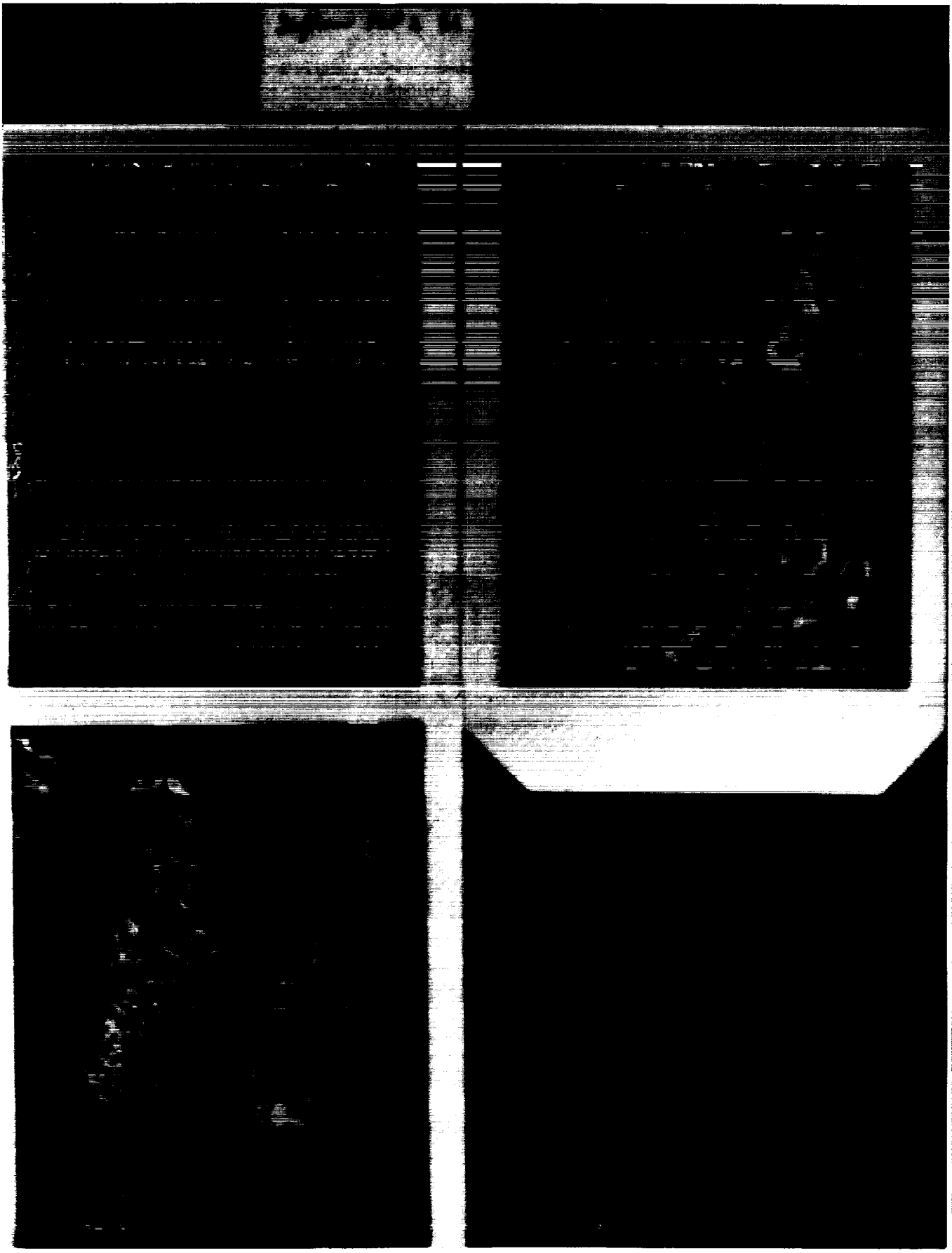

ORIGINAL PAGE IS
OF POOR QUALITY

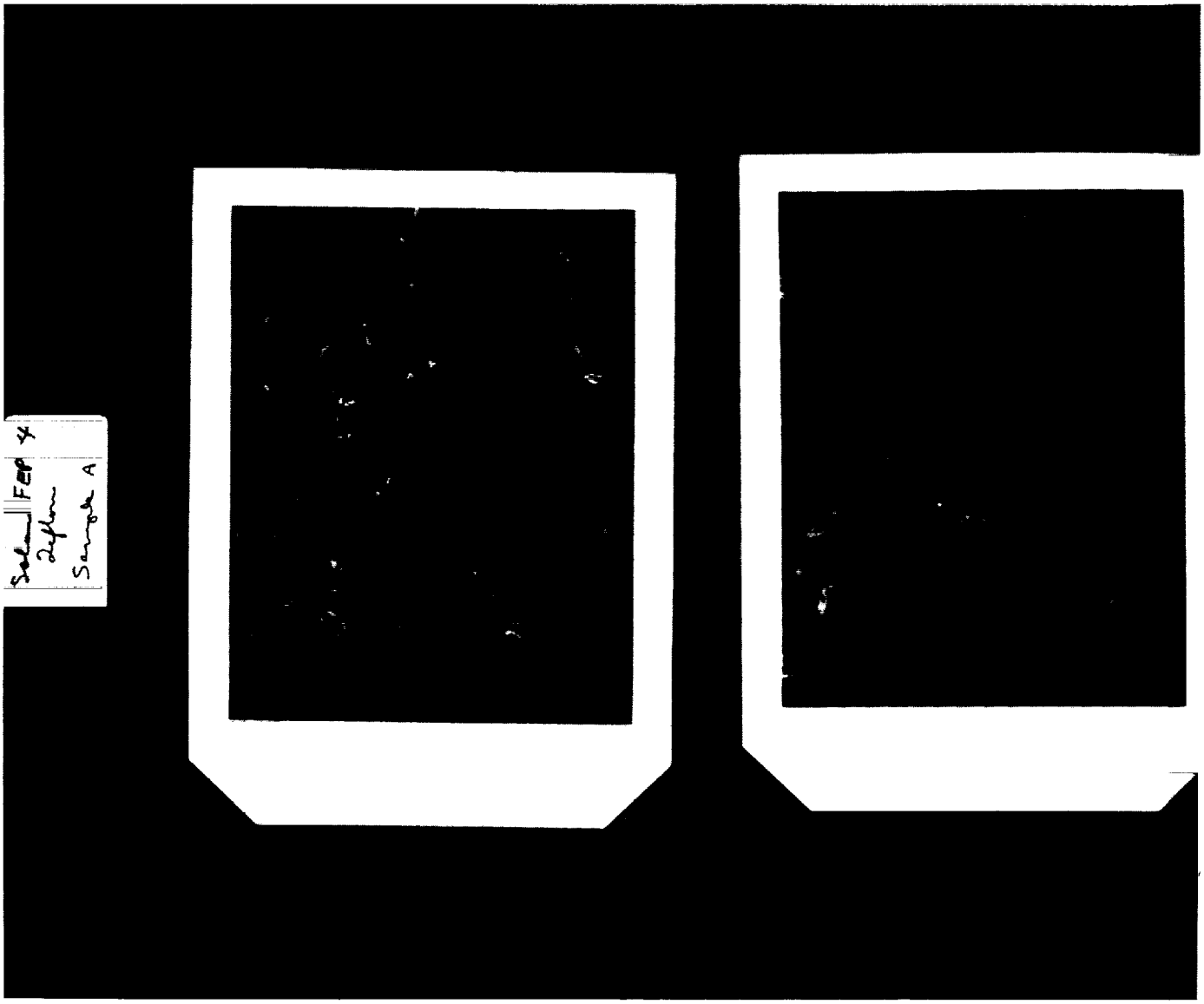

Figure 5.

(This page intentionally left blank)

PRELIMINARY RESULTS OF SMM EXPOSED ALUMINIZED KAPTON AND SILVERED TEFLON

Presented at the SMM Results Meeting
NASA Goddard Space Flight Center
May 9-10, 1985

by

Beatrice Santos-Mason
NASA-Langley Research Center
Hampton, VA 23665

INTRODUCTION

Early Space Shuttle flights revealed that organic materials, such as those used in thermal control blankets and paints in the payload bay, were adversely affected in the low-Earth orbit (LEO) environment.[1] Examination of eroded surfaces on these early flights and materials experiments performed on subsequent flights led to the conclusion that atomic oxygen present at Shuttle operating altitudes was responsible for surface degradation.[1,2]

These tests, which provided reaction rate data on polyimides[2,3], were highly accelerated. They obtained, in only a matter of hours, a total atomic oxygen fluence representative of exposure over several years. The Solar Maximum Repair Mission (Shuttle Mission 41-G) in April of 1984, during which the failed attitude control system (ACS) was replaced, provided a rare opportunity to study some of those same materials exposed in real time to atomic oxygen and ultraviolet (UV) radiation. The satellite was in low-Earth orbit for 4 years. Its outer surfaces were subjected to atomic oxygen, ultraviolet radiation or some combination thereof, depending on their location on the satellite. The replacement and retrieval of the ACS module from Solar Maximum Mission afforded the first opportunity to examine long-term exposure polymer specimens. This report presents preliminary results of studies of the microscopic surface effects on silvered Teflon* (Ag/Teflon) and aluminized Kapton* (Al/Kapton) used for thermal control on the Solar Maximum Satellite.

MATERIALS EXPOSURE

Due to the configuration of the satellite and its direction of travel, there were three types of exposure of thermal control blanket material: atomic oxygen and UV exposure, atomic oxygen exposure, or UV exposure. Some of the silvered Teflon was exposed on the backside (silver surface) as well as the front side (Teflon surface) due to open channels in the satellite. Aluminized Kapton was exposed only on the frontside (Kapton surface). The type of exposure will be specified for each sample discussed.

ALUMINIZED KAPTON

Atomic Oxygen and UV Exposure

The majority of the ACS module was covered with overlapping layers of aluminized Kapton thermal blanket. After assembly of the satellite and prior to launch, the blanket was wiped down with an alcohol-based solvent. Upon examination of the returned module exposed for 4 years in LEO, the blanket material appeared dull, in contrast to its original glossy appearance. The affected surface showed the pattern of streaks apparently created during the wipe down stage. Immediately adjacent to these streaks were areas that had the glossy, unexposed appearance. There were no obvious delineations indicating sharp edges or corners around which the material may have been wrapped to protect the "non-wiped" blanket area from direct atomic oxygen impingement.

*Identification of commercial products in this paper is provided to adequately describe the materials and does not constitute official endorsement, expressed or implied, of such products or manufacturers, by NASA.

In Figure 1, a scanning electron micrograph (SEM) of one of the inner layers of unexposed Kapton blanket surface is shown. It has a generally smooth appearance with minor surface scratches probably created during normal handling. The interface of the "wiped" and "non-wiped" area from an exposed outer layer appears in figure 2, with the "wiped" area on the left. Even at this low magnification, surface damage is more apparent and more abundant in the wiped area compared to the adjacent non-wiped area or to the unexposed specimen of figure 1. The microscopic tracks may have been caused by dust, micrometeoroids, or space debris in the LEO environment.

A much closer look at the affected region is shown in figure 3, now at the same magnification as figure 1. If one examines these tracks in detail, as shown in figure 4, one can see that there are holes within these structures. A circular depression is illustrated in figure 5. It also appears in the lower right hand corner of figure 2. Note the recurrence of holes within this structure as well. It seems as though these sub-micron sized holes occur preferentially in damaged or stressed areas.

At the interface between the wiped and non-wiped areas, as seen at high magnification in figure 6, another surface feature is noticeable. The material appears to have been attacked from underneath the surface, and in some cases the top layer of material is "left behind". A close up in figure 7 shows a tunnel-like structure passing beneath a very thin top layer. Figure 8 shows an even closer view of a curled edge of this top layer in the upper left corner of the photograph. This tunneling suggests that a protective layer exists on the Kapton surface, whereas the unprotected bulk is attacked by atomic oxygen through defects in the surface or diffusion of the oxygen through it.

A Kapton specimen exposed to atomic oxygen plus a limited amount of UV, shown in figure 9, does not have the same surface morphology as the previously discussed specimens. Its surface appears somewhat rough with wavelike structures created on the surface, but there are no holes. A close up of a typical area, figure 10, confirms this.

Atomic Oxygen Exposure

Figure 11 shows a Kapton specimen which was constantly in shadow, yet exposed to atomic oxygen impingement. Its surface is quite similar to that shown in figure 9, which was also exposed to limited UV. The magnified view of this sample (figure 12) is also very similar to figure 10. If these two sets of figures are compared (Figs. 9 and 10 to Figs. 11 and 12), an interesting observation can be made. That is, even though their morphologies are nearly identical, the features of figs. 9 and 10 are much larger than those of Figs. 11 and 12. The variation of atomic oxygen impingement angle and UV exposure may have created this difference. Another feature worth nothing is the directionality of the wavelike structures. This is visible when a comparison is made between figures 9 and 12. Apparently, figure 12 is rotated approximately 180° from figure 9. This directionality, related to vehicle travel through space and, therefore, atomic oxygen impingement, was also observed on STS-8.[3]

Silicon Contamination

A section of Kapton located near a satellite vent hole was examined. This specimen was subjected to solar and atomic oxygen exposure. Figure 13 reveals the surface to be thoroughly covered with what was determined by EDAX (Energy Dispersive Analysis of X-rays), to be silicon. In figure 14, a detail of this contaminant is shown. Silicone potting compounds were used in the satellite, which explains the appearance of this contaminant near a vent hole.

SILVERED TEFLON

Atomic Oxygen and UV Exposure

The louvers located on the ACS module were covered in some areas by silvered Teflon. The samples discussed in this paper were taken from the outer edges of the louver frame.

Teflon side

An unexposed sample of Teflon is shown in figure 15. Its surface is fairly smooth in texture. Again, some surface damage, probably created during handling, is evident.

The Teflon side of the silvered Teflon sample which was exposed to both atomic oxygen and UV is shown in figure 16. A higher magnification of a typical area is shown in figure 17, which reveals the three-dimensional nature of the cones. This view is taken from as nearly perpendicular to the sample as possible. The apparent tears in the material were caused by overheating of the sample at high magnification by the electron beam of the SEM.

This is in direct contrast to previous atomic oxygen exposure experiments aboard the Shuttle, which showed Teflon to be extremely stable. It had the lowest reaction efficiency of all materials tested.[2,5] In fact, the surface morphology seen here for Teflon is very similar to the Kapton morphology caused by atomic oxygen exposure.[3]

Silver side

Silvered Teflon used for space application has a thin coating of Inconel applied to protect the silver surface. In the SEM examinations described herein, the Inconel (Cr, Ni, Fe) was detected by EDAX.

A Silvered Teflon sample had its silver side exposed to both atomic oxygen and solar UV. When observed with the naked eye, the exposed sample appeared to have had some silver removed from the area which saw direct UV. Under the SEM, as one went from the unaffected silver area to the affected and finally depleted silver area, there were definite surface changes. Figure 18 illustrates the unexposed silver side of a silvered Teflon specimen.

In figure 19, regularly shaped bodies, which resemble grain bodies, can be seen. These bodies shrank in size and the boundaries around them appeared to progressively degrade as the "silver-depleted" area was approached.

Figure 20 illustrates this concept. In figure 21, the boundaries seem to have disappeared, and the bodies themselves are now degrading. EDAX did not show any difference in composition between the boundaries and the bodies. Both areas contained silver and Inconel. Also in figure 21, the underlying Teflon is visible. In figure 22, where most of the silver is absent from the surface, Teflon has the familiar spiked appearance, as seen with Kapton on STS-8.[3] Figure 23 shows these structures in detail. It appears as though these spikes are generated by "peeling away" from the main bodies (see upper portion of photograph).

Atomic Oxygen Exposure

Teflon side

In figure 24, a Teflon sample was exposed to the velocity vector of atomic oxygen. A closer view is given in figure 25. Its surface appears rough compared to unexposed Teflon (figure 15), but the damage is insignificant when compared to the previously discussed specimens.

Silver side

In figure 26, a view of the atomic oxygen-exposed silver side is shown. The first stages of oxidation appear to have taken place. A close up of the whitish (oxidized) areas are given in figure 28. Oxidation of silver by atomic oxygen was observed in an STS-4 experiment, in which the silver was completely oxidized.[4]

CONCLUDING REMARKS

The most adversely affected Kapton specimens were those exposed to both atomic oxygen and UV. Their surface morphology was somewhat similar to those previously observed in earlier experiments: the difference being the absence of the cone-like structures. The holes observed within the "tracks" and "craters" presented an intriguing problem. They may occur only in areas of internal stress within surface defects. These defects may have existed in the film prior to launch, but more likely, the majority were created by space debris during exposure. The mechanism of atomic oxygen and UV interaction that caused these holes to form is not yet understood.

Another interesting feature was the substructure found at the boundary zone of the "wiped" and "non-wiped" area. The material just below the surface was preferentially attacked. This suggested diffusion of atomic oxygen through the surface and reaction with the underlying polymer. If this reacted material then increased in volume, the resulting stress could have caused it to break away from the bulk. This process may have caused the apparent tears seen in the top layer and eventually removed it. Further investigation should determine the composition of the "non-wiped" portion to determine why it was not attacked.

Kapton specimens exposed to atomic oxygen appear virtually unaffected compared to those exposed to atomic oxygen and UV. This is also true for the specimen exposed to atomic oxygen and limited amounts of UV. There is essentially no difference between these two samples.

The most surprising result from these data was the attack on Teflon by combined atomic oxygen and UV. No such degradation was noted on earlier Shuttle experiments on Teflon. The cone structures created in the Teflon are, as previously mentioned, reminiscent of earlier polyimide data. Also, the removal of the silver/Inconel coating indicates that temperature cycling caused cracking and loss of the coating from Teflon as the satellite moved from sunlight to shadow.

It is important that the role of UV in atomic oxygen degradation be understood. The Solar Max Satellite was exposed to orders of magnitude more UV than any Shuttle exposures obtained to date. Therefore, it must be established whether there is some difference between the previous Teflon flown and that flown on Solar Max, or if UV causes a synergistic degradation effect when combined with atomic oxygen.

REFERENCES

1. Leger, L. J.: Oxygen Atom Reaction with Shuttle Materials at Orbital Altitudes. NASA Tech. Memorandum 58246, May 1982.

2. Leger, L. J.: Oxygen Atom Reaction with Shuttle Materials at Orbital Altitudes-Data and Experiment Status. AIAA-83-0073, AIAA 21st Aerospace Sciences Meeting, Jan. 1983.

3. Slemp, W. S.; Santos-Mason, B.; Sykes, G. F.; and Witte, W. G.: Effects of STS-8 Atomic Oxygen Exposure on Composites, Polymeric Films and Coatings. AIAA-85-0421, AIAA 23rd Aerospace Sciences Meeting, Jan. 1985.

4. Peters, P. N.; Linton, R. C.; and Miller, E. R.: Results of Apparent Atomic Oxygen Reaction of Ag, C, and Os Exposed During the Shuttle STS-4 Orbits. Journal of Geophysical Research, Vol. 10, July 1983, pp. 569-571.

5. Leger, L. J.; Visentine, J. T.; Kuminecz, J. F.: Low-Earth Orbit Atomic Oxygen Effects on Surfaces. AIAA-84-0548, AIAA 22nd Aerospace Sciences Meeting, Jan. 1984.

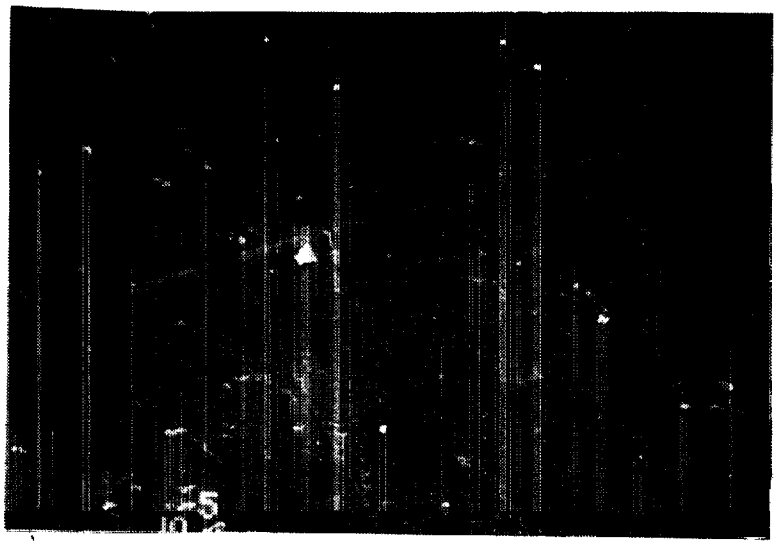

Figure 1. Unexposed Kapton from inner layer of thermal control blanket (1000x).

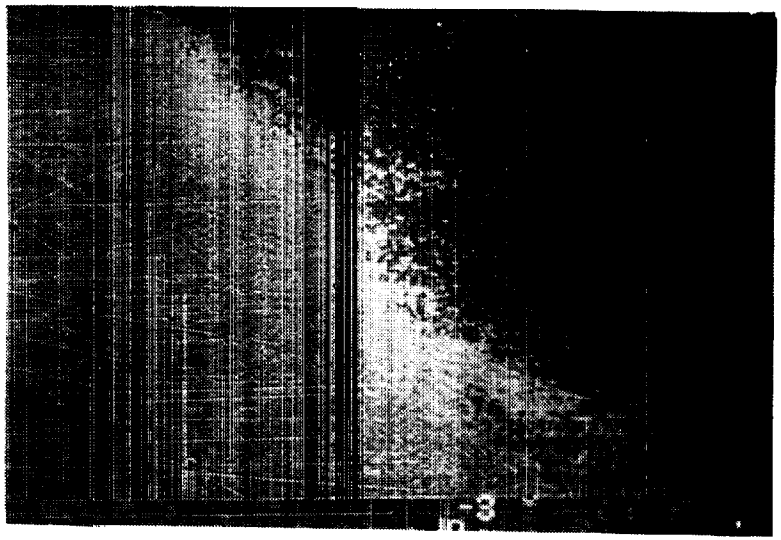

Figure 2. Kapton exposed to atomic oxygen and UV, showing "wiped" and "non-wiped" boundary (50x).

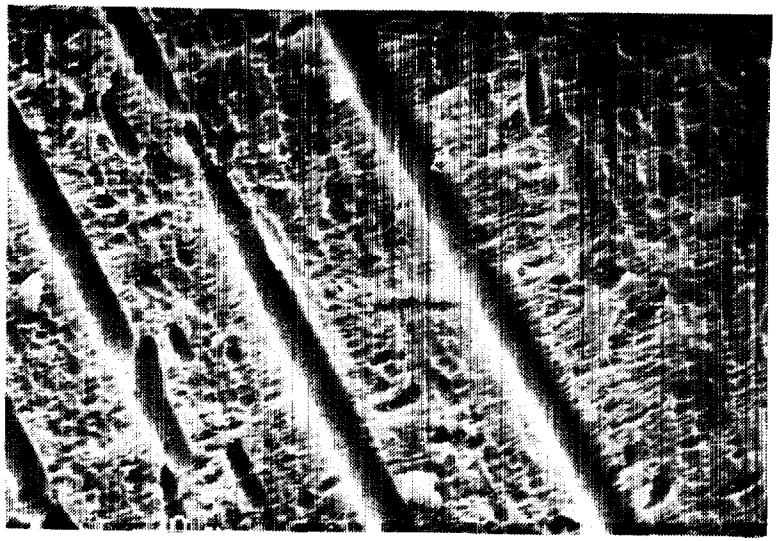

Figure 3. Kapton exposed to atomic oxygen and UV from "wiped" section (1000x).

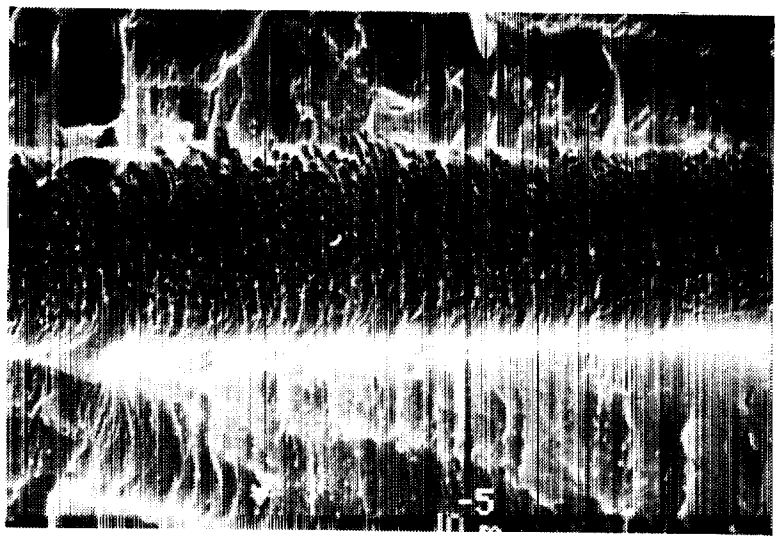

Figure 4. Magnified view of striated structures in Fig. 3. (5000x).

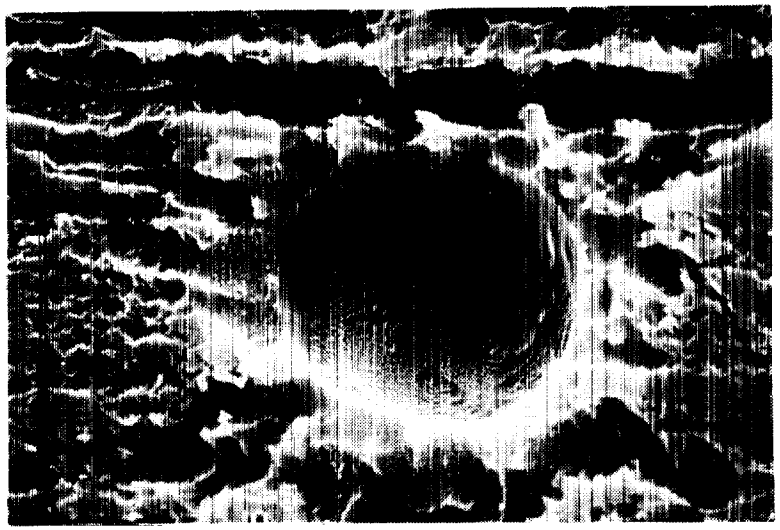

Figure 5. Kapton exposed to atomic oxygen and UV from "wiped" section showing "crater" and inner structure (2000x).

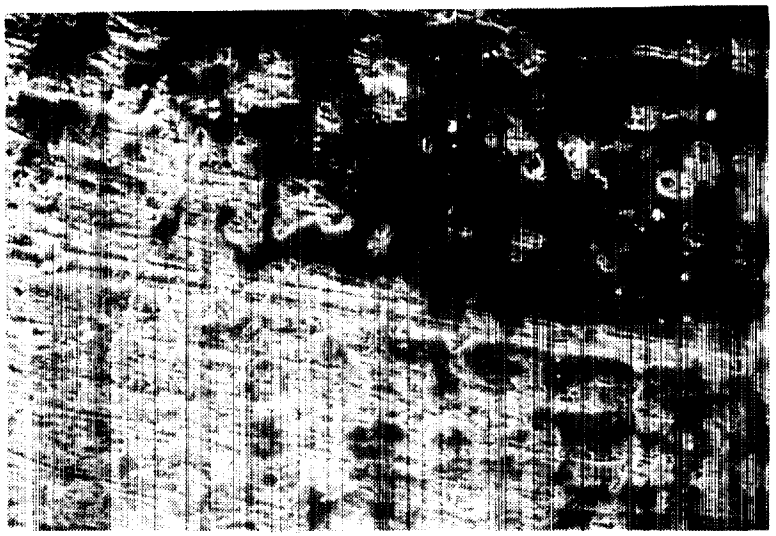

Figure 6. Kapton detail of boundary of "wiped" and "non-wiped" section of fig. 2 (500x).

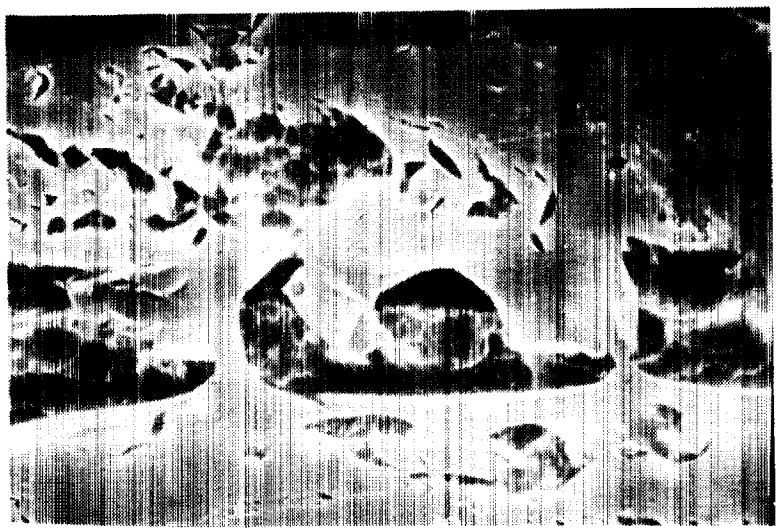

Figure 7. Kapton detail of Fig. 6 showing underlying structure (5000x).

Figure 8. Kapton detail of Fig. 6, showing structure of top layer (10,000x).

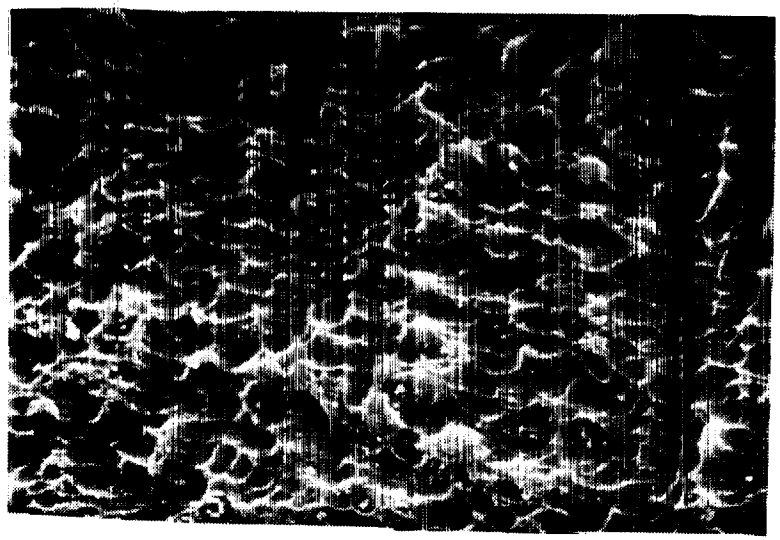

Figure 9. Kapton exposed to atomic oxygen and limited UV (1000x).

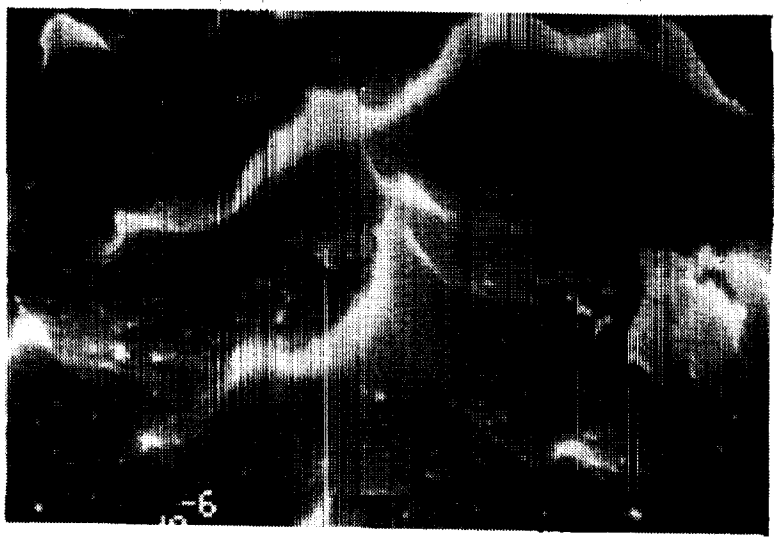

Figure 10. Detail of Kapton exposed to atomic oxygen and limited UV (10,000x).

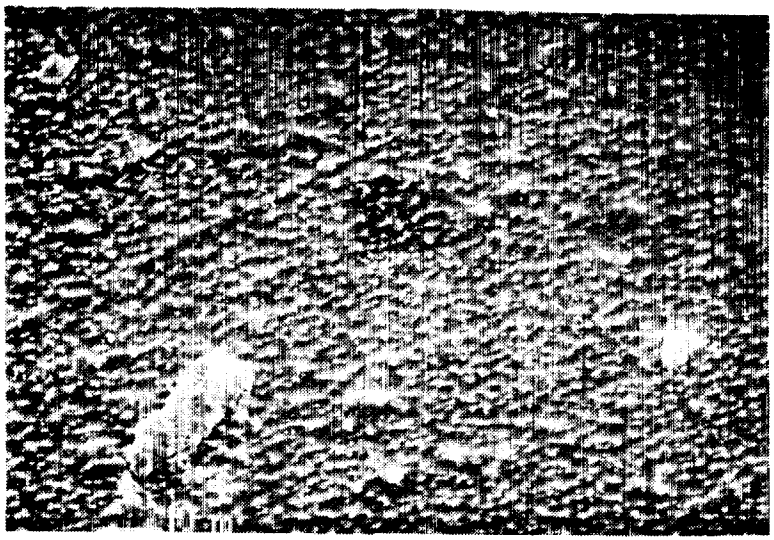

Figure 11. Kapton exposed to atomic oxyygen (1000x).

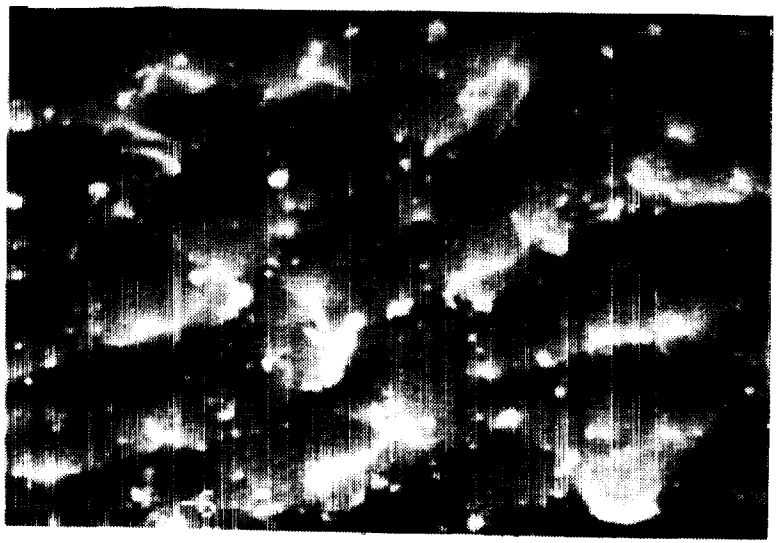

Figure 12. Detail of Kapton exposed to atomic oxygen (10,000x).

Figure 14. Detail of silicon contaminated Kapton surface (10,000x).

Figure 13. Kapton surface exposed to UV showing silicon contaminant (1000x).

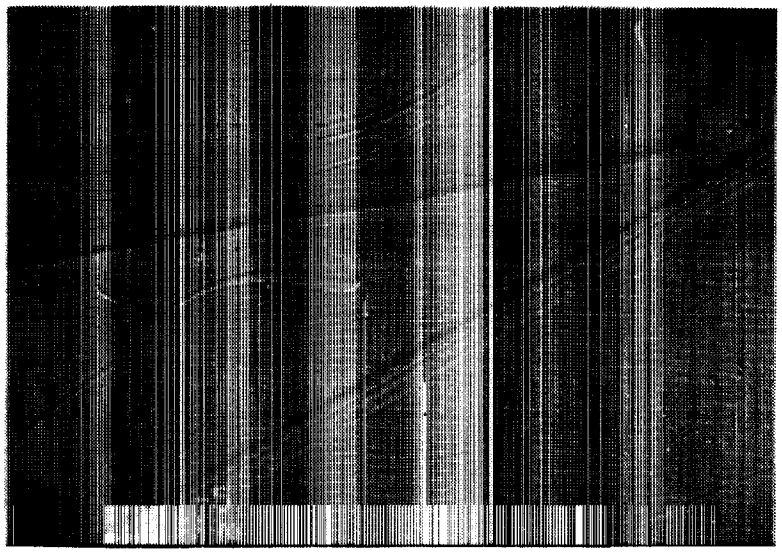

Figure 15. Unexposed Teflon side of Ag/Teflon (1000x).

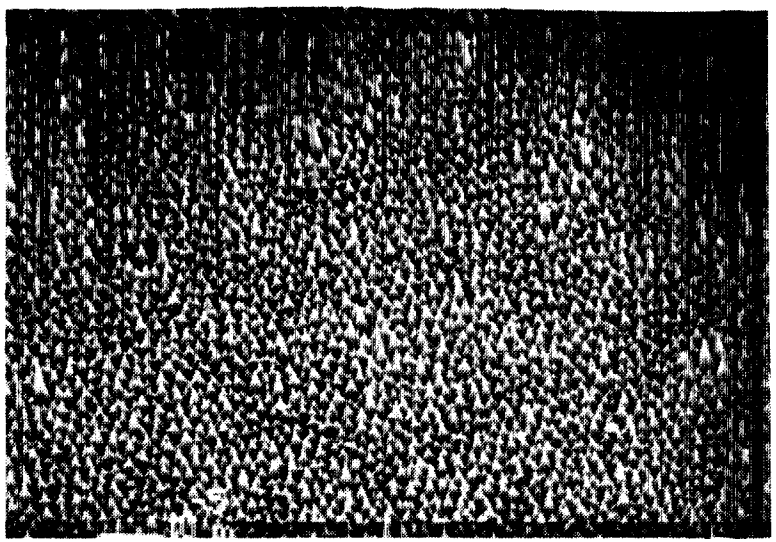

Figure 16. Teflon exposed to atomic oxygen and UV (1000x).

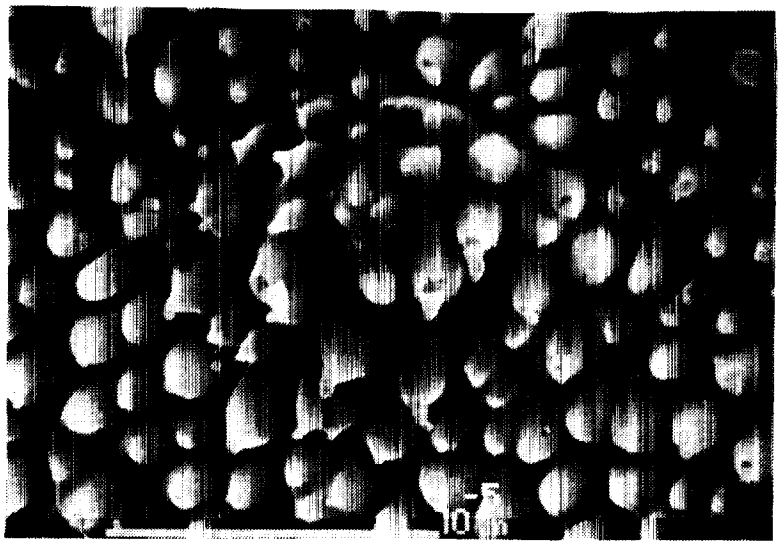

Figure 17. Detail of Teflon exposed to atomic oxygen and UV (5000x).

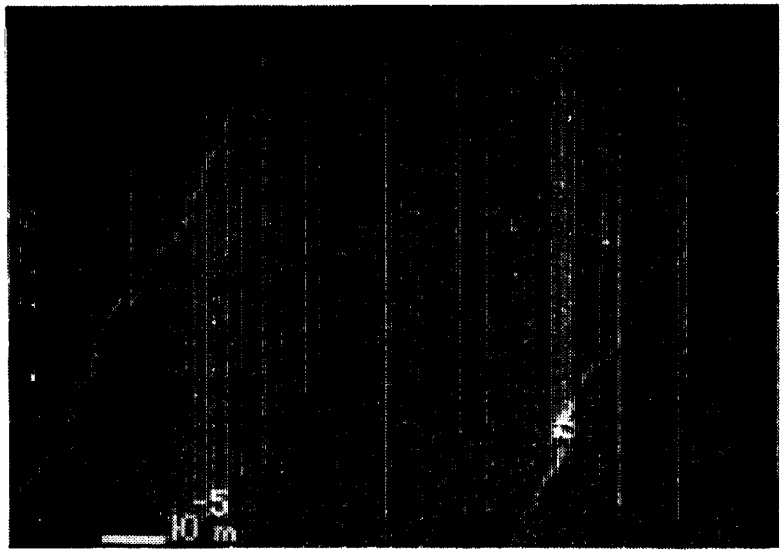

Figure 18. Unexposed silver side of Ag/Teflon (1000x).

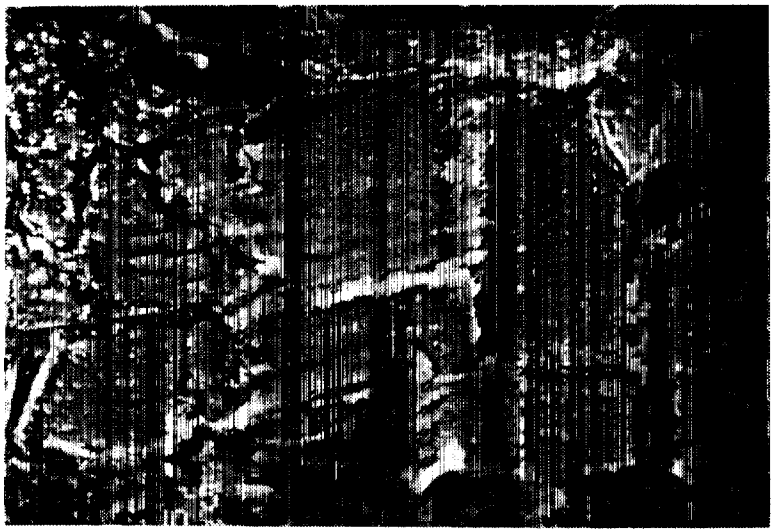

Figure 19. Silver surface exposed to atomic oxygen and UV, adjacent to silver-depleted area (1000x).

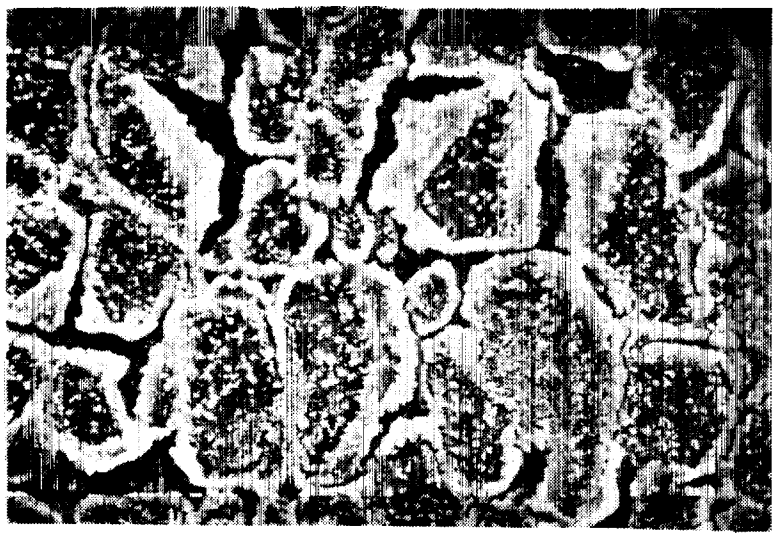

Figure 20. Silver surface exposed to atomic oxygen and UV, approaching silver-depleted area (1000x).

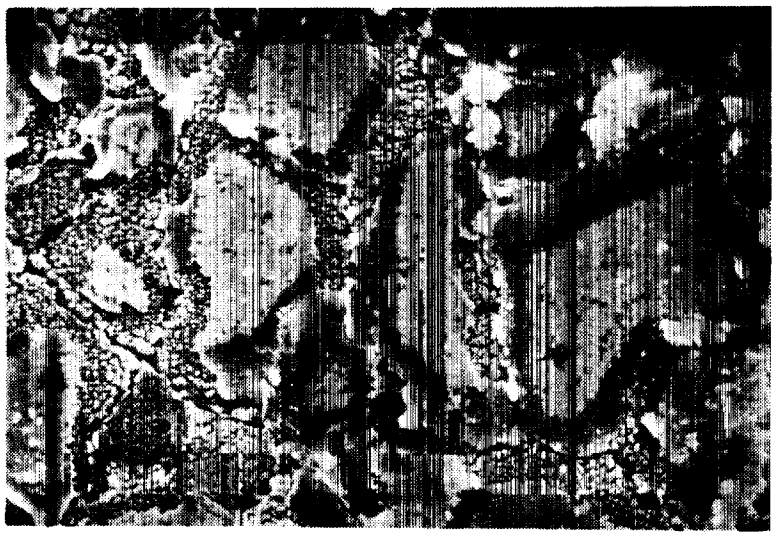

Figure 21. Silver surface exposed to atomic oxygen and UV, nearing silver-depleted area showing underlying Teflon (2000x).

Figure 22. Silver surface in area of near total silver depletion, showing remaining Teflon structure (1000x).

Figure 23. Detail of silver depleted surface showing Teflon Structure (10,000x).

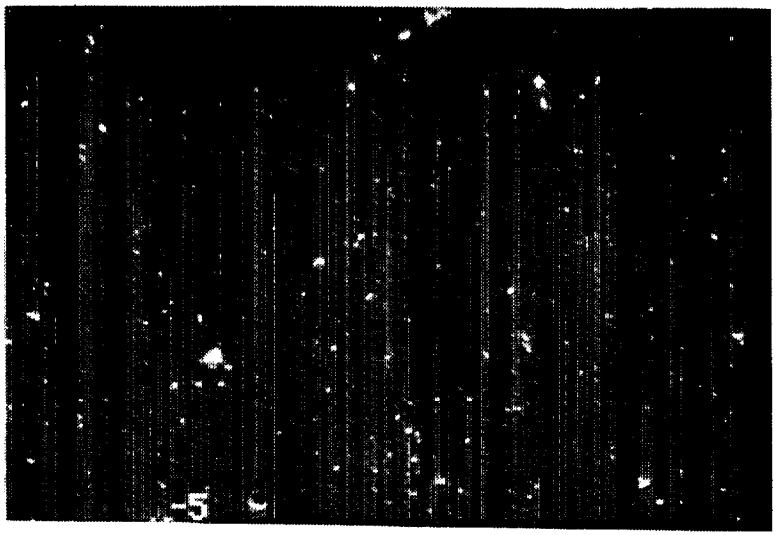

Figure 24. Teflon surface exposed to atomic oxygen (1000x).

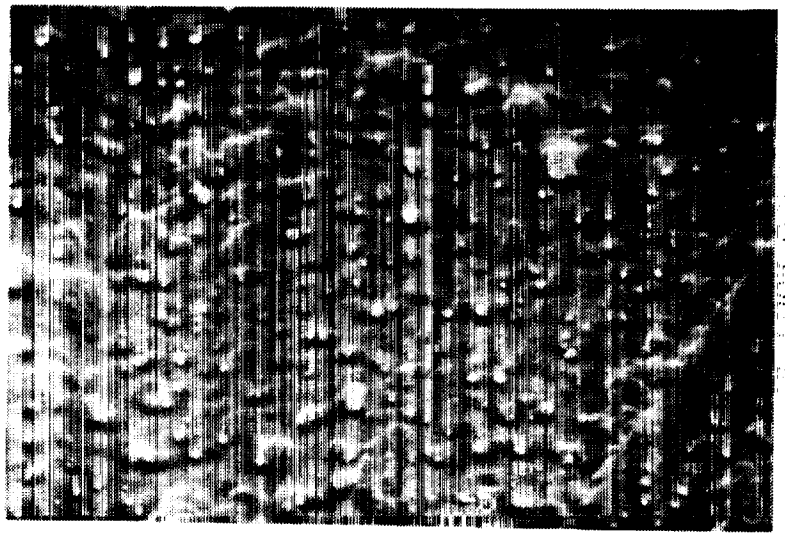

Figure 25. Detail of Teflon surface exposed to atomic oxygen (5000x).

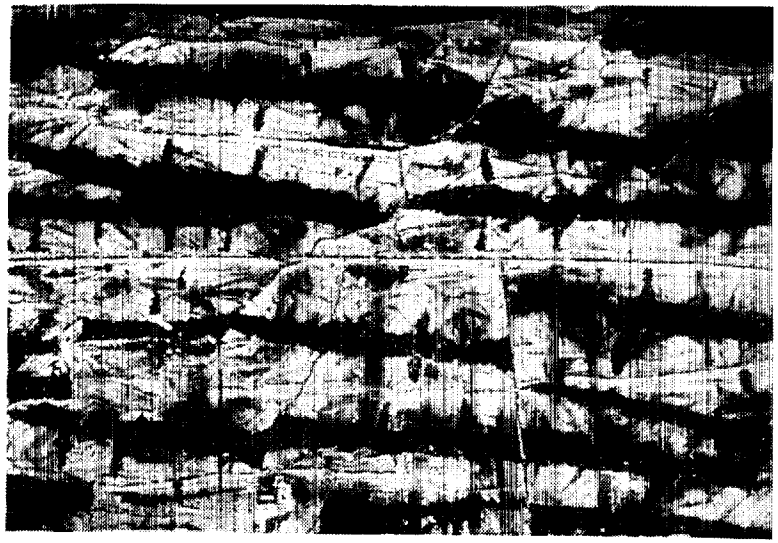

Figure 26. Silver surface exposed to atomic oxygen (200x).

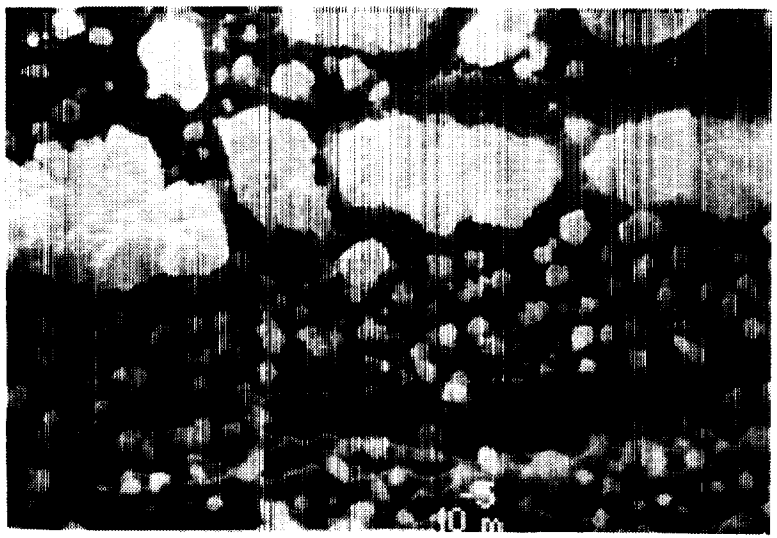

Figure 27. Detail of Fig. 26 showing light area (oxidized) of silver surface exposed to atomic oxygen (5000x).

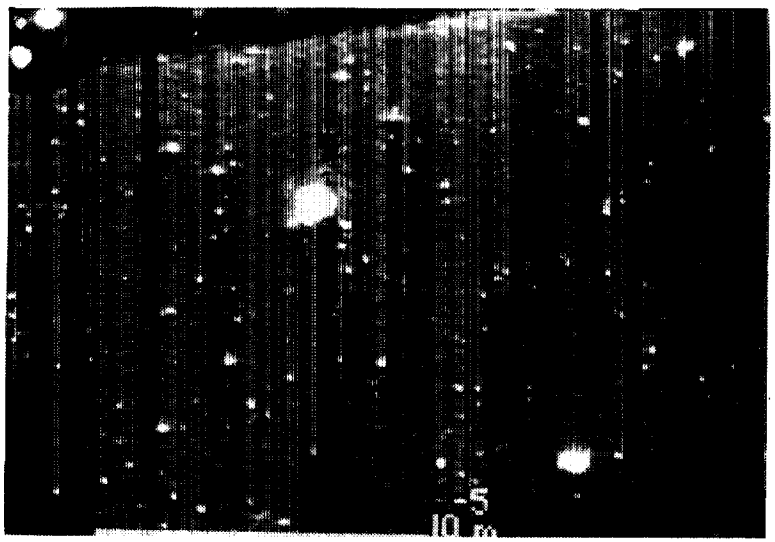

Figure 28. Detail of Fig. 26 showing dark area (non-oxidized) of silver surface exposed to atomic oxygen (5000x).

TEFLON, KAPTON SURFACE AND BULK EFFECTS

J. C. Robinson, M. McCargo

Lockheed Missiles & Space Company

TEFLON,KAPTON SURFACE AND BULK EFFECTS

MATERIALS DESCRIPTION

LMSC received for evaluation samples 13A and 17B of 2mil aluminized/kapton thermal blanket (approximately 80 square inches of twelve layers) and samples T1 and T3 of FEP Teflon flexible OSR (20 square inches). Their location on the solar maximum ACS is shown in Fig. 1.

The Kapton top layer of the thermal blanket (sample 13A exposed, Fig. 2) had been exposed to the LEO atomic oxygen environment and shows the surface degredation due to atomic oxygen attack resulting in a diffuse character over most of the surface. The backside Kapton layer (unexposed, Fig. 2) appeared to the eye to be in the virgin condition. Sample 17B exhibited similar properties, but was, in large part, covered with Kapton adhesive tape and it was not possible to obtain usable specimens for analyis. Sample T1 of the FEP-OSR (exposed) shows signs of heavy degredation including attack on the Ag/Inconel backside by UV and atomic oxygen. On the other hand, sample T3 (unexposed due to partial shading) was only slightly fogged on the teflon side and the Ag/Inconel appeared untouched. See Fig. 3.

To evaluate the analytic techniques prior to analyzing the flight materials laboratory specimens of 2 mil Al/Kapton and FEP teflon OSR were exposed in an oxygen plasma reactor for 2 hours to simulate the degredation effects of a 40 hour shuttle flight in the LEO environment. One FEP teflon specimen was exposed directly on the Ag/Incontel side as was the case for flight specimen T1.

ANALYSIS PROGRAM

A number of physical and chemical analyses were proposed in the initial experimental plan submitted to NASA, but due to the magnitude and type of degradation observed in the SMM and laboratory specimens, the candidate analyses were limited to those listed in the following table:

TABLE I ANALYTICAL TECHNIQUES

INFRARED	Infrared Spectroscopy ATR	Electron Spectroscopy Chemical Analysis ESCA	Secondary Electron Microscopy SEM	RAMAN Spectroscopy	Mass Spectroscopy
13A	Y	Y	Y		
T1	Y	Y	Y		
T3	Y	Y	Y		
Kapton Blank	Y	Y	Y	N	N
FEP Teflon Blank	Y	Y	Y	N	N

Y = Analysis completed
N = Analysis discontinued

These tests were first conducted on the oxygen plasma exposed specimens and blanks to determine their viability before attempting to analyze the flight materials.

RESULTS

Secondary ION Mass Spectroscopy

The Ar+ SIMS spectra obtained from the kapton specimens added little or no new information to the ESCA data. Fragmentation data obtained from the Teflon specimens was of greater detail, but added nothing to the ESCA data. Since the desired information could be generated by ESCA alone, the SIMS studies were discontinued.

Mass Spectroscopy

The mass spectroscopy data on the base line materials were obtained using a Townsend oxygen discharge to generate the spectra. The data obtained contained many uncertainties and added no new information to the ESCA results and were, therefore, discontinued.

Raman Spectroscopy

The Raman spectra excited by the 5145 (green) laser line were obtained for the unexposed and laboratory exposed FEP flexible OSR material. Spectral differences were noted as extra low intensity lines at 961 Cm-1 and 803 Cm -1 in the plasma exposed specimens. No interpretation of these data could be made. In addition, exposure of the Kaplon to the green line laser produced intense flouresence which precluded the collection of any meaningful data. Within the limits of time and funding, no useful data from the Raman spectroscopy could be obtained and these experiments were discontinued.

Infra Red Spectroscopy

All Kapton and FEP Teflon specimens, blanks, lab exposed and SMM flight materials were analyzed by Fourier Transform Infrared spectroscopy in a micro attenuated reflectance accessory. No oxidation was noted at the 1720-1750 CM-1 carbonyl region and it's not apparent from the infrared spectrum that any structural or chemical changes were effected on the flight Kapton or FEP teflon specimens.

Electron Spectra for Chemical Analysis (ESCA)

XPS Investigations of Teflon Specimens. The surface and in-depth compositional XPS data obtained from various Teflon specimens are discussed below and summarized in Table II.

TABLE II SURFACE COMPOSITION OF TEFLON DETERMINED BY XPS

SPECIMEN	SURFACE COMPOSITION (Atomic Percent) C	F	O	Si	OTHERS DETECTED	COMMENTS
(a) BASE MATERIALS						
TEFLON SIDE	32.1	66.0	1.5	0.4		CF_2/CH 14
SPU 40A	29.7	69.8	0.4	.1		CF_2/CF_2CH
INCONEL SIDE					NI,CR,F,O,C	7/ 3/2.5/
(b) LAB EXPOSURES						
(2 hours plasma)						
TEFLON SIDE XPOS.	28.7	71.2	0.1			CF_3CF(293 suggested 10/1
INCONEL SIDE XPOS						
TEFLON SIDE MEASURED	29.0	71.0	0.1			
(c) FLIGHT DATA						
T3 TEFLON SHADED	23.1	33.3	30.2	13.4		Si is SiO
T3 TEFLON SPU 40A	27.5	45.7	16.6	10.1		CF_2/CH 7/
T3 TEFLON SPU 126A	33.3	47.7	11.4	7.6		tSiO_2 150
T1 TEFLON EXPOSED	33.3	64.1	2.6	0		cF_3 obser
SPU 40A	39.3	60.3	0.4	0		cF_2/CH 14
T1 INCONEL EXPOSED					Ag,F,CF,CH,O,Ni	
SPU 40A					Ag,F,CF+,CH+,Hi+	

a) Teflon Unexposed: An FEP Teflon specimen, coated on the backside with 1 mil Ag and 1mil Inconel, was examined in the virgin (unexposed) condition. The surface of the uncoated side showed C, F, small amounts of oxygen (1.5 atomic percent) and Si (0.4 atomic percent). The overall concentration estimates and the C intensity ratio in CF_2 and CH bonds are listed in Table II. The presence of few -CH (or C-C) bonds at surface and their decrease upon sputtering to 40 A depth suggests the origin of CH is adventitious carbon at this surface.

Sputtering to 40 A depth decreased the oxygen and silicon concentrations, suggesting that Si is also a surface contamination (possibly a silicone) either from manufacturing or processing of Teflon. The Inconel coated surface showed Ni, Cr, F, O and C.

b) Teflon Directly Exposed 2 hr. to O-Plasma: Surface of this specimen consisted of very little oxygen (0.1 atomic percent) and no detectable silicon. This result in conjunction with DF_n/CH_n bond ratio of 10/1 suggests the cleanup of prevailing surface contamination, e.g., Si and hydrocarbons. Most importantly, the data indicates that little or no oxygen bearing products remain at the surface, suggesting that either they do not form or volatilize readily upon formation.

c) Teflon Indirectly Exposed to O-Plasma: In preparing this specimen, Teflon was covered by aluminum foil and the Inconel side was exposed 2 hours to oxygen plasma. The Teflon side was examined by XPS and was found to be very similar to Specimen a, above.

d) SMM Teflon T3: The unexposed (shaded from atomic oxygen during SMM flight) front surface of SMM Teflon showed large amounts of silicon (13 atomic percent) and oxygen (30 atomic percent). The survey spectrum and high resolution peaks of C and Si are shown in Fig. 2. Si peak position indicates a highly oxidized form, such as SiO_2. Sputtering in steps followed by XPS analysis provided and estimate of 150 A Thickness for the SiO_2 islands. SiO_2 appears to cover over 40% of the surface.

e) SMM Teflon T1, Exposed Back Surface: The metallized back surface showed Ag, F, O, Ni and carbon present in CH_{n-} and CF_{n-} bond forms. the predominance of Ag at this surface suggests its diffusion through Inconel. Sputter removal of 40 A reduced Ag, CF, CH, F and O peaks while increasing Ni. The indication is that silver diffused through Inconel layer and covered the surface.

f) SMM Teflon T1, Exposed Front Surface: This Teflon surface was directly exposed to atomic oxygen during SMM flight. The surface showed small amounts of oxygen, only slightly greater than virgin

Teflon (Specimen a). Silicon was not detected at the surface (0.,1 atomic percent). Carbon at the surface is predominant in the CF_2 the virgin surface.

XPS Investigation of Kapton Specimens. Virgin Kapton, laboratory plasma exposed and SMM Kapton specimens were studied by XPS and their results are summarized in Table III.

TABLE III SURFACECOMPOSITION OF KAPTON, AS DETERMINED BY XPS

SPECIMEN	C	O	SI	N	AL	CL	OTHERS DETECTED	COMMENT
(a) BASE MATERIAL								
KAPTON SIDE	65.5	25.8	2.7	2.9	3.1	0.1	Na	CH/CO/C=0
KAPTON SIDE SPU 20A	76.6	14.5	0.7	4.1	4.0	-0.1	Na	7/1/7/1.2
KAPTON SIDE SPU 84A	88.3	6.2	0.4	3.4	1.7	0.1	-	
(b) LAB EXPOSED								
(2 hours plasma)								
KAPTON SIDE	43.4	41.6	8.3	4.6	1.4	0.1	Na	CH/C-0 7/3
SPU 20A	50.7	34	8.3	4.6	1.6	0.2	Na	
SPU 105A	58.2	27.2	7.7	4.6	1.9	0.2	Na	
SPU 270A	73.0	16.3	4.5	4.0	2.1	0		
(c) FLIGHT MATERIAL								
13A KAPTON DULL SURF	52.2	35.9	6.3	4.7	0.4	0	0.5F	
13A KAPTON SHINY SURF	56.9	32.7	4.4	5.4	0.2	0.1	0.4F	CH/C-0 7/2
SPU 42A	80.4	12.2	2.2	5.2	-	-	0.0F	
SPU 126A	85.7	8.2	1.6	4.4	-	-	0.1F	
SPU 270A	87.4	6.7	1.2	4.5	-	-	0.1F	

a) Unexposed Kapton: Front surface of virgin Kapton (with 2 mils of vapor deposited aluminum on the backside) was examined by XPS, prior to exposure to plasma. XPs spectra indicated presence of C, O, N and

small amounts of Si and Al at the surface. Si is possibly a contamination during preparation or processing of Kapton, while Al is likely a deposit occurred during the backside metallization. Ion sputtering of the surface to a depth of 20 A reduced much of the silicon, suggesting its origin to be of a silicone type. Further sputtering to a depth of 84 A reduced the aluminum level to less than half its value, implying an aluminum thickness of about 80 A.

b) Kapton Exposed 2 hour to Oxygen Plasma: XPS spectrum from this surface is shown in Fig. 3 and indicates a high level (9 atomic percent) of silicon. Based on its precise peak position, silicon could be determined to be preset in the Sio_2 form. Sputtering to 270 A (see Table II) reduced Si, while increasing Al. Based on this sputtering data, the thickness of SiO_2 may be estimated at 300A. It is also to e noted that SiO_2 layer is not contiguous, and may be assumed to be present in the form of islands, with an average surface coverage of 20 to 30%. Aluminum is present in the open areas, as well as below the SiO_2 islands. Further, the surface $C{=}O/CH_n$ bond ratio was found to be high (3/7) compared to virgin Kapton, indicating a reaction of surface carbon with oxygen.

c) SMM Kapton 13 A, Front Side, Dull Surface: This specimen was cut up from he 0A and 1A segments of LPARL grid and exhibited a dull surface on one side and a relatively shiny surface on the other. Compositional differences at these surfaces were, however, small as indicated in Table II.

d) SMM Kapton 13 A, Front Side, Shiny Surface: XPS survey spectrum from surface showed a relatively high amount (4.4 atomic percent) of Si, as compared to virgin Kapton, Specimen a. High resolution spectrum shows that silicon is in a highly oxidized form, similar to SiO_2. The SiO_2 thickness is estimated at 50 A, much thinner than the laboratory O-plasma exposed specimen, but thick compared to virgin Kapton. Fluorine at 0.5 atomic percent level was observed at both dull and shiny surfaces of SMM samples, while it was absent at all the other Kapton surfaces. The source of fluorine may be the Teflon present in the vicinity during the SMM flight. The ration of $C{=}O/CH_n$ bonds at surface was found to be high (2/7), again indicating oxygen reaction with surface carbon.

Secondary Electron Microscopy

All Kapton and FEP Teflon specimens, blanks, lab exposed, and SMM flight materials were analyzed by secondary electron microscopy. The results are presented in Fig. 4 through Fig. 19. Impact craters about 1um in diameter were observed at a frequency of about 10 per Cm^2 on the unexposed SMM Teflon Surfaces and approximately 3 per Cm^2 on the metallized back surfaces of the SMM Kapton and Teflon. No impact features were observed on the SMM Kapton termal blanket beyond the first layer of Al/Kapton. The exposed FEP Teflon (Ti) was erroded by the atomic oxygen to a degree that observed any impact features which may have been present.

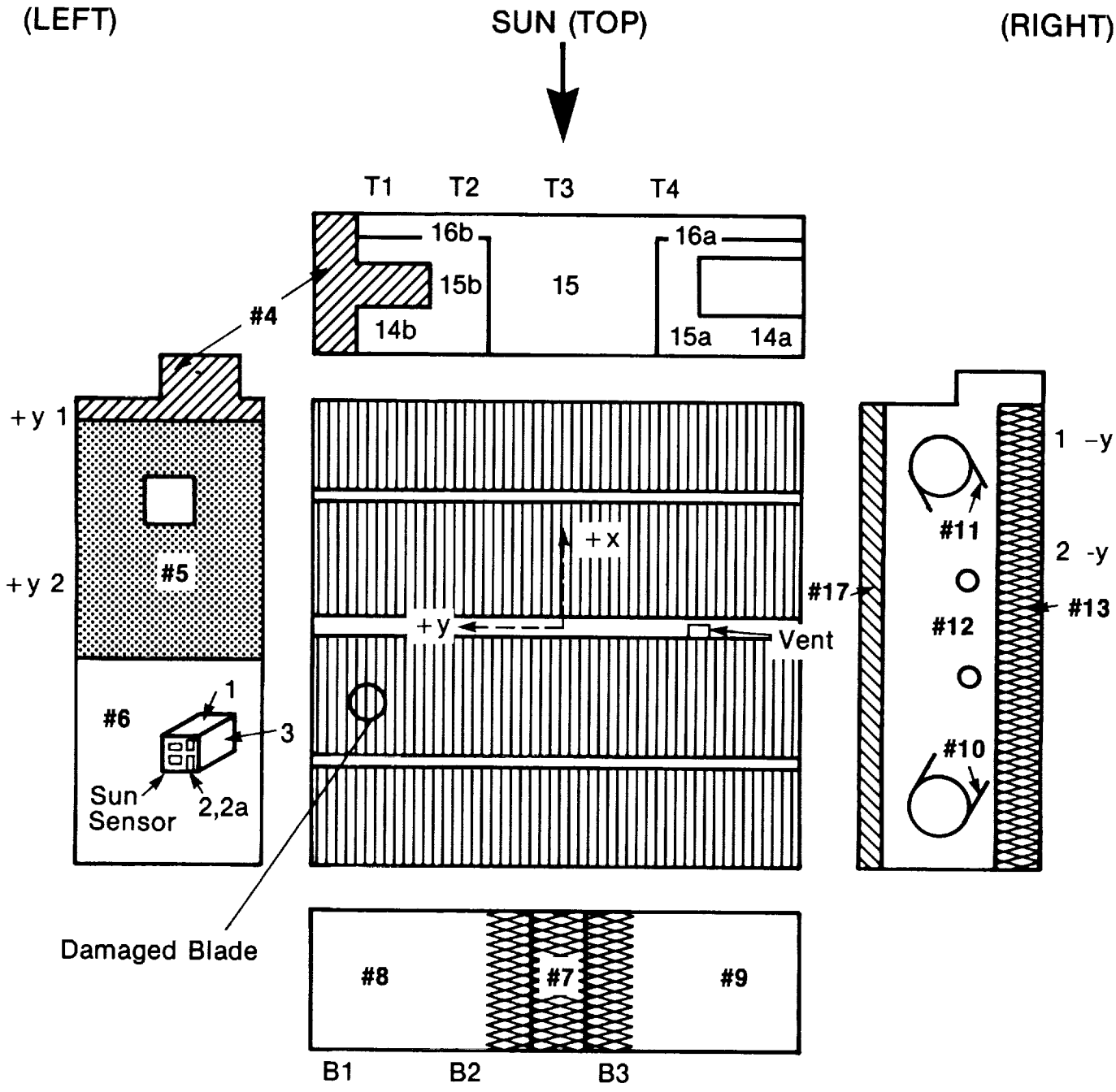

Figure 1
SOLAR MAX ACS
MLI Blanket Picce # References

Figure 2 Exposed and Unexposed Kapton Sample 13A

T 1

BACK

EXPOSED

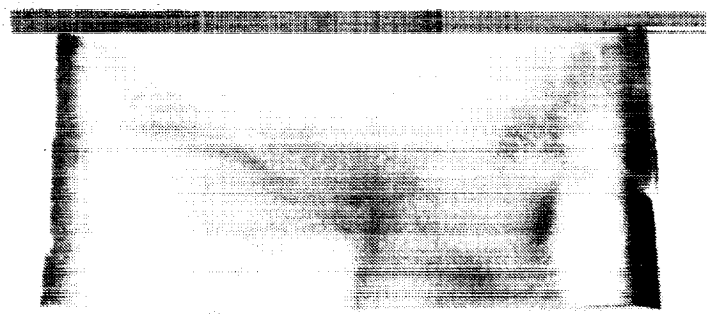

T 1

FRONT

EXPOSED

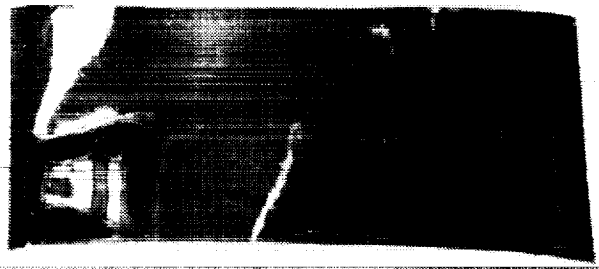

T 3

FRONT

UN EXPOSED

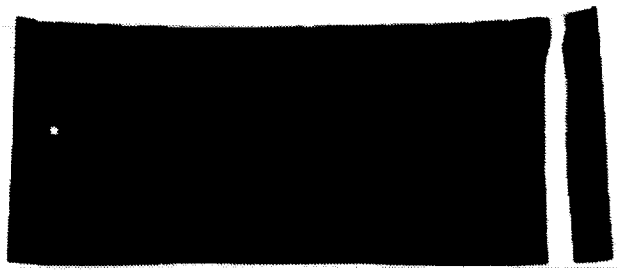

T 3

BACK

UN EXPOSED

Figure 3 T_1 Exposed FEP Teflon. T_3 Unexposed FEP Teflon

Figure 4 Blank Kapton Exhibiting Featureless Surface Typical of Virgin Kapton

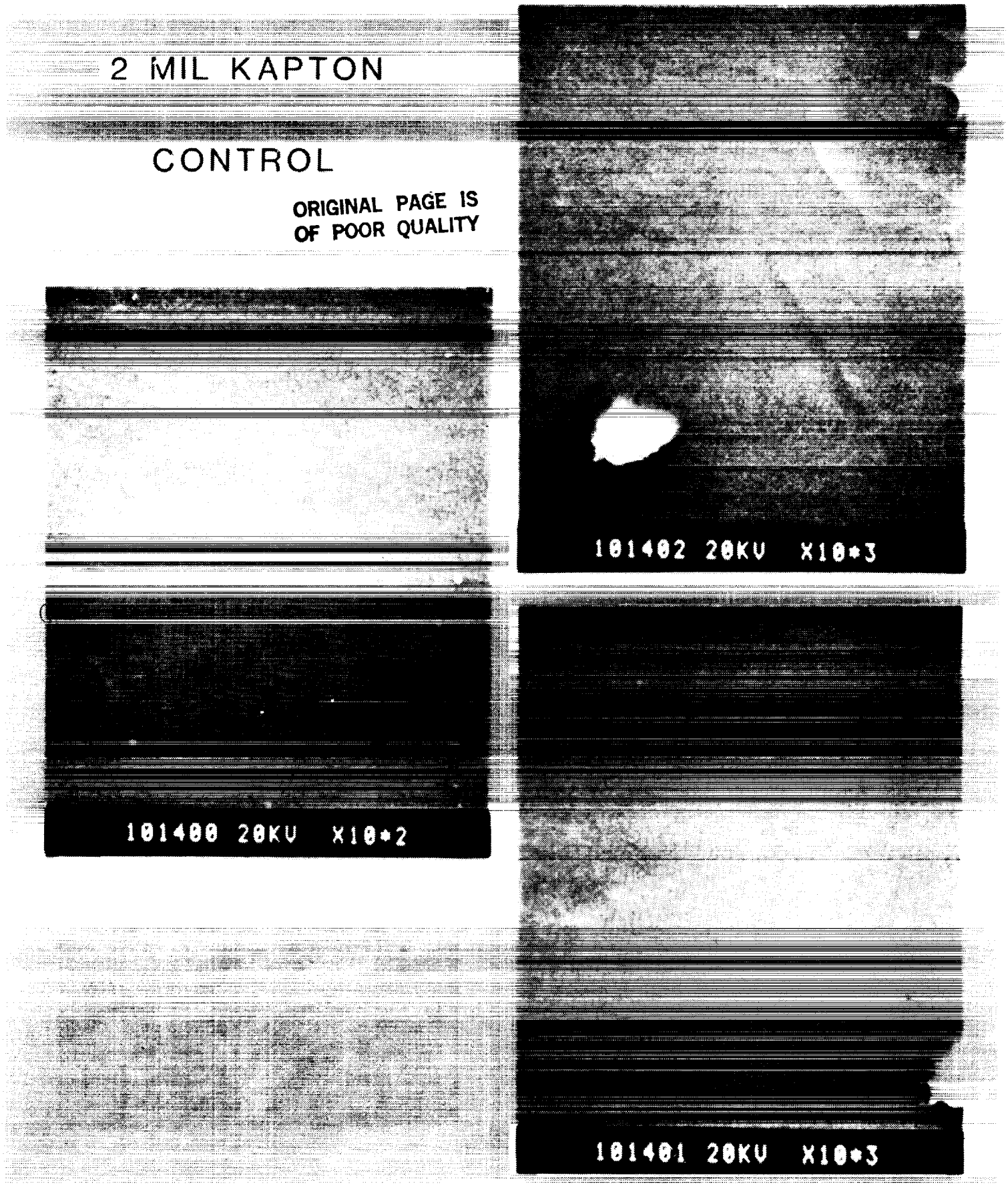

Figure 5 Kapton After 2 Hours Laboratory Exposure to Atomic Oxygen Showing Cuspate Erosion of Surface and Fine Debris Dispersed at High Points on the Surface

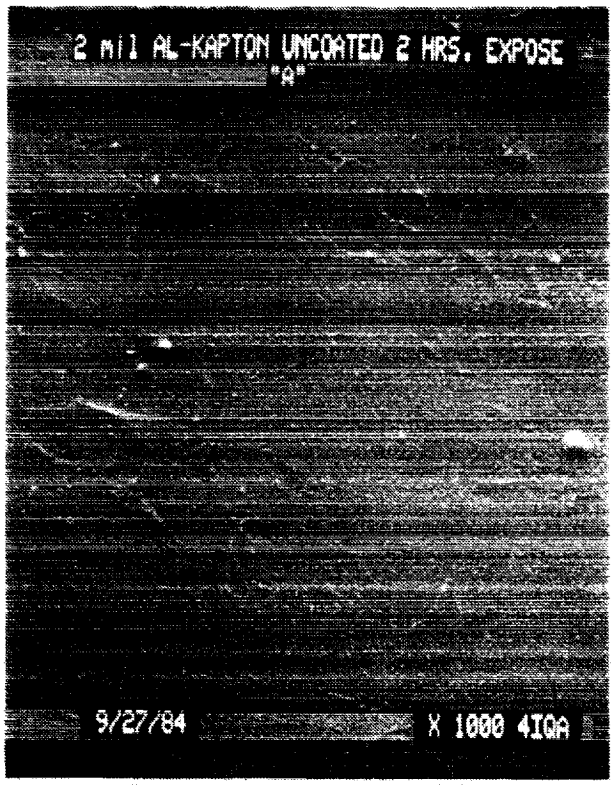

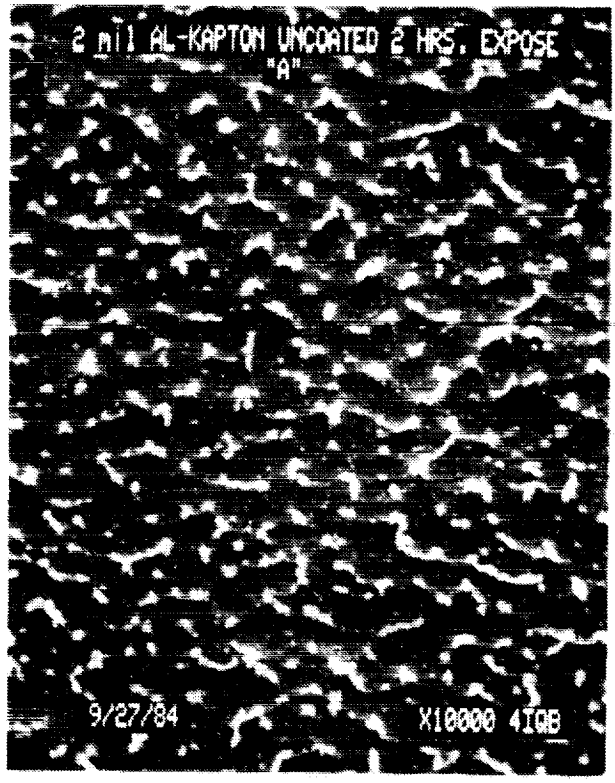

KAPTON

PLASMA EXPOSURE

2 HOURS

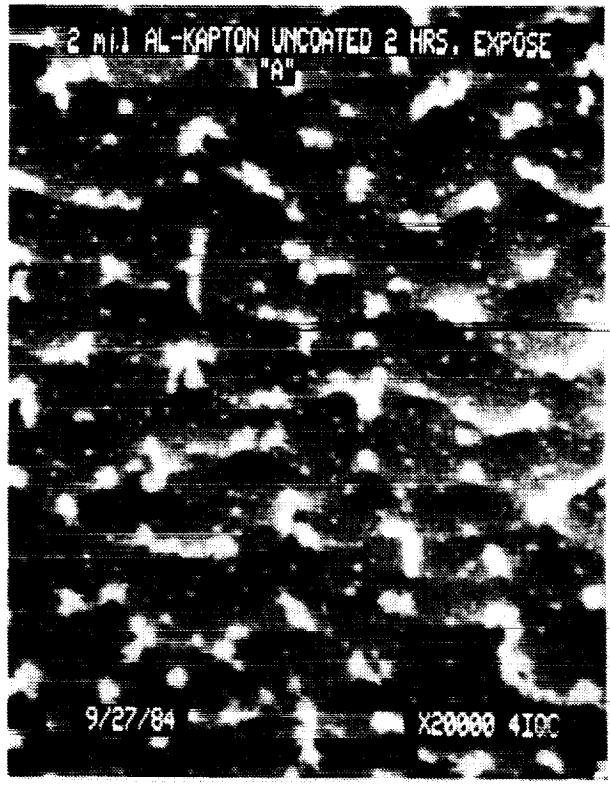

Figure 8 13A Kapton Top layer. The Surface Morphology is Similar to that of the Laboratory Exposed Specimen, but More Erosion Has Taken Place

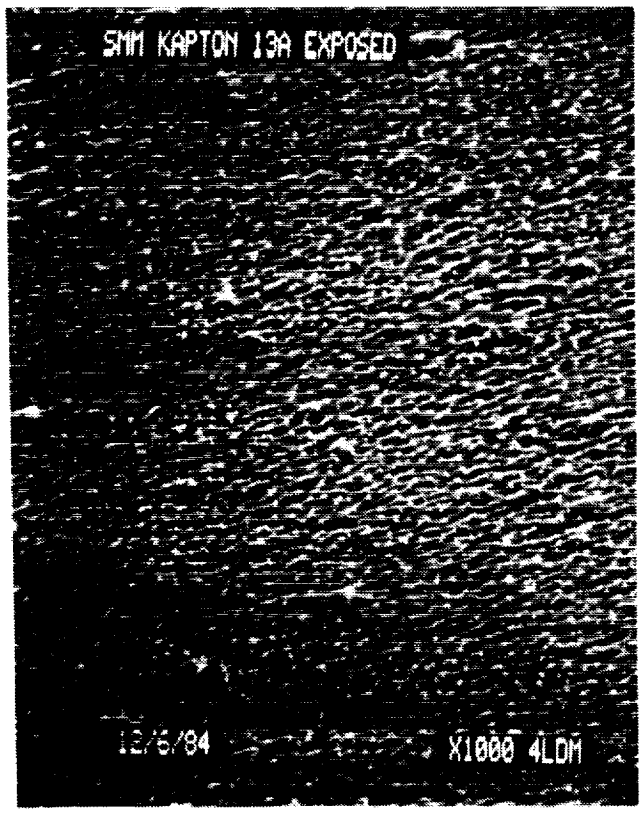

13A KAPTON

TOP LAYER

Figure 7 13A Kapton Bottom. This Layer Has Not Been Exposed to A/O and Shows Only the Indentations Due to Manufacturing and Handling.

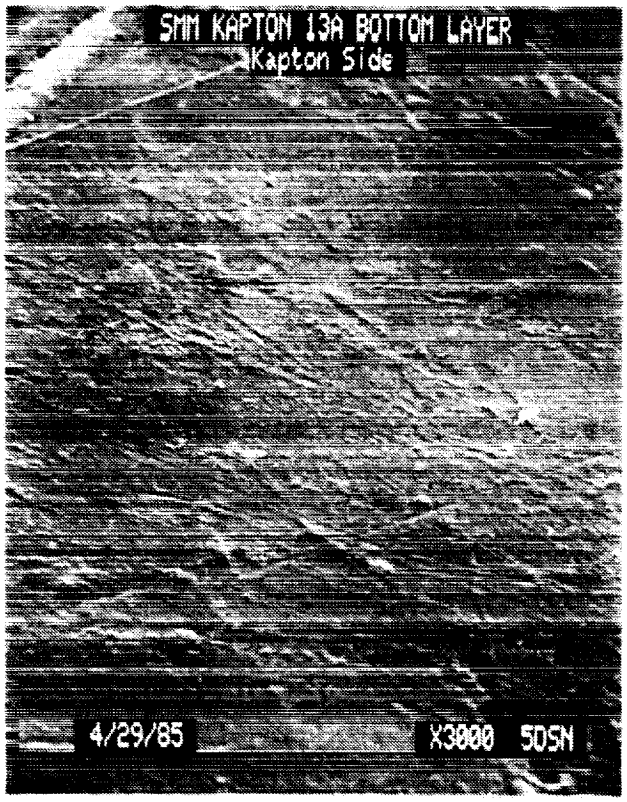

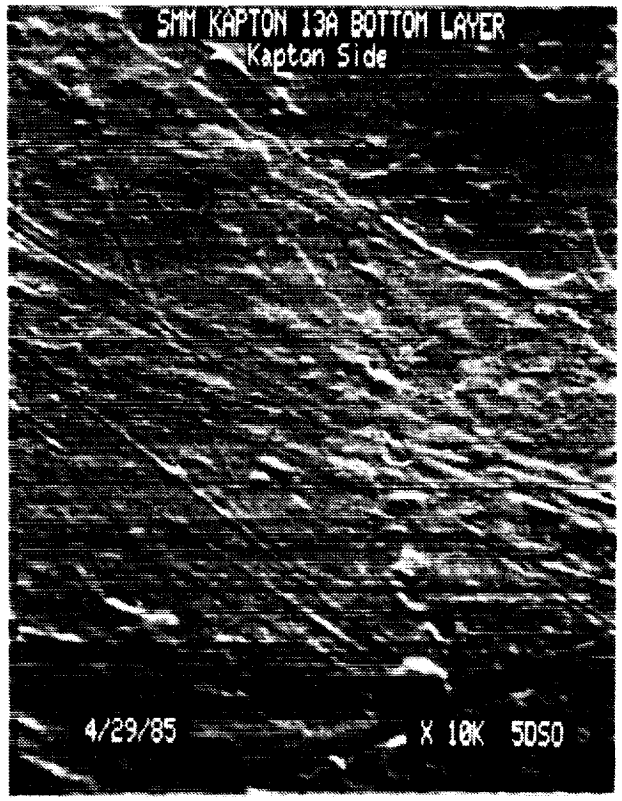

13A KAPTON

BOTTOM LAYER

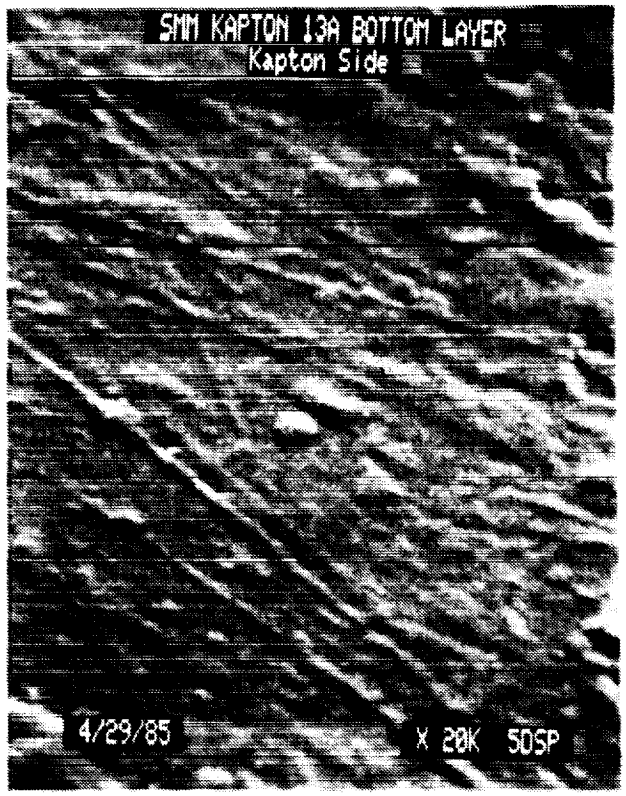

ORIGINAL PAGE IS
OF POOR QUALITY

Figure 8 FEP Teflon Blank. Typical FEP Teflon Surface. Indentations Due to Manufacturing and Handling

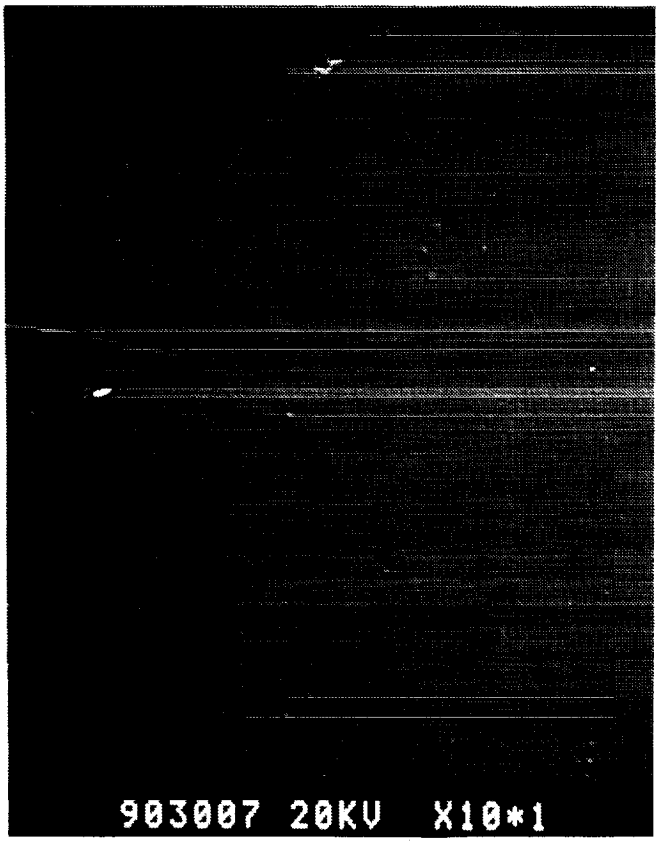

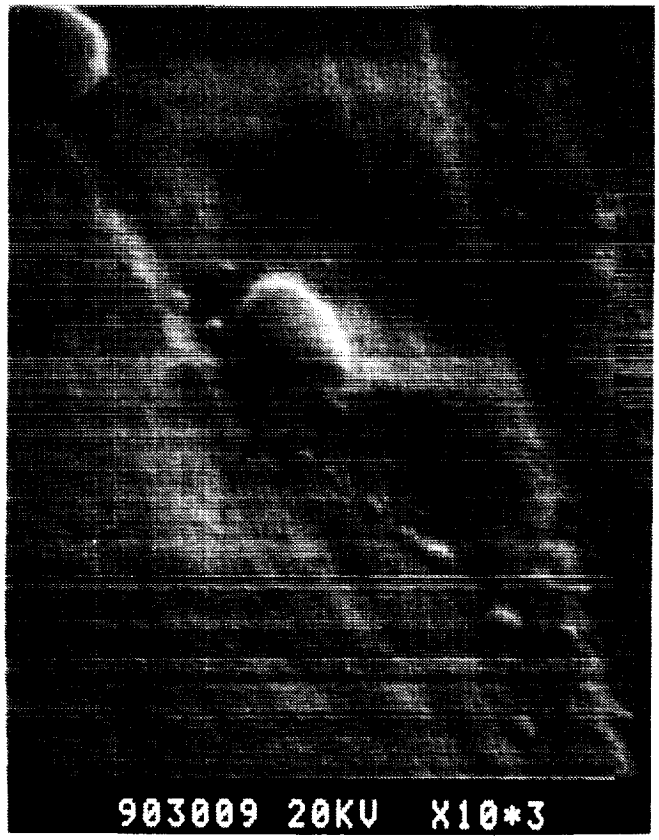

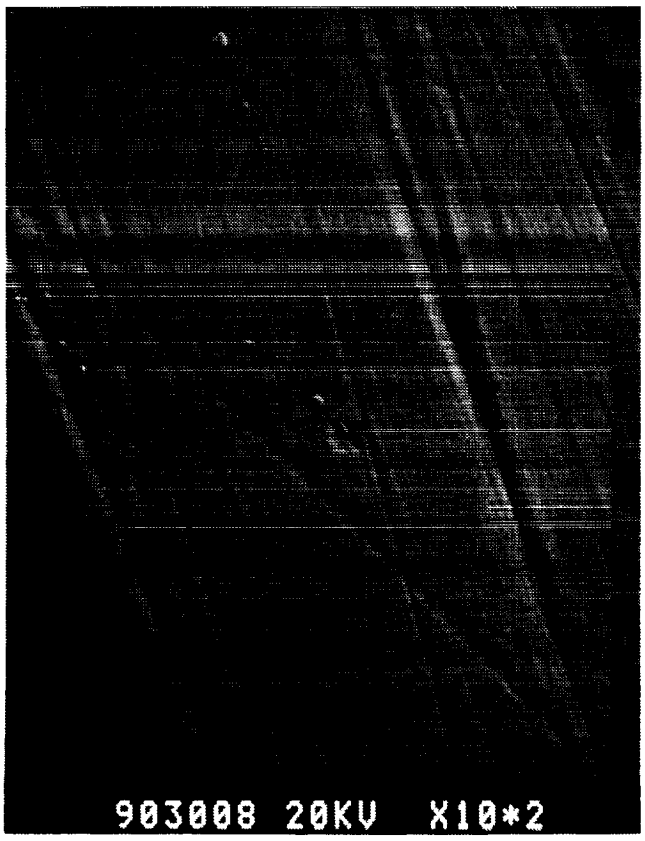

Figure 3 FEP Teflon After 2 Hours Plasma Exposure. Surface Has Granular Texture and Beginnings of Polygonization with Eroded Striations Remaining from Original Texture

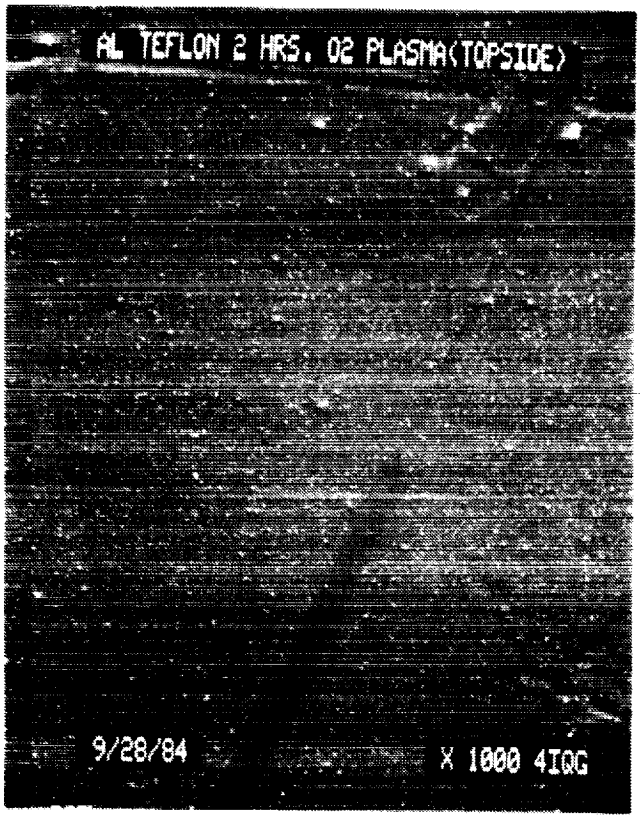

FEP TEFLON

PLASMA EXPOSURE

2 HOURS

Figure 10 FEP Teflon After 2 Hours Plasma Exposure on the Ag/Inconel Surface. Growth of Ag along Grain Boundaries and Cracks in the Inconel Over Coat Has Occurred.

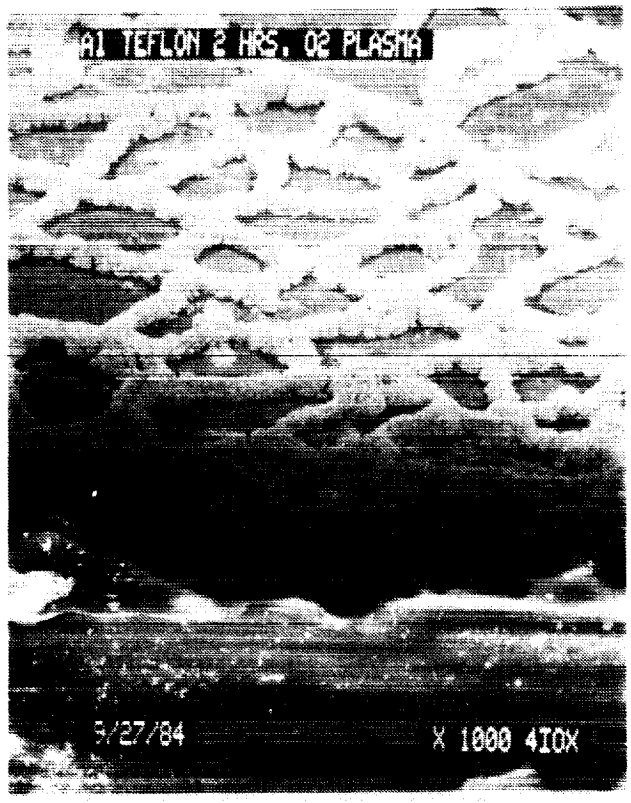

FEP TEFLON

INCONEL/Ag SIDE

PLASMA EXPOSURE

2 HOURS

Figure 11 T1 FEP Teflon Exposed. This Specimen, Subjected to Increased Temperature and Atomic Oxygen, is Highly Eroded to Cone Texture with Rosettes of the Underlying Ag Growing through Cracks

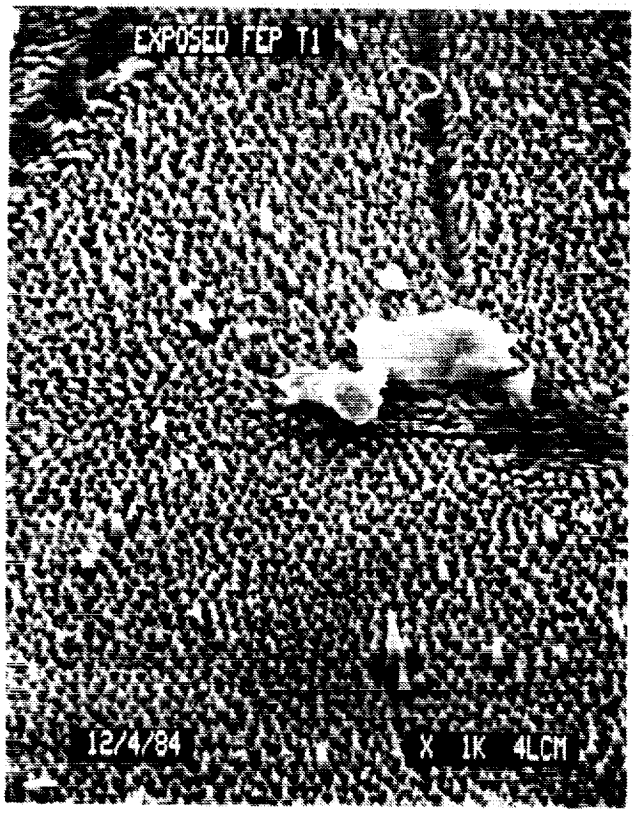

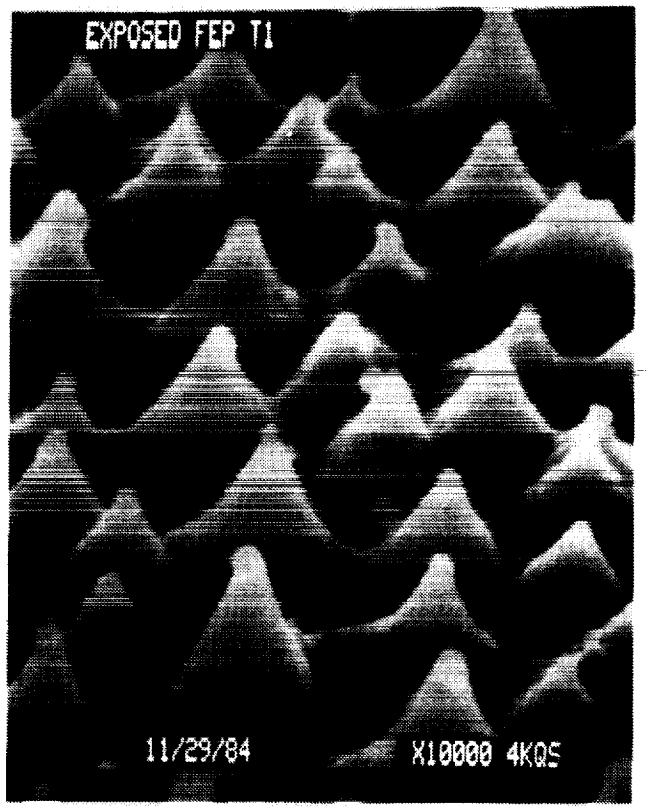

T1 FEP TEFLON

EXPOSED

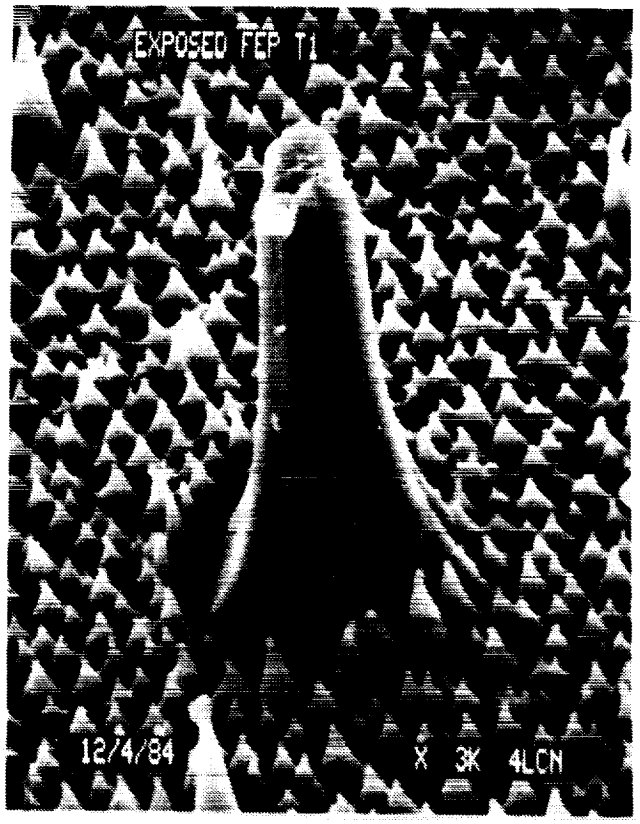

Figure 12 T1 FEP Teflon Exposed Ag/Inconel Side. The Morphology is Similar to that of the Laboratory Exposed Ag/Inconel with Ag Growing Through Cracks and Grain Boundaries in the Inconel Overcoat. At High Magnification it is Possible to Observe Regions in which the AG/I has been Totally Removed and the FEP Teflon Textured Surface is Visible.

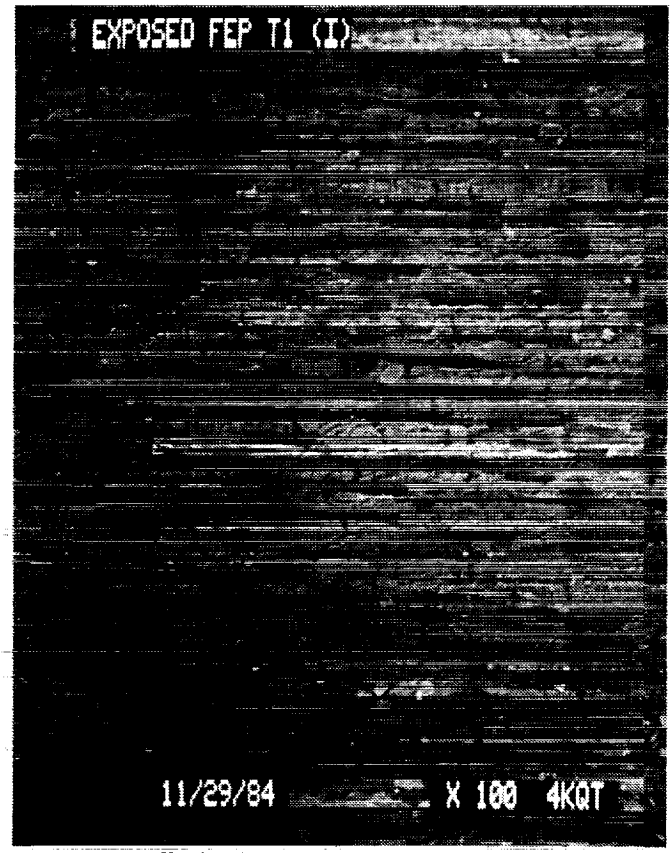

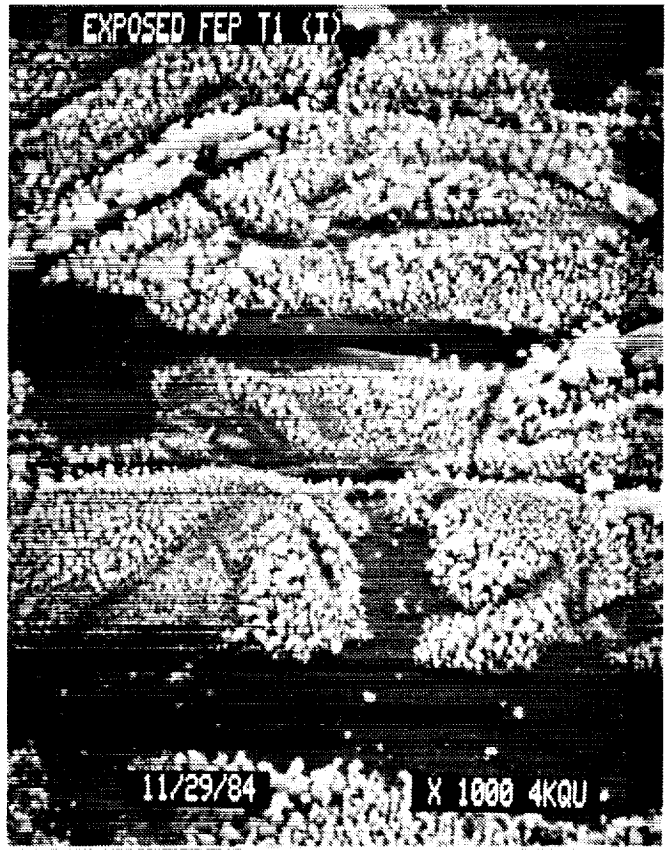

T1 FEP TEFLON

INCONEL/Ag SIDE

EXPOSED

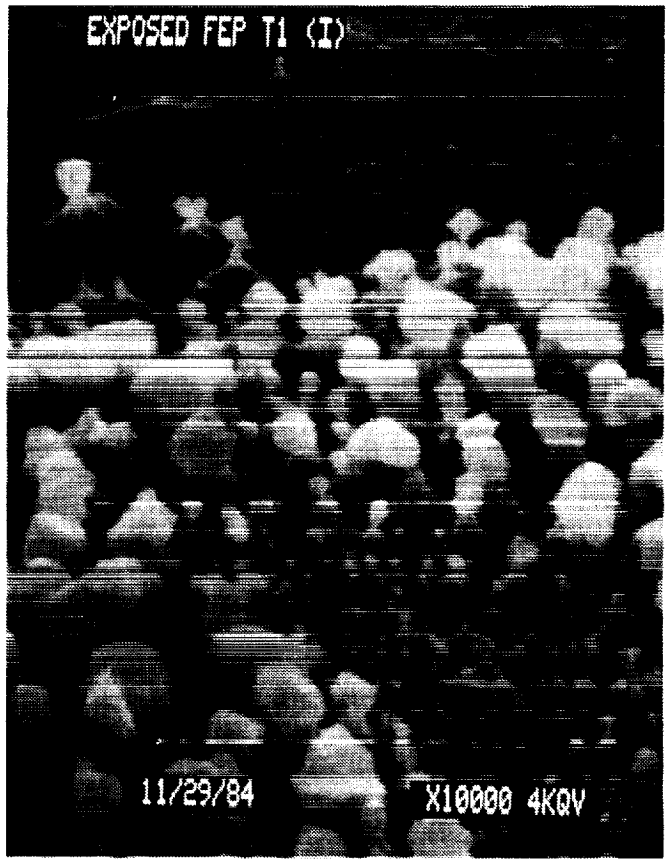

Figure 18 T3 FEP Teflon unexposed (shaded). The surface is highly pockmarked and impact craters are observed.

T3 FEP TEFLON UNEXPOSED (SHADED)

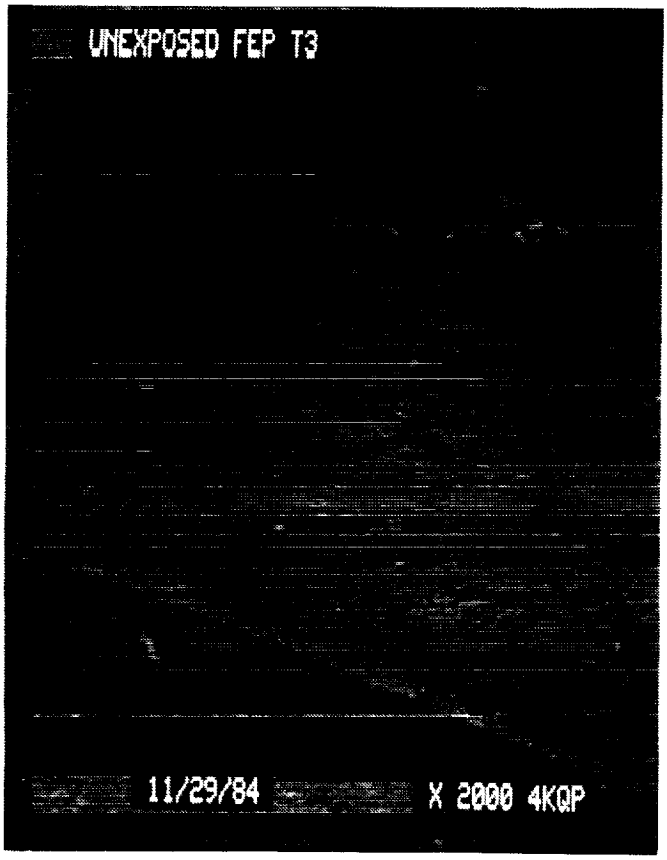

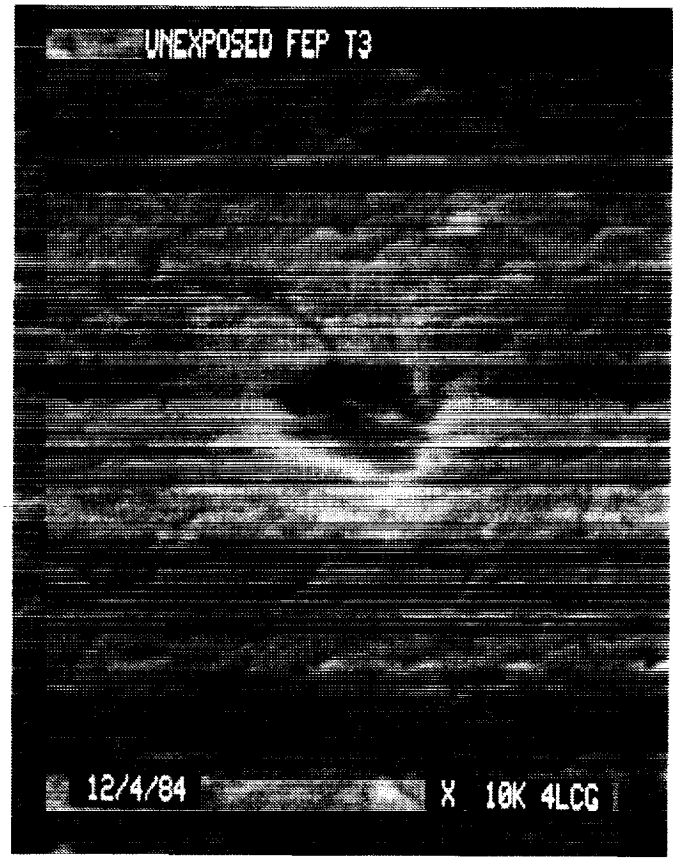

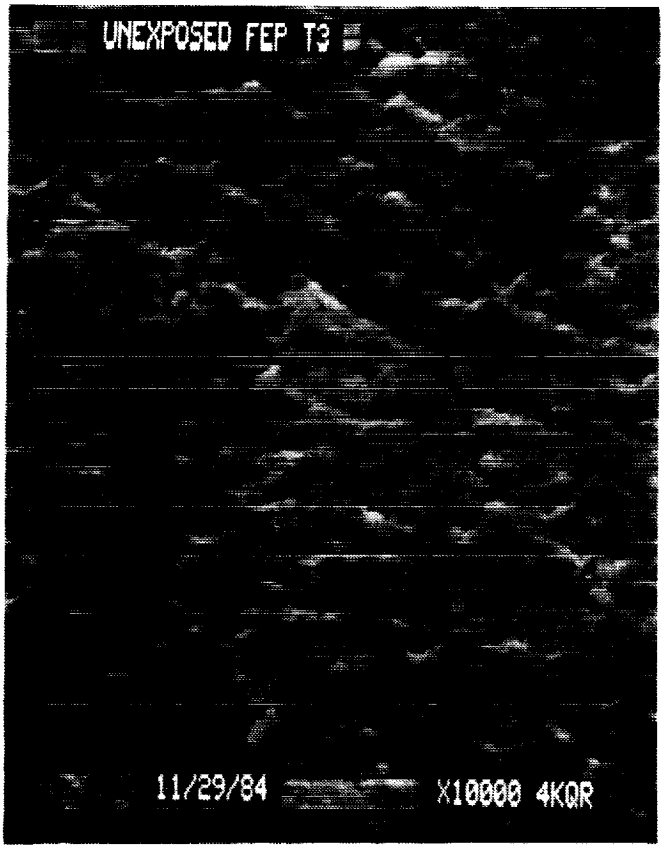

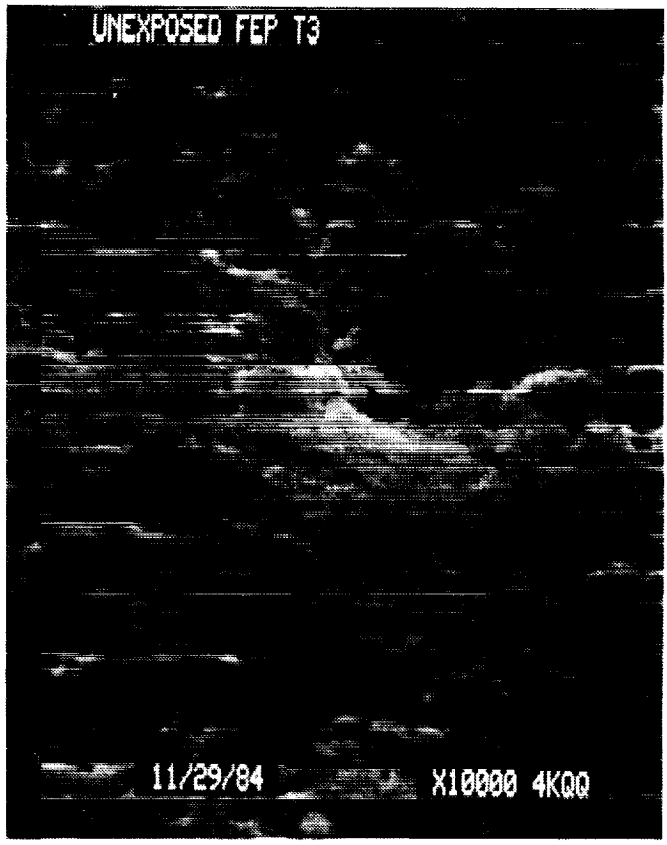

Figure 14. T3 FEP Teflon unexposed shaded Ag/Inconel side Ag growth is limited to major cracks. Impact crater 2 mm in diameter.

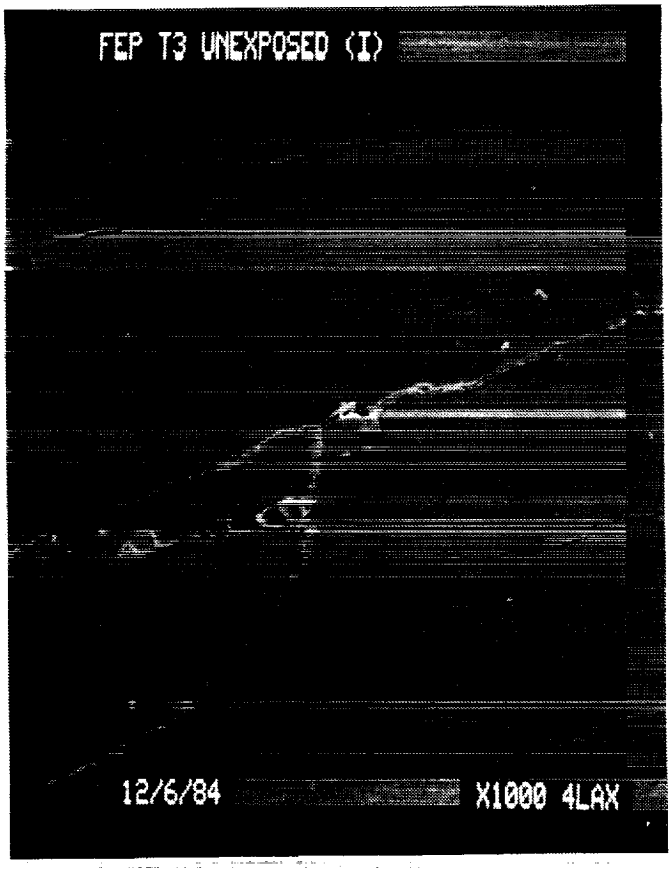

T3 FEP TEFLON

INCONEL/Ag SIDE

UNEXPOSED (SHADED)

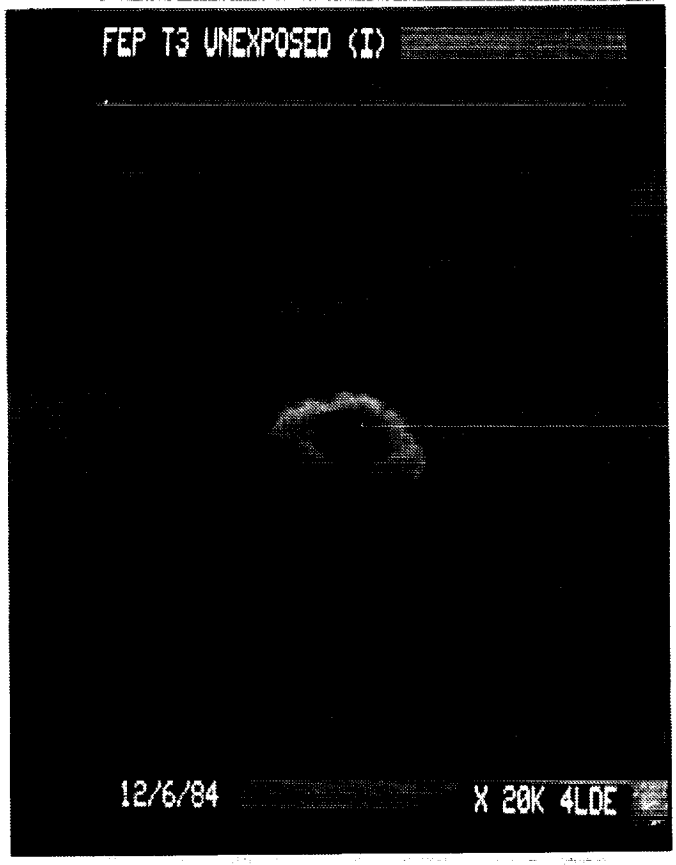

Figure 15 T3 Examples of impact craters entrance and exit in FEP Teflon.

T3 MICRO METEORITE CRATERS

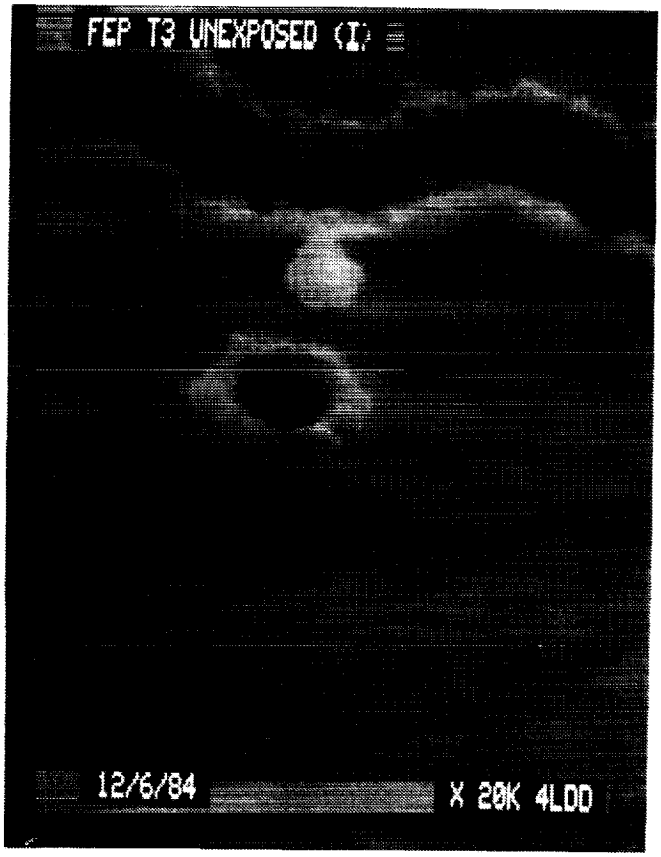

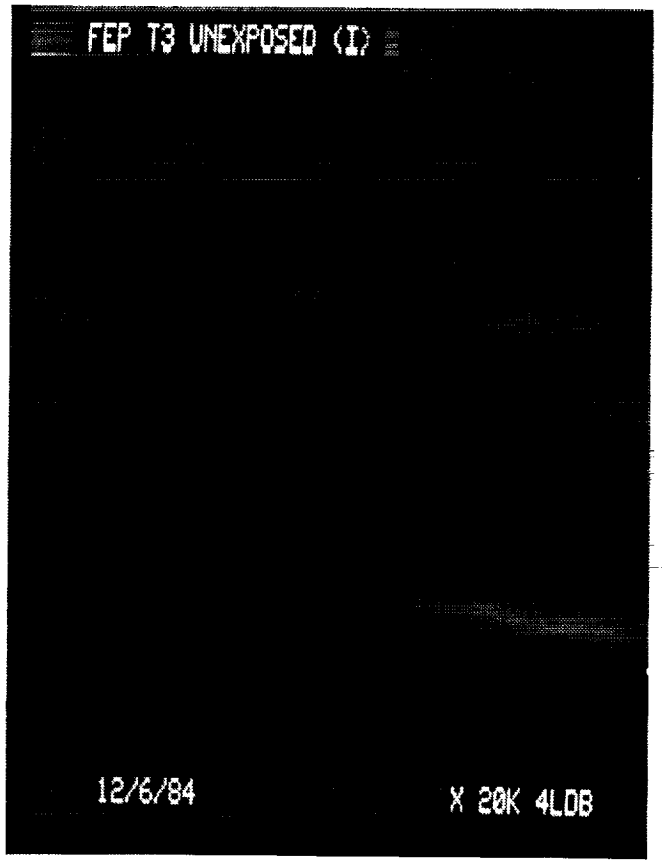

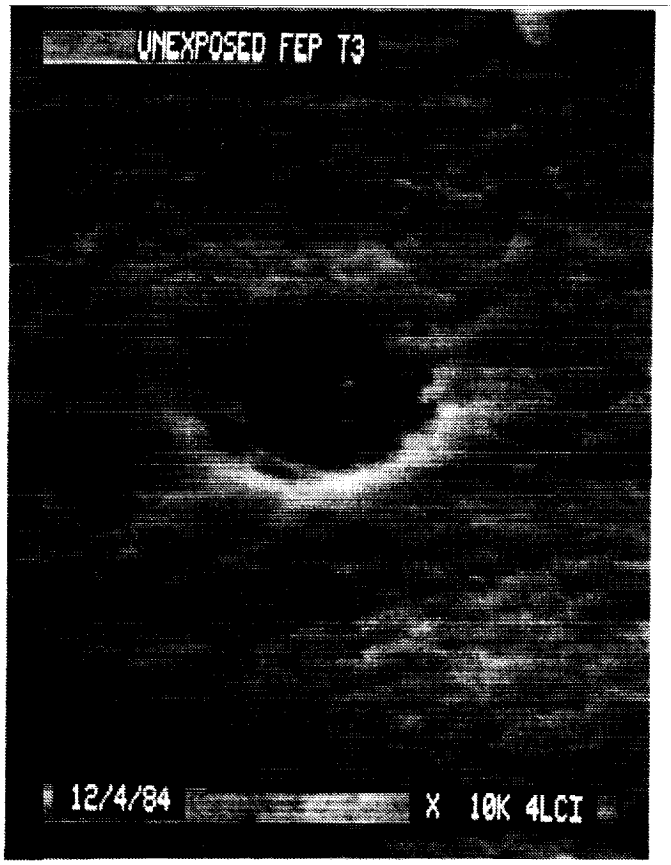

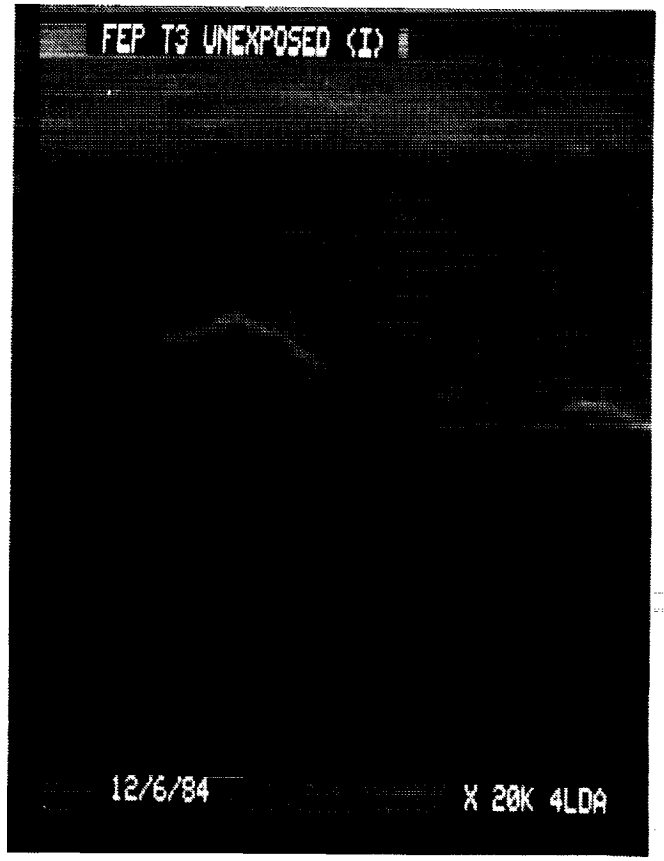

Figure 16 T3 Examples of impact craters entrance and exit in FEP Teflon.

T3 FEP TEFLON UNEXPOSED MICRO METEORITE CRATERS

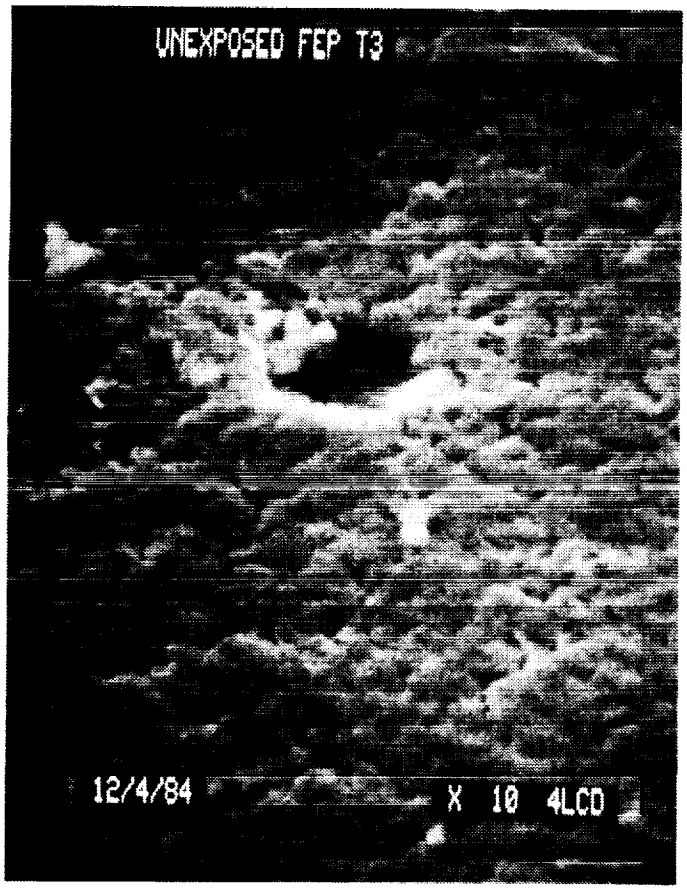

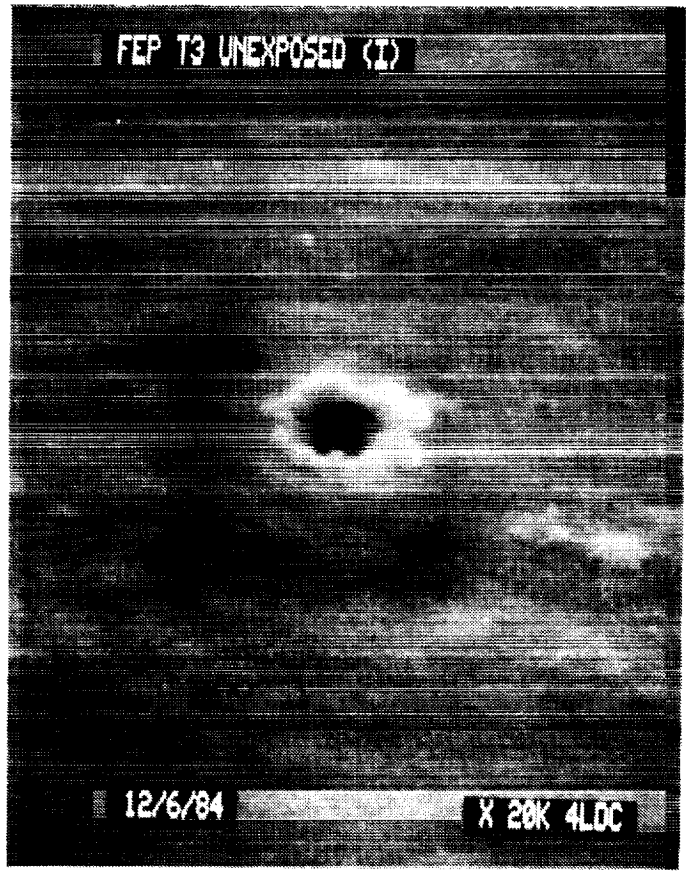

Figure 17 13A Kapton Top layer possible impact.

Crater on eroded Kapton surface. These are generally not visible because of erosion texture on the Kapton surface.

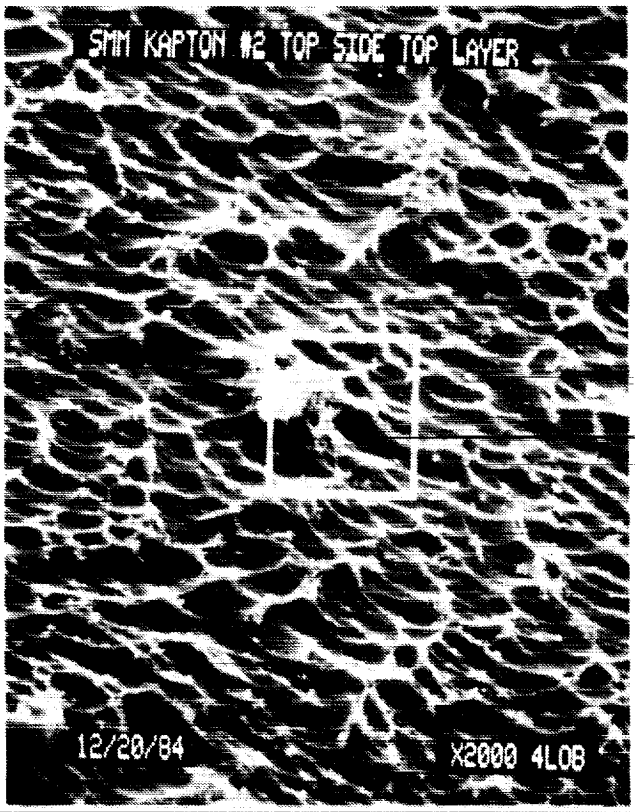

13A KAPTON TOP LAYER

MICRO METEORITE

CRATER

ORIGINAL PAGE IS
OF POOR QUALITY

Figure 13 13A Kapton #2 side of top layer. Exit impact craters on Al side of top layer of Kapton.

13A MICRO METEORITE CRATERS

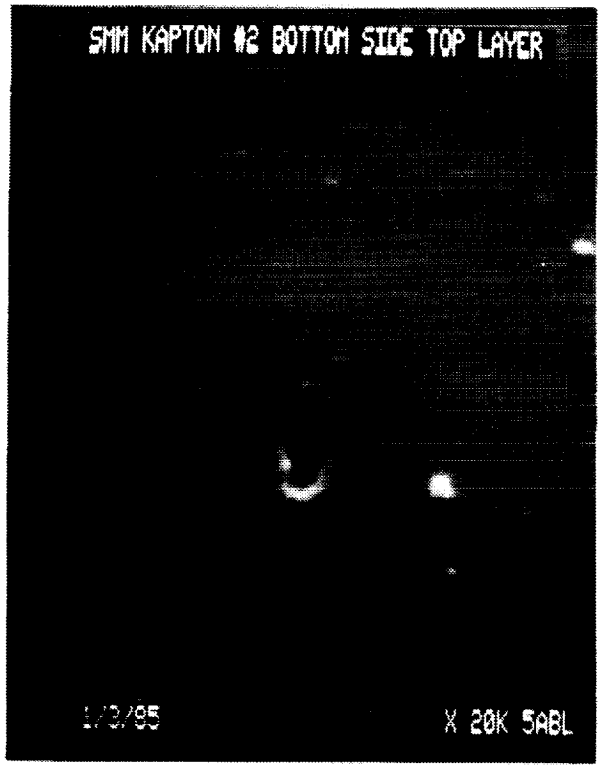

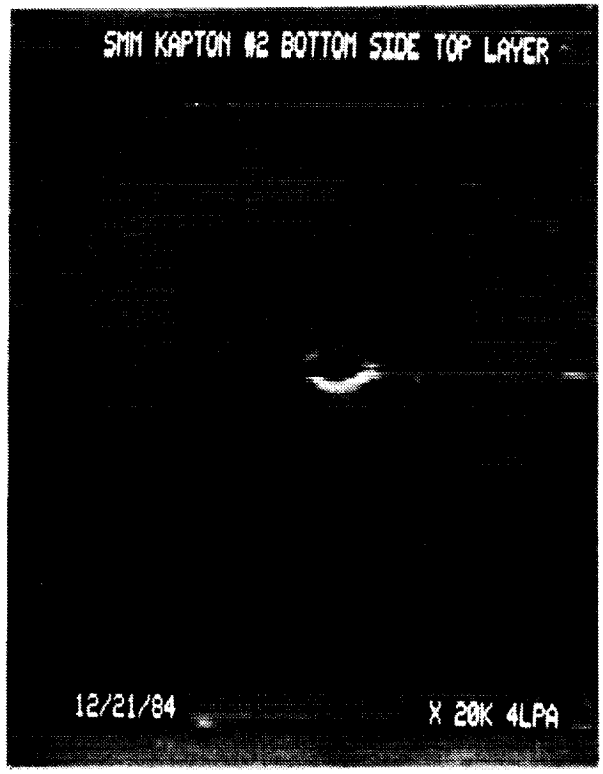

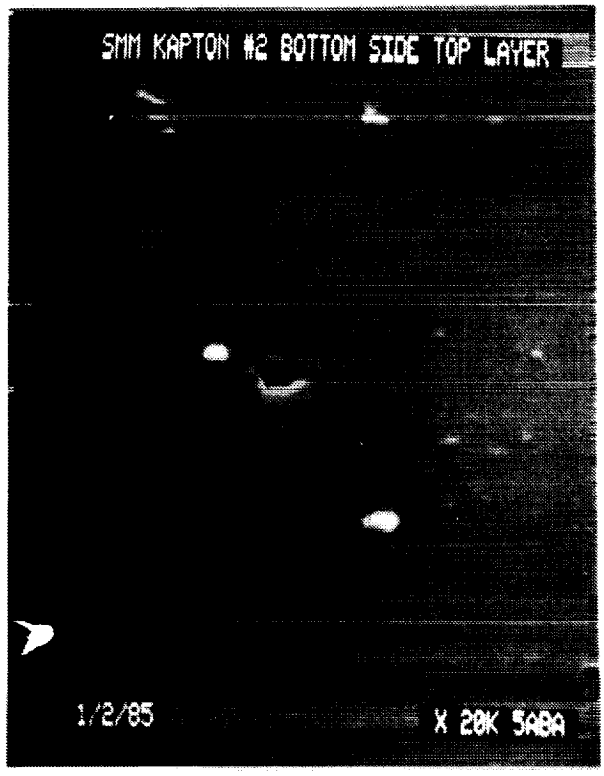

Figure 13 13A Kapton Bottom Layer Al side.

Typical aluminized surface with no impact craters visible.

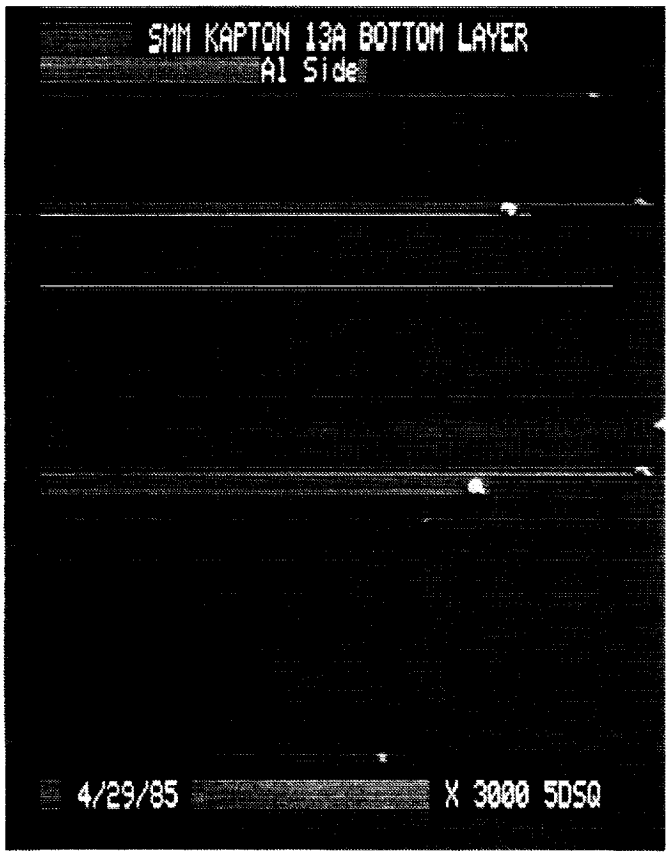

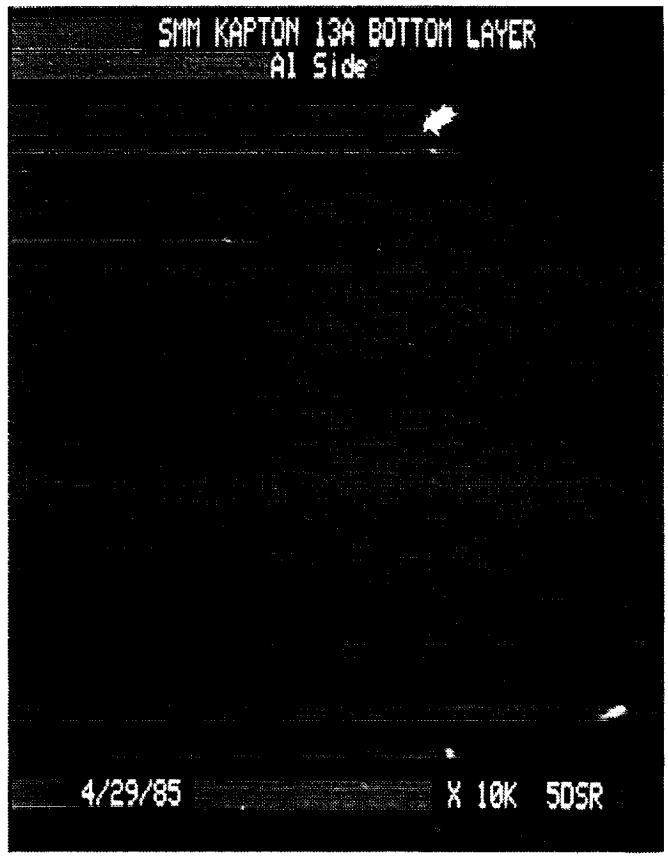

13A KAPTON

BOTTOM LAYER

Al SIDE

ORIGINAL PAGE IS
OF POOR QUALITY

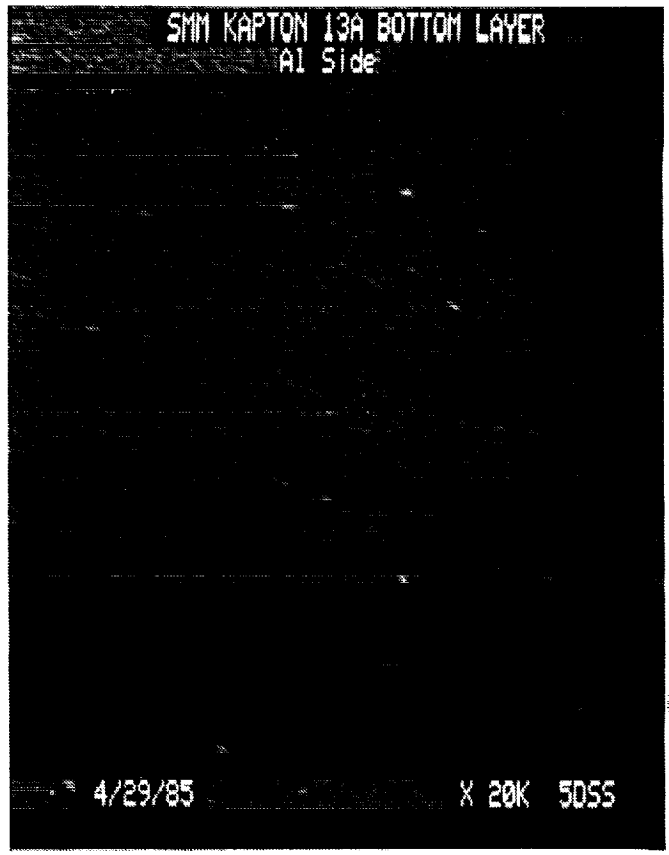

(This page intentionally left blank)

(This page intentionally left blank)

Analysis of Normal and Transparent Silver Teflon

Presented at

Solar Max Repair Mission
Materials Degradation Workshop

9-10 May 1985

NASA/Goddard Space Flight Center

Dr. Wayne K. Stuckey
Dr. Alan A. Galuska
Joe Uht

Samples of Inconel/silver/Teflon exposed to solar radiation, and atomic oxygen on Solar Max were brought to The Aerospace Corporation for microcharacterization. Those samples exposed to atomic oxygen from the metallic side had become transparent while those exposed from the Teflon side remained reflective. The objective of our analysis was to determine the difference between the transparent and non-transparent material. Microcharacterization of these Inconel/silver/Teflon samples was performed using scanning electron microscopy with windowless energy dispersive X-ray analysis (SEM/EDX), secondary ion mass spectrometry (SIMS), and X-ray photoelectron spectroscopy (XPS).

SEM/EDX Analysis

Our principal specimen is an Inconel/silver/Teflon film in which the metalized surface has been partially exposed to atomic oxygen. As shown in Figure 1, there are at least three structurally different regions (A, B and C) of interest. Region A is the unexposed area. The abundant cracks have produced a grainy microstructure with reaction product protruding from the boundary regions. As shown in Figure 2, the grain surface and reaction product are primarily silver, nickel, and carbon. Region B is transition area exposed to a moderate dose of atomic oxygen. Cracking in this region is more severe and has resulted in a greatly reduced grain size. In addition, as shown in Figure 3, the boundary region has begun to erode with reaction product being dispersed over the surface. Despite these structural changes, the EDX analysis reveals that the surface is still composed primarily of silver, carbon and nickel. Region C is the completely exposed material. The grains have largely been eroded away leaving cone-like formations. As shown in the EDX spectrum of Figure 4, silver and nickel have largely been removed. High carbon and fluorine signals characteristic of Teflon remain. Unexpectedly, significant quantitites of oxygen were not detected in the areas exposed to atomic oxygen.

To determine the mechanism of crack propagation, samples of Inconel/silver/Teflon exposed to solar radiation alone, solar radiation and atomic oxygen, and neither solar radiation or atomic oxygen were examined.

The sample exposed to neither environment showed few cracks. In contrast, substantial cracking was observed in the solar irradiated sample, and cracking plus erosion was observed in the material exposed to atomic oxygen and solar radiation. Examples of crack propagation in material exposed to only solar radiation is presented in Figure 5. The most probable cause of the cracking is the thermal expansion mismatches of the film materials combined with the variation in temperature experienced by Solar Max. In addition, the cracking appears to be more prevalent in areas that have experienced greater mechanical stress. A combination of thermal and mechanical factors may be responsible for the observed cracking.

In all cases, the cracking was accompanied by the presence of a reaction product in the cracks. SEM micrographs and EDX spectra of this particulate matter are shown in Figure 6. The reaction product was insulating in nature and composed primarily of silver, carbon, fluorine, and chlorine. The fluorine concentration was found to vary quite dramatically from sample to sample while the carbon, silver, and chlorine signals remain fairly constant. The source of chlorine has not yet been determined.

The SEM investigation of the observed material degradation is summarized pictorially in Figure 7. Due to thermal or mechanical factors, cracks are initiated and propagated. A silver containing reaction product is then produced in the cracks. This reaction product then flakes off leaving underlying layers exposed. Finally, the grain boundaries are eroded until most of the grain has been consumed. A cone-like surface structure, which is composed primarily of carbon and fluorine with trace amounts of silver, remains.

SIMS Analysis

In addition to SEM/EDX analysis, SIMS mass spectra and ion images were taken from the metallized surface of the Inconel/silver/Teflon films. SIMS mass spectra of the metallic surface unexposed, partially exposed, and fully exposed (to transparency) to atomic oxygen are presented in Figure 8. The constituents of the Inconel (nickel, chromium, and iron) dominate the spectrum

of the unexposed metallized region. Fairly high signals from elemental contaminants (sodium, aluminum, silicon and potassium) and silver are also apparent. As expected for the non-degraded surface, the carbon and fluorine peaks are only present at low levels.

Upon partial exposure to atomic oxygen, the Inconel and contamination peaks are greatly reduced while the silver, carbon, and fluorine peaks have increased. It appears that the Inconel layer has been largely removed exposing the underlying layers of silver and Teflon (The Teflon is exposed through cracks in the silver layers.) In addition to the changing elemental intensities, fluorinated carbon peaks (CF^+, CF_2^+, CF_3^+, and $C_3F_3^+$) are apparent. These peaks are not characteristic of pure Teflon, and may be attributed to the breakdown of the polymer chain upon exposure to atomic oxygen.

Upon more intense exposure, an increase is observed in the carbon intensity relative to the silver intensity. This indicates that most of the silver layer has been removed. In addition, the fluorine and the fluorinated carbon intensities have decreased relative to carbon. This may indicate that the Teflon surface has been depleted of fluorine.

Ion micrographs of nickel, silver, fluorine and oxygen from the unexposed and exposed metallized surfaces are presented in Figures 9 and 10, respectively. The ion micrographs from the unexposed region show that the grains are composed of nickel with silver and fluorine apparent in the cracks. In addition, trace quantities of oxygen are localized to the nickel grains. In contrast to the unexposed region, the ion micrographs from the exposed region show that most of the nickel and much of the silver has been removed. The fluorine and oxygen signals appear to trace the silver distribution rather than the nickel or Teflon (dark areas) distributions.

From these ion micrographs and mass spectra the degradation of the exposed material may be described in the following manner. During atomic oxygen exposure, first the Inconel and then the silver layers are being removed. The Teflon surface is being broken down, resulting in the depletion of fluorine

from the surface. The unexpectedly low signal levels observed for oxygen indicate that no stable (non-volatile) oxygen compound has been formed in significant quantities on the metallized surfaces. The oxygen that is present segregates to the metallic areas.

XPS Analysis

The atomic oxygen exposed and unexposed metallic surfaces were also analyzed by XPS to determine any differences in their chemical form. Prior to analysis, the samples were coated with a thin layer of Au for binding energy calibration. The XPS spectra of the unexposed and exposed surfaces are presented in Figures 11 and 12, respectively. The spectrum of the unexposed surface shows the presence of Inconel constituents (nickel and chromium), oxygen, carbon and a trace of silver. The high energy shoulder of the Ni2p3 peak, as well as the position of the oxygen peak, indicate that an extremely thin nickel oxide has been produced on the surface. The carbon peak is positioned at 284.6 eV which is characteristic of graphitic carbon.

In contrast to the unexposed material, the XPS spectrum of the surface exposed to atomic oxygen shows no evidence of Inconel. The Inconel has been removed resulting in increased silver, carbon, and fluorine concentrations at the surface. The silver and fluorine binding energies correspond to silver metal and Teflon, respectively. The carbon peak is split into a doublet with one peak corresponding to fluorinated carbon and the other corresponding to graphitic carbon. This doublet indicates bond breaking in the Teflon resulting in fluorine depletion. This depletion is further substantiated by a comparison of the fluorine to carbon concentration ratio for the Teflon surface and the degraded metallized surface. The ratio changes from ~2 for the Teflon to ~1 for the degraded material. Unexpectedly, there is no evidence of oxide production on the exposed surface. In fact, the normalized oxygen signal from the exposed surface is a factor of seven lower than that from the unexposed surface.

Conclusion

While the mechanism of the Inconel/silver/Teflon film degradation (transparency) has not been completely elucidated, many important features of the process have been identified. These features are briefly summarized in Table 1. The transparent material had a cracked mosaic-like surface structure which can be attributed to thermal effects. Unexpectedly, only trace quantities of oxygen were observed on the surface. A reaction product composed primarily of silver, carbon, fluorine and chlorine was observed protruding from the cracks. This material was easily detached leaving the underlying regions exposed. During oxygen exposure, most of the Inconel layer and much of the silver layer are removed. In addition, the SIMS and XPS analyses indicate that a Teflon reaction has taken place. Fluorine is liberated resulting in a fluorine depleted Teflon surface. While this reaction is not fully understood, it is likely that silver in the presence of atomic oxygen has catalyzed the breakdown of the Teflon. This hypothesis is currently being examined in greater detail.

SPACE AND ENVIRONMENTAL EFFECTS

(EXPOSED SILVER ON TEFLON)

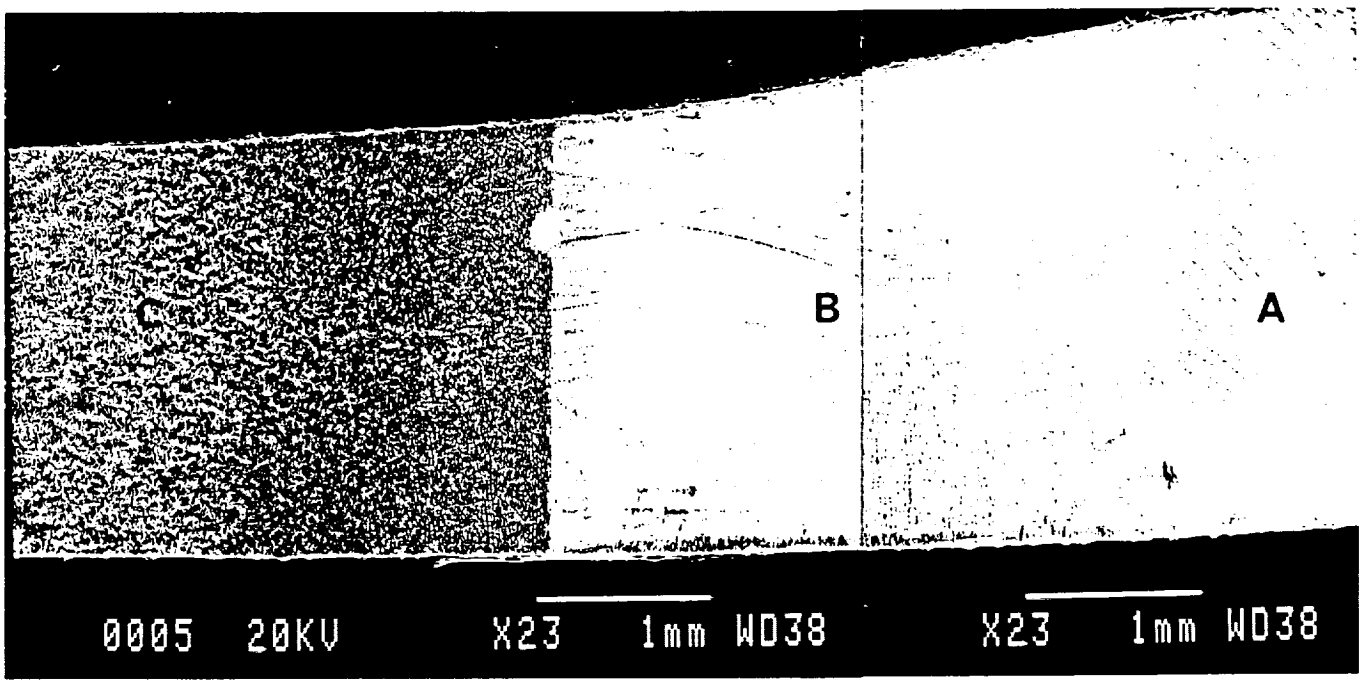

FIGURE 1

A. UNEXPOSED METAL REGION

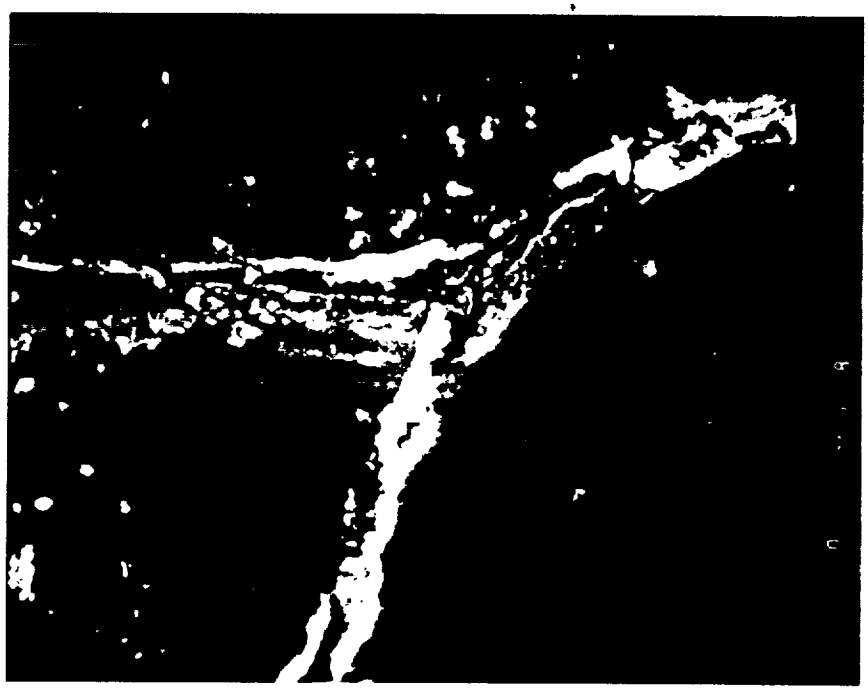

10μ

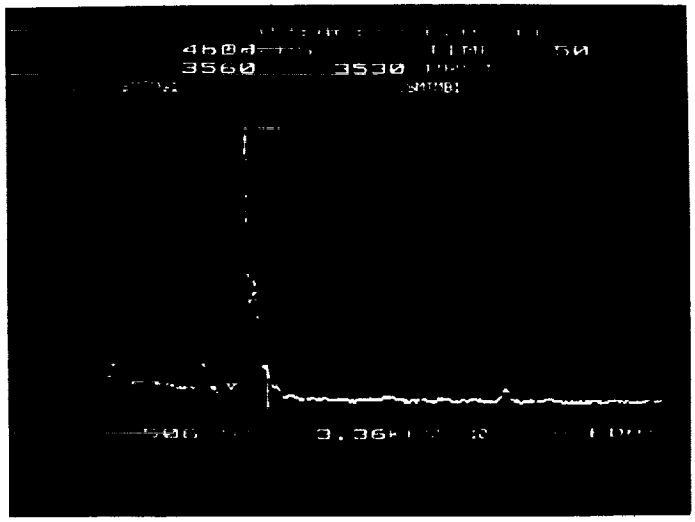

FIGURE 2

B. TRANSITION REGION

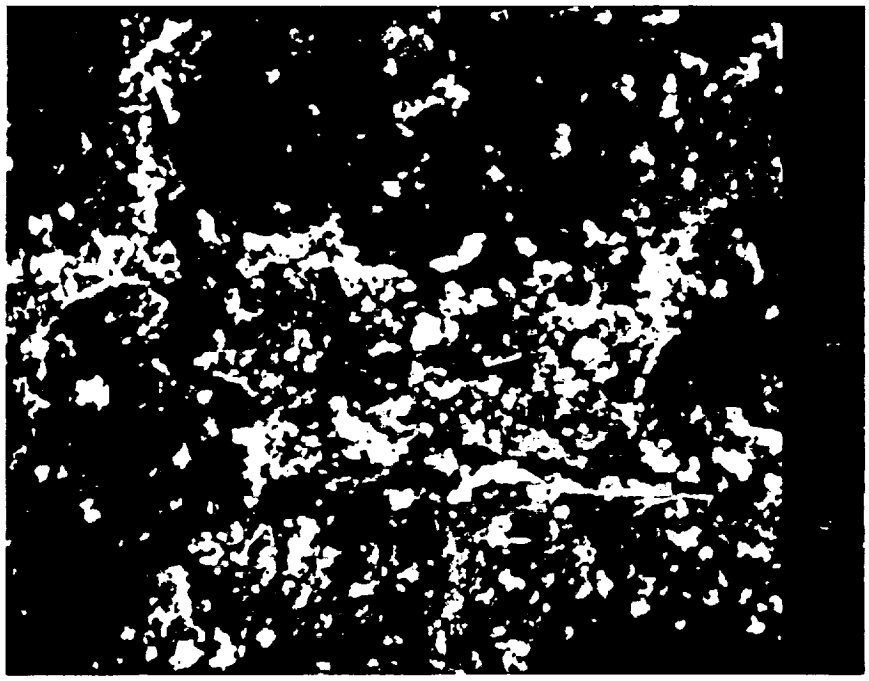

10μ

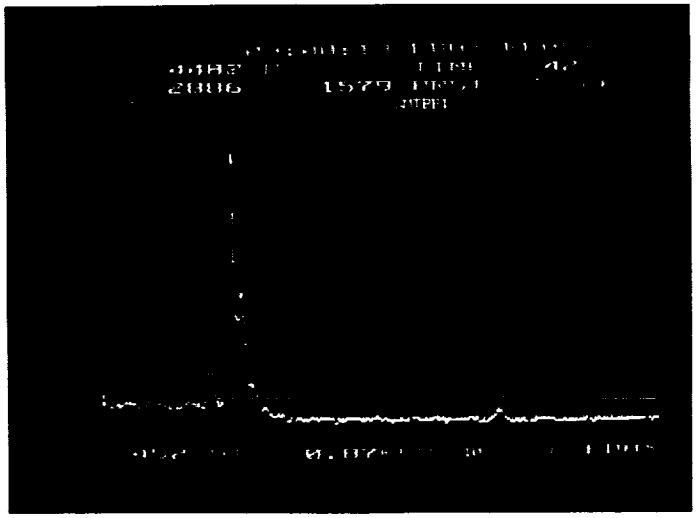

FIGURE 3

C. EXPOSED REGION

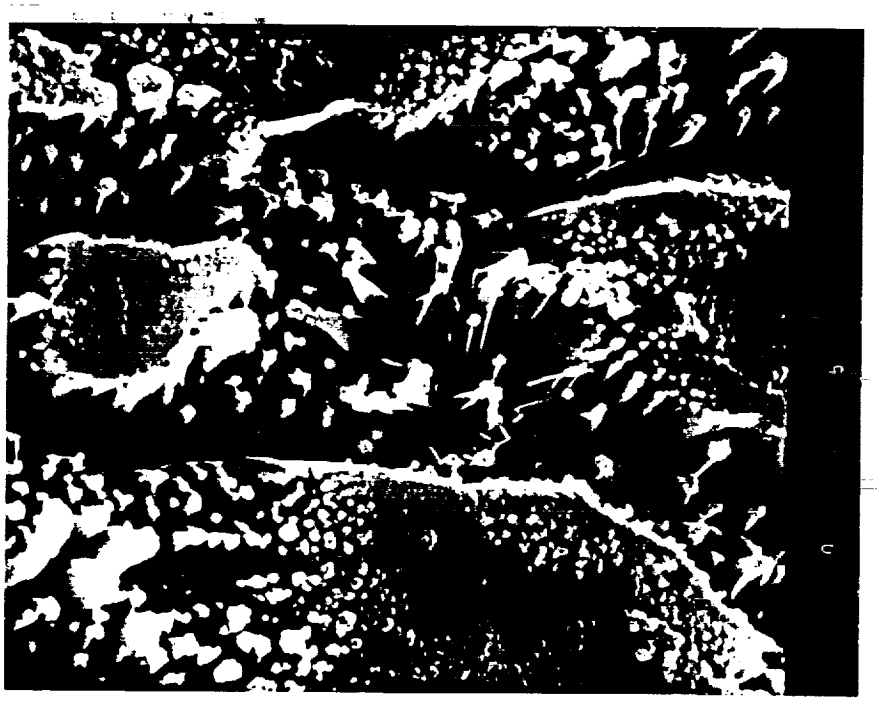

10μ

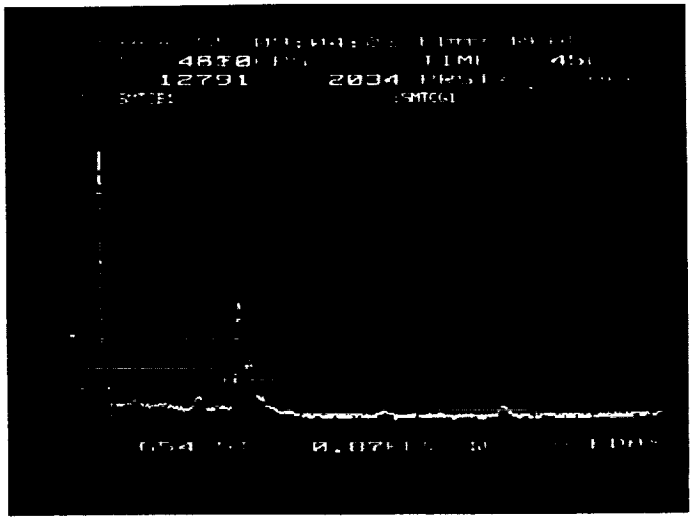

FIGURE 4

(Unexposed Material)

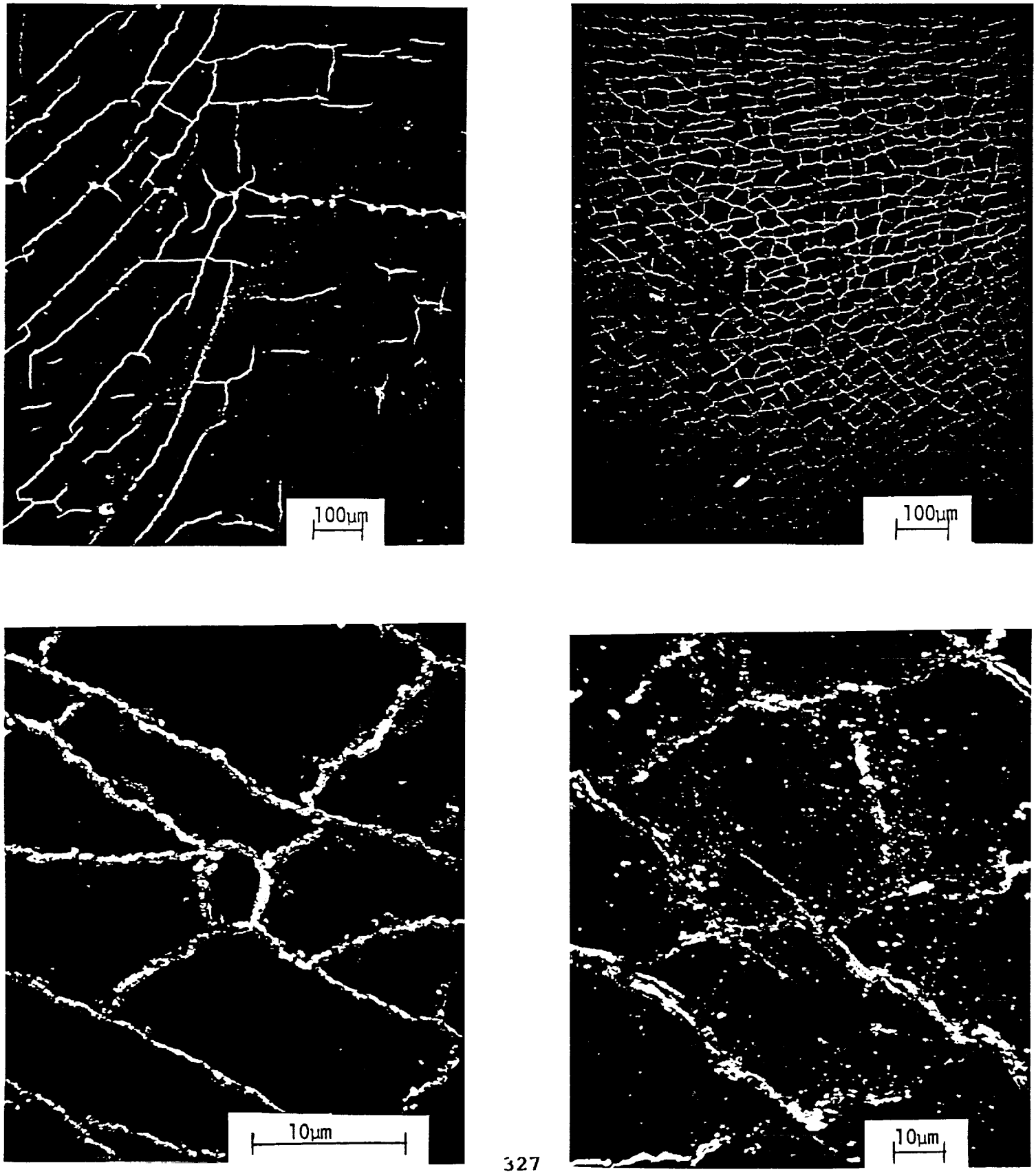

FIGURE 5

REACTION PRODUCT PROTRUDING FROM SURFACE CRACKS

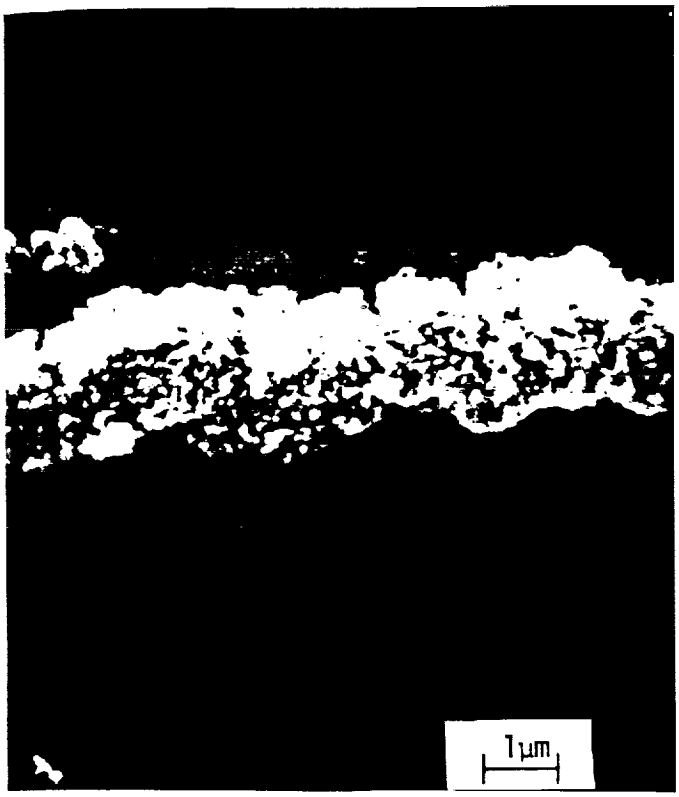

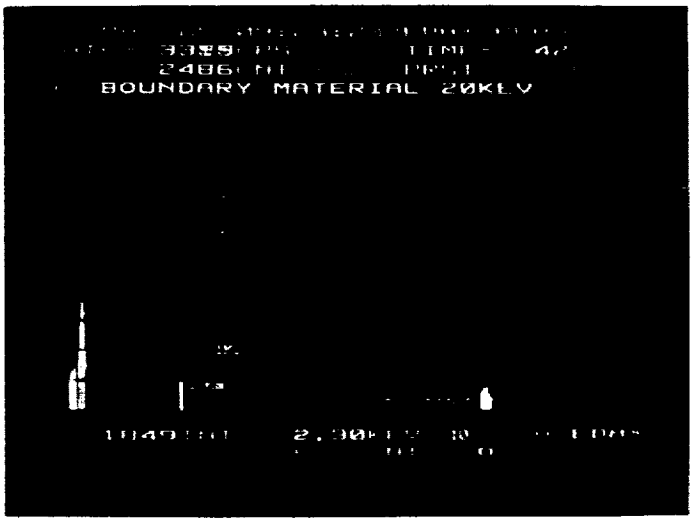

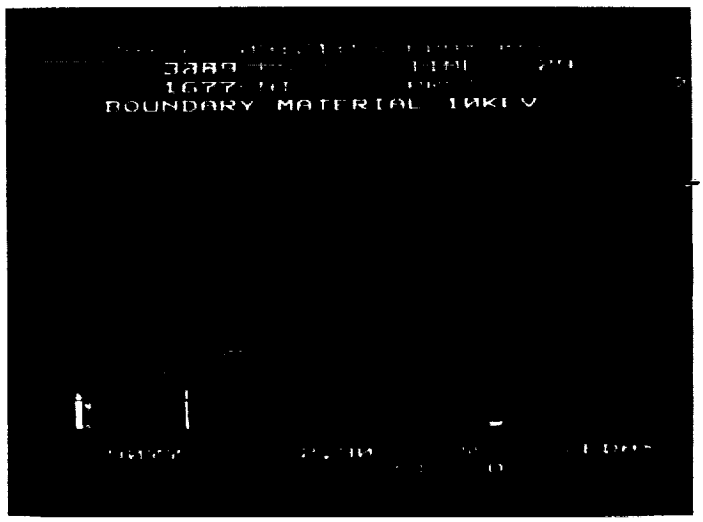

FIGURE 6

SURFACE DEGRADATION OF EXPOSED MATERIAL

ORIGINAL PAGE IS
OF POOR QUALITY

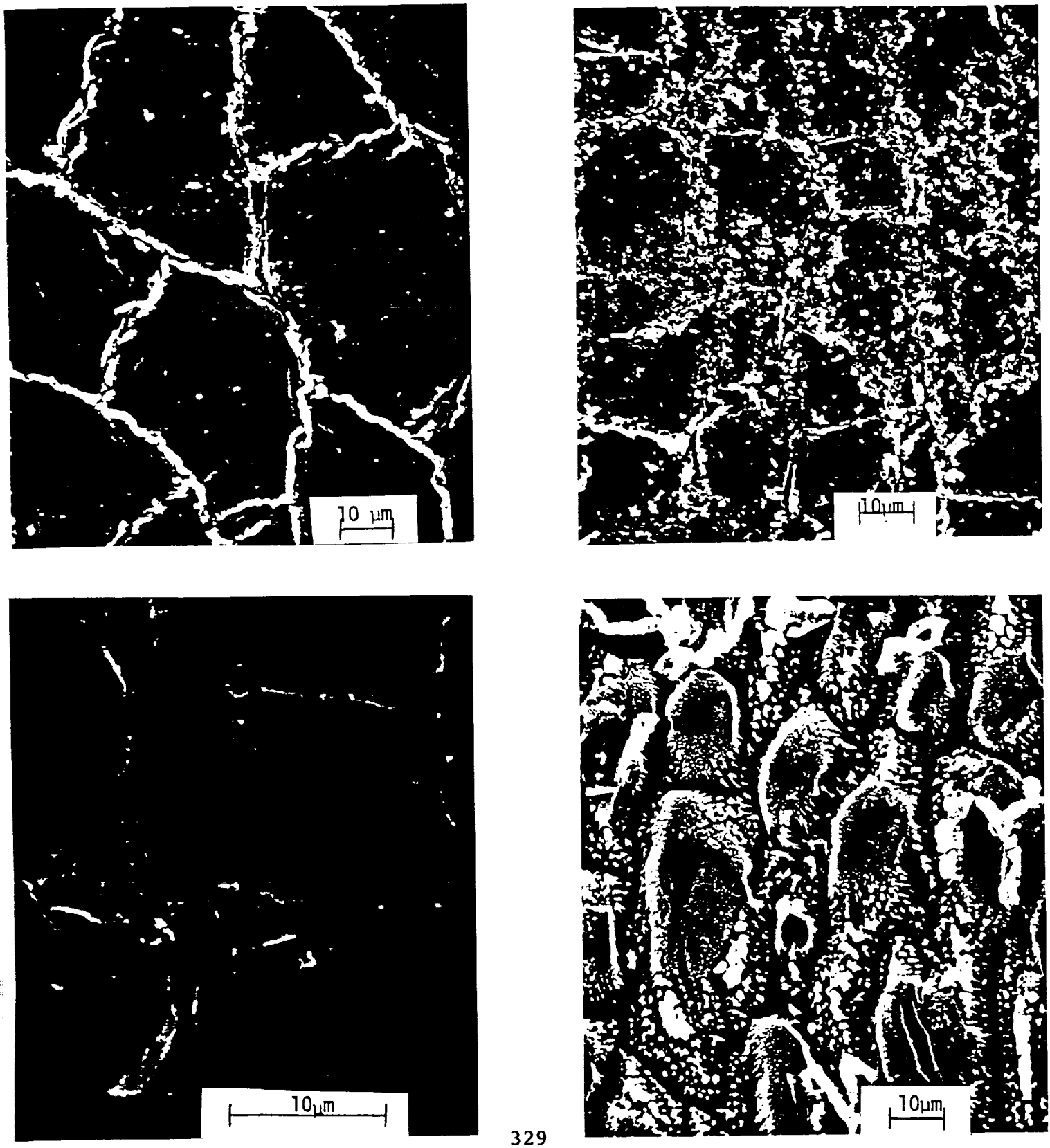

FIGURE 7

ORIGINAL PAGE IS
OF POOR QUALITY

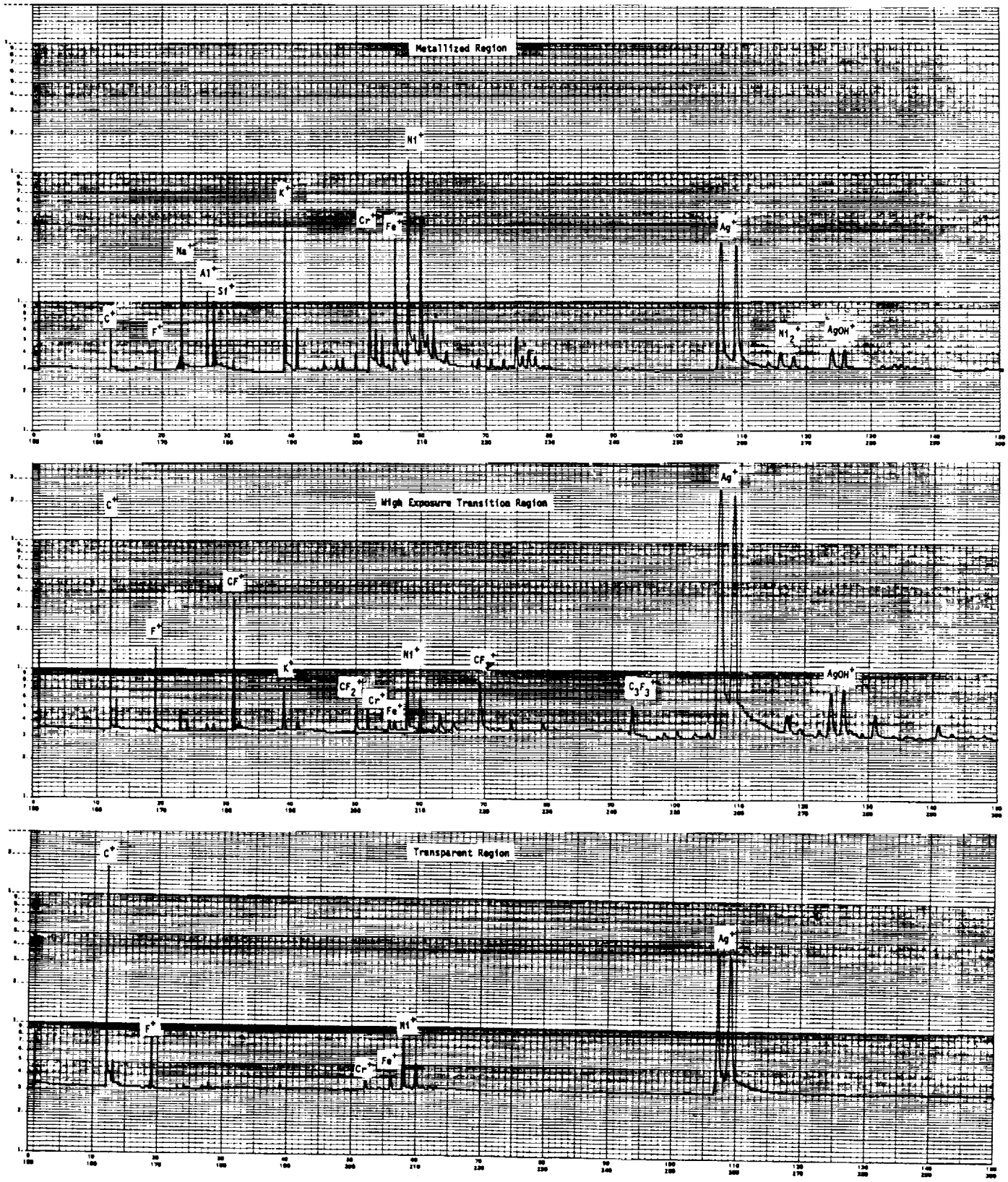

FIGURE 8

UNEXPOSED METAL REGION

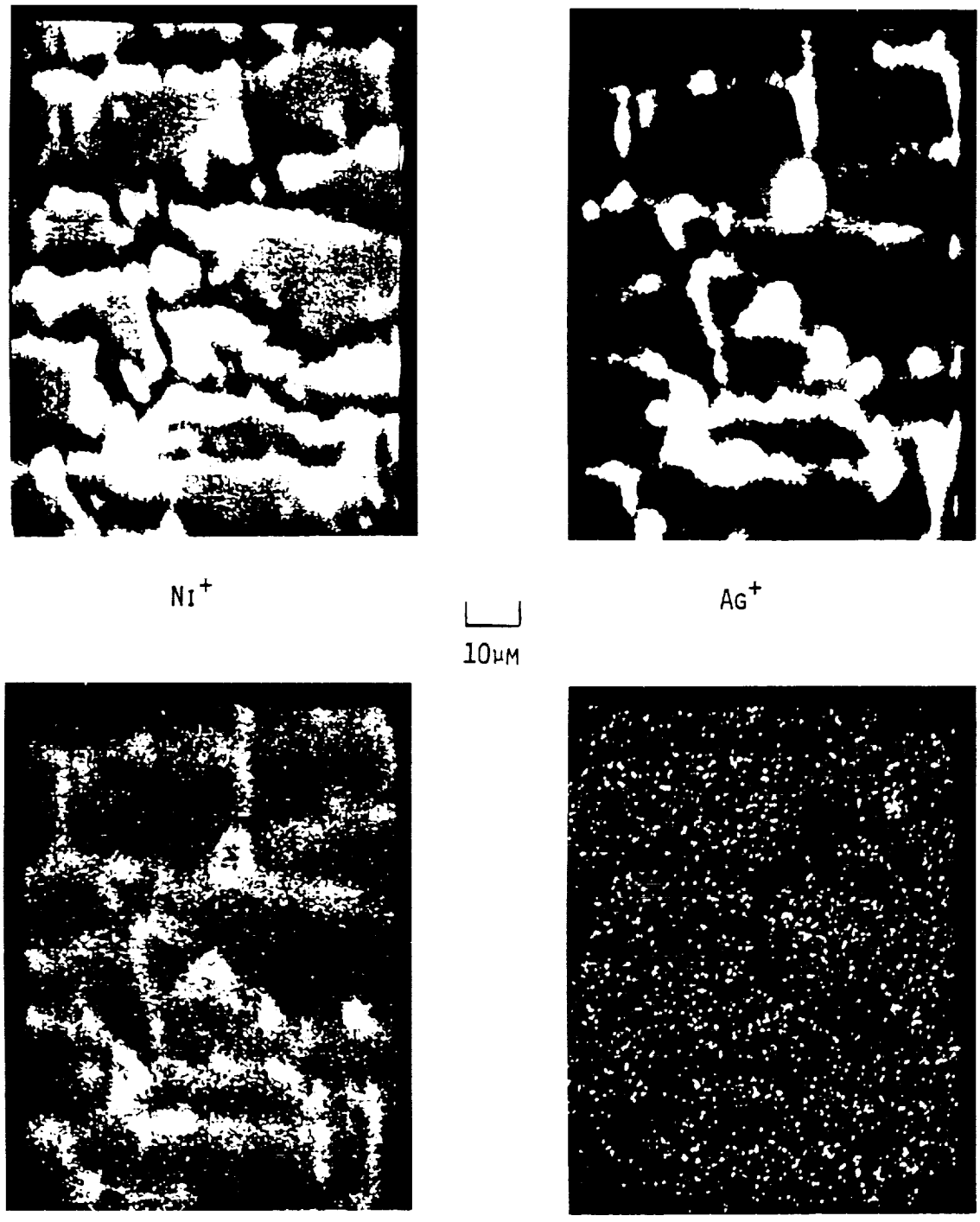

FIGURE 9

EXPOSED METAL REGION

Ni^+

Ag^+

10μM

F^+

O^+

FIGURE 10

XPS SPECTRUM OF UNEXPOSED REGION

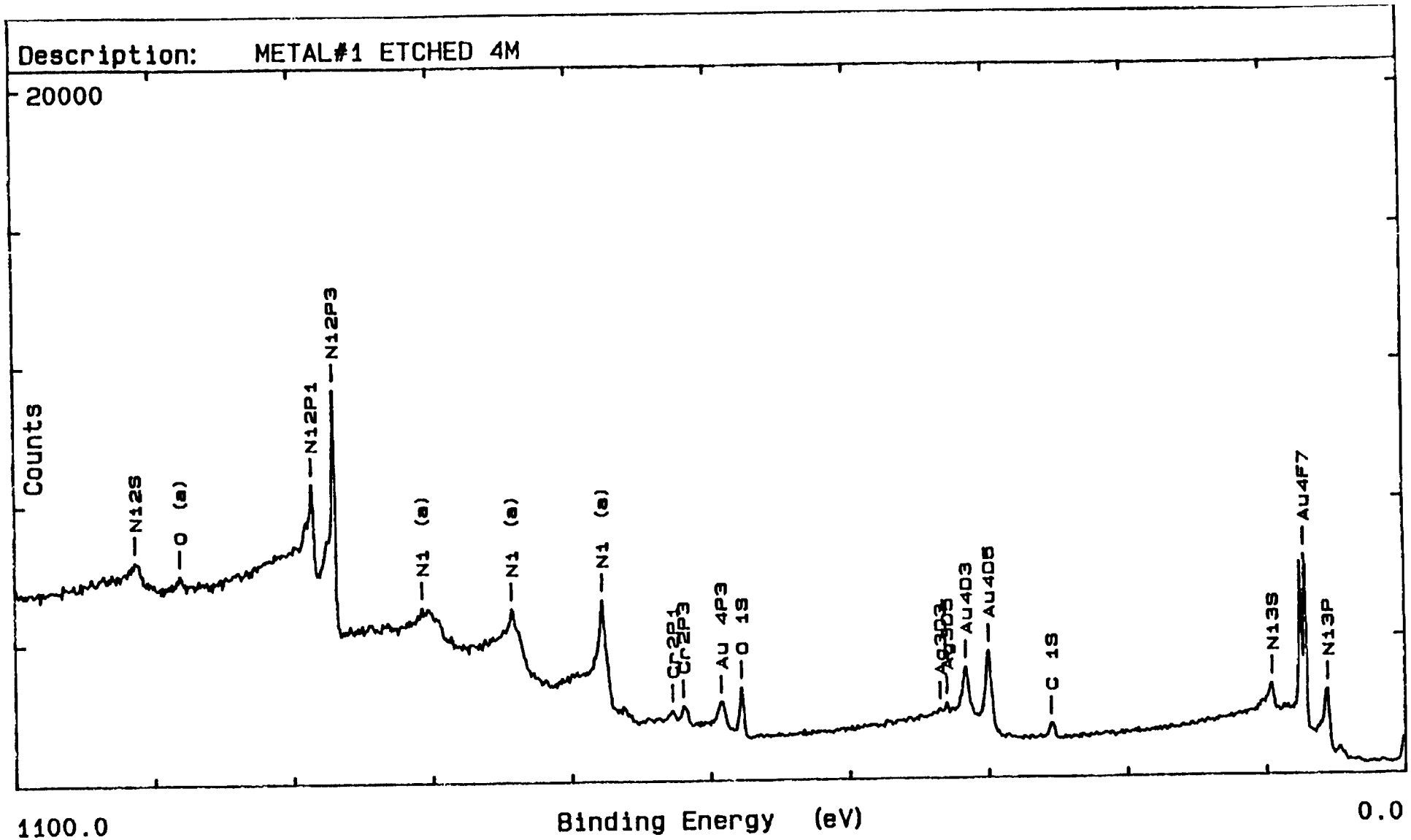

FIGURE 11

XPS SPECTRUM OF EXPOSED REGION

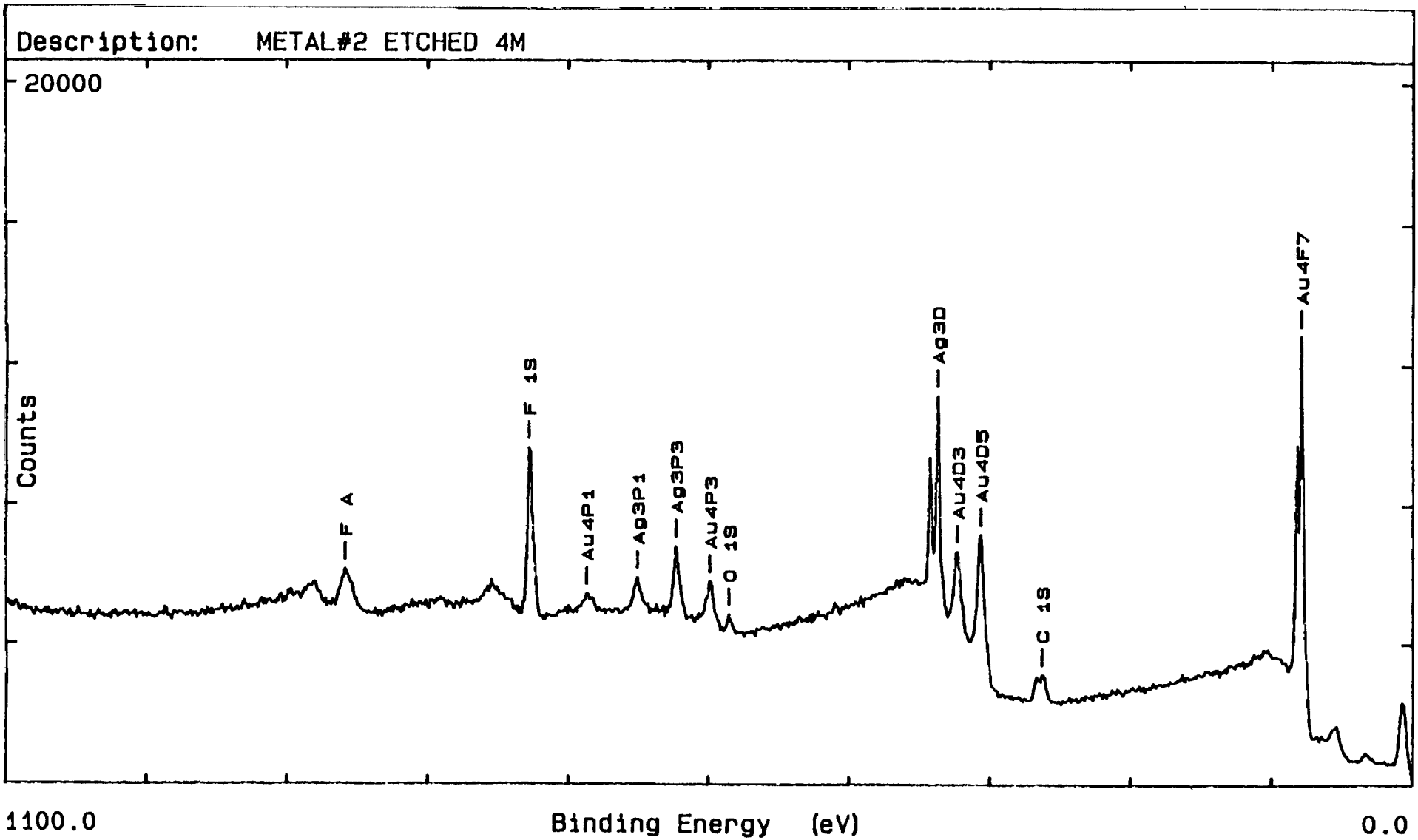

FIGURE 12

TABLE I SUMMARY

- REACTION AT CRACK SITES
  - OXYGEN NOT DETECTED
  - MATERIAL EASILY DETACHED
  - LOSS OF MATERIAL FROM CRACK EDGES
- SILVER LOSS IN TRANSPARENT REGION
  - SILVER INCREASES AT SURFACE IN TRANSITION REGION
  - SILVER LOWER AND INHOMOGENOUS IN TRANSPARENT REGION
  - NICKEL (INCONEL) LOW IN ALL REGIONS
- TEFLON REACTIONS SUGGESTED
  - FLUORINE DETECTED ON SURFACE OF METAL AND IN CRACKS
  - CARBON/FLUORINE RATIOS VARY
- REACTIONS NOT FULLY UNDERSTOOD

(This page intentionally left blank)

DEGRADATION STUDIES OF SMRM TEFLON

Ranty H. Liang, Keri L. Oda and
Shirley Y. Chung

Applied Mechanics Technology Section
Jet Propulsion Laboratory
California Institute of Technology
Pasadena, CA 91109

A working group was organized to study materials and components of the Solar Max Satellite (SMS) that was returned by the STS 41C. These materials were exposed in space for 50 months and represent the only real-time long-term exposure data available to date. We were invited by Goddard Space Flight Center (GSFC) to participate in the studies of these materials.

In our molecular modeling of material and energetic oxygen atom interaction we pointed out the importance of developing correlation between accelerated exposure data from STS and some real-time data. In particular, we predicted that teflon which showed no detectable degradation on various STS flights may be susceptible to atomic oxygen degradation under real-time conditions. Initial inspection of returned SMS samples showed that teflon suffered visual damage such as cracking and yellowing. We had selected and received 4 SMS teflon samples which were exposed to different space environments (i.e. O atom, UV etc.).

Four teflon samples were received and their exposure conditions are listed in Table I. Figure 1 is a picture of all four samples. Sample C, T_2 and B_1 are 5 mil. thick teflon tape coated with 1500Å of silver and 100Å of inconel. Sample T_1 is the same teflon tape laminated on a 5 mil thick Kapton.

Table I. Teflon Samples and Exposure Conditions

SAMPLE	Exposure conditions
C_1	Sample not exposed to O atom nor UV
T_1	High O atom, High UV
T_2	Medium O atom, no UV
B_1	High O atom, no UV

ESCA analyses were carried out on the surface of these samples and results are listed in Table II.

Table II. ESCA Analyses of Teflon Samples

SAMPLE	C_1	C_2	C_3	C_4	C_5	C_6	F_1	Si_1	Si_2
UNEXPOSED	4.9	4.0	3.7	3.4	25	2.2	48		1.0
B_1	4.2	0.9	2.6	2.4	22	3.4	56	2.2	3.1
T_1	2.0	1.9	3.2	5.5	24	4.7	53	?	?
B_1	1.6	1.3	1.5	2.5	30	2.5	58		
T_2	3.6	3.1	3.1	3.0	24	3.6	53	0.3	0.5
T_2	15	3.4	4.8	1.1	8.9	1.6	24	?	?

C_1 = CH C-C
C_2 = COH C-O-C
C_3 = COOH COOC
C_4 = CF_2-CH_2
C_5 = CF_2-CF_2
C_6 = CF_2O, CF_3
Si_1 = SILICONE
Si_2 = SiO_2

Figure 1. Teflon Samples from Solar Max Satellite (SMS).

It is not surprising to find that surfaces of these samples were contaminated as evident by the detection of Si as well as hydrocarbon (C_1) by ESCA. Surface of regular teflon which has a chemical structure of (CF_2)'s should be composed of 33% fluorocarbon (C_2) and 67% fluorine (F) with no hydrocarbon (C_1). C_1 on these teflon was first thought to be from siloxane which was physically deposited onto the teflon surface as contaminants. However, detection of C_4 which is a fluorocarbon chemically bounded to a hydrocarbon revealed that these teflon tapes are not pure fluorocarbons (i.e. $-CF_2-$). Table III shows the -CH- to $-CF_2-$ ratios (R) of all four samples. Samples B_1 and T were evaluated at two different locations in order to determine magnitude of experimental error. It is evident that the ratio $R=(C_4/C_5+C_6)$ decreases as a function of oxygen atom exposure. This is in agreement with our molecular model in which the reaction rate of energetic oxygen atoms with hydrocarbons is much higher than that with fluorocarbons. It is interesting to note that sample B_1 which was exposed to high dose of oxygen atoms shows a larger decrease in R as compared to sample T_2 which was exposed to medium dose of oxygen atoms. Sample T_1 on the other hand, exhibits an increase in R as a result of exposure.

TABLE III. $-CH_2-$ to $-CF_2-$ ratios (R) of all Four Samples

SAMPLE	$R = [C_4/(C_5 + C_6)]$
UNEXPOSED	12.5%
B_1	9.4%
B_1	7.7%
T_2	10.9%
T_2	10.5%
T_1	19.2%

Rheovibron measurements were carried out on these samples in order to determine possible bulk property changes. Figure 2 is a plot of tensile modulus as a function of temperature. All three exposed samples exhibit loss of modulus. Both samples B_1 and T_2 showed 15% decrease while sample T suffered a 30% decrease, in modulus.

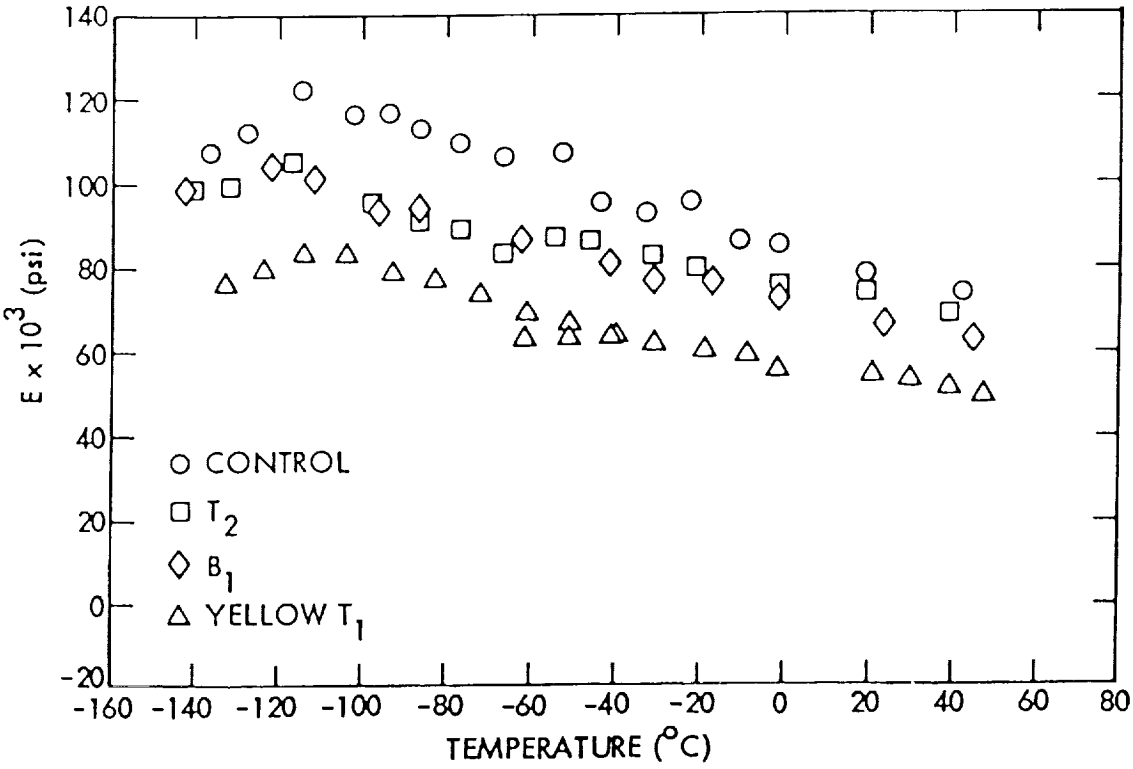

Figure 2. Plot of Tensile Modulus as a Function of Temperature

Table IV summarizes the preliminary findings. The SMS teflon tape sample is not pure fluorocarbon, but copolymer of fluorocarbon and hydrocarbon. In the case of only O atom interaction, our model predicts that hydrocarbons will be more susceptible to degradation than fluorocarbon (i.e. decrease in R value) with very little formation of unsaturation (i.e. no yellowing). Both phenomena were being observed on sample B_1 and T_2. Sample T_1 which was exposed to both O atoms and UV showed different modes of degradation. This leads to the conclusion that synergistic effects of UV and O atom cannot be neglected in designing ground based testing. Additional studies are planned to evaluate the decrease in modulus. GSFC is also planning to have JPL look at additional SMS samplesin order to study synergistic effects of O atom and UV.

Table IV. Summary of Preliminary Findings

SAMPLE	B_1, T_2	T_1
EXPOSURE CONDITIONS	O ATOM	O ATOM + UV
$R = CH_2/CF_2$	DECREASE	INCREASE
YELLOWING	VERY LITTLE	EXTENSIVE
TENSILE MODULUS	DECREASE (15%)	DECREASE (30%)

SOLAR MAXIMUM THERMAL SURFACE ASSESSMENT

*G. D. Rhoads
Lockheed Missiles & Spacecraft Co., Sunnyvale, California

ABSTRACT

The in-flight repair of the Solar Maximum Spacecraft provided the first opportunity to make actual measurements of thermal control surfaces after 4 years exposure in low earth orbit. Defective hardware was replaced by astronauts and returned to earth while protected from re-entry damage in the Shuttle Payload bay. A preliminary thermal surface assessment was made soon after retrieval in support of Space Telescope and other current spacecraft programs. This included visual examination and measurement of Kapton and Teflon film to determine change in thermal radiative properties after 4 years exposure to solar radiation and reaction with atomic oxygen. Comparative measurements were made with a portable solar reflectometer used for inspection of spacecraft hardware. Post flight measurements and observations reveal significant surface changes that further confirm Kapton mass loss predictions made prior to Solar Maximum repair. Details of thermal surface application, measurements and experimental results are presented and discussed in this paper.

INTRODUCTION

The Solar Maximum retrieval and repair mission (SMRM) provided the first opportunity to measure in-flight thermal surface degradation after 4 years in a low earth orbit and to compare the results with short term Shuttle measurements. The SMM spacecraft was launched February, 1980 into a circular orbit at 570 KM altitude and 28.8 inclination angle. Progressive loss of attitude control greatly reduced mission performance after September, 1980. Plans were then made for the first Shuttle repair mission which was initiated after atmospheric drag reduced SMM altitude to 498 KM. Astronauts successfully replaced the defective attitude control system (ATS) during SMM retrieval and redeployment in April, 1984. The ATS and associated hardware was returned to earth while protected from re-entry damage in the payload bay. Special handling and contamination controls were used to protect flight surfaces after re-entry and during shipment to NASA Goddard Space Flight Center.

---

*Staff Engineer, Spacecraft Thermodynamics

Exterior thermal control surface materials were removed for examination prior to the Post Flight Studies Workshop held at NASA GSFC, June, 1984. Visual examinations were made by attendees while surfaces were protected by clear plastic containers. A preliminary assessment was made after the workshop to determine change in surface properties of significance to the Space Telescope and other low earth orbiting (LEO) spacecraft. The assessment included visual examination and measurements of exposed Kapton and Teflon film with a portable solar reflectometer. Details of thermal surface measurements, application and experimental results are presented in this paper.

ENVIRONMENTAL DAMAGE EFFECTS

Spacecraft temperature control is highly dependent on the stability of thermal surfaces exposed to the damaging space environment. Surface material damage and deposition of contaminants typically increase solar absorptance which raises temperatures and may exceed design limits. Surface degradation in LEO was attributed primarily to ultraviolet radiation and spacecraft contamination prior to Shuttle flight experiments (Ref. 1).

Recent LEO flight experiments reveal atomic oxygen reactions which may have a very significant effect on thermal surface performance and life. Many materials returned from Shuttle flight reveal various degrees of surface damage and mass loss (Ref. 2, 3). This is attributed to reaction of the atomic oxygen (AO) component of the neutral atmosphere and is highly dependent on AO density which increases exponentially with lower altitude. Reaction efficiencies have been determined for many spacecraft materials based on Shuttle exposures of short duration. Values have been derived by comparing mass loss or equivalent thickness loss with the estimated AO fluence incident during flight. Reaction efficiencies are summarized in Table 1 for Kapton, FEP Teflon and other common materials for comparison purposes. These values were obtained from measurements made by Leger and other investigators during Shuttle STS-3 through STS-8 (Ref. 4, 5, 6). Averages are shown where mass loss measurements and fluence estimates were available for more than one experiment.

FLIGHT SURFACES

Most SMM exterior surfaces were covered with Kapton multilayer insulation (MLI) blankets including 4 sides and the back of the attitude control system. Each MLI blanket was protected with a front and back cover consisting of 2 mil Kapton aluminized on the inside surface. Silverized FEP Teflon film was fastened to the perimeter of the thermal louver assembly which was used to regulate temperature of the attitude control system. The Teflon film is 5 mil thick with a reflective layer of silver and protective overcoating of Inconel on the back side. All Kapton MLI and Teflon film was removed from the ACS and protected by clear plastic containers to minimize contamination and

handling damage. Location of the ACS and thermal control surface materials are shown in Figure 1 and Table 2.

Kapton and Teflon thermal surfaces were exposed to variable solar and atomic oxygen flux depending on location with respect to the top of the sun-pointing spacecraft. Top surfaces of the ACS received near maximum solar fluence while other surfaces received little direct solar exposure. Partial loss of attitude control early during the mission reduced solar pointing accuracy to an uncertain $\pm 15^{\circ}$ and a roll rate of 1° per sec as shown in Figure 2. This prevents accurate prediction of solar fluence and atomic oxygen fluence during the 4 year mission.

KAPTON MASS LOSS PREDICTIONS

Kapton mass loss predictions were made prior to SMM retrieval using a recently reported method that combines existing atmospheric property and data and the principles of orbit mechanics to derive the total atomic oxygen fluence incident on spacecraft surfaces (Ref. 7). Table 3 shows the predicted AO fluence incident on the SMM spacecraft from launch to projected time of recovery. The total Ram fluence was calculated to be 2.18 E21 per cm during the 4 year period. This result agreed well with the preliminary estimate of 2.14 E21 per cm made by NASA GSFC (Ref. 8).

Mass loss was derived from the product of the adjusted fluence and the Kapton reaction efficiency. The adjusted fluence incident on SMM multilayer insulation covers was assumed to be Ram x $1/\pi$ for a spinning, sun pointing spacecraft in a circular orbit. The predicated mass loss is 0.7 mil based on a Shuttle measured reaction efficiency of 2.6 E-24 per AO Atom. This agrees well with NASA GSFC post flight measurements of 0.5 to 0.8 mil equivalent Kapton mass loss (Ref. 8).

Kapton mass loss predictions were more recently confirmed during a flight experiment in a LEO (Ref. 11). It was predicted that 2 mil thick Kapton would be completely removed after 5 to 7 days exposure to atomic oxygen in flight. Flight performance data indicated total Kapton removal occurred within 6.25 days. Flight confirmation of Kapton mass loss is summarized in Table 4.

SURFACE MEASUREMENTS AND APPARATUS

Thermal surfaces were visually examined prior to measurement to identify specimens representing the full range of exposure. Clean room facilities and methods were used to minimize handling and contamination damage. Representative specimens were selected from exposed thermal surfaces and divided into areas of maximum and minimum change. Control specimens were selected from overlapped areas and from the back side of MLI blankets which were not exposed to solar radiation or the direct impingement of atomic oxygen.

Experimental error was reduced by making comparative measurements where possible. The effects of material manufacturing variables were minimized by measuring large MLI blankets where areas of maximum change could be compared with areas of minimum change on the same sheet of Kapton. Recorded measurement values represent an average of at least 3 measurements of a given area.

A portable solar reflectometer was used to make comparative measurements of selected areas of Kapton and Teflon (Ref. 9). The instrument consists of a measurement head and an electronic readout assembly which can be carried in a small suitcase. The head contains an integrating sphere with a tungsten-halogen lamp source and 4 filtered detectors. The detectors are adjustable and cover the UV, Blue, Red, and IR range of the solar spectrum. Detector outputs are electronically added to provide integrated solar reflectance values. Direct digital readout is provided at the electronic assembly with resolution to 0.001 and repeatability of $\pm$ 0.003 reflectance units.

Resolution and repeatability are enhanced by automatic zeroing and lamp control. Measurements are normally made every 8 seconds through a 1 inch diameter measurement port.

Performance and accuracy were confirmed by comparison with the Cary Model 17 D Spectrophotometer (Ref. 10). There was good agreement based on measurements of 9 different thermal surface materials made without separate adjustments as shown in Table 5. Improved accuracy was later obtained by simple adjustment of gain control using calibration specimens previously measured in the laboratory. An aluminized Teflon calibration standard with a predetermined $\alpha_s = 0.14$ was used to adjust gain for SMM measurements. The calibration standard was checked frequently during the SMM measurements to minimized drift due to electronic interference.

RESULTS AND OBSERVATIONS

Representative measurements of 6 sample areas of silverized Teflon and 4 sample areas of aluminized Kapton film are summarized in Table 6. Each sample is identified with respect to visual appearance and location on the SMM spacecraft. Post flight solar absorptance values were determined from a minimum of 3 solar reflectance measurements made of each sample area. Typical pre-launch values are included for comparison purposes.

Silverized Teflon post flight results revealed a small increase in solar absorptance < 0.04 as represented by 80 to 90% of exposed areas. These areas appear unchanged and remain highly specular based on comparison with the unflown calibration standard. The remaining 10 to 20% is darkened and crazed with small metalized areas of silver and Inconel missing from the back surface. Measurements of the darkened areas confirm a large increase of $\alpha_s = 0.22$ to 0.29. The damaged areas appear to have been subjected to higher temperatures due to loss of attitude

control and greater solar exposure. Most of the damaged Teflon was unsupported and subject to exposure on both sides.

Visual examination and solar absorptance measurements revealed little evidence of surface contamination based on the highly specular appearance of 80 to 90% of the silverized Teflon. A possible exception was noted where solar absorptance of sample area 17 B increased from $\alpha_s = 0.06$ to 0.28. This area appears to have been discolored by outgassing products from an adjacent SMM vent.

The Kapton muti-layer insulation measurements reveal a small increase in solar absorptance of $\Delta\alpha_s < 0.04$ with a large visual decrease in surface specularity (increased optical scattering). These surface property changes compare qualitatively with measurements made during Shuttle flights STS-3 through STS-8. The changes are also consistent with the SMM atomic oxygen fluence estimate and Kapton mass loss measurements mentioned previously. The diffuse appearance of degraded SMM Kapton is similar to Kapton removed from Shuttle STS-8 where measured mass losses are 0.7 and 0.4 mil, respectively.

CONCLUSION

Preliminary measurements of thermal control surfaces have been completed after 4 years exposure on the SMM spacecraft. The data confirm Kapton mass loss due to atomic oxygen reaction in a low earth orbit. Small increases in Kapton solar absorptance and large decreases in specularity are consistent with previous mass loss and surface property measurements. Small changes in most Teflon surfaces are attributed to a lower atomic oxygen reaction rate. Greater damage to small unsupported areas of Teflon requires further evaluation. The overall change in surface properties was not significant in terms of SMM performance. Greater mass loss and change in surface properties can be expected with more reactive materials or increased atomic oxygen fluence.

REFERENCES

1. McCargo, M., Spradley, L.W., Greenberg, S.A., McDonald, S.L., "Review of the Transient Degradation-Contamination of Thermal Coatings", NASA Contract NAS 8-26004, May, 1971.

2. Leger, L.J., "Low Earth Environment Interaction With Vehicle Surface-Material Effects," NASA Shuttle Environment Workshop, Washington, D.C., October 5-7, 1982.

3. Leger, L.J., Visentine, J.T., Schliesing, J.A., "A Consideration of Atomic Oxygen Interactions with Space Station," AIAA Paper 85-0476, 1985.

4. Leger, L.J., "Oxygen Atom Reactions with Shuttle Materials at Orbital Altitudes-Data and Experimental Status," AIAA Paper 83-0073, 1983.

5. Visentine, J.T., Leger, L.J., Kuminecz, J.F., Spiker, I.K., "ST-8 Atomic Oxygen Effects Experiment," AIAA Paper 85-0415, 1985.

6. Whitaker, A.F., Little, S.A., Harwell, R.J., Griner, D.B. DeHaye, R.F., "Orbital Atomic Oxygen Effects on Thermal Control and Optical Materials - STS-8 Results," AIAA Paper 85-0416, 1985.

7. Lee, A.L., Rhoads, G.D., "Prediction of Thermal Control Surface Degradation Due to Atomic Oxygen Interaction", AIAA Paper 85-1065, June, 1985.

8. Triolo, J., Park, J., Private Communications, May 25 and August 20, 1985.

9. Devices and Services Co, Dallas, Texas, "Solar Spectrum Reflectometer," Vendor Data, 1984.

10. Rhoads, G.D., "Thermal Surface Inspection Apparatus Investigation", Lockheed Missile & Space Co. Internal Communication, TXA-3083, 1982.

11. Knopf, P.W., Martin, R.J., Dammann, R.E., McCargo, M., "Correlation of Laboratory and Flight Data for the Effects of Atomic Oxygen on Polymeric Materials", AIAA Paper 85-1066, June, 1985.

ORIGINAL PAGE IS
OF POOR QUALITY

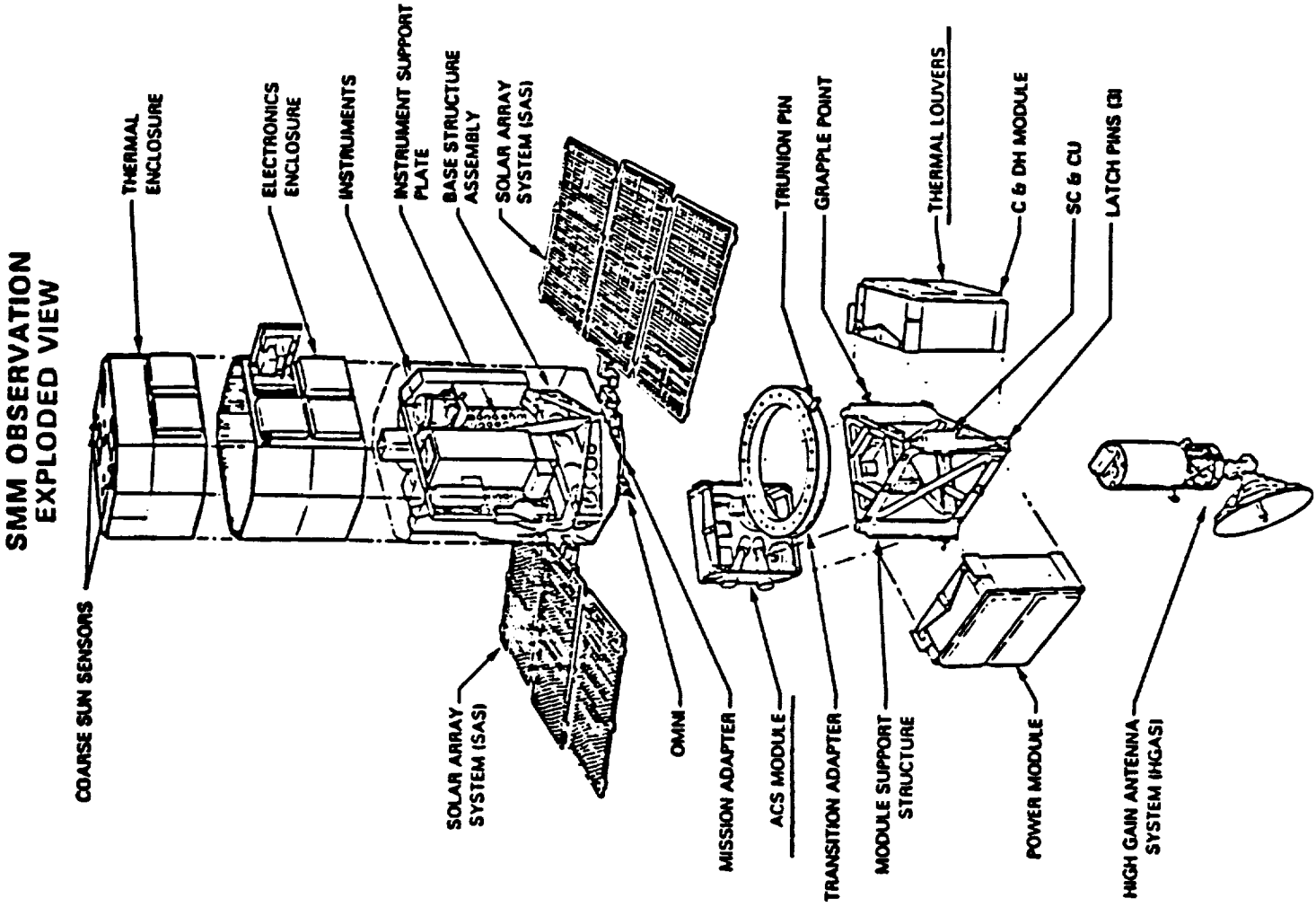

Figure 1

SMM SPACECRAFT TUMBLE RATES

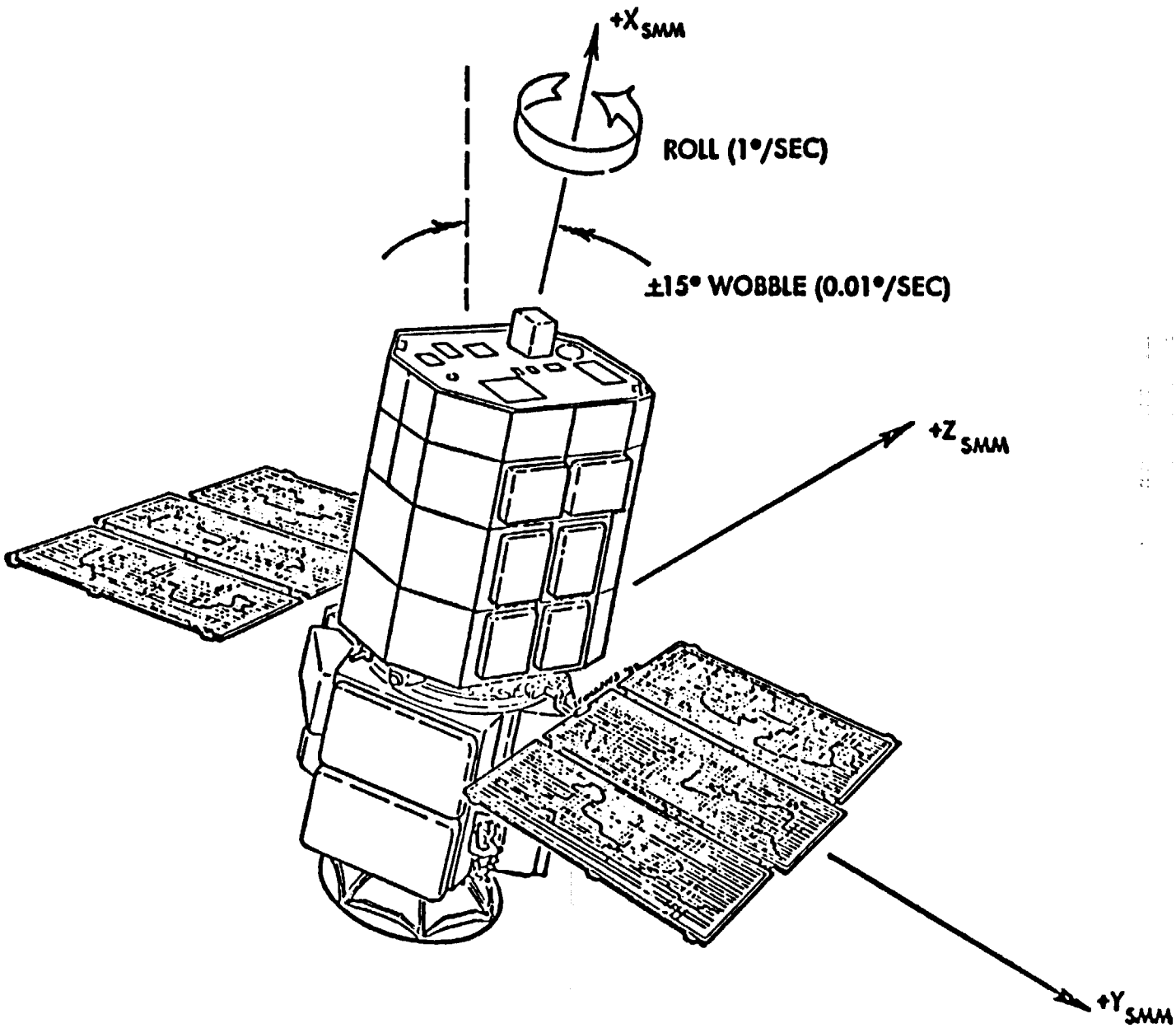

Figure 2

Table 1 Reaction efficiency of thermal control surface materials.

Typical Thermal Control Surface	AO Reaction Efficiency 10^{-24} cm^3/AO Atom
Kapton Polyimide Film	2.6
Carbon Filled Kapton Polyimide Film	2.5
Mylar Polyester Film	2.85
Clear Tedlar Film	2.89
White (TiO_2) Filled Tedlar Film	0.6
TFE and FEP Teflon Film	$<$ 0.03
Z302 Gloss Black Polyurethane Paint	4.5
Z306 Matt Black Polyurethane Paint	0.85
Z853 Gloss Yellow Polyurethane Paint	0.75
Z276 Gloss White Polyurethane Paint	0.85
401-C10 Flat Black Velvet Epoxy Paint	0.67
High Temperature Graphite Paint	3.3
S-13 GLO Flat White Silicone Paint	No Measurable Change
Green Potassium Silicate Paint	No Measurable Change
Graphite Epoxy T300/934 Composite	2.5
Graphite Al Metal Matrix Composite	No Measurable Change
Silver Foil Solar Array Interconnects	0.47 - 1.47
Glassy Carbon	0.8
Molded Graphite	0.85

Table 2

PART, DESCRIPTION, AND LOCATION

PART#	DESCRIPTION
#1	Upper (sun) side of sunsensor (+x facing)
#2,2a	Lower side of sunsensor (-x facing) and +z facing
#3	backside of sunsensor (-z facing)
#4	upper left (+y, +x) corner
#5	top half of sunsensor side blanket
#6	bottom half of sunsensor side blanket
#7	middle-top of bottom blanket
#8	left of bottom
#9	right of bottom
#10	lower star-tracker
#11	upper star-tracker
#12	BOS (bright object sensor)
#13a&b	star tracker side pieces
#14a&b	upper right and left pieces
#15a&b	pieces under 14 a and b
#16a&b	pieces under 15 a and b
#17	star tracker left side piece
T1,2,3,4	teflon pieces on the top
B1,2,3	teflon pieces on the bottom
+y1,2	teflon pieces on the left
-y1,2	teflon pieces on the right

NUMBER ASSIGNMENT FOR PART AS A FUNCTION OF THE BOX

BOX#	PIECE#'s
1	8, 14A+B
2	7,9
3	+y2, -y2, B1, 13A + B
4	+y1, -y1, C3, 12
5	6, 6A
6	1, 2, 2A, 3, 4
7	10, 11
8	5
9	17A,B BR, BL, C1,2,4 T1, 2, 3, 4 B2,3
10	G4

In Bag: 15A&B, 16A&B

Table 3 AO Fluence of Solar Max Mission Satellite

	1980	1981	1982	1983	1984	Total
Avg. altitude, km	570	552	534	516	498	
Time, hours	8030	8760	8760	8760	2920	37230
Avg. $F_{10.7}$	197	204	174	120	138	
Avg. K_p	3	3	4	3	4	
Avg. AO Density, cm^{-3}	2.45+07	3.24+07	3.70+07	2.91+07	4.49+07	
AO fluence, cm^{-2}	3.78+20	4.46+20	6.27+20	4.67+20	2.58+20	21.76+20

Table 4 Flight Confirmation of Predicted Kapton Mass Loss

Mission	Ram Fluence (cm^{-2})	Adjusted Fluence	Predicted Kapton Loss (mil)	Actual Kapton Loss (mil)
Shuttle STS-8 41.2 hrs @ 222 km	3.87E20	3.87E20	0.39	0.2 to 0.5
Solar Max Mission 4 years @ 570 to 498 km	21.8E20	6.94E20	0.7	0.5 to 0.8
LEO Flight Experiment (six day exposure)	-----	19.0E20	2.0	1.9 to 2.1

Table 5

SSR-ER SOLAR REFLECTOMETER MEASUREMENTS

Sample Description and Orientation	Solar Reflectance ρ_s Air Mass "2" SSR-ER	Solar Absorptance α_s Air Mass "2" SSR-ER	Solar Absorptance α_s Air Mass "0" SSR-ER	Solar Absorptance α_s Air Mass "0" LMSC Cary 17D
B-3 3003 Aluminum Sheet ∥	0.862 0.863 0.866	0.136	0.144	0.170
B-3 3003 Aluminum Sheet ⊥	0.852 0.858 0.854	0.145	0.135	
B-7 Flat Black Chemglaze	0.040 0.040 0.039	0.960	0.962	0.957
B-6 White Thermatrol Silicone Enamel ∥	0.892 0.893 0.893	0.107	0.160	0.171
B-6 White Thermatrol Silicone Enamel ⊥	0.891 0.891 0.890	0.109		
B-5 7075 Clad Aluminum Sheet ∥	0.801 0.800 0.803	0.198	0.202	0.234
B-5 7075 Clad Aluminum Sheet ⊥	0.828 0.821 0.823	0.176		
B-4 2024 Clad Aluminum Sheet ∥	0.746 0.742 0.738	0.258	0.264	0.287
B-4 2024 Clad Aluminum Sheet ⊥	(No striation noted)			
B-1 Aluminized FEP Teflon 2nd Surface (5mil)	0.867 0.867 0.866	0.133	0.134	0.132
19FB Silverized Fused Silica OSR	0.973 0.973 0.972	0.027	0.039	0.05 (Typical)
159 Anodized Titanium Foil	0.275 0.276 0.270	0.723	0.708	0.71 (Typical)
Armalon Black PTFE Teflon Glass Cloth (Unetched)	0.046 0.045 0.046	0.954	0.956	0.94 (Typical)

Table 6

SMM THERMAL SURFACE SOLAR ABSORPTANCE

Thermal Control Surface Description	Solar Absorptance Typical Prelaunch α_s	SMM Post Flt α_s	Apparent Change $\Delta\alpha_s$
T1, AgFEP Film, Unsupported Sunlit end, Worst case, Wrinkled, Frosty, Partial Trans	0.05 - 0.07	0.3 to 0.4	0.29
T3, AgFEP Film, Unsupported center area of same strip above, Looks new, A ~ 80%	0.05 - 0.07	0.09 to 0.11	0.04
17B, AgFEP Film Strip, Bonded to MLI, End of strip, Worst case, Obvious yellow contamination coating	0.05 - 0.07	0.28	0.22
17B, AgFEP Film Strip, Bonded center area of same strip above, Looks new, A ~ 90%	0.05 - 0.07	0.06 to 0.08	0.01
-Y2, AgFEP Film, Unsupported strip, Looks new	0.05 - 0.07	0.06 to 0.07	0.005
+Y2, AgFEP Film, Unsupported strip, Looks new	0.05 to 0.07	0.06 to 0.07	0.005
17B, Al Kapton MLI cover, Exposed front side, Looks like STS-8 samples	0.37 to 0.41	0.42	0.03
17B, Al Kapton MLI Cover, Same as above, Protected back side, Looks new	0.37 to 0.41	0.396	0.006
13A, Al Kapton MLI Cover, Exposed front side, Looks like STS-8 samples	0.37 to 0.41	0.425	0.035
13A, Al Kapton MLI Cover, Same as above, Protected front side by overlap, Looks new	0.37 to 0.41	0.39	0.000

ATTENDEES
SMRM DEGRADATION STUDY WORKSHOP
May 9-10, 1985

FACILITY/ORGANIZATION	NAME	TELEPHONE
GSFC/732	E. Abrams	301-344-6071
GSFC/311.2	R. Anstead	301-344-7123
GSFC/732	N. Carosso	301-344-7295
GSFC/408	F. Cepollina	301-344-5913
GSFC/408	R. Davis	301-344-7703
GSFC/711.2	J. Day	301-344-6691
GSFC/408	K. Dolan	301-344-8289
GSFC/616	M. Dublin	301-344-5475
GSFC/750.1	T. Gehringer	301-344-5771
GSFC/435	L. Gonzales	301-344-0272
GSFC/311.1	J. Henegar	301-344-5345
GSFC/408	J. Jew	301-344-0059
GSFC/754.2	L. Kauder	301-344-5309
GSFC/420	M. Lauriente	301-344-5690
GSFC/HAO	R. Lee	301-344-7077
GSFC/717	J. Mangus	301-344-0508
GSFC/Sperry	A. Marquez	301-344-6486
GSFC/313	R. Marriott	301-344-8833
GSFC/732	T. Michalek	301-344-6952
GSFC/BFEC	M. Mijslinski	301-344-8625
GSFC/712.2	P. Newman	301-344-8421
GSFC/408	G. Ousley, Jr.	301-344-6756
GSFC/404	G. Ousley, Sr.	301-344-8073
GSFC/313.2	J. Park	301-344-6368
GSFC/725	J. Scialdone	301-344-6862
GSFC/403	A. Seivold	301-344-6511
GSFC/301	W. Smith	301-344-7935
GSFC/732.2	J. Triolo	301-344-8651
GSFC/313.1	J. Uber	301-344-8469
Aerospace Corporation:	W. Stuckey	213-648-7389
Applied Research Corp.:	S. Auer	301-459-8442
BASD:	J. Austin	303-939-4435
Case Western Res. Univ.:	D. Hoffman	216-368-4012
Comsat:	J. Reisenweber	301-428-4565
CRC (Canada):	D. Zimcik	613-998-2187
Dornier:	E. Langeluddecke	202-861-0200
Fairchild:	M. Bay	301-428-6057
	B. Bloom	301-428-6259
	R. Eby	301-428-6455
	H. Frankel	301-428-6800
	R. Karam	301-849-6380
	L. Sprott	301-428-6385
General Electric:	G. Racetti	215-354-1672

SMRM DEGRADATION STUDY WORKSHOP
MAY 9-10, 1985

FACILITY/ORGANIZATION	NAME	TELEPHONE
ILC:	S. Lloyd	302-335-3911 X353
	J. Martin	302-335-3911 X213
	J. Zelon	302-335-3911 X430
Johns Hopkins Univ.:	R. Benson	301-953-6241
	R. Fristrom	301-953-6221
	R. Maurer	301-953-5000 X4009
	O. Manuel Uy	301-953-5004
Jet Propulsion Lab:	R. Liang	818-354-6314 FTS 792-6314
Johnson Space Center:	D. McKay	713-483-3818 FTS 525-3818
	J. Visentine	713-483-4564 FTS 525-4564
Langley Research Center:	B. Sands-Mason	804-865-4555
Lewis Research Center:	T. Miller	216-433-4000 X6626
	H. Nahra	216-433-4000 X6626
Lockheed:	G. Cunnington	415-424-2397
	B. Retrie	408-742-8244
	D. Rhoads	408-743-2399
	J. Robinson	415-424-2440
Marshall Space Flt. Ctr.:	R. Linton	205-453-2009
Martin Marietta:	L. Bareiss	303-977-8713
	D. Merschel	303-977-8707
MDAC:	M. Moriarity	314-233-4473
MNC/NOLA:	A. Daech	504-255-3617
	B. Webber	504-525-3617
NASA/HQ:	R. Weinstein	301-469-3847
OAO:	P. Carosso	301-345-0750 X0272
Perkin Elmer:	C. Carey	203-797-5106
Rockwell:	H. Rockoff	213-922-0637
Schonstedt	J. Rippingale	703-471-1050
Science & Eng. Assoc.:	R. Rantanen	303-790-1572
Sperry:	C. Sutter	602-869-1323
Teledyne:	J. Ritter	818-886-2211 X2807
TRW:	F. Cottrell	213-535-2706
	D. Hewitt	213-535-9550
	K. Smith	213-297-2054
Consultant, WASH, DC	R. Kruger	202-362-0839